Ph.D. Course in:

"Food and Human Health"

XXXVI Cycle

Dissertation Title:

# "**Oil Structuring for Improving Healthy and Sustainable Diets**"

**Ph.D. Student**
Ciuffarin Francesco

**Supervisor**
Prof. Sonia Calligaris

**2024**

*One of the greatest challenges of our World is knowing enough about a subject to think you're right, but not enough of the subject to know you're wrong.*

*Neil deGrasse Tyson*

# TABLE OF CONTENTS

# PREFACE

The present thesis, titled "Structuring Oil for Developing Healthy and Sustainable Diets", represents the culmination of three years of my studies, research, exploration, and curiosity about Food Science.

Undertaking this "research journey", as I like to call it, has been both challenging and rewarding. It has provided me with the opportunity to taste in depth the academic research on fats and to contribute, in my modest way, to the ever-growing body of knowledge on this actual topic.

I would like to express my sincere gratitude to Sonia Calligaris and the FoodTech Group of the University of Udine, whose guidance, support, and expertise have represented a fundamental part of this process. Their energy, motivation, and mentorship have not only shaped the trajectory of this research but have also contributed significantly to my personal and academic growth.

The decision to explore oleogels as fat replacers was motivated by a deep-seated concern about climate change, and the sustainability of our diets was one of the topics to which my expertise could contribute. As I entered the intricate rabbit hole of oleogels, I was reminded of the importance of taking into account every aspect of the supply chain, from ingredient production to the processing, formulation, and consumption of food products. Only by thinking globally, the goal of more sustainable diet patterns can be achieved.

This thesis is structured into three parts, in which oleogels are studied regarding the crystallization properties based on different processing conditions, the possibility of using hydrophilic gelators, and finally their nutritional properties. While the chapters are almost self-contained, together form a cohesive narrative that seeks to formulate more sustainable fat ingredients.

I hope that this work not only contributes to the existing literature but also sparks further inquiry and discussion in the field. It is my fervent desire that readers find this thesis informative, engaging, and thought-provoking.

Ivo 🙋🏼‍♂️

November 2023

# SUMMARY

In response to the nutritional and environmental issues that emerged recently on fats, there has been in the last decades an exponential growth of research in the field of oleogel and oleogelation. Oleogels are defined as semisolid materials entrapping large quantities of oil. These innovative materials are explored mainly as promising solutions to reduce trans and saturated fatty acids in foods, but also as potential delivery systems for bioactive molecules. Possible applications include bakery and confectionery items, plant-based meat alternatives, dressings, sauces, chocolates, spreads, and margarine products. It should be said that the consumer acceptability of these products strictly depends on the functionalities of solid fats, such as animal fats, tropical oils, or chemically modified shortenings. Despite the interest in oleogels, the use of oleogels in food industries is still in the early stages. This can be attributed to several challenges associated with Regulatory constraints, imposing restrictions on the use of some proposed gelators, or lack of knowledge about the functionalities of oleogels in complex food systems and their further behavior in the human body.

This doctoral project was designed to increase the knowledge surrounding oleogel and oleogelation. To this aim, both conventional and unconventional oleogelation strategies have been explored. The initial part of this research was dedicated to the study of the oil structuring ability of lipophilic gelators, considering the impact of oil minor components on oleogel structure as well as the potential use of novel technologies for a process-driven structuring of fats. In particular, the potential of high-pressure technology was considered. The second section was focused on exploring innovative oleogelation procedures mainly considering the ability of nanostructured porous materials to entrap oil. In this context cellulose, pea proteins, and whey proteins were considered as oleogelators. Finally, the third part of the thesis was designed to study the fate of oleogels in the human body to close the circle in studying structure-function relationships.

The outcomes of the research contribute to increasing the existing knowledge on oleogels and oleogelation strategies, taking in mind the importance of improving the nutritional functionalities of the existing lipid-containing foods as well as in the development of novel foods. I hope that the thesis results will be useful in assisting researchers and food managers in the attempt to design healthy and sustainable food products assuring at the same time a memorable eating experience during food consumption. Every food innovation is likely doomed to failure if the pleasure of consumers is not reached.

# 1. INTRODUCTION

## 1.1. Challenges of the Modern Food System

The food system is currently facing multiple challenges. On one hand, there is the need to ensure the sustainability of the food system for future generations, and, on the other, there is the need to reduce the health burdens associated with the over- or under-nutrition of the population (Figure 1).



Figure 1. Multifaced challenge of the 21st Century food system.

Consumers, particularly the younger generations, are becoming more conscious of these concerns and are gradually adopting more conscientious consumption behaviors (EIT Food, 2021). Nonetheless, it remains evident that it is imperative to instigate measures at all levels to promote sustainable development. In this context, the food system has a significant environmental impact, accounting for approximately one-third of global greenhouse gas (GHG) emissions. Food production alone occupies 40% of the Earth's land surface and consumes at least 70% of the planet's freshwater resources (Crippa et al., 2021). Moreover, a

large number of steps are needed to obtain a food product: starting from farming, harvesting or coughing, transporting, processing, packaging, distributing, storing, and finally consumer manipulation. Each of those steps produces a significant amount of $CO_2$ emissions (Aschemann-Witzel et al., 2023) with an environmental impact that varies significantly from food products. Broadly speaking, there are three sets of food groups with different impact per calorie: plant-based foods have the lowest impact; eggs, dairy, poultry, pork, and most of the fish run into 5 to 20 times the impact of the lower-$CO_2$-emitting products; some fish, as well as meat from cattle, goats, and sheep, have upwards of 20 to 100 times of plant-based food (M. Clark et al., 2020). These differences are largely driven by the resources that are needed to produce each food.

Given the increase in the global population, a dietary transition that includes more calories from plant-based foods is suggested as a strategy to mitigate the large environmental impact of the food system (Springmann et al., 2018). It has been estimated that a global transition to a more plant-based diet would be able to reduce food-related GHG emissions by 50-70%, bringing benefits to other aspects of the environment, such as biodiversity (Clark & Tilman, 2017; IPCC, 2019). Hence, governmental agencies, funding programs, and a growing number of consumers are actively promoting the adoption of lower carbon footprint alternatives to animal products, aiming to enhance both environmental sustainability and human health advantages.

Beyond sustainability concerns, it's imperative to recognize that dietary patterns not only raise sustainability concerns but are also one of the pivotal factors influencing health outcomes. Numerous chronic diseases are directly correlated to excessive and unbalanced food intake, culminating in severe health complications, including obesity, type II diabetes, hypertension, and cardiovascular diseases, typically linked to the excessive consumption of sugars, fats, and sodium. On the other side, an inadequate essential nutrient intake increases frailty worsening important functional abilities, such as immunity, bone health, and cognitive functions (Rémond et al., 2015).

Based on these considerations, as part of the European Green Deal, which aims to transform the EU into a modern, resource-efficient, and competitive economy with net zero emissions of greenhouse gases by 2050, in 2020 the European Commission, released a programmatic document titled "Farm to Fork Strategy" (Figure 2). This document describes the correlation between a healthy population and the transition to a more sustainable food system. The aim is to accelerate our transition to sustainable food systems and to ensure, at the same time, that everyone has access to sufficient safe, nutritious, and sustainable food (European Commission, 2020). To do that, the EU policies are implementing a systemic approach to achieve four overarching priorities (Figure 2):

- *Nutrition for sustainable and healthy diets*, by tackling malnutrition and overnutrition, fostering healthy aging through nutrition, and developing new protein alternatives for plant-based diets.
- *Food systems to support a healthy planet*, by developing climate-smart food systems that adapt to climate change, conserve natural resources, and help to reduce the flow of greenhouse gases into the atmosphere, boosting biodiversity, healthy ecosystems, and soils and fostering environmentally friendly sustainable agriculture and aquaculture.
- *Circularity and resource efficiency*, by achieving zero food waste, reducing water and energy use by more industrial food processes, encouraging more local food, using sustainable and biodegradable food packaging, and reducing plastics in food.
- *Innovation and empowering communities*, by fostering sustainable and accessible food for all towns, cities, and regions, and raising awareness and getting people engaged in food science and local food policy.
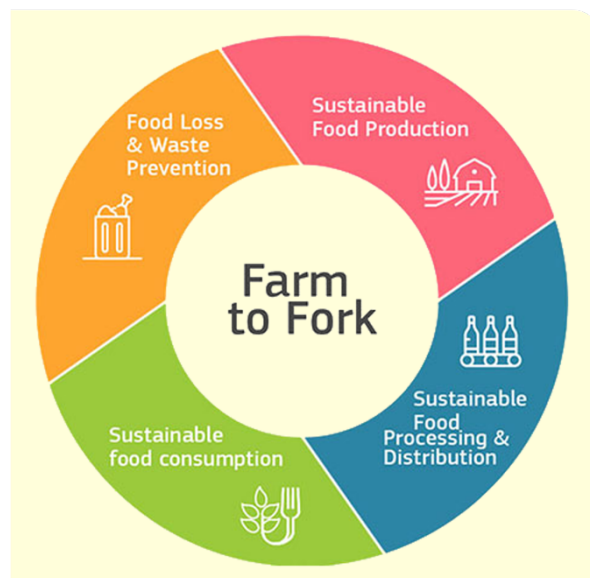


Figure 2. Farm to Fork Strategy programmatic summary (European Commission, 2020).

A redesign to healthier and more sustainable food products is much needed to achieve the results required by EU goals. This involves both the reformulation of traditional food products and the creation of entirely new ones.

Some examples are the plant-based alternatives that in the last five to ten years landed on the market (Xiong, 2023). These alternatives offer not only a wider variety of healthy options but are also more environmentally friendly. Examples are plant-based meat and fish alternatives, crafted from ingredients like legumes, grains, and vegetables, that mimic the taste and texture of meat while significantly reducing the carbon footprint associated with

livestock production (Heller & Keoleian, 2018; Saget et al., 2021). Similarly, dairy alternatives made from soy, almond, oat, or coconut provide nutritious alternatives to dairy milk, often requiring less land, water, and resources in their production (Apovian, 2016). Furthermore, traditionally consumed foods can be reformulated to reduce levels of calories, sugar, fat, and salt to fight chronic diseases, such as obesity, diabetes, heart disease, and hypertension (M. Clark et al., 2020).

The design of the modern food system is the result of centuries of discoveries, often serendipitous, that have profoundly influenced our culinary traditions. These discoveries brought all of us food products that are part of our diets and our culture. However, boosting the transition from a traditional-based diet to a more sustainable and healthier one needs to rethink food, while maintaining its sensorial aspect (FAO, 2017).

Nevertheless, achieving food formulations that retain sensory qualities akin to traditional products is a complex task. Many attempts have been made to replicate the appearance of conventional products with plant-based alternatives, but they often fall short on the sensory aspect. This challenge has been central to the decline in market share observed in recent years, following the peak in sales in 2020 (Wilson, 2023). Another concern pertains to the substantial presence of saturated fats in meat substitutes, which is essential for providing structural integrity to the product but poses a noteworthy health-related drawback. For these reasons, further research is needed to address these challenges.

## 1.2. Issues Associated with Fat Consumption

From a nutritional point of view, the excessive intake of fats is worldwide recognized as one of the burdens of modern society, being closely associated with the increasing risk of development of many non-communicable diseases (*e.g.,* coronary heart disease, type II diabetes, obesity, stroke, metabolic syndrome, and other cholesterol maladies) (Hooper et al., 2020). On the other hand, oils are known for their potential cardiovascular benefits, reducing the levels of LDL cholesterol and improving overall heart health.

Unfortunately, the removal of saturated fats, without compromising all the technological and sensory aspects, is considered an extremely difficult task. On the other hand, their complete substitution with unsaturated fats is also partially negative from a nutritional point of view. In particular, dietary saturated lipids are considered essential for the structural integrity of cell membranes, and to produce hormones, including testosterone and estrogen, which present a positive effect on brain function and cognitive health, increasing bone calcium absorption and reducing their turnover, and supporting immune defense (Gómez-Pinilla, 2008).

Generally, lipids rich in saturated fatty acids are commonly referred to as fats, and these can be sourced from both animals and plants. Animal-derived fats can be found in meat and dairy products, while vegetable ones are present in some tropical fruits, such as coconut, shea, and palm. On the other way around, lipids from plant sources, like sunflower seeds, nuts, and olives, are mainly rich in unsaturated fatty acids and are known as oils (O'Brien, 2004).

Lipids consist of a complex mixture of triacylglycerols (TAGs), which are molecules comprising a glycerol backbone linked to three fatty acids. These fatty acids can be categorized based on the chain length and presence/number of double bonds along their chains, influencing both the three-dimensional shape of the carbon chain and its physical behavior. Fatty acids are categorized as unsaturated when one or more double bonds are present in their molecular structure, preventing close packing and decreasing the crystallization temperatures. In contrast, saturated fatty acids lacking double bonds easily pack together with the formation of crystals at room temperature.

The proportion of saturated and unsaturated fractions in a food lipid determines the lipid's behavior at specific temperatures. When subjected to temperatures lower than their melting points, TAG molecules undergo nucleation due to the limited solubility of the higher melting point molecules. This process facilitates the development of an interconnected three-dimensional crystalline network, formed by growing and interacting crystals held together by

non-covalent forces. Over time, these crystals group form clusters, contributing to the formation of larger structures bonded by weak forces (Miyashita, 2017; Sato et al., 1999). Understanding these complex interactions between saturated and unsaturated fractions and their crystalline behavior is fundamental to comprehend the physical properties of lipid-based materials (Figure 3).
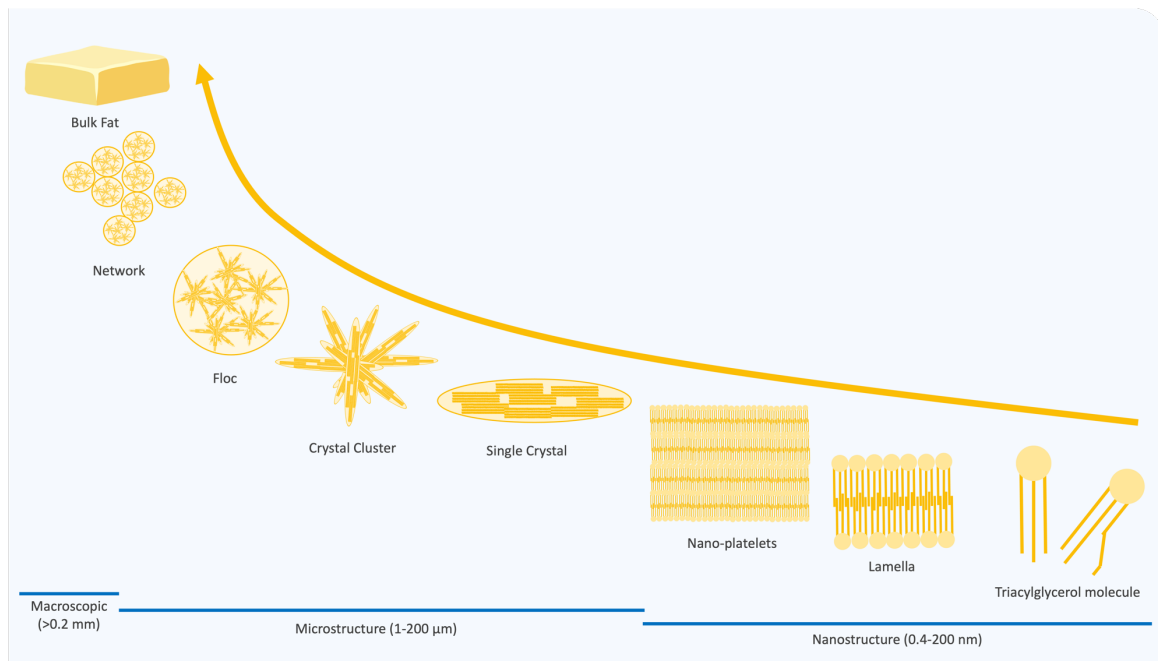


Figure 3. Structural hierarchy in a fat crystal network from molecules to the material.

The distinction between fats and oils significantly influences their roles in food formulations. From a practical standpoint, fats exhibit a solid state at room temperature, contributing to the texture and sensory experience of various food products. Beyond their natural occurrence in products like meat, fish, and dairy, fats also serve as ingredients added to foods to enhance taste, texture, and other sensory aspects. Items like baked goods, chocolates, and spreads frequently utilize solid fats to improve their palatability and consumer appeal (Marangoni et al., 2012). Interestingly, the application of these fats is increasing in plant-based formulations, where they are used to enhance both structural and sensory functionalities. Table 1 presents the main technological roles of fats in food formulations.

Table 1. Technological contribution of saturated fats in food formulations (Patel et al., 2020; R. C. da Silva et al., 2023).

| Food Category | Technological Contribution |
|---|---|
| Bakery | Lamination, favoring aeration for volume and uniform cell structure, lubrification for tenderness and texture, moisture stabilization by retaining long-term softness, structuration, aroma dissemination and permanence of flavor, etc. |
| Meat | Structuring, moisture stabilization, sensorial properties (*i.e.*, color, softness, juiciness, etc.) |
| Chocolate | Stabilization to prevent the blooming, and structuration by giving consistency and fragility, sensorial aspects, etc. |
| Spreadable Creams | Structuring in terms of consistency and spreadability, sensorial aspects, stabilization of the water-dispersed droplets, etc. |
| Dairy | Spreadability of butter and cheese spreads, structure of whipped cream, texture of cheese, and creaminess of ice cream, etc. |

Being these solid fats highly appreciated for their technological functionalities in foods, in the past, the chemical hydrogenation of oils was applied to mimic animal fats functionalities in food formulations by using as starting materials more economical plant-based oils. As is well known, hydrogenation consists of the conversion of liquid oils into fats by chemically removing double bonds in the carbon chain. Unfortunately, it is also well demonstrated that hydrogenation leads to the formation of *trans* fatty acids (TFAs), which have serious health risks (Cerqueira & Castro, 2023). In response to the health concerns associated with *trans* fats, the Food and Drug Administration (FDA) acted in 2015 by determining that partially hydrogenated oils are not generally recognized as safe (GRAS). The European Commission released a Regulation to limit the use of trans fats to 2 g per 100 g of total fat in food products the maximum allowed quantity (Reg. EU No 1169/2011). These regulatory actions demonstrate the commitment of regulatory authorities to promote healthier food choices and protect public health from the harmful effects of trans fats.

As an alternative, the industry sharply increased the use of naturally plant-sourced saturated fatty acids, deriving from tropical oils, such as palm, coconut, and shea oil and their fractionated fractions. Fat fractionation is a process used to separate the high melting fractions from low melting components of fat (Sangwal & Sato, 2018). Given that, palm oil has become one of the most widely utilized sources of fats in foods due to its cost-effectiveness, desirable texture, and rheological properties, excellent resistance to oxidation, and extended shelf life (Tan et al., 2021). Unfortunately, tropical oils (*e.g.*, palm and coconut oils) are sources of saturated fatty acids, like animal fats. Additionally, the use of palm oil opens sustainability issues associated to the extensive deforestation and habitat loss in Southeast Asia rainforests and other biodiverse regions, including South America (Vijay et al., 2016).

Therefore, today there is an increasing demand for healthier and *trans* fatty acid-free alternatives able to mimic the fat functionalities. In this context, the possibility to structure plant-based oils into gel-like materials called oleogels is one of the most promising sustainable strategies.

# 1.3. Oleogel and Oleogelation Strategies

Oleogels are solid-like materials obtained by exploiting the properties of selected molecules in forming a three-dimensional network able to entrap a high quantity of liquid oils (Marangoni & Garti, 2011b) (Figure 4). The resulting material can be tailored to obtain a wide range of mechanical properties or specific functional properties (*i.e.*, melting point or texture) (Martins et al., 2018).



Figure 4. Example of a phytosterol-based oleogel formed by 90% (w/w) of liquid oil and shaped in the nickname of the author.

The development of oleogels can be traced back to 1946 when a lithium soap of 12-hydroxy stearic acid (12-HSA) was employed in lubricating greases (Fraser, 1946). In 1992, a new vegetable oil-based oleogel was developed. This was achieved by melting ethyl-cellulose at 140 °C and incorporating perfume before the solidification of the mixture, resulting in a transparent oleogel that was recommended for cosmetic purposes (AIACHE et al., 1992). Early applications of oleogels also encompassed areas such as waste oil disposal, oil spill recovery, and art conservation (Abdallah & Weiss, 2000; Terech & Weiss, 1997). The use of structured liquid oil was then transferred to the pharmaceutical and cosmetical sectors, in which they were employed for several purposes, including the treatment of cellulite (Morales et al., 2009), and make-up (Co & Marangoni, 2012a; Martinez et al., 2019).

The main reason for the large use of these materials by the pharmaceutical and cosmetic industries relies on their possible use as drug-delivery matrices, especially for lipophilic molecules (Sagiri et al., 2014). It was only in 2003 that structured liquid oils were proposed for food applications as possible substitutes for saturated fats (Daniel & Rajasekharan, 2003), but only in the last ten years the research efforts on this topic progressively increased (Figure 5).
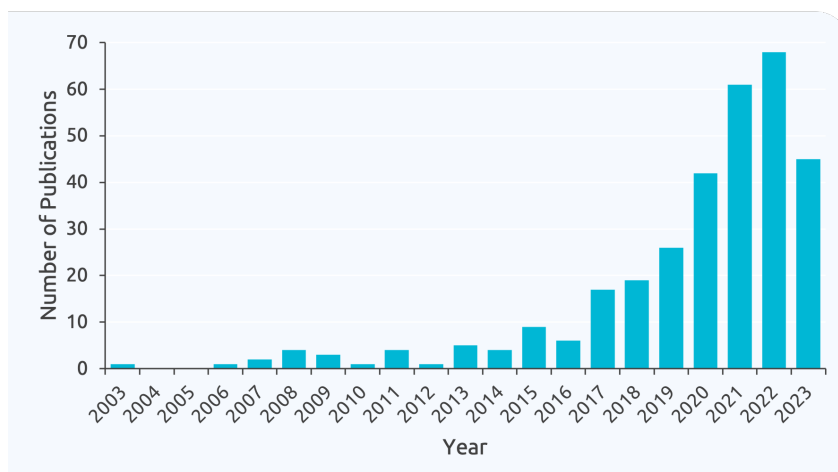
Figure 5. Publications with the word "oleogel" or "organogel" in the title retrievable in the Web of Science database.

The sharp increase reported by the literature publications is a symptom of interest in this topic driven by new regulatory patterns and consumer demand.

This growing body of knowledge surrounding oleogels would open exciting possibilities for revolutionizing food formulations and addressing health and sustainability concerns in the food industry, especially when considering lipid-containing products, such as bakery products, plant-based meat alternatives, dressings, sauces, chocolates, spreads, containing animal fats, tropical oils or chemically modified shortenings. As previously described, the consumers' acceptability of these products strictly depends on the functionalities of the plastic fats used in the formulation.

# 1.4. Oleogel Preparation Methodologies

Today, oleogels can be obtained by using different molecules able to assemble and entrap liquid oil. Basically, molecules used in oleogelation can be classified based on their affinity with oil. Lipophilic molecules, which have an inherent oil affinity, can be directly dispersed into edible oil under defined physicochemical conditions to form a network that physically entraps the liquid oil. This approach, known as *direct oleogelation*, was developed earlier and has been extensively studied and applied in food prototypes. Examples of gelators applicable in this context are fatty acids, monoglycerides, fatty alcohols, waxes, ethylcellulose, and phytosterols (Zhao et al., 2022).

In recent years, there has been a significant increase in studies on the possibility of using hydrophilic molecules as oleogelators. This is much more challenging because it involves the use of hydrophilic molecules, such as proteins and polysaccharides, and requires the initial dissolution of the polymer in a water-based system. Water has to be further removed before oil addition (Gravelle, 2023). For this reason, this approach falls under the name of *indirect oleogelation*.

It should be considered that all proposed oleogelators can be used as single gelators or in combination. Thus, oleogels can be also categorized into mono-component-based oleogels, prepared by a single oleogelator, and multi-component-based or hybrid oleogels, prepared by using two or more oleogelators (Co & Marangoni, 2012b).

Their capability to form a network entrapping oil and thus oleogel structures can be steered by selecting the proper gelator or their combination. Given that, the following general characteristics must be considered for the successful implementation in food formulation of an oleogel (Marangoni & Garti, 2011a):

- *Food-grade*. The structurant should meet the regulatory requirements in the attempt to apply it for food applications. This aspect often limits the exploitation of many proposed gelators that are labeled as additives limiting their concentration in the final product.
- *Economic*. Costs associated with the choice of the oleogelator should be carefully considered with the expected application to be readily available and affordable. However, the final price of food products could hinder the application of high-cost gelators if additional benefits are present.
- *Efficient*. The ability to structure at low concentration is fundamental, not only from the economic point of view but also to limit the risk of overdosing. However, if a healthier gelator is economical and doesn't compromise the sensorial characteristics, its ability to structure at low concentration becomes less important.

- *Functional from a technological point of view.* The final oleogel feature should mimic the technological functionality of the fat matrix that aims to substitute in terms of rheological and sensory properties.
- *Versatile.* Ideally, the same gelator, or a slightly modified version, could be used for different food applications. That aspect can be considered a key point for broadening oleogel diffusion. Moreover, the oleogelator needs to withstand traditional food processing treatments.
- *Sustainable.* Selecting an appropriate oleogelator involves evaluating its sourcing, production processes, and overall carbon footprint. Opting for oleogelators derived from renewable and responsibly managed sources, with minimal environmental impact during their lifecycle, aligns with sustainability goals, and potentially allows the reuse and the reduction of waste promoting circular economy practices.

Over the last decade, a considerable high number of structuring molecules has been identified. Both direct and indirect oleogelation strategies have advantages and disadvantages. In the following paragraphs, a detailed description of the different oleogelation strategies that could be strategically exploited to prepare fat analogs will be provided, describing the advantages and disadvantages associated with each technique and each gelator, also providing a comprehensive understanding of their potential applications and limitations.

# 1.5. Oleogelation with Lipophilic Gelators through the Direct Method Approach

The direct oleogelation approach represents the simplest, and the easiest scaling-up strategy for oleogel production involving the direct dispersion of one or multiple lipophilic oleogelators into the selected liquid oil (Scharfe & Flöter, 2020). The preliminary gelator dispersion in oil has to be carried out at a temperature that allows the complete melting and solubilization of the gelator. After that, a cooling step is performed to induce the formation of the network in which liquid oil is entrapped and represents the continuous phase (Marangoni & Garti, 2018).

Different categories of molecules can be used, comprising low molecular weight (*e.g.*, waxes, fatty acids, fatty alcohols, monoglycerides, phytosterols) and high molecular weight gelators (*e.g.*, ethylcellulose and chitin). The common characteristic of these molecules relies on their ability to directly self-assemble in a network when dispersed into the oil under specific physicochemical conditions.

To obtain a satisfactory gelation, the gelator must present a high solubility in the lipid solvent. If the gelator is insoluble in the solvent, it may precipitate; whereas if it is excessively soluble, it may only interact with the solvent and hinder the formation of a gel network (Blake et al., 2014).

Despite these common characteristics, the network formed by lipophilic molecules could have a different nature based on the gelator characteristics (Figure 6):

- *Crystalline network.* This network consists of structured arrangements of crystals in liquid oil. The crystal clusters within the network interact by intermolecular forces, such as van der Waals forces, and hydrogen bonds, creating a three-dimensional network. Crystalline networks can vary in size, shape, and complexity depending on the gelator features and processing parameters. Examples are:
  - *Monoglycerides* (MG) are lipid molecules with a polar structure, consisting of a single fatty acid esterified to a glycerol molecule. Having an amphiphilic nature, monoglycerides find widespread applications as polar lipids in numerous food products. Cakes, bakery items, margarine, frozen desserts, and spreads are just a few examples of food products where monoglycerides are commonly used.

When introduced into liquid oil, these molecules have the capability to self-assemble, forming an inverse crystalline lamellar phase (Verstringe et al., 2015). The agglomeration of the crystalline lamellar clusters in a dendritic crystal shape, which is easily visible under the polarized light microscope. Several factors influence the physical properties of this type of oleogel, like the polarity of the solvent, MG chain length, cooling rate, and shear, and the presence of minor components (da Pieve et al., 2010; Ojijo et al., 2004; Valoppi et al., 2017)

- o *Waxes* are very promising oleogelators, being able to crystallize in a three-dimensional network with a high oil-binding capacity at low concentrations (1-10%, w/w) (Manzoor et al., 2022). In the case of waxes, the coexistence of high- and low-melting temperature susceptible waxes provides interesting viscoelastic, visual, and textural properties (Doan et al., 2017; Tavernier, Doan, et al., 2017). Some of the influencing factors are related to the chemical composition of the wax and the oil used, but also external factors, such as cooling and shear rate, and storage time (Doan et al., 2018). However, restrictions in their use as food additives impair their extensive use in food formulations.

- *Polymeric network. This* is another type of network that is characterized by a three-dimensional structure formed by interconnected polymer chains creating complex entanglements characterized by unique properties, such as mechanical strength, elasticity, and stability.

  - o *Ethylcellulose* is a linear polysaccharide derived from cellulose by replacing the hydroxyl end groups with ethyl end groups. The different degrees of substitution at the basis of the different behavior in oil and water: for values ranging between 1.05 and 1.50, the molecules are soluble in water, and in the range of 2.4 and 2.5 are soluble in organic solvents (Davidovich-Pinhas et al., 2015). In this case, hydrogen bonds are responsible for the interactions between the polymer strand and network formation. The oil represents a passive filler in the gel matrix, not affecting the gel mechanical properties. The ethylcellulose-based oleogel mechanical performances are directly correlated to the polymer molecular weight as well as the cooling rate, the gelling setting time, and the oil considered (Davidovich-Pinhas, 2019).

- *Fibrillar network.* Another possible type of structure that can be exploited for oil structuring in the fibrillar network. It is mainly formed by the self-assembly or

aggregation of molecules resulting in a three-dimensional network that provides mechanical strength, stability, and unique gel properties (Martins, 2023).

o Among various gelators available, *phytosterols*, a family of plant-produced molecules, stand out because of their natural origin and healthy effects. More importantly, they have positive health implications for the phospholipid-based cell membrane structure and the ability to lower cholesterol levels in the blood. One of the most promising molecule combinations giving a fibrillar network entrapping oil is represented by a mixture of γ-oryzanol with β-sitosterol, or stigmasterol, which self-assemble into nanoscale hollow tubes (Scharfe et al., 2019). Subsequently, these tubes aggregate into bundles, forming a three-dimensional network that fills the space, resulting in translucent and firm gels. This tubular network exhibits a high level of transparency (Scharfe et al., 2019). Some of the parameters affecting the gel are represented by the polarity of the solvent used and the micro components eventually present in it.
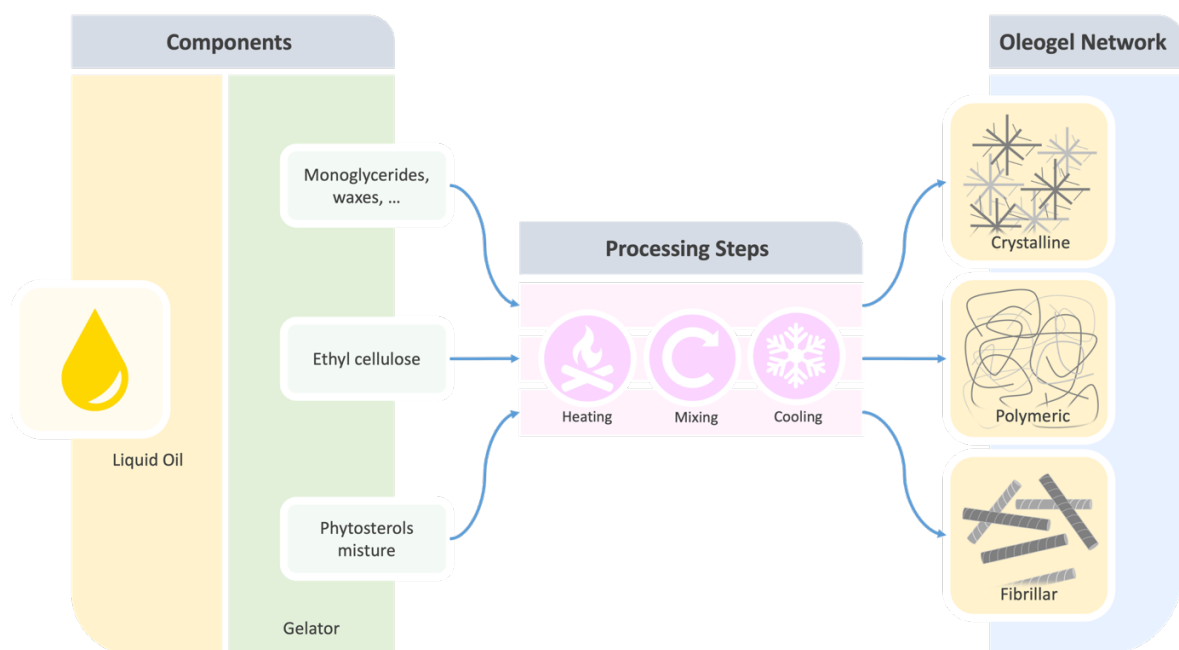


Figure 6. Schematic representation of the possible network obtained by using lipophilic gelators.

The various networks here described illustrate the immense potential of lipophilic gelators to structure liquid oil, resulting in oleogels with diverse mechanical and technological properties due to their diverse physio-chemical characteristics, as summarized in Table 2. This aspect opens possibilities for their application in various food formulations.

Table 2. Lipophilic gelators for oleogel formation, gelling properties, and regulatory aspects.

| Gelator | Melting Temperature (°C) | Minimum Gelling Concentration (%, w/w) | EU Regulatory Aspects | Reference |
|---|---|---|---|---|
| Monoglycerides | 60-65 | 4.0 | E471 | Y. Zhang et al., 2023 |
| Rice Bran Wax | 70 | 5.0 | E908 | Doan et al., 2015, 2017 |
| Sunflower Wax | 72 | 1.0 | Not approved | Doan et al., 2015, 2017) |
| Bees Wax | 50 | 1.5 | E901 | Doan et al., 2015, 2017 |
| Candelilla Wax | 57 | 1.0 | E902 | Doan et al., 2015, 2017 |
| Carnauba Wax | 61 | 2.0 | E903 | Doan et al., 2015, 2017 |
| Berry Wax | 16 | 1.0 | Not approved | Doan et al., 2015, 2017 |
| β-sitosterol/ γ-oryzanol mixture | 85-90 | 8.0 | E499 | Martins et al., 2022 |
| Ethylcellulose | 130-140 | 2-10 | E462 | Bampidis et al., 2020; Gravelle et al., 2018 |
| Sorbitan Monostearate | 70 | 17 | E491 | Sagiri et al., 2016 |

Despite the direct approach requiring easy process unit operations, different drawbacks should be described. The gelator dissolution can be achieved only by reaching high temperatures, thus promoting oil oxidation (Chen et al., 2011). To reduce oxidation development, some strategies can be applied, such as reducing the heating time and temperature as much as possible and carrying on the process in dark conditions and under nitrogen flow. Moreover, the network physical stability during storage should be considered. In a study involving extra virgin olive oil-based oleogel, Alongi et al. (2022) showed that all oleogels made of MG, waxes, and ethylcellulose experienced a reduction in their mechanical properties due to molecular reorganization events (Alongi et al., 2022). Similar results were obtained by Giacomozzi et al. (2021) considering monoglycerides-based oleogels.

Another relevant issue of direct oleogelation methods is associated with the belonging of the gelators to the additives list (Table 2). This aspect impairs the food industry from using them in food formulations, especially in Europe, where the *clean label* policy requested by consumers is very strong (Edenbrandt & Lagerkvist, 2023). Monoglycerides, as an example, can be used only in *quantum satis* in food formulation and reported on the label with the number E471 (Reg. EU No 1129/2011).

# 1.6.  Process-Driven Structuring of Lipid Crystalline Networks

As already described in Paragraph 1.2, fat crystalline networks are formed by crystals that form larger aggregates upon clustering together. These aggregates finally create a continuous network, whose structure at the nano-, micro-, and macro-scale affects the fat functionalities in foods.

It has been widely demonstrated that both composition and processing conditions affect fat crystal network structure (*e.g.*, crystal size, morphology, and interactions among crystalline particles) and thus, its functionality (Acevedo & Marangoni, 2015; Ramel et al., 2016). This is true not only for fats made of triacylglycerols but also for oleogels structured by a crystalline network.

By employing appropriate processing conditions, the crystalline structure of a given matrix can be effectively controlled and manipulated. Temperature cooling rate and the application of shearing are the most common processing factors taken under control to steer fat crystallization. The rate applied to cool down the system and the associated undercooling affects the type of polymorphic form as well as the shape and dimensions of crystals (Werner-Cárcamo et al., 2023). Additionally, it has been demonstrated that the shear applied on the fat matrices during cooling can drive both nucleation and crystal growth in terms of the thickness of nanocrystal platelets and polymorphic transition rate (Campos & Marangoni, 2014; Maleky et al., 2011). In fact, as reported by Nguyen et al. (2020), static crystallization tends to form spherulite-like crystals, under β form, whereas spherical clusters of β' were observed when dynamic crystallization was performed, enhancing the hardness of the fat matrix.

Recently, high-intensity ultrasound (US) was proposed to improve the physical and functional properties of lipids by tailoring their crystallization behavior (Gregersen et al., 2019; Povey, 2017) with low associated processing costs. In this context, the US has demonstrated its capability to efficaciously steer the structural and textural properties of fat by increasing the crystallization rate, hardness, and elasticity of the crystalline network characterized by smaller crystals and a sharper melting profile (Martini, 2013; Wagh et al., 2016). Several sonication conditions can be applied to modulate the crystallization, including the acoustic power level, pulse mode, duration, temperature, crystallization stage in which the US is applied, as well as other processing variables (Wagh et al., 2016).

Additionally, some earlier studies also highlighted that this target could be reached by applying high-pressure processing (HPP) (Zulkurnain et al., 2016). High-pressure processing

stands out as a non-thermal approach in food technology and pressure treatments in the food sector are today commonly employed to extend the shelf life of products. The capability of hydrostatic pressure to steer fat crystallization has been scarcely investigated in the literature. From a thermodynamic point of view, the changes in both molar volume ($\Delta V$ = 6-41 mL mol$^{-1}$) and enthalpy ($\Delta H$ = 100-300 kJ mol$^{-1}$) associated with fats melting are known to be always positive (Hagemann & Rothfus, 1983; Hiramatsu et al., 1989; Zulkurnain et al., 2016b). According to the Clausius-Clapeyron equation, this implies that the melting temperature of lipids will always increase with the increase in pressure (10-20 K MPa$^{-1}$), which thus promotes the crystallization of these materials (Brown, 2023; Zulkurnain et al., 2016b). The volume reduction associated with fat crystallization is also based on its kinetic pressure dependence. Due to the negative activation volume of fat solidification ($\Delta V^{\neq} < 0$), the kinetic rate of fat crystallization exponentially increased with pressure according to the Eyring equation (Zulkurnain et al., 2016b).

Coherently with these theoretical principles, previous studies have examined the influence of pressurization on lipid crystallization, revealing its potential not only in boosting the phenomenon but even in promoting the formation of smaller crystals. In particular, Zulkurnain et al. (2016a, 2019) focused on the impact of pressure on the crystallization behavior of a blend of fully hydrogenated soybean oil with 10-30% (w/w) soybean oil content at pressures ranging between 100 and 600 MPa. The Authors reported how an increase in pressure resulted in a decrease in crystal size, an increase in crystallization rate, and a more thermally stable crystal network. The effect of pressurized crystallization was even shown to steer fat morphology, concerning polymorphic transformation. However, this effect appeared to be highly variable, being particularly dependent on the matrix nature. For instance, while Tefelski et al. (2008) and Kościesza et al. (2010) showed that crystallization under pressure (60-450 MPa) greatly favored the α form of oleic acid and triolein, Oh & Swanson (2006) observed no significant morphological changes by applying up to 600 MPa during cocoa butter solidification.

Based on these earlier studies, the feasibility of HPP technology for fat crystallization is certainly worthy of further investigation given its possible scaling up. It should be considered that HPP technology is nowadays shifting from a novel to a mature technology with a continuously growing amount of commercial equipment applied as an alternative to heat pasteurization. Their high price has been already pointed out by other authors as the main limitation of a worldwide commercial application (Cacace et al., 2020). Future innovations are thus needed to increase the economic sustainability of HPP equipment. In this regard, it should be noted that as the pressure required for the process decreases, its costs also decrease, mainly resulting from the decrease in the vessel wall thickness required to withstand pressure (Bermejo-Prada et al., 2017; Cacace et al., 2020). Thus, the possibility of

applying moderate hyperbaric treatments (< 200 MPa) could boost the industrial application of fat crystallization under pressure.

# 1.7. Oleogelation with Hydrophilic Gelators through the Indirect Method Approach

Hydrophilic polymeric components and particles have gained significant attention recently due to their extensive commercial availability, approved use in food products, and cost-effectiveness compared to other lipophilic gelators (Patel, 2018). Nonetheless, hydrophilic molecules cannot be directly dispersed in lipophilic media, like oil. Therefore, indirect approaches have been developed to use these molecules as building blocks to structure oil.

Several strategies have been developed in recent years to exploit hydrophilic molecules as oleogelators:

- *Emulsion-template.* Various food polymers, such as proteins and modified polysaccharides, have amphiphilic properties that enable them to stabilize oil-in-water emulsions. In the literature examples of these systems are represented by proteins or modified cellulose combined with polysaccharides or surfactants (thickeners), such as xanthan gum, resulting in emulsions with viscoelastic properties (Espert et al., 2020; Patel, Rajarethinem, et al., 2015; Patel & Dewettinck, 2015).

The basic mechanism relies on the initial formation of a stable emulsion. The oleogel is then formed by water removal (Tavernier, Patel, et al., 2017a) (Figure 7). The emulsion formulation is the key factor in successfully preparing oleogel by this method because the network formed in water might retain oil upon water evaporation without collapsing (Espert et al., 2020; Patel, Cludts, Bin Sintang, et al., 2014). In fact, the determining factors in developing firmly structured oleogels using the emulsion-templated approach are the initial interface rigidity and stability of the primary emulsion.

The primary drawback of this approach is the risk of oil oxidation when employing air drying, typically carried on at ~60 °C (Espert et al., 2020). Another difficulty that has to be faced is the formation of a stable emulsion, able to withstand the drying process without collapsing and, subsequently, the shear forces that occur during the food processing (Tavernier, 2018).
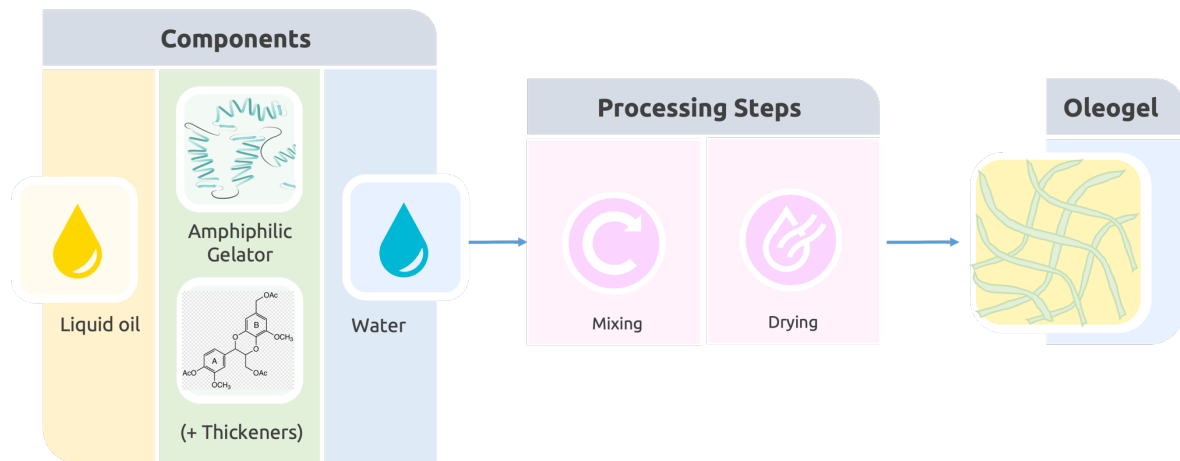
Figure 7. Schematic representation of the emulsion template-based oleogel.

- *Solvent exchange*. This procedure is based on the formation of a network in the aqueous medium by a polymer. Then, the polarity of the solvent is progressively decreased by the introduction of an intermediate solvent, being either ethanol, acetone, or tetrahydrofuran. Finally, the organic solvent is substituted with an oil, obtaining an oleogel with 80-90% (w/w) of oil. By modulating the polymer concentration and the processing conditions it is possible to modify the rheological properties of the final oleogel. In fact, the final oleogel characteristics are mainly dependent on the properties of the gel network, the polarity of the intermediate sample, and the kinetics of the solvent exchange procedure. This technique was well documented by De Vries et al. (2015) concerning the solvent exchange procedure to form protein-based oleogels from pre-set hydrogels.

  Some of the drawbacks associated with this technique rely on the use of solvents, such as tetrahydrofuran and acetone, which are not common in food production and are also considered toxic (Fowles et al., 2013; Umeh et al., 2021). The necessity of their use drastically limits the applicability of this oleogelation approach in food formulations.



Figure 8. Schematic representation of the solvent exchange template-based oleogel.

- *Dried-template.* A third indirect approach for oil structuring has been developed. In this approach, a hydrogel (*i.e.*, aqueous gel) or a foam structured by using hydrophilic molecules, is first dried. The resulting material has a porous structure, that can absorb oil leading to the formation of oleogels (Manzocco et al., 2021). The literature highlights three prevalent approaches: the foam template, where foam is created and the aqueous part is then dried through freeze-drying (FD); the cryogel template, involving hydrogel formation followed by FD; and the aerogel template, where a hydrogel is dried using a supercritical fluid (Buchtová & Budtova, 2016).

The dehydration process to obtain the final oleogel is considered the critical step because the pore size modifies extensively the capacity of the material to absorb oil and form a network. If traditional hot air drying (HAD) is used, a structural collapse due to the capillary forces generated by water migration is generally experienced (Patel, 2020). For that reason, different drying strategies were implemented over time (Figure 9).

The easiest, well-established, and environmentally friendly drying process is freeze-drying (FD). The process involves an initial formulation of a hydrogel that is further frozen. The water is then removed via sublimation under a vacuum in a freeze-dryer, and a cryogel is obtained (Nowak & Jakubczyk, 2020). The freezing step stands as a crucial parameter that demands careful consideration. Specifically, the growth of ice crystals plays a pivotal role in determining the final morphology of the cryogel. If the freezing process is carried on quickly, smaller ice crystals are generated, and thus the resulting pores in the final dried material are also small (Luo et al., 2022). Moreover, during freeze-drying (FD), the sublimation of ice crystals prevents the formation of liquid-vapor interfaces, thereby avoiding the capillary surface tension that typically occurs in hot air drying. Consequently, the resulting material exhibits enhanced porosity and structural performance compared to conventional hot air-drying methods (Fricke & Tillotson, 1997). However, it is essential to note that the formation and growth of ice crystals during hydrogel freezing can lead to localized polymer chain collapse and concentration. As a result, the cryogel may exhibit large pores and non-porous pore walls in certain regions (Assegehegn et al., 2019). By playing with different process parameters during the freezing process the desired porosity and structural characteristics of the cryogel can be obtained.

To further reduce structural collapse during drying, a novel approach called supercritical-$CO_2$ drying (SCD) has been recently proposed (Şahin et al., 2018). Supercritical-$CO_2$ drying is a process designed to remove solvents from a material while preserving its structure and properties. This technique uses supercritical carbon dioxide, which is achieved when $CO_2$ is heated and pressurized beyond its critical point.

In this state, carbon dioxide exhibits properties of both gas and liquid, making it a powerful solvent (Weibel & Ober, 2003), with a wide range of applications, including drug delivery systems, tissue engineering, and food processing (Jahed et al., 2023). To enable SCD for hydrogel drying, a pre-processing step is required, due to the low solubility of water in supercritical carbon dioxide. The hydrogel needs to be converted into an alcohol-gel by replacing water with a highly $CO_2$-soluble solvent, such as acetone or ethanol (Şahin et al., 2018). This process, known as "solvent exchange" and previously described, allows an efficient removal of the solvent with supercritical carbon dioxide by maintaining its structure. The resulting material, commonly called "aerogel", is an extremely porous structure that retains the polymer's original structure, capable of absorbing significant quantities of liquid oil (Manzocco et al., 2021). Supercritical-$CO_2$ drying is widely regarded as the gold standard in drying techniques, offering several advantages over traditional methods like air or vacuum drying and freeze-drying. These advantages include fast drying times if the solvent exchange step is not considered, superior preservation of material structure and properties, and suitability for a wide range of materials (Weibel & Ober, 2003). However, it comes with the trade-off of high usage of $CO_2$-miscible solvents, which can be a costly factor in the process. Despite this drawback, the use of supercritical-$CO_2$-drying remains a promising approach due to its ability to overcome the challenges associated with conventional drying methods, making it an attractive option for various applications in materials science and beyond.
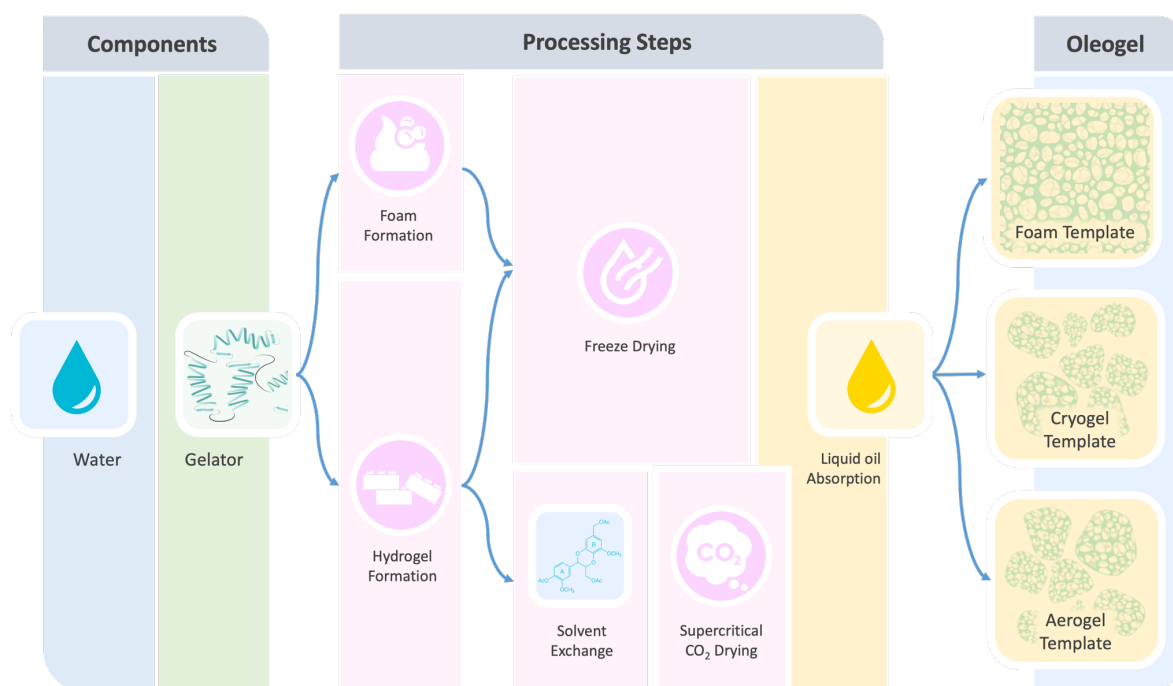


Figure 9. Schematic representation of the foam, cryogel, and aerogel template-based oleogel.

Table 3 shows the literature examples of oleogels prepared by using the indirect methods previously described. This provides valuable insights into the diverse range of possibilities for creating oleogels using hydrophilic gelators.

Table 3. Examples of possible oleogel formulation via different indirect strategies.

| Method | Initial System | Structurant | Final Oil Content (%, w/w) | Process Applied | Reference |
|---|---|---|---|---|---|
| Emulsion template | 60% O/W emulsion | Soy Protein Isolate + κ-carrageenan | 60 | 60 °C HAD | Tavernier, Patel, et al., 2017b |
| | | Gelatin + xanthan gum | 95-99 | 70 °C HAD, FD | Patel & Dewettinck, 2015 |
| | | Sodium caseinate + Xanthan gum + Guar gum | >94.5 | 70 °C HAD, FD | Abdolmaleki et al., 2020 |
| | 80% O/W emulsion | Whey proteins + low methoxy pectin | 80 | 35 °C HAD | Wijaya et al., 2017 |
| Solvent Exchange | Hydrogel | Whey protein isolate | 84-90 | Stepwise solvent exchange | De Vries et al., 2015 |
| | | Whey, potato, egg, pea, and soy protein isolates | 94 | Acetone as the intermediate solvent | Feichtinger et al., 2022 |
| | Gel-like aqueous suspension | Cellulose nanofibrils | 98 | Methanol as the intermediate solvent | Roman et al., 2021 |
| Dried Template | Foam | Gelatin + xanthan gum | 95-97 | FD | Abdollahi et al., 2020 |
| | | Rice bran proteins | 95 | FD | Wei et al., 2022 |
| | | Hydroxypropyl methylcellulose, pectin | - | | Jiang & Bai, 2022 |
| | Cryogel | Alginate + soy proteins | 92 | FD | Chen & Zhang, 2020 |
| | | Egg white protein + Xanthan gum | 94 | FD | Jaberi et al., 2020 |
| | | Whey protein isolates | 80 | SFD | Plazzotta et al., 2020 |
| | | κ-carrageenan | 80 | Lettuce as a filler | Plazzotta et al., 2019 |
| | | Alginate + Gelatin | 95 | FD | Li et al., 2022 |

| | Whey protein isolates | 80 | SCD and FD | Plazzotta et al., 2020 |
|---|---|---|---|---|
| | κ-carrageenan | 80 | Lettuce as a filler | Plazzotta et al., 2019 |
| Aerogel | Egg proteins | 20-94 | Cold-set hydrogel | Alavi & Ciftci, 2023 |
| | Whey protein isolates + carboxymethyl chitosan | <84 | SCD | Zhao et al., 2023 |
| | Whey and Potato protein isolates | 70-84 | SCD | Jung et al., 2023 |

Hot air drying (HAD), freeze-drying (FD), supercritical-$CO_2$ drying (SCD).

The various techniques presented in Table 3 highlight the complexity involved in the application of hydrophilic molecules-based oleogels. As retrievable from the literature on indirect methodologies, there are a significant number of papers claiming to deal with oleogels. It is debatable whether all these materials can be considered true oleogels, considering both their physical properties and oil content. As reported by Marangoni & Garti (2018), most definitions of a gel exhibit at least two of three common motifs:

1. a substantially diluted (*i.e.*, predominantly liquid phase) chemical composition;
2. rheological properties of a solid;
3. the existence of some form of interconnected structure that is responsible for #2 despite #1.

The distinction between oil-particle aggregates (like dough) and oleogel remains unclear, and this issue is pivotal when focusing on emulating saturated fats. As shown in Table 3, the literature contains a broad spectrum of oleogels with varying oil content, ranging from 20% to 95% (w/w). Notably, these oleogels exhibit different performances, but it is not clear reading the literature if at least two of the three motifs reported above are respected (in many cases the presence of a network is only hypothesized) and the systems are not diluted at all. Additionally, the capacity to mimic fat functionalities is not in all cases well studied.

In conclusion, indirect approaches represent the new frontiers of oleogelation due to the possibility of using widely accepted, recognizable, and trustworthy hydrophilic biopolymers commonly labeled as ingredients and not categorized as additives. Interestingly, these oleogelators in food have a nutritional value beyond their structuring function (*i.e.*, in the case of protein or fiber use) that could justify any potential increase in the final product's cost (Patel, 2018). Moreover, this strategy opens the possibility to use components eventually recovered from food processing and production side streams (*i.e.*, proteins and fibers) offering sustainable structuring solutions, which are in line with the principles of the circular

economy promoted by the EU (European Commission, 2020). Embracing these molecules as oleogel building blocks represents an op an opportunity to create innovative and sustainable food products that cater to consumer preferences for clean labels and improved benefits contributing to food production.

# 1.8. Oleogel for Food Applications

Over the last decade, significant advancements have been made in the field of fat mimetics, driven by the necessity to find effective strategies for replacing trans and saturated fats. However, to successfully replace saturated fats (solid fat) with unsaturated fats (liquid oil) in food products without compromising sensory and quality characteristics, the properties of the fat alternative must emulate those of the solid fat. As previously described (paragraph 1.2), edible fats, from a structural standpoint, belong to a unique category of soft matter made of triglycerides that crystallize into various polymorphic states creating a crystal network (Marangoni et al., 2012). For these reasons, the incorporation of so-called fat mimetics needs to reduce unhealthy fats with mono- and polyunsaturated fats, and simultaneously, provide technological functionalities comparable to those of traditional fats.

As listed in Table 4, oleogels have been tested as a fat substitute in many food products including meat products, dairy, spreads, confectionaries, and pastries. As can be noted, the good capability of oleogels to mimic fat functionalities (*e.g.*, spreadability, texture, mouthfeel, and emulsion stabilization) has been demonstrated in many food prototypes (Perța-Crișan, Ursachi, Chereji, Tolan, et al., 2023; Puscas et al., 2020; Zhao et al., 2022). In any attempt to replace fats, the first critical issue is to find the best-performing oleogel in terms of rheological properties and compatibility with other ingredients present in the formulation. In fact, it cannot be underestimated the role of the interactions among components considering the food complexity. Moreover, the oleogel performance must be maintained during food processing and storage.

Table 4. Examples of oleogel applications in food product formulation.

| Food Category | Food Product | Liquid oil used | Gelator used | Degree of Fat Substitution (%) | References |
|---|---|---|---|---|---|
| Meat Products | Frankfurter | Soybean oil | Rice bran wax | 100 | Wolfer et al., 2018 |
| | Meat patties | Sesame, linseed oil | Beeswax, Phytosterols | 25, 50 | Martins et al., 2019; Moghtadaei et al., 2018 |
| | Cooked salami | Canola oil | Ethylcellulose | 50 | Woern et al., 2021 |
| | Sausage | Soybean oil | Rice bran wax | 42 | Tarté et al., 2020 |

| | Product | Oil | Oleogelator | Concentration | Reference |
|---|---|---|---|---|---|
| | Pork burger | Olive oil, linseed oil, and fish oil | Beeswax | 100 | Gómez-Estaca et al., 2019 |
| | Beef burger | Soybean oil | Beeswax | 25, 50 | Moghtadaei et al., 2018 |
| Dairy Products | Processed cheese product | High oleic soybean; soybean oil | Rice bran wax, Ethylcellulose, and Sunflower wax | 100 | Huang et al., 2018; Park et al., 2018 |
| | Cheese cream | Soybean oil | Rice bran wax | 100 | Park et al., 2018 |
| | | Soybean oil | Rice bran wax, Ethylcellulose | 100 | Bemer et al., 2016 |
| | Ice cream | Oleic sunflower oil | Rice bran wax | 100 | Zulim Botega et al., 2013) |
| | Margarine | Soybean oil | Candelilla wax | 100 | da Silva et al., 2018 |
| | Filling cream | Sunflower oil | Monoglycerides | 100 | Giacomozzi et al., 2018; Palla et al., 2021 |
| Confectionaries | Chocolate paste | Sunflower, pomegranate seed and palm oil | Shellac wax, monoglycerides, beeswax, and propolis wax | 50 | Fayaz et al., 2017 |
| | | Sunflower oil | Hydroxypropyl-methylcellulose | 50 | Espert et al., 2021 |
| | | Sunflower oil | Whey protein aerogel particles | 100 | Plazzotta et al., 2023 |
| | Filling | Rice bran and palm; canola | Beeswax; hydroxypropyl methylcellulose and methylcellulose | 50, 75, 100 | Doan et al., 2016; Tanti et al., 2016 |
| Pastries | Cookie | Refined hazelnut oil | Beeswax and sunflower wax | 100 | Pandolsook & Kupongsak, 2017) |
| | | Soybean and high oleic sunflower oil | Candelilla wax | 100 | da Silva et al., 2021 |
| | Cake | Sunflower; cotton and high oleic sunflower | Rice bran wax; carnauba wax | 100 | Oh et al., 2017; Pehlivanoglu et al., 2018 |
| | Sweet pan bread | Rice bran oil | Candelilla wax | 25, 50, 75, 100 | Jung et al., 2020 |
| | Biscuit | Sunflower oil | Rice bran wax | 100 | Principato et al., 2021 |

| | | | | |
|---|---|---|---|---|
| Muffin | Sunflower oil | Candelilla wax | 100 | Jeong et al., 2021 |
| | High oleic sunflower oil | Monoglycerides | 100 | Giacomozzi et al., 2018 |
| Sponge cake | Sunflower oil | Beeswax | 100 | Dikhtyar et al., 2021 |
| Maize tortillas | Canola oil | Candelilla wax | 100 | Vernon-Carter et al., 2020 |
| Sponge cake, biscuits, laminated pastry | High oleic sunflower oil | Monoglycerides | 50 | Deniz Gunez et al., 2020 |

As Table 4 illustrates, the predominant type of oleogel employed in food formulations are those formed with lipophilic gelators. This prevalence can be attributed to the fact that they were largely studied before indirect methods were developed. In the reported examples, fat replacement with oleogels ranged from partial to total substitution. This can be explained by the limitation in the use of some gelators from a regulatory point of view and the reduced performances of the fat replacer. A general improvement in the fatty acid profile was in any case obtained, with the need for some adjustments in terms of sensory attributes and technological properties (Perța-Crișan et al., 2023).

A common mistake in the definition of the best-performing oleogel is the simple comparison of the mechanical and rheological properties of the oleogel in comparison to the fat intended to be substituted. For this reason, the interactions among the food formulation ingredients should be carefully evaluated. For instance, as documented by Patel et al., (2014) the presence of an oleogel made of methylcellulose in the dough could affect the crosslinking of the gluten network, considerably increasing the hardness and chewiness of the final product.

Considering all the examples presented in Table 4, it is clear that oleogels represent a promising alternative to saturated fats in a great variety of food products. However, to boost the oleogel application in the food industry by converting them into a real alternative to conventional fats, there is the need to strengthen the research activity mainly in the attempt to find out green-clean label fat alternatives as well as on the formulation-process interactions with the final aim to satisfy the sensory perception of consumers in tasting a new food formulation.

# 1.9. Health Benefits of Oleogels

Besides the above-described technological functionalities, oleogels are also recognized for enhancing the health properties of food formulation beyond the enhanced lipid profile.

Over the past decade, there has been a significant increase in scientific awareness concerning the crucial role of food structure in affecting the health functionalities of food. Particularly, in the case of oleogels, researchers have been studying the intricate relationship between the composition and structure of oleogels and their health performances, such as bioaccessibility, lipolysis, and digestibility. Table 5 reports literature evidence on the effect of oleogel on lipid digestion and the delivery of lipophilic components.

In the literature, studies have shown that oil structuring can impact both lipid digestibility (Ashkar et al., 2019; Calligaris et al., 2020; Marangoni et al., 2007; Marangoni & Garti, 2011b; O'Sullivan et al., 2017; Plazzotta et al., 2022) and the bioaccessibility of lipophilic compounds present in the oil (Calligaris et al., 2020; Dent et al., 2022; N. Luo et al., 2021; Salvia-Trujillo et al., 2017). Oleogels based on lipophilic oleogelators were found to reduce the extent of lipolysis (Calligaris et al., 2020; O'Sullivan et al., 2017; Ashkar et al., 2019). This effect is attributed to the presence of the oil structuring network, which hinders the activity of lipases on triacylglycerols. In general, the more resilient the network is against destructuring during digestion, the slower the digestion rate of the oil (Okuro et al., 2020). Remarkably, these *in vitro* digestion simulation findings are supported by some in vivo studies conducted by Tan and colleagues (2017a), demonstrating the ability of oleogelation to modulate post-prandial plasma triglycerides, glycemia, and appetite in comparison to the assumption of unstructured oil (Tan, et al., 2017a; Tan, et al., 2017b; Tan, et al., 2017c).

Contrarily, the digestion of oleogels structured by hydrophilic molecules has received much less attention. Recently, Plazzotta et al. (2022) studied the gastrointestinal behavior of oleogels containing whey proteins. These Authors showed a higher intestinal lipolysis extent of the oleogel in comparison to unstructured oil. It has been hypothesized that the oleogel structure, associated with the presence of proteins could favor oleogel destructuring and thus lipolysis (Plazzotta et al., 2022).

These results on the effect of oleogel structure on lipolysis could open new horizons for their possible use as tools to improve food health functionality as well as energy management deriving from lipid ingestion.

Other evidence published in the literature pointed out that not only can digestion be modulated by oleogelation, but also the bioaccessibility of lipophilic compounds. This can be achieved by controlling the gastrointestinal behavior of the oleogel through the selection of the proper oleogelator (Calligaris et al., 2020), and the relative concentration (Dent et al.,

2022). For instance, Li et al. (2019) reported that the bioaccessibility of curcumin loaded in an oleogel structured by β-sitosterol and lecithin was higher than the one of curcumin in unstructured oil.

Oleogels were proposed as delivery and protecting systems of lipophilic bioactive compounds in foods but also during digestion in the human body. In foods, oleogel structure was claimed as effective in protecting the entrapped oil or bioactive components from oxidation during storage. This capacity has been attributed to the decrease of the reactant mobility within the oleogel network (Alongi et al., 2022; Bascuas et al., 2020; Fu et al., 2020; Gao & Wu, 2019). For instance, recently it has been demonstrated that oleogelation protected the bioactive polyphenols in extra virgin olive oil during storage at different temperatures (Alongi et al., 2022). These Authors hypothesized that the differences in oxidation kinetics in structured and unstructured oil could rely on a different location of minor components inside the oleogel network. Similarly, curcuminoids in sunflower oil-based oleogels were protected from oxidation during storage (Calligaris et al., 2020). These results open the door to the possibility of using oleogelation strategies to deliver the bioactive lipophilic molecules proper of the extra virgin olive oil (EVOO).

Table 5. Summary of *in vitro* or *in vivo* studies exploring oleogel effect on lipid digestion and micro. components.

| Oleogel Composition | Carried molecule | Digestion method | Assessment | Reference |
|---|---|---|---|---|
| Candelilla wax + Canola oil | Fatty acids | Static method | Influence of oleogel amount in starch digestion rate | Alvarez-Ramirez et al., 2020 |
| Ethylcellulose / mono- and di-glycerides / phytosterols mix + Canola oil | Fatty acids | *In vitro* intestinal digestion | Free fatty acid release (%) using pH-stat method | Ashkar et al., 2019 |
| Phytosterols mix + Sunflower oil | Fatty acids | Static gastrointestinal digestion | Free fatty acid release (%) using pH-stat method; Interfacial binding of lipase using potentiometric titration | Dong et al., 2020 |
| Rice bran wax + Rice bran oil | Fatty acids | *In vivo* rat digestion | Blood parameters: lipid profile, triacylglycerols, total cholesterol, free fatty acids, HDL and LDL cholesterol. | Limpimwong et al., 2017 |
| Monoglycerides + Canola oil | Fatty acids | *In vivo* human study | Postprandial blood analysis TAG, FFA, glucose, and insulin response. | Wright et al., 2014 |

| | | | | |
|---|---|---|---|---|
| Monoglycerides / rice bran wax / phytosterols mix + sunflower oil | Curcumin | Static INFOGEST protocol | Free fatty acid release (%) using pH-stat method; Curcuminoid bioaccessibility | Calligaris et al., 2020 |
| Candelilla wax + Nut oils | β-carotene | Static INFOGEST protocol | β-carotene bioaccessibility | Li et al., 2021 |
| Ethylcellulose + Canola oil | β-carotene | *In vitro*, static, with simulation of fastened conditions | Moles of FFA released and lipolysis; β-carotene bioaccessibility | O'Sullivan et al., 2017 |
| β-sitosterol and lecithin + Corn oil | Curcumin | *In vitro* intestinal digestion | Curcumin bioaccessibility; free fatty acid release (%) using pH-stat method. | Li et al., 2019 |
| Rice bran wax + sunflower oil | Curcumin | Static INFOGEST protocol | Curcumin bioaccessibility. | Dent et al., 2022 |

In summary, there is an emerging interest regarding the potential use of oleogels not only to enhance food nutritional profile but also to promote further health benefits. However, it should be said that these findings are currently fragmented and there is a need to reinforce the research activities to better understand oleogel health functionalities.

# 1.10. Final Considerations on Oleogels

In conclusion of this introduction, the topic "oleogels" is an actual, multifaceted, and dynamic area of research considering the broad spectrum of technological and nutritional aspects associated with it. Throughout this introduction section, the most recent literature was revised comprising the methodologies of oleogel preparation, their manifold applications as fat mimetics, their possible impact on lipid digestion and bioavailability, and their role in addressing health and environmental concerns. Figure 10 summarizes the different functionalities of oleogels (technological, nutritional, and environmental) considering their possible application (as fat replacers or delivery systems for bioactive molecules).
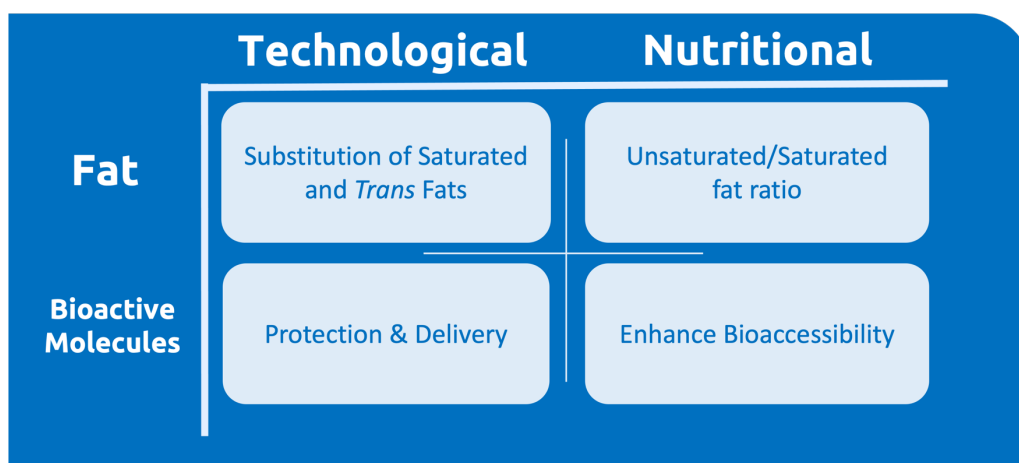


Figure 10. Key open questions associated to oleogelation.

Despite the huge amount of available literature, many challenges are still open to favor the transition from fats to oleogels in food products. From a *technological point of view*, innovation in oleogel preparation methodologies and relevant gelators is needed to solve Regulatory and technical issues impairing the large industrial application of oleogels. To this aim, research efforts are needed to deeply study the effect of formulation and processing conditions able to impact the final oleogel performances by considering both "conventional" (*i.e.*, direct methodologies) and novel oleogelation strategies (*i.e.*, indirect methodologies). It should be remembered that novel indirect strategies for oleogelation are under development, especially to solve the Regulatory issues associated with the use of food additives providing clean-label solutions. In this context, the selection of biopolymers is pivotal to face the *sustainability aspects* associated with the development of novel food ingredients. Only by solving these open questions, it would be possible to boost the escalation of oleogels from a laboratory level to an industrial scale. Additionally, should not be

underestimated the overall impact of oleogelation on the *nutritional and health functionalities* of food containing oleogels. Thus, aspects such as the fatty acid digestion behavior as well as the bioavailability of bioactive molecules included in the oleogel structure need to be clarified.

This doctoral journey aimed to tackle some of these open challenges by trying to improve existing oleogelation methodologies as well as design novel ones, with in mind the overall consumer acceptance that today considers not only food safety and sensory properties (essential pre-requisites), but also the potential additional health functionalities of food as well as its impact on the environment.

# AIM & OUTLINE OF THE THESIS

This Ph.D. thesis aimed to tackle some of the questions still open around the structuring of plant-based oils into oleogels, intended to be used as an alternative to saturated fats and/or as functional ingredients for delivering health functionalities.

The research framework is thus divided into the following three parts and its visually represented in Figure 11:

- *Part 1.* Oil structuring through direct approach (Chapters 2-3)
- *Part 2.* Oil structuring through indirect approach (Chapters 4-8)
- *Part 3.* Health functionalities of oleogels (Chapters 9-10)



Figure 11. Outline of the research.

## PART 1. OIL STRUCTURING THROUGH DIRECT APPROACH

The first part of this thesis focused on the application of the direct methodology exploiting the oil structuring ability of lipophilic gelators. We studied the possibility of structuring extra virgin olive oil (EVOO), representing a peculiar oil characterized by an optimally balanced fatty acid profile and by the presence of minor components, such as polyphenols, with demonstrated health-promoting properties. These positive nutritional features make EVOO an optimal candidate for designing healthy foods. This awareness is boosting the research efforts toward the development of ingredients and foods enabling an increase in EVOO consumption. In this thesis, the influence of micro-components on EVOO oleogelation was investigated in Chapter 2.

Furthermore, in Chapter 3 it has been studied a completely novel approach to drive oil structuring. In particular, the capability of hydrostatic high-pressure treatments to steer fat crystallization was initially demonstrated considering a mixture of sunflower oil structured by triacylglycerols (*i.e.*, palm stearin). This chapter should be considered as a proof-of-concept opening the way for further research efforts on process-driven oil structuring.

## PART 2. OIL STRUCTURING THROUGH INDIRECT APPROACH

In this second part of the doctoral thesis, the possible application of hydrophilic molecules to structure liquid oil by using indirect methodologies was investigated. To this aim, the dried template approach was selected as a particularly interesting strategy for a possible scaling up in the attempt to prepare novel ingredients for cold oil gelation. It should be remembered that this methodology comprises the following steps: hydrogelation, drying, and finally oil absorption. It was clearly stated in the introduction the fundamental importance of the drying process to maintain as much as possible the structure formed by the polymer in the hydrogel because this structure drives the ability of the molecule to entrap oil.

Cellulose was first considered, being the most abundant biopolymer on Earth today frequently discharged as waste. In Chapter 4 the focus was on the possibility of obtaining cellulose-based dried porous materials able to entrap oil. Furthermore, Chapter 5 was dedicated to the improvement of the functionalities of cellulose-based porous materials in forming oleogels with a solid-like behavior able to mimic that of plastic fats.

The study moved to proteins in Chapter 6 and Chapters 7 and 8 by considering pea proteins and whey proteins, respectively. Also in this case, dried porous materials were developed and their ability to form oleogels was assessed.

## PART 3. HEALTH FUNCTIONALITIES OF OLEOGELS

The third part of the thesis was dedicated to the study of the digestion behavior of some of the oleogels developed in this work (Chapters 9 and 10). In particular, the oleogels containing extra virgin olive oil and prepared by both direct and indirect approaches were investigated both for their lipolysis degree and polyphenol bioaccessibility during *in vitro* digestion. Additionally, cellulose oleogels containing sunflower oil were *in vitro* digested to elucidate the role of cellulose structure during digestion.

# PART 1

# OIL STRUCTURING THROUGH DIRECT APPROACH

Lipophilic gelators (*i.e.*, monoglycerides, waxes, and γ-oryzanol/β-sitosterol mixture) were initially considered to produce oleogel through a direct approach. These gelators, due to their affinity for oil, are easily dispersible in it, exerting their structuring capability by creating crystalline/fibrillar networks able to physically entrap oil. The choice of a lipophilic gelator, its concentration, and the specific oil employed contribute to the overall mechanical properties of the oleogel. Although the oil structuring capabilities of lipophilic gelators are widely documented in the literature, only a limited amount of information was retrievable on their performances when structuring extra virgin olive oil (EVOO). Thus, Chapter 2 was dedicated to the study of the role of the polyphenol content on the structuring behavior of liposoluble gelators in extra virgin olive oil.

Furthermore, with in mind the potentialities of crystalline networks to structure oil, the research in Chapter 3 was dedicated to the study of the feasibility of the application of a novel technology to drive fat crystallization. The selected novel technology was Hydrostatic High Pressure (HHP) which is scarcely studied for oil structuring but has already been applied by the food industry for other purposes, such as food pasteurization. To this aim and considering the reduced literature on that topic, we decided to develop the research by considering as starting fat blend sunflower oil structured by means of a crystal network made of saturated triacylglycerols deriving from palm stearin. This chapter should be considered as a proof-of-concept opening for further research efforts on process-driven oil structuring.

# 2. ROLE OF THE POLYPHENOL CONTENT ON THE STRUCTURING BEHAVIOR OF LIPOSOLUBLE GELATORS IN EXTRA VIRGIN OLIVE OIL

## 2.1. Introduction and Aim of the Study

EVOO, a key component of the Mediterranean diet, is renowned for its impact on both culinary traditions and health. Beyond its distinct flavor, it is rich in monounsaturated fats, vitamins, and antioxidants, exerting specific effects on the prevention of cancers, type II diabetes, obesity, and metabolic syndrome prevention (Buckland & Gonzalez, 2015), with additional benefits evidenced in genetic and aging studies (Menendez et al., 2013; Piroddi et al., 2017). Among micro-components that can be found in EVOO, polyphenols are particularly important, given their health-promoting properties, showing antioxidant, anti-inflammatory, cardioprotective, neuroprotective, anticancer, antidiabetic, antiobesity, antisteatotic, and antimicrobial effects (Cicerale et al., 2012; Fabiani, 2016; Parkinson & Cicerale, 2016; Rigacci & Stefani, 2016; Rodríguez-Morató et al., 2015).

The role of polyphenols on the structural and rheological properties of EVOO-based oleogels prepared by exploiting the gelling ability of lipophilic gelators (*i.e.*, saturated monoglycerides, rice wax, sunflower wax, or a mixture of γ-oryzanol and β-sitosterol) was investigated. These gelators were selected based on their well-known ability to gel plant-based oils (Co & Marangoni, 2012b; Martins et al., 2018; Plazzotta et al., 2022), including EVOO (Alongi et al., 2022), and are characterized by the capacity of assemble into oil. Monoglycerides and waxes form crystalline tridimensional networks in oil (da Pieve et al., 2010; Doan et al., 2015), whereas the mixture of γ-oryzanol and β-sitosterol assembles into a fibrillar network (Bot et al., 2008).

In the literature, only a few reports highlighted the impact of microcomponents present in the oil on the oleogel structure (Scharfe et al., 2019; Valoppi, Calligaris, Barba, et al., 2017).

This aspect appears of fundamental importance in view of using oleogels in food formulations.

To unravel the effect of the presence of polyphenols on oleogel structure, polyphenols were selectively removed from EVOO before gelation with 10% (w/w) of each gelator. This concentration was considered to be able to generate firm oleogels with high oil holding capacity (Alongi et al., 2022). The structural characteristics of oleogels were assessed by different methodologies, including rheology, polarized light microscopy, calorimetry, synchrotron XRD, and FTIR. Results demonstrated the polyphenol structuring ability when mixed with some of the considered gelators, such as monoglycerides and waxes.

Results here presented have been published in Open Access in:

Ciuffarin, F., Alongi, M., Peressini, D., Barba, L., Lucci, P., & Calligaris, S. (2023). Role of the polyphenol content on the structuring behavior of liposoluble gelators in extra virgin olive oil. Food Chemistry, 412, 135572. https://doi.org/10.1016/j.foodchem.2023.135572

## 2.2. Materials and Methods

### 2.2.1. Materials

Commercial extra virgin olive oil (EVOO) was used. Myverol™ saturated monoglycerides (fatty acid composition: 0.24% C12:0, 0.88% C14:0, 60.1% C16:0, 38.4% C18:0, 0.26% C20:0, 0.07 other; melting point 68.05 ± 0.50 °C) were purchased from Kerry Bioscience (Bristol, UK); rice bran wax (Karl Wax GmbH & Co. KG, Reinbek, Germany) was kindly provided by Spica Srl (Sulmona, Italy); sunflower wax purchased from Kahlwax GmbH & Co. KG (Reinbek, Germany), β-sitosterol (75.5% β-sitosterol, 12.0% β-sitostanol, 8.4% campesterol, 3.0% other) and γ-oryzanol (99% purity) were purchased from Nutraceutica S.r.l. (Monterenzio, Italy). Hydroxytyrosol, tyrosol, and tocopherol (α, γ, and δ-tocopherols) analytical standards, as well as all the other analytical grade reagents, were purchased from Sigma Aldrich (Milan, Italy).

### 2.2.2. Sample Preparation

#### 2.2.2.1. Polyphenol Removal from EVOO

Polyphenols were removed from EVOO by using the official COI/T.20/Doc No 29 method. In particular, oil was mixed in a 2:5 (v/v) ratio with a methanol/water (80:20, v/v) solution, vortexed for 3 min, sonicated for 25 min, and centrifuged at 5,000 rpm for 15 min. The oil fraction was recovered, and the same procedure was repeated 4 times. Afterward, the oil cleared from polyphenols (No-P) was mixed with the untreated oil (High-P) in a 1:1 ratio (v/v) to obtain a sample with an intermediate polyphenol content (Medium-P).

#### 2.2.2.2. Oleogel Preparation and Storage

Oleogels were prepared by following the methodologies reported by Calligaris et al. (2020). In particular, 10% (w/w) of saturated monoglycerides (MG), rice waxes (RW), sunflower waxes (SW), or a mixture of β-sitosterol and γ-oryzanol (PS) (2:3 w/w), were added to the three oil samples having different polyphenol content. The mixtures were stirred in the dark at temperatures higher than the gelator melting point (i.e., 80 °C for MG, RW; SW, 90 °C for PS) until the complete melting of the gelator, which required about 20 min for MG, RW or SW, and 25 min for PS. MG, RW, and SW oleogels were cooled and stored at room temperature (20 °C) in dark conditions, while PS oleogel was cooled at 4 °C for 12 h before being stored at 20 °C. All samples underwent analysis 48 hours post-preparation to enable network setting.

### 2.2.3. Analytical Determinations

#### 2.2.3.1.  Oil Fatty Acid Composition

In order to determine fatty acid composition (%), the methyl-esters were prepared according to the COI/T.20 Doc No 33 method. Samples were methylated before injection in Thermo Trace (Thermo Fisher, Waltham, Massachusetts, USA) 1300 gas chromatograph equipped with a FID detector and an auto-sampler. A fused silica column, SP-2330 (60 m length × 0.32 mm i.d. × 0.20 μm film thickness), was used. Helium was employed as a carrier gas, with a flow through the column of 1 mL min$^{-1}$. The temperatures of the injector (split) and detector (FID) were both set at 250 °C. An injection volume of 1 μL was used. The operating conditions were as follows: oven temperature was held at 165 °C for 5 min, then increased by 3 °C min$^{-1}$ to 210 °C and held for 10 min. The split ratio was 1:50. Results were expressed as a percentage of relative area.

#### 2.2.3.2.  Peroxide Values

The peroxide number was determined based on the method COI/T.20/ Doc. No 35 Rev.1. Briefly, 5 g oil were weighed, added to 25 mL of isooctane/acetic acid (2:3, v/v) solution, and shaken for 5 minutes. An aliquot of 1 mL of freshly prepared potassium iodate saturated solution was added and the samples were shaken for another 1 min. Afterward, 25 mL water was added to stop the reaction, and 2 mL of a 10 g L$^{-1}$ soluble-starch dispersion was added. Finally, samples were titrated with a 0.01 M sodium thiosulfate solution. The peroxide value (PV) was expressed as milliequivalents of active oxygen (mEqO$_2$) per kg of oil and computed by Eq. (1):

$$PV = V \cdot M \cdot 1000 \qquad \text{Eq. (1)}$$

where V is the volume of the sodium thiosulfate solution, M its concentration, and m the oil mass.

#### 2.2.3.3.  Absorbance at 232 and 270 nm

Absorbance was measured at 232 and 270 nm according to the method COI/T.20/Doc. No 19/Rev.5. Briefly, 0.25 g of sample was added with cyclohexane to 25 mL. Samples were properly diluted and absorbance at 232 and 270 nm was recorded (UV-2501PC, UV–VIS Recording Spectrophotometer, Shimadzu Corporation, Kyoto, Japan).

#### 2.2.3.4.  Diglycerides Composition

Oil composition was analyzed using the method COI/T.20 Doc No 32 based on gas chromatography (GC Carlo Erba HRGC-5160, Milano, Italia). In particular, 0.1 g of oil was added

with 1 mL of internal standard (dinonadecanoine in methyl-tertbutyl-ether, 0.1%). An aliquot of 30 μL of this solution was dried by a gentle nitrogen stream, added with 200 μL of silylation reagent and 200 μL of pyridine, mixed, left for 20 min to allow the complete reaction, and dried before adding 1 mL of n-heptane. Aliquots of 1 μL of the sample were injected (on column injection) at 80 °C eluted under helium pressure of 55 kPa. 80 °C have been held for 1 min, then oven temperature increased from 80 to 340 °C in 41 min (2 min at 80 °C, 20°C min$^{-1}$ from 80 to 300 °C, 5 °C min$^{-1}$ from 300 to 340 °C, and 20 min at 340 °C). A Mega SE52 (8 m long, 0.32 μm in diameter, 0.10 μm film thickness) column was used. Diglycerides were detected by a FID detector at 350 °C and quantified based on Equation 2:

$$A\% = \frac{Ax \cdot ms}{As \cdot m} \cdot 100 \qquad\qquad \text{Eq. (2)}$$

where *Ax* is the area corresponding to the peak of a single diglyceride, *As* is the area corresponding to the internal standard peak, *ms* is the added amount (mg) of internal standard, and *m* is the amount (mg) of the sample.

### 2.2.3.5.    Hydroxytyrosol and Tyrosol Quantification

Hydroxytyrosol and tyrosol were extracted from 2 g of the sample according to the official COI/T.20/Doc No 29 method. Acid hydrolysis was applied following the procedure suggested by Rovellini (2017). UHPLC analysis was performed using an Agilent Poroshell 120 EC-C18 reversed-phase column (2.7 μm particle size, 4.6 × 150 mm) on a Shimadzu Nexera UHPLC System (Shimadzu Nexera, Kioto, Japan) equipped with dual pump LC-30AD, on-line degasser DGU-20AS, column oven CTO-30A, autosampler SIL-30AC, and diode array detector (SPD-M20A) following the operative conditions described by Lucci et al. (2020). Polyphenol quantification was obtained through calibration curves in the range of 10–600 ng of tyrosol and hydroxytyrosol injected on-column with R$^2$ values higher than 0.999, in all cases. Polyphenol content in oil was calculated as the sum of hydroxytyrosol and tyrosol values.

### 2.2.3.6.    Tocopherol Quantification

Tocopherol was identified and quantified in accordance with the method reported by Lucci et al. (2020). Briefly, UHPLC analysis was realized using a Shimadzu Nexera (Shimadzu, Kyoto, Japan) coupled with the same components used for polyphenols analysis and a fluorescence detector RF-20Axs with double acquisition channels and a 12 μL cell. The detector was set at 296 nm and 325 nm for exciting and emission wavelengths, respectively. Oil samples were diluted in 2-propanol for reaching a 100 mg/mL concentration and 1μL was injected on the column as a compromise between sensibility and column capacity. The chromatographic separation was performed using an Agilent Eclipse PAH column (1.8 μm particle size, 4.6 x 50 mm) used under isocratic conditions with solvent A (methanol) and B (acetonitrile) in the ratio

60/40 (v/v) and a total flow of 600 μL min$^{-1}$. The oven temperature was set to 30 °C. The injected volume for each sample was 1 μL. Tocopherols were quantified using a calibration curve for δ, β+γ, and α respectively in the range 0.05 – 100 ng injected on the column with R$^2$ values higher than 0.999.

### 2.2.3.7. Oil Viscosity

Oil viscosity was measured using a rotational rheometer (Haake Rheostress 6000, Thermo Scientific, Karlsruhe, Germany), controlled through the RheoWin v.4.60.0001 software package (Thermo Scientific, Karlsruhe, Germany). Briefly, 20 mL oil was poured in a concentric cylinder geometry (CC25 DIN Ti) and rested for 5 min before testing. The flow behavior was determined at 20 °C from 0.3 to 100 s$^{-1}$ of shear rate under steady state conditions (Haake UTM temperature controller unit, Thermo Scientific). Since a typical Newtonian behavior was observed, viscosity was a constant value defined as the ratio between shear stress and shear rate (Newton's law).

### 2.2.3.8. Wax Fatty Acids Esters Length

Crude rice wax and sunflower wax fatty acid compositions were obtained following the method of Wijarnprecha et al. (2018) with some modifications. An aliquot of 0.100 g of crude wax was dispersed in 4 mL of hexane, then 0.5 mL of the wax-containing solution was hydrolyzed with 2 N ethanolic KOH (ethanol:water 80:20, v/v) for 8 hours. The fatty acid ethyl esters (FAEE) analysis was performed on a Thermo-Trace 1300 (Thermo Scientific, Waltham, MA, USA) GC system, equipped with a flame ionization detector. Separation was carried out on an SP2330 (Supelco, Bellefonte, PA, USA) fused silica capillary column 30 m long, 0.25 mm ID, and 0.20 μm stationary phase film thickness. Samples of 1 μL were injected with a split ratio of 25:1. Helium was used as carrier gas at a flow rate of 1 mL min$^{-1}$. The injector and detector were stabilized at 250 °C, the column held at 170 °C for 2 min, then increased to 210 °C at a rate of 2 °C min$^{-1}$ and maintained at 210 °C for 20 min.

## 2.2.4. Oleogel Characterization

### 2.2.4.1. Macroscopic Appearance

Gel images were acquired by using an image acquisition cabinet (Immagini and Computer, Bareggio, Italy) equipped with a digital camera (EOS 550D, Canon, Ota City, Tokyo, Japan) and 60 mm lens with 2.8 focal aperture (Canon, Ota City, Tokyo, Japan). The digital camera was placed on an adjustable stand positioned 40 cm in front of a black cardboard base where the sample was placed. The light was provided by four 23 W frosted photographic floodlights, in

a position allowing minimum shadow and glare. Other camera settings were: shutter time 1/250 s, f/2.8, and focal length 60 mm. Images were saved in jpg format.

### 2.2.4.2. Polarized Light Microscopy

Samples were prepared by depositing a drop of a molten gel onto a heated glass microscope slide. The molten gel was pressed with a glass cover slip to ensure a sample thin enough for the measurement. Slides were allowed to cool at room temperature for 48 hours before imaging at 20 °C. Images were taken at 40x and 400x magnification using a Leica EC3 digital camera, elaborated by the Leica Suite Las EZ software (Leica Microsystems, Heerbrugg, Switzerland), and saved in jpg format.

### 2.2.4.3. Oil Binding Capacity

The oil binding capacity (OBC) was determined by weighing about 1 g oleogel and was allowed to be set directly into a microcentrifuge tube. Samples were centrifuged at 10,000 rpm for 15 min at 20 °C (Mikro 120, Hettich Zentrifugen, Andreas Hettich GmbH, and Co, Tuttlingen, Germany) and decanted the excess oil. The samples were weighed and OBC was expressed as the percentage of oil retained by the oleogel.

### 2.2.4.4. Viscoelastic Properties

The rheological properties of oleogels were determined using a controlled stress rheometer (Haake Rheostress 6000, Thermo Scientific, Karlsruhe, Germany). Aliquots of about 4 g of sample were gently transferred on a 35-mm parallel-plate geometry system, and the measuring gap and temperature were set at 2 mm and 20 °C, respectively. Due to the brittle texture of PS oleogel, samples were preliminarily prepared by carefully cutting, with a sharp knife, cylinders of 2-mm height and 35-mm diameter able to fit within the parallel-plate geometry gap to avoid gel breaking during loading. Samples were equilibrated for 5 min before testing to allow stress relaxation. Viscoelastic properties were evaluated using oscillatory stress sweep and frequency sweep tests. The former was performed to determine the upper limit of the linear viscoelastic region (LVR) and was carried out at 1 Hz and a stress amplitude in the range of 0.1–1000 Pa for MG, RW, or SW, and 100-5000 Pa for PS. The frequency sweep test was carried out at a constant stress amplitude selected within LVR, and a frequency range of 0.1–10 Hz. Storage modulus (G'), loss modulus (G"), and loss tangent (tan $\delta$ = G"/G') were measured. The critical stress ($\sigma_c$), where the G' value of the *plateau* reduces by 10% during the stress sweep test, was used as an index of oleogel resistance to shear stress (Doan et al., 2017). Viscoelastic parameters were compared at 1 Hz.

### 2.2.4.5.    Thermal Analysis

A TA4000 differential scanning calorimeter (Mettler-Toledo, Greifensee, Swiss) connected to a GraphWare software TAT72.2/5 (Mettler-Toledo) was used for DSC analysis. Heat flow calibration was achieved using indium (heat of fusion 28.45 J g$^{-1}$). Temperature calibration was carried out using hexane (melting point – 93.5 °C), water (melting point 0.0 °C), and indium (melting point 156.6 °C). Aliquots of 60-80 mg oleogels were weighed in 100 µL aluminum DSC pans and heated from 20 to 100 °C at 5 °C min$^{-1}$ in the DSC cell under nitrogen flow (20 mL min$^{-1}$) while using an empty pan as a reference. The temperature corresponding to the transition peak (T$_{peak}$), and the melting enthalpy (ΔH) were computed (STARe, ver.8.10, Mettler-Toledo).

### 2.2.4.6.    Fourier Transform Infrared (FTIR) Measurement

Oleogels infrared spectra were recorded using an FTIR spectrophotometer, equipped with an ATR accessory and a Zn-Se crystal allowing the direct collection of IR spectra on a sample without any preparation (Alpha-P, Bruker Optics, Milan, Italy). A background scan of the clean crystal was acquired before sample scanning. Spectra were collected at 25 ± 1 °C in the range 4000 – 400 cm$^{-1}$ at a resolution of 4 cm$^{-1}$ and with 32 co-added scans. Data were processed by the OPUS software (version 7.0, Bruker Optics).

### 2.2.4.7.    Synchrotron X-ray Diffraction (XRD) Analysis

X-ray diffraction patterns were recorded at the X-ray diffraction beamline 5.2 at the Synchrotron Radiation Facility Elettra in Trieste (Italy). The X-ray beam emitted by the wiggler source on the Elettra 2 GeV electron storage ring was monochromatized by a Si(111) double crystal monochromator, focused on the sample and collimated by a double set of slits giving a spot size of 0.2 x 0.2 mm. A drop of the sample was lodged into a nylon pre-mounted cryoloop 20 mm for crystallographic experiments (0.7 – 1.0 mm) (Hampton Re- search HR4-965, Aliso Veijo, CA, USA). The sample temperature was controlled by means of a 700 series cryocooler (Oxford Cryosystems, Oxford, UK) with an accuracy of ~1 °C. Analyses were performed at 20 °C. Data were collected at a photon energy of 8.856 keV (l 1⁄4 1.4 Å), using a 2M Pilatus silicon pixel X-ray detector (DECTRIS Ltd., Baden, Switzerland). Bidimensional patterns collected with Pilatus were calibrated by means of a LaB6 standard and integrated using the software FIT2D (Hammersley, 2016). The indexing of the XRD patterns obtained by the crystalline phases was performed using the program WinPLOTR (Roisnel & Rodríguez-Carvajal, 2001) and Checkcell.

### 2.2.5. Statistical Analysis

Results are averages of three measurements carried out on two replicated experiments and are reported as means ± standard deviation. Analysis of variance (ANOVA) was performed using R (version 3.2.3, The R Foundation for Statistical Computing, Vienna, Austria). Bartlett's test was used to check the homogeneity of variance and the Tukey test was used to test for differences between means ($p < 0.05$).

# 2.3.  Results and Discussion

## 2.3.1. Chemical Characterization

Table 6 shows the chemical characteristics of the EVOO samples having different polyphenol content.

Table 6. Polyphenol (PP) content, diglyceride ratio (1,2 DAGs / 1,3 DAGs), tocopherols, absorbance at 232 (K232) and 270 nm (K270), peroxide value (PV), acidity index, and viscosity of the control oil (High-P), the oil-containing intermediate polyphenol content (Medium-P) and the polyphenol removed oil (No-P).

| Oil Sample | PP Content (mg/kg) | 1,2/1,3 DAGs | Tocopherols (mg/kg) | $K_{232}$ | $K_{270}$ | PV (mEq $O_2$/kg) | Acidity | Viscosity (mPa s) |
|---|---|---|---|---|---|---|---|---|
| High-P (control) | 322.9 ± 10.7 [a] | 1.25 ± 0.00 [a] | 354.59 ± 2.13 [a] | 2.24 ± 0.08 [a] | 0.06 ± 0.01 [a] | 7.6 ± 0.1 [b] | 0.41 ± 0.01 [a] | 77 ± 1 [a] |
| Medium-P | 173.0 ± 9.3 [b] | 1.31 ± 0.26 [a] | 340.87 ± 2.31 [b] | 2.13 ± 0.11 [ab] | 0.04 ± 0.01 [a] | 8.9 ± 0.1 [a] | 0.32 ± 0.01 [b] | 78 ± 2 [a] |
| No-P | n.d. | 1.39 ± 0.03 [b] | 340.80 ± 3.26 [b] | 1.84 ± 0.06 [b] | 0.06 ± 0.01 [a] | 9.1 ± 0.2 [a] | 0.24 ± 0.02 [c] | 74 ± 3 [a] |

n.d. not detectable.

[a-c] indicate significant differences among the different oils ($p < 0.05$).

It can be noted that the procedure applied to remove polyphenols from EVOO was effective, as no polyphenols were detected in the No-P sample (Table 6). The other two oils presented 322.9 mg kg$^{-1}$ (High-P) and 173.0 mg kg$^{-1}$ (Medium-P) as polyphenol content. The procedure applied to remove polyphenols allowed to retain all EVOO quality parameters in a range complying with the compulsory limits reported in the REG CEE n.2568/91. In particular, no oxidation phenomena were triggered since neither the peroxide value nor the $K_{232}$ and $K_{270}$, revealed the formation of conjugated dienes and trienes. Moreover, the method applied did not affect the fatty acid profile (Table 7). Lastly, no more than 5% polyphenol depletion was detected for all gelators (data not shown).

Table 7. Fatty acid profile (% w/w) of EVOO before (High-P) and after polyphenol removal (No-P) and of the wax ester fraction of sunflower and rice waxes.

| Fatty Acid | Oil composition (%) | | Wax composition (esters, %) | |
|---|---|---|---|---|
| | No-P | High-P (control) | Rice | Sunflower |
| C16:0 | 7.9 | 7.7 | 24.0 | 14.9 |
| C16:1 w9 | 0.1 | 0.1 | n.d. | n.d. |
| C16:1 w7 | 0.2 | 0.2 | n.d. | n.d. |
| C17:0 | 0.0 | 0.0 | 0.2 | 1.1 |
| C17:1 w8 | 0.0 | 0.0 | n.d. | n.d. |
| C18:0 | 2.3 | 2.0 | 4.7 | 5.0 |
| C18:1 w9 | 80.1 | 80.7 | 64.0 | 23.8 |
| C18:2 w6 | 8.0 | 8.1 | 0.76 | 29.6 |
| C20:0 | 0.4 | 0.3 | 1.3 | 17.9 |
| C18:3 w3 | 0.6 | 0.5 | 0.6 | 1.4 |
| C20:1 w9 | 0.3 | 0.2 | n.d. | n.d. |
| C22:0 | 0.1 | 0.1 | 2.1 | 3.4 |
| C24:0 | 0.0 | 0.0 | 2.3 | 3.0 |
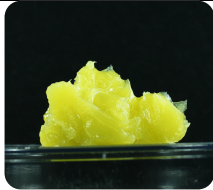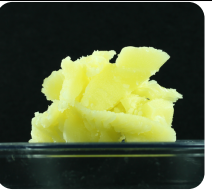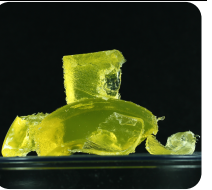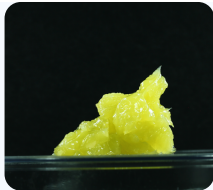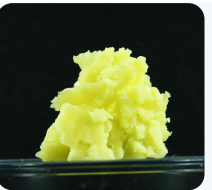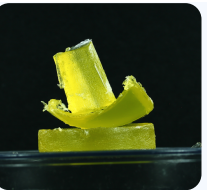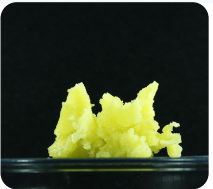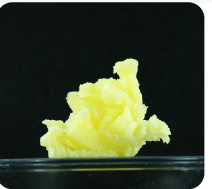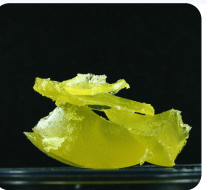
n.d. not detectable.

Additionally, it should be noted that no polarity changes are expected upon polyphenol removal. In fact, the dielectric constant of EVOO reported in the literature is comparable to that of vegetable oils undergoing the refining process (Lizhi et al., 2008).

### 2.3.2. Oleogel Properties

The visual appearance of the EVOO oleogels prepared by using the three different oils and the selected gelators is reported in Table 8.

Table 8. Macroscopic visual appearance of oleogels prepared with 10% (w/w) of monoglycerides, rice bran waxes, sunflower waxes, or the mixture β-sitosterol and γ-oryzanol (2:3 w/w) in EVOO having decreasing polyphenol content.

| Sample | Monoglycerides | Rice Bran Wax | Sunflower Wax | Phytosterols |
|---|---|---|---|---|
| High-P (control) | | | | |
| Medium-P | | | | |
| No-P | | | | |



EVOOs were successfully structured into solid-like materials with self-standing behavior and a visual appearance differing depending on the gelator considered (Table 8). MG and wax-based oleogels were opaque systems, whereas PS showed a translucent appearance, in agreement with the literature (Alongi et al., 2022). No visual differences can be appreciated as a function of oil polyphenol content. All the samples showed an oil binding capacity higher than 99% with no oil release upon centrifugation (data not shown).

To obtain information on oleogel microstructure, viscoelastic properties in both linear (small strain) and non-linear (large strain) regimes were investigated. Figure 12 shows the rheological behavior of the samples; whereas Table 4 the relevant G' and G" at 1 HZ, the tan δ, and the critical stress.
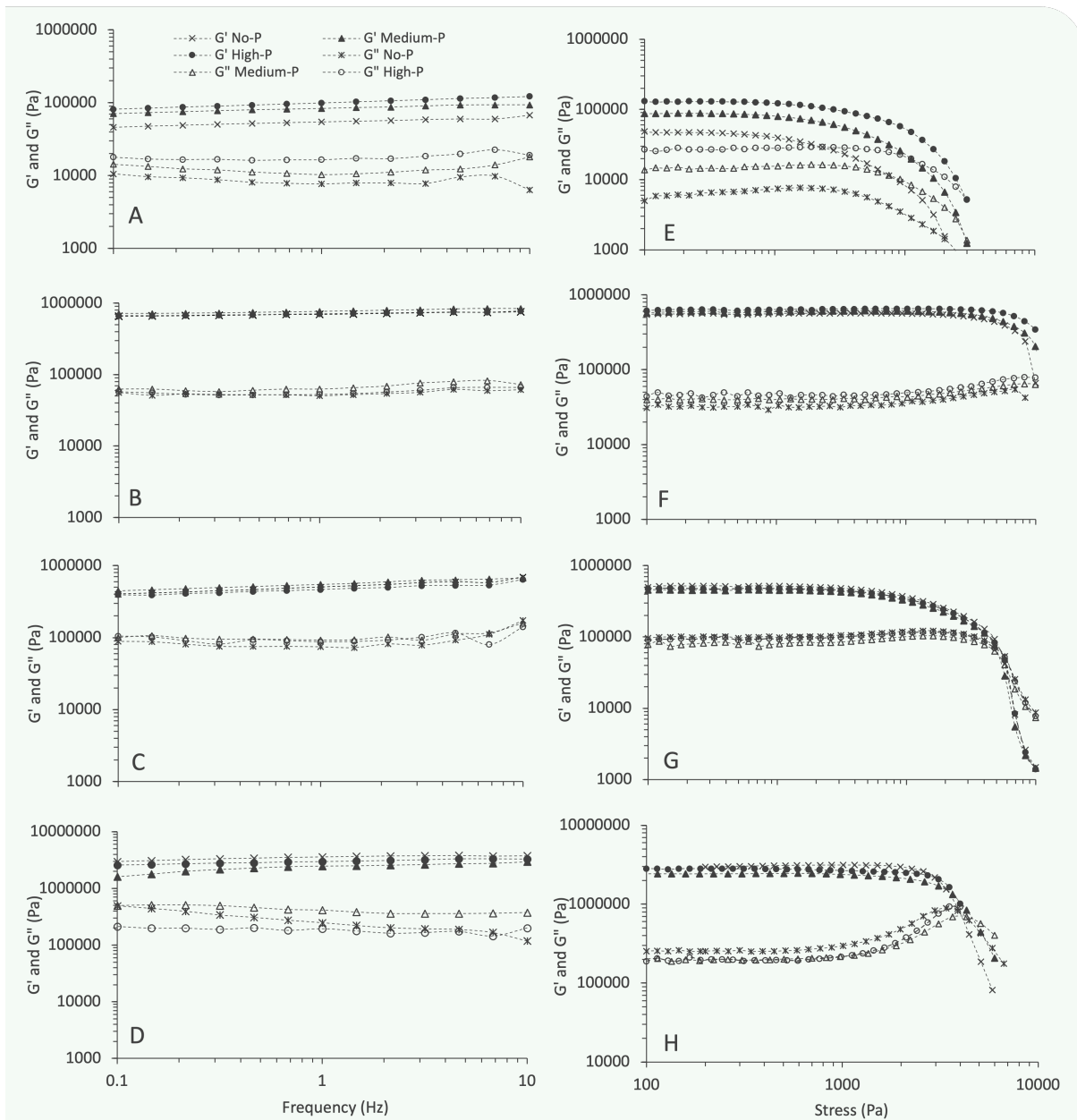
Figure 12. Frequency and oscillatory stress sweep curve of EVOO oleogels containing 10% (w/w) monoglycerides (A, E), rice bran wax (B, F), sunflower wax (C, G), or a mixture of β-sitosterol and γ-oryzanol (D, H) prepared with EVOO having different polyphenol content.

Figure 12 A-D reports the results of the frequency sweep test performed in LVR. As expected for gels, G′ exceeded G″ for all the frequency ranges indicating that the elastic component is dominant. Additionally, a weak dependence of moduli on frequency was observed, which is characteristic of viscoelastic solids. Rheological parameters at a frequency of 1 Hz were used to compare the samples (Table 9).

Table 9. Rheological parameters (G′, G″, Tan δ at 1 Hz, and critical stress) of oleogels containing 10% (w/w) monoglycerides (MG), rice bran wax (RW), sunflower wax (SW), and a mixture of β-sitosterol and γ-oryzanol (PS) prepared with No-P, Medium-P, and High-P

| Oleogelator | Sample | $G′ × 10^4$ (Pa) | $G″ × 10^4$ (Pa) | Tan δ | Critical stress (Pa) |
|---|---|---|---|---|---|
| MG | High-P (control) | 9.3 ± 1.0 [a] | 1.5 ± 0.2 [a] | 0.165 ± 0.012 [a] | 12.32 ± 1.16 [a] |
| | Medium-P | 8.2 ± 1.7 [a] | 1.3 ± 0.4 [ab] | 0.155 ± 0.003 [a] | 12.29 ± 2.95 [a] |
| | No-P | 6.2 ± 0.7 [b] | 0.8 ± 0.1 [b] | 0.130 ± 0.010 [b] | 7.61 ± 1.37 [b] |
| RW | High-P (control) | 68.1 ± 4.3 [a] | 5.0 ± 0.2 [a] | 0.076 ± 0.002 [a] | 464.95 ± 7.06 [a] |
| | Medium-P | 68.1 ± 6.7 [a] | 5.5 ± 0.5 [a] | 0.079 ± 0.002 [a] | 317.56 ± 3.52 [b] |
| | No-P | 68.7 ± 9.9 [a] | 5.4 ± 0.5 [a] | 0.074 ± 0.004 [a] | 287.10 ± 17.60 [c] |
| SW | High-P (control) | 57.1 ± 9.7 [a] | 9.1 ± 1.6 [a] | 0.164 ± 0.002 [a] | 39.18 ± 3.74 [a] |
| | Medium-P | 45.7 ± 8.1 [a] | 7.7 ± 1.7 [a] | 0.169 ± 0.010 [a] | 41.05 ± 4.31 [a] |
| | No-P | 50.5 ± 0.2 [a] | 8.6 ± 0.8 [a] | 0.171 ± 0.018 [a] | 39.87 ± 4.17 [a] |
| PS | High-P (control) | 239.9 ± 2.2 [a] | 20.9 ± 3.6 [a] | 0.084 ± 0.006 [a] | 1966.5 ± 364.8 [a] |
| | Medium-P | 216.0 ± 9.1 [a] | 17.8 ± 2.6 [a] | 0.082 ± 0.008 [a] | 1745.5 ± 202.9 [a] |
| | No-P | 255.0 ± 12.2 [a] | 23.7 ± 1.1 [a] | 0.087 ± 0.009 [a] | 1999.5 ± 388.6 [a] |

[a-c] indicate significant differences among oils with different polyphenol content containing the same gelator ($p < 0.05$).

For RW, SW, and PS oleogels, no significant differences in linear viscoelastic parameters were observed between samples with and without polyphenols ($p > 0.05$). In contrast, MG-containing polyphenols exhibited higher G′ and tan δ at 1 Hz compared to the oleogel obtained from EVOO cleared from polyphenols. These results indicate that the matrix of MG structured with High-P oil has more elastic interactions in the crystalline network. It can be inferred that polyphenols can interact with the crystal network reinforcing it by forming additional junction points. It can be hypothesized that polyphenols could interact with the polar moieties of the oleogel structure through hydrogen bounding, thus contributing to the stability of the gel network. The MG-based oleogel obtained from the High-P also presented a slightly greater degree of viscous behavior compared to the sample with No-P, suggesting that the weak interactions promoted by polyphenols were broken down when shear stress was applied to the material, producing an increase in energy dissipation (viscous character) due to the presence of slippery layers.

Oleogelator type influenced the rheological behavior according to a previous investigation (Fayaz et al., 2020). PS gave the highest and MG the lowest elastic modulus among gelators attributed to differences in oleogel microstructure (Table 9). The former made the strongest gels mainly due to the ability to self-aggregate into PS tubular elements, promoting the formation of a three-dimensional network (Calligaris et al., 2014).

Figure 12 E-H shows the results of the oscillatory stress sweep test at 1 Hz, which are useful to determine the limit of the LVR. In the linear region, both viscoelastic moduli are not stress-

dependent (*plateau*) because the applied stresses produce a proportional strain response (reversible deformation). The upper limit of LVR was 7.6-12 Pa for MG, 93-124 Pa for RW, 39-41 Pa for SW, and 880-990 Pa for PS oleogels. The critical stress ($\sigma_c$) corresponding to the shear stress above which structure breaking occurs, was obtained from G' profile (Figure 12 E-H). The upper limit of LVR and $\sigma_c$ was identical for MG and SW oleogels because they both resulted from the G' curve. In contrast, the limit of LVR was lower than $\sigma_c$ for RW and PS samples since the former was evaluated using the G" profile (narrower *plateau* than G'). Above the $\sigma_c$ value, the matrix is subjected to permanent deformation due to the breaking up of the inner structure (Patel, Babaahmadi, et al., 2015). The $\sigma_c$ parameter, which reflects the resistance of the gel network to shear stresses, decreased in the following order: PS > RW > SW > MG (Table 9).

Comparing samples with crystalline network, SW gave $\sigma_c$ values much lower than RW revealing differences in the intensity of interactions in their networks. Similar evidence was previously reported for these waxes added to medium-chain triacylglycerols (Fayaz et al., 2021). Based on these results, SW samples were weaker than RW. Generally, the number and intensity of interactions influence network strength. Probably, differences in $\sigma_c$ values between waxes are mainly due to the intensity of interactions since the samples differed slightly in the number of elastic interactions (frequency sweep results, Table 9). These differences were attributed to the chemical compositions of waxes. As reported by Doan et al. (2017), the ester fraction in the waxes represents about 93-96% of the total components. However, this fraction is characterized by a different composition of fatty acids. As can be noted in Table 7, RW was characterized by a prevalence of esters containing oleic acid C18:1, whereas SW showed a higher variability of fatty acids in the ester fraction with C18:1, C18:2, and C20:0 fatty acids as main components. The different wax composition is expected to produce a different ester arrangement, with crystals characterized by a less ordered structure with a lower number of elastic interactions in the case of SW. These crystals are expected to be more susceptible to mechanical stresses compared to those obtained from the tighter and more ordered packing of RW esters (Doan et al., 2017). Similar findings were actually reported in the literature showing that the crystalline network of SW breaks down more easily at the same applied force in comparison with RW (Fayaz et al., 2020; Patel, Babaahmadi, et al., 2015).

The concentration of polyphenols affected the features of oleogels to different extents depending on the network. PS- and SW-based oleogels did not show significant changes in the critical stress between samples with and without polyphenols (Table 9). On the contrary, the magnitude of $\sigma_c$ was significantly higher for MG and RW samples containing polyphenols, indicating a structuring effect ($p < 0.05$), that can be attributed once again to the formation of junction points in the crystalline network through polyphenols. For RW, $\sigma_c$ increased also with polyphenol content, resulting in 11-62% higher compared to No-P.

Looking at the non-linear regime (Figure 12 E-H), both G' and G" decreased as stress amplitude increased for MG-based oleogels due to network breakage. For PS samples, G" showed an increase followed by a decrease as stress (or strain) rose revealing a weak strain overshoot behavior (Hyun et al., 2002). Therefore, a characteristic of the PS network is to resist deformation (increase in G") before breaking.

Based on G' and tan δ at 1 Hz from frequency sweep (LVR) and $\sigma_c$ values (Tavernier, Doan, et al., 2017), MG and SW gave the weakest and PS the strongest oleogels (Table 9).

The impact of polyphenols was then studied with calorimetric analysis. Figure 13 shows the melting curve of the samples.



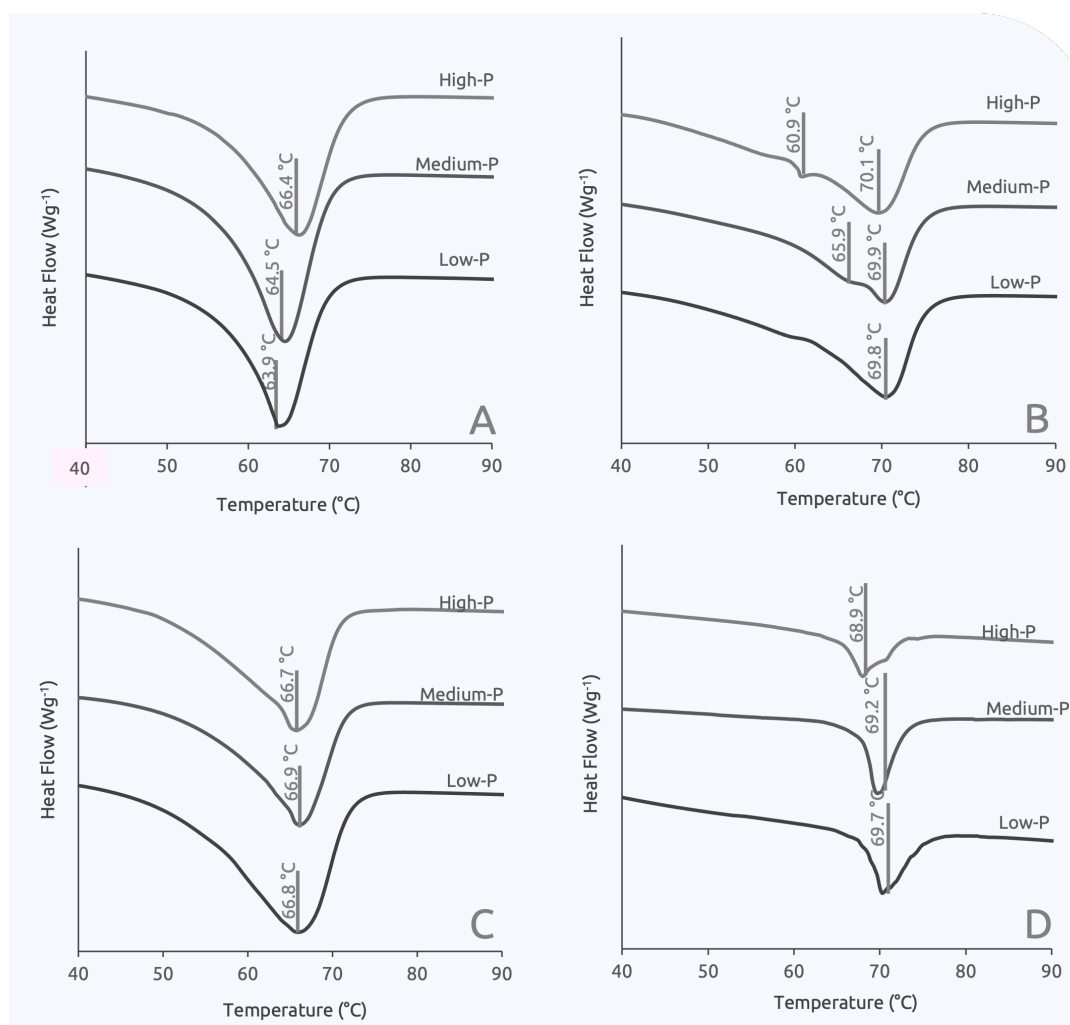Figure 13. Melting calorimetric curves of oleogels containing 10% (w/w) monoglycerides (A), rice bran wax (B), sunflower wax (C), and a mixture of β-sitosterol and γ-oryzanol (D) prepared with No-P, Medium-P and High-P oils.

All oleogels revealed broader endothermic peaks with lower $T_{peak}$ in comparison to the neat gelators (Figure 14). This result is expected and in agreement with the literature and is

associated with the initial disintegration of the network in oil followed by the melting of crystals in MG, SW, and RW-based oleogels or the de-structuring of the tubules in the PS-containing sample (Alongi et al., 2022).
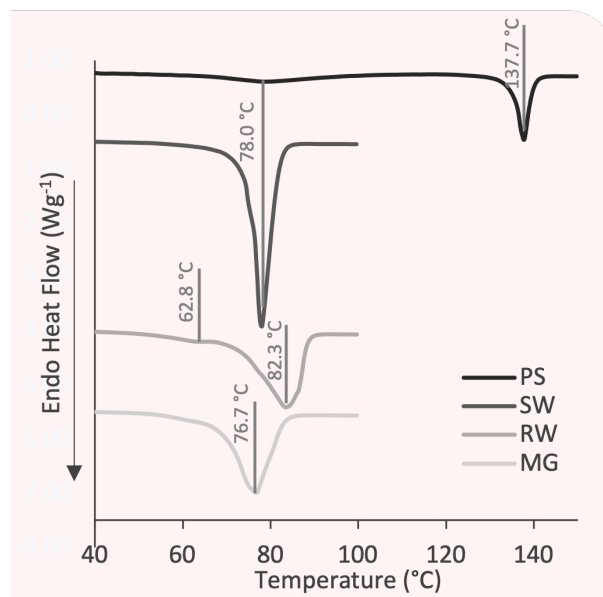


Figure 14. Melting calorimetric curves of oleogelators monoglycerides (MG), rice bran waxes (RW), sunflower waxes (SW), and a mixture of β-sitosterol and γ-oryzanol (PS).

Considering the effect of polyphenol content (Figure 13), MG-oleogels presented a progressive decrease of the $T_{peak}$ as the polyphenol content also decreased, indicating a reduction in the network's strength as polyphenols in the matrix decreased. It can be hypothesized that the absence of polyphenols reduced the number of junction points able to stabilize the network, making the latter more susceptible to melting at lower temperatures. Moving to RW-containing samples, two melting events can be noted in the High-P sample ($T_{peak}$' at 60 °C e $T_{peak}$'' at 70 °C). These can be associated with the crystallization of two fractions, as also noted in the neat gelator (Figure 14). Interestingly, the peak at the lowest temperature disappeared as the polyphenol in the matrix decreased, confirming that polyphenols may play a critical role in stabilizing the crystalline RW network, ultimately affecting oleogel behavior.

The differences in the oleogel properties previously described can be associated with the microscopic features of the network. Thus, polarized light microscopy was performed on samples containing crystals (MG, RW, and SW, Table 10). It should be remembered that as well known in the literature, it is not possible to image the network formed by the mixture of phytosterol with sterol-esters because they form tubules with dimensions that are considerably smaller than the wavelength of visible light (Bot et al., 2008; Calligaris et al., 2014).

Table 10. Microscopic appearance of oleogels containing 10% (w/w) monoglycerides (MG), rice bran waxes (RW), sunflower waxes (SW), and a mixture of β-oryzanol and δ-sitosterol (PS) prepared with No-P, Medium-P and High-P oils. Magnification: 40x and 400x.
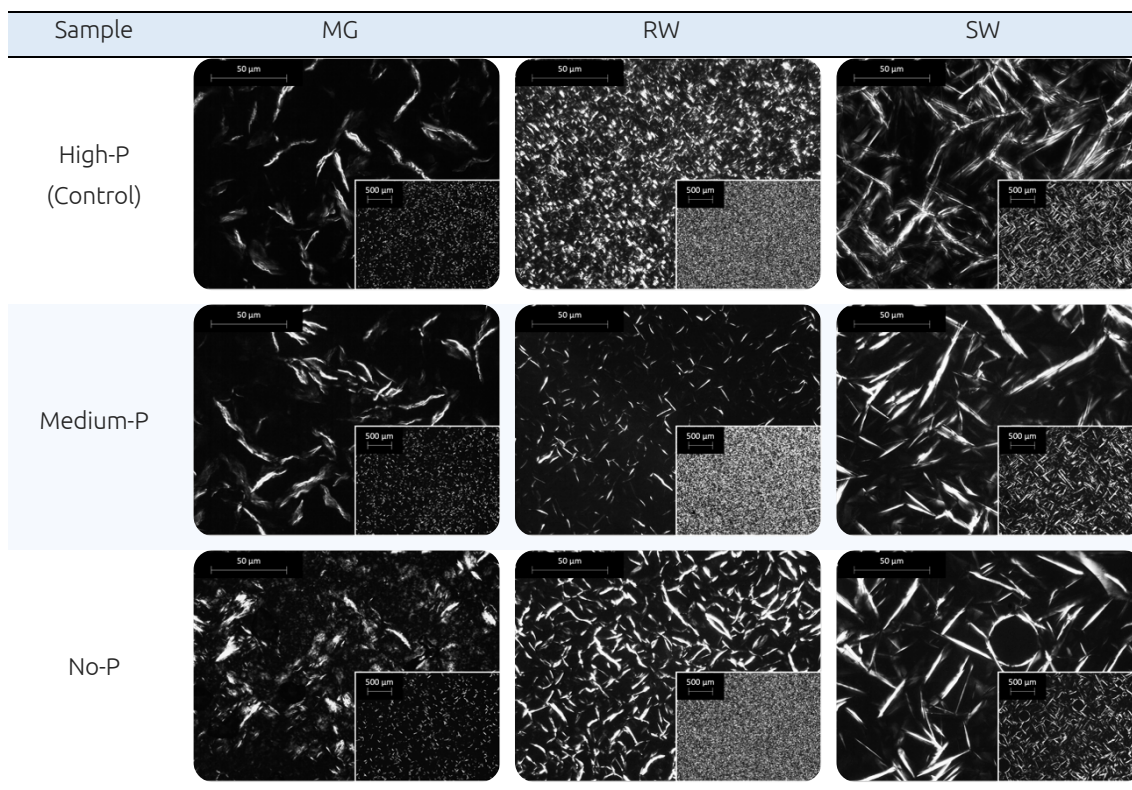


The crystalline networks formed by MG, RW, and SW are well appreciable in the microscopy images reported in Table 10 in which bright areas are the crystals and the dark zones that fill the space correspond to the liquid oil.

The MG in the control EVOO formed a network made of randomly dispersed needle-like crystals. As reported in the literature, MG organized itself into an inverse lamellar phase with a *β*-subcell packing in oil (da Pieve et al., 2010). Considering waxes, SW showed needle-like crystals, whereas RW formed spherulites well dispersed in the matrix. Respectively, these results agree with Doan et al. (2015) and Fayaz et al. (2020) and can be associated with the different chemical compositions of waxes (Table 7) leading to a different crystal morphology.

The progressive lower content of polyphenols in the samples determined differences in the oleogel network structure, especially in MG- and RW-containing samples, whereas the SW oleogel network seems to be comparable among No-P, Medium-P, and High-P oils. In MG and RW samples, different crystal morphology and density were recorded from the control samples. In the case of RW, the morphology of the crystals appeared to change from spherules to needle-like crystals with a higher dimension. In the MG-based oleogel, crystals were more randomly dispersed with fewer connections.

The network structure changes associated with the polyphenol content confirmed the importance of these components in the network formation in MG and RW. It can be inferred that in both cases polyphenols participate in the network strengthening and reinforcing the connections among crystals, possibly creating new junction points. As described by other authors, olive polyphenols display surface activity (Di Mattia et al., 2014; Giacintucci et al., 2018). Hence, it can be hypothesized that they are located near polar moieties in MG and RW favoring and increasing the degree of interactions among crystals (Shang et al., 2021).

The ineffectiveness of polyphenols in reinforcing SW oleogel compared to RW could be attributed to the lower gel strength (Table 9) associated with a different wax composition (Table 2). As previously reported Fayaz et al. (2020) SW produces dendritic crystals larger than the spherulitic ones obtained from RW, in which the potential contribution of polyphenols to the gel network was probably masked. Finally, the results on PS-based oleogels indicated that polyphenols did not interact with the tubule formation between $\beta$-sitosterol and $\gamma$-oryzanol, even though other authors evidenced that the micro- and nano-structural properties of the tubular self-assembled system were affected by the presence of phenolic moieties under different gelling conditions, such as gelator concentration and ratios, and cooling rate (Martins et al., 2022).

To evaluate the molecular interactions in the samples, FT-IR spectroscopy was performed (Figure 15).
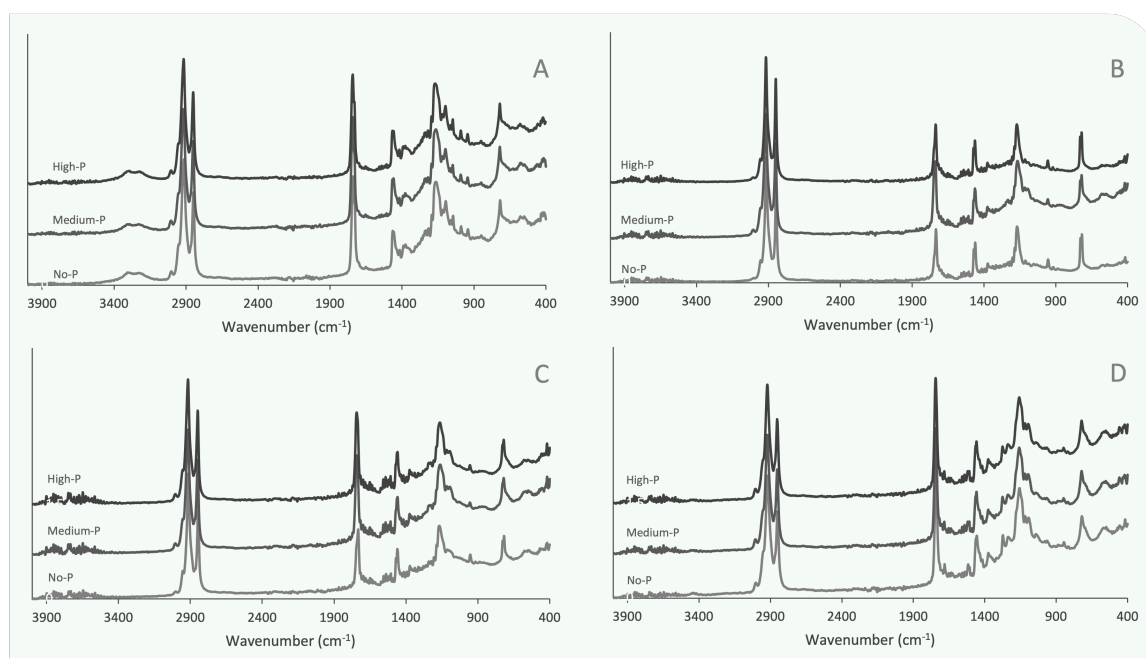


Figure 15. FT-IR signals of oleogels containing 10% (w/w) monoglyceride (A), rice bran wax (B), sunflower wax (C), and a mixture of β-sitosterol and γ-oryzanol (D) prepared with No-P, Medium-P, and High-P oils.

All oleogel spectra presented the typical bands associated with triglycerides, being the major components of EVOO, such as the double peak in 3000-2800 cm$^{-1}$ region (alkane sp$^3$ C-H stretching vibration of ethyl and methyl groups) and a smaller one at 1700 cm$^{-1}$ (stretching vibration of carbonyl group C=O) (Singh et al., 2013). The region below 1500 cm$^{-1}$ is commonly called the "fingerprint region" and here most of the differences are due to the intermolecular feature of each compound which is expressed by a complex set of bands.

The FT-IR spectra of samples were different depending on the gelator, however, no differences were detected among samples with different polyphenol content. As reported by Öğütcü & Yilmaz (2014), intermolecular hydrogen bonds should appear as medium-intensity bands in the bands at 3450–3550 cm$^{-1}$ wavenumber range, and intramolecular hydrogen bonds as medium-intensity bands in the 3540–3570 cm$^{-1}$ wavenumber range. Since no signals relevant to hydrogen bonds in the FT-IR spectra were recorded, this means probably that polyphenols did not chemically interact with the gelators, but only Van der Waals interactions occurred.

Finally, to understand the crystal polymorphs formed in the samples, synchrotron XRD analyses were performed (Figure 16).
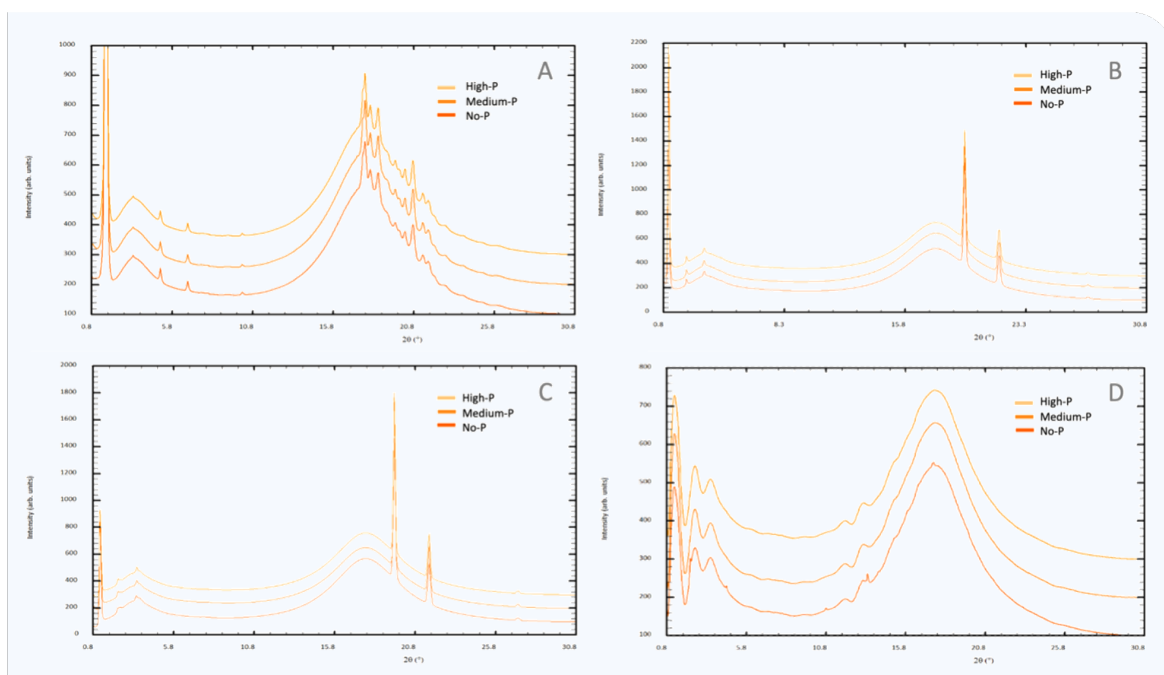


Figure 16. X-ray diffraction patterns of EVOO oleogels containing 10% (w/w) monoglycerides (A), rice bran wax (B), sunflower wax (C), and a mixture of β-sitosterol and γ-oryzanol (D) at increasing concentrations of polyphenols.

These patterns are in agreement with data reported in the literature (Fayaz et al., 2017; Valoppi et al., 2017). MG showed a multitude of peaks in the WAXD region, attributable to $\beta'$

polymorphic form crystals typical of the 2D planar hexagonal packing of glycerol head groups (C. H. Chen & Terentjev, 2009). The two waxes-based samples presented two peaks in the WAXD region along with the previously observed and oil-related SAXD peaks. WAXD peaks appeared to be very similar not only inside the same gelator group but also between the two different waxes and this can be explained by the same form $\beta'$ polymorphic form (Valoppi et al., 2017). Different levels of polyphenols do not contribute to crystal conformation in all samples, which is highlighted by the absence of peak deviations detected between the three different oils used in oleogel preparation.

Based on these results, it can be inferred that polyphenols were able to generate additional interactions among crystals in MG and RW modifying the microstructural organization of the networks and thus the macrostructure. On the contrary, nano-level crystals maintained their original morphology.

# 2.4. Conclusions

Results acquired in this Chapter evidenced that polyphenols could differently impact the structure of oleogels. While no networking capacity was noted in phytosterol- and WS-based oleogels, the role of EVOO polyphenols was noted in MG- and RW-containing samples. in these samples, it was hypothesized that polyphenols participated in the network strengthening and reinforcing the connections among crystals, creating new junction points thanks to their surface activity near polar moieties. The different behaviors observed can be associated with the compositional differences among the oleogelators considered. Overall, this study confirmed the strong importance of minor components of vegetable oils in affecting the micro- and macro-structure of oleogels.

# 3. EFFECT OF HYDROSTATIC PRESSURE TREATMENTS ON THE CRYSTALLIZATION BEHAVIOR OF PALM STEARIN-SUNFLOWER OIL BINARY SYSTEMS

## 3.1. Introduction and Aim of the Study

The capability of hydrostatic pressure to steer fat crystallization is presented in this Chapter. Previous studies have examined the influence of pressurization on lipid crystallization, revealing its potential not only in boosting the phenomenon but also in promoting the formation of smaller crystals. For these reasons, this Chapter aimed to study the crystallization behavior of binary blends containing sunflower oil and increasing concentrations (80, 90, and 100%, w/w) of palm kernel stearin under moderate pressure treatments (200 MPa). After the treatments, samples were removed from the vessel and analyzed for mechanical (compressive dynamometry), rheological (oscillatory rheology), thermal (differential scanning calorimetry, nuclear magnetic resonance), microstructural (optical microscopy), and nano-structural (synchrotron X-ray diffractometry) properties. Samples crystallized at atmospheric pressure (0.1 MPa) were used as references. Results could enlarge the potentialities of the HPP process in the food lipid sector.

# 3.2. Materials and Methods

### 3.2.1. Sample Preparation

Samples were prepared by mixing palm kernel stearin (kindly donated by a local company specialized in shortenings for bakery purposes) and sunflower oil (Giglio Oro), obtaining blends with 80, 90, and 100% (w/w) palm stearin content. These blends were chosen as hypothetical shortening to be used in lipid-containing foods. Samples were initially set at 70 °C for 25 min in a thermostatic bath. Aliquots of twenty-gram of each sample were heat-sealed into polyethylene/ethylene vinyl alcohol/polypropylene pouches (5 × 15 cm; 80 µm thickness, water vapor permeability < 1 g m$^{-2}$ 24 h$^{-1}$; Niederwieser Group S.p.A., Campogalliano, Italy) with minimal headspace (Orved, VM-16, Musile di Piave, Italy). Before pressurization, packaged samples (5 × 15 × 1 cm) were heated again at 70 °C for 25 min to ensure complete melting and delete the memory of crystallization.

### 3.2.2. Hyperbaric Crystallization

A hydrostatic pressure unit assembled by Comer Srl (Bologna, Italy) was used. It consisted of a screw-capped water-tight steel vessel (maximum pressure: 200 MPa; capacity: 2 L, Hystat, Slaithwaite, Huddersfield, UK) pressurized by a Haskel International high-pressure pump (Burbank, CA, USA). The pressure-mediating fluid was an aqueous solution containing 0.2% (w/w) potassium sorbate and 0.2% (w/w) sodium benzoate (Carlo Erba Reagents Srl, Milan, Italy) to prevent mold proliferation in the fluid reservoir tank. The pressurizing fluid temperature was maintained at 20 ± 1 °C by placing the working unit in a temperature-controlled room. The plastic pouches containing the melted samples (70 °C) were anchored to 10 g-weights and positioned inside the steel vessel. Samples were immediately pressurized (50 MPa min$^{-1}$) at 200 MPa. This pressure was thus reached within 4 min, and maintained for increasing time from 1 to 24 h. After pressurization, all samples were further kept in the vessel for 24 h at 0.1 MPa before analysis to allow samples to complete setting pressure (0.1 MPa) in the vessel for the same storage time. Control samples were treated as above described by placing them in the hyperbaric vessel for 48 h at ambient pressure (0.1 MPa) conditions.

### 3.2.3. Analytical Determinations

#### 3.2.3.1. Cooling Rate

Control samples crystallized at 0.1 MPa were equipped with a thermocouple data logger (Digital 2 Channel K-Type Thermometer Thermocouples, Gain Express Holdings Ltd., Hong

Kong) to monitor samples temperature. For technical reasons it was not possible to measure temperature during pressurization.

### 3.2.3.2. Firmness

Firmness was measured by a uniaxial compression test using an Instron 4301 (Instron LTD., High Wycombe, UK). Samples were removed from pouches without further modification and tested at 20 °C using a 6.2 mm diameter cylindrical probe mounted on a 1000 N compression head at a 25 mm/min crosshead speed. Force-distance curves were obtained from the compression tests and firmness was taken as the maximum force (N) required to penetrate the sample for 2 mm.

### 3.2.3.3. Rheological Analysis

The rheological properties of samples were determined using a controlled stress rheometer (Haake Rheostress 6000, Thermo Scientific, Karlsruhe, Germany). Aliquots of about 4 g of sample were gently transferred on a 35-mm parallel-plate geometry system, and the measuring gap and temperature were set at 2 mm and 20 °C, respectively. Samples were equilibrated for 5 min before testing to allow internal stress relaxation. Viscoelastic properties were evaluated using oscillatory stress sweep and frequency sweep tests. The former was carried out to determine samples linear viscoelastic region (LVR), that was defined as the stress domain in which samples storage modulus (G') did not decrease more than 10%. The stress sweep was performed by applying a stress ramp from 1 to 10000 Pa at a frequency of 1 Hz. Samples critical stress ($\sigma^*$) was identified as the shear stress required to induce a 10% reduction in G'. The frequency sweep test was carried out at a constant stress belonging to the LVR, by decreasing the oscillatory frequency from 10 to 0.1 Hz. Storage modulus (G'), loss modulus (G''), and loss tangent ($\tan \delta = G''/G'$) were measured, and their values at 1 Hz were considered for sample comparison.

### 3.2.3.4. Differential Scanning Calorimetry (DSC)

A DSC-3 Star$^e$ system (Mettler-Toledo, Greifensee, Swiss) equipped with Star$^e$ software (v.8.10) was used for DSC analysis. Heat flow calibration was achieved using indium (heat of fusion 28.45 J/g). Temperature calibration was carried out using hexane (m.p. -93.5 °C), water (m.p. 0.0 °C), and indium (m.p. 156.6 °C). Approximately 20 mg-aliquots of each sample were weighed in 100 µL aluminum DSC pans and analyzed. An empty pan was used as a reference for all the analyses. The thermal properties of samples crystallized at 0.1 and 200 MPa were determined by heating from 20 to 100 °C at 5 °C/min under nitrogen flow (20 mL/min). Transition peak temperature ($T_{peak}$), onset temperature ($T_{on}$), and melting enthalpy ($\Delta H$) were computed using the STARe software (v. 8.10, Mettler-Toledo).

Additional trials were performed to simulate the cooling profile during the pressurization process. To this aim, the following temperature profile (*e.g.*, cooling rate) was applied: 70 °C for 25 min, 70 – 43 °C at -40.0 K min$^{-1}$, 43 – 32 °C at -6.6 K min$^{-1}$, 32 – 25 °C at -3.2 K min$^{-1}$, 25 – 20 °C at -3.0 K min$^{-1}$, 20 °C for 30 min).

### 3.2.3.5. Solid Fat Content (SFC)

$^{1}$H relaxometry was performed at 20.0 ± 0.1 °C using a low resolution $^{1}$H nuclear magnetic resonance (LR-NMR) spectrometer (20 MHz, the MiniSpec, Bruker Biospin, Milan, Italy). Approximately 4 g of the sample was placed into an NMR tube (10 mm in diameter) and sealed with Parafilm®. $^{1}$H Free Induction Decay ($^{1}$H FID) experiments were performed to investigate the protons relaxing signals. $^{1}$H FIDs were acquired using a single 90° pulse, followed by a dwell time of 7 µs, a recycle delay of 3 s, and an acquisition window of 0.1 ms, with 4 scans and 150 data points. The curves were fitted with the bi-Gaussian method (Eq. 1) proposed by Declerck et al. (2018):

$$FID_{fit} = FID_{Solid} \cdot e^{-0.5\left(\frac{t}{T^*_{2,Solid}}\right)^2} + FID_{Liquid} \cdot e^{-0.5\left(\frac{t}{T^*_{2,Liquid}}\right)^2} \qquad \text{Eq. 1}$$

The model fit was done with the *fitting* function, available in Matlab R2022 (Matlab, Mathworks, Natick, USA). For the fit, different parameters were used. For $FID_{Solid}$ and $FID_{Liquid}$, the maximum and minimum value of the FID signal was used, respectively, restricted to positive values. A value of 13 µs was selected as starting value for T*$_{2;Solid}$. Moreover, a minimum and a maximum value of 5 µs and 22 µs for T*$_{2;Solid}$, respectively, were specified to obtain physically realistic values for the T$_2$ value of solids. Finally, a starting value of 2 ms was selected for T*$_{2;Liquid}$.

For the solid fat content (SFC) estimation, Eq. 2 was used:

$$SFC = \frac{FID_{Solid}}{FID_{Solid} + FID_{Liquid}} \cdot 100 \qquad \text{Eq. 2}$$

### 3.2.3.6. Polarized Light Microscopy (PLM)

Samples were prepared by depositing a small amount of sample onto a glass microscope slide covered with a glass coverslip and applying a small pressure to ensure the sample was thin enough for the measurement. Images were taken at 20 °C at 40× magnification using a Leica EC3 digital camera, elaborated by the Leica Suite Las EZ software (Leica Microsystems, Heerbrugg, Switzerland), and saved in jpeg format.

### 3.2.3.7. Synchrotron X-ray Diffraction (XRD)

X-ray diffraction patterns were recorded at the X-ray diffraction beamline 5.2 at the Synchrotron Radiation Facility Elettra in Trieste (Italy). The X-ray beam emitted by the wiggler

source on the Elettra 2 GeV electron storage ring was monochromatized by a Si(111) double crystal monochromator, focused on the sample, and collimated by a pinhole of the radius of 0.2 mm. Analyses were performed at room temperature. Data were collected at a photon energy of 8.856 keV (1.4 Å), by means of a 2M Pilatus silicon pixel X-ray detector (DECTRIS Ltd., Baden, Switzerland). Bidimensional patterns collected with Pilatus were calibrated by means of a LaB6 standard and integrated using the software FIT2D (Hammersley et al., 1996). The indexing and the peak profile parameters refinement of the XRD patterns obtained by the crystalline phases were performed using the programs WinPlotr and Checkcell (Laugier and Bochu, 2000; Roisnel and Rodríguez-Carvajal, 2001). The cell was orthorhombic, a=5.08(1), b=68.59(1), c=7.93(1). Two peaks belonging to the same crystallographic direction, identified as 0 2 0 and 0 4 0, were chosen for every one of the three samples crystallized at ambient pressure and of the three samples crystallized at 200mPA. Their Pseudo-Voigt parameter has been optimized at values ranging from 13 to 58%, along with full width at half maximum of intensity (FWHM) and position, and this data allowed to estimate crystallite volumes and non-uniform strain along the chosen direction, according to Hosemann ideal-paracrystal theory (Enzo et al., 1988; Hindeleh & Hosemann, 1991).

### 3.2.4. Data Analysis

Data were expressed as the mean ± standard error of different experimental replicates based on the analysis (sample cooling profile was obtained by 2 repetition, mechanical and thermal properties as at least 2 replicates of two repetitions, SFC as 4 replicates on a single repetition, microscopy appearance as single experiments, and XRD by a single repetition). Statistical analysis was performed by using R v. 4.2.3 (The R Foundation for Statistical Computing). ANOVA test was used to determine statistically significant differences among means ($p < 0.05$). Bartlett's test was used to check the homogeneity of variance ($p \geq 0.05$) and the Tukey test was used as a post hoc test ($p < 0.05$). Non-linear regression analysis was performed by using Excel (Microsoft, Redmond, Washington, USA). The goodness of fit was evaluated based on the determination coefficient ($R^2$).

# 3.3. Results and Discussion

### 3.3.1. Samples Cooling

Preliminary trials were initially conducted to gain insight into the thermal behavior of samples during the cooling phase inside the hyperbaric vessel. Since the measurement of temperature during pressurization was not technically possible, the cooling curves of samples containing 80, 90, and 100% (w/w) palm stearin in sunflower oil heated at 70 °C were recorded at ambient pressure (Figure 17 – red dotted line).
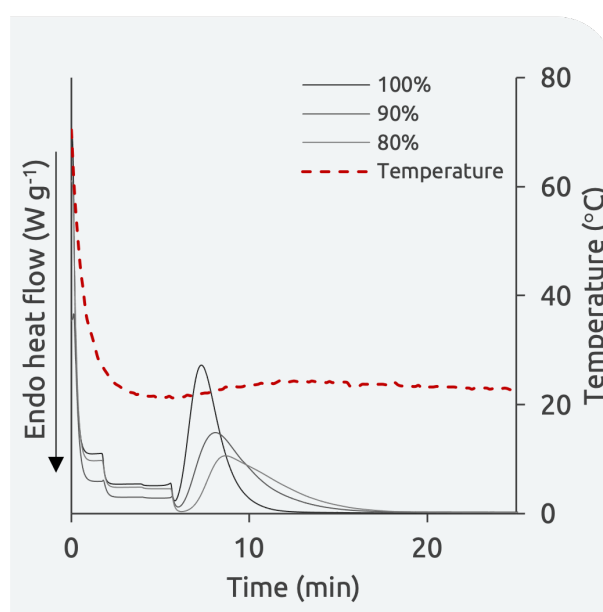


Figure 17. DSC thermograms of samples containing increasing concentrations of palm stearin (80, 90, 100%, w/w) in sunflower oil cooled from 70 to 20 °C and further maintained at 20 °C for 25 min. The red dotted line shows the recorded temperature of the samples in the hyperbaric vessel.

As expected, the sample temperature rapidly decreased to 20 °C in approximately 4 min (Figure 17 – red dotted line). Then, a very broad temperature peak extending up to 30 min was observed, which was likely caused by the heat released by sample exothermic crystallization. It should be noted that, based on the very low adiabatic heating of the pressure-mediating fluid (*i.e.*, water) and short pressurization time (*i.e.*, < 4 min), the same thermal profile could be expected for samples under pressure (Ardia et al., 2004). To identify the occurrence of crystallization during sample cooling, the cooling profile reported in Figure 17 was simulated in DSC equipment (Figure 17 – grey continuous lines), with the cooling rate profile reported in paragraph 3.2.3.4. Exothermic crystallization peaks were detected in all samples after 6 to 8 min at 20 °C and persisted for up to 20 min. Based on these results and

assuming that samples were likely to show a similar thermal behavior under pressure, palm stearin-sunflower oil systems were maintained in the hyperbaric vessel for at least 1 h after insertion to ensure they reached thermal equilibrium.

### 3.3.2. Structural Properties

The effect of the application of hyperbaric conditions during fat crystallization was firstly evaluated considering samples structural properties, with particular reference to firmness and rheological parameters (Table 11 and Figure 18).

Table 11. Firmness and rheological parameters (storage modulus, G' at 1 Hz; critical stress, σ*; loss tangent, tan δ) of samples containing increasing concentrations of palm stearin (80, 90, and 100%, w/w) in sunflower oil and crystallized at 0.1 or 200 MPa.

| Palm stearin (%, w/w) | Pressure (MPa) | Firmness (N) | Critical stress $\sigma^*$ (Pa) | $G' \times 10^4$ (Pa) | tan δ |
|---|---|---|---|---|---|
| 80 | 0.1 | 8.62 ± 1.19[e] | 587.8 ± 21.0[cd] | 240.4 ± 31.3[bc] | 0.124 ± 0.014[b] |
| | 200 | 18.44 ± 1.06[c] | 1974.5 ± 35.6[bc] | 303.3 ± 29.2[bc] | 0.079 ± 0.014[de] |
| 90 | 0.1 | 13.93 ± 1.67[d] | 2169.0 ± 64.9[bc] | 491.9 ± 36.5[bc] | 0.104 ± 0.006[cd] |
| | 200 | 34.07 ± 3.72[b] | 4344.0 ± 48.7[a] | 681.3 ± 27.1[ab] | 0.051 ± 0.001[e] |
| 100 | 0.1 | 30.67 ± 3.37[b] | n.d. | n.d. | n.d. |
| | 200 | 59.29 ± 2.19[a] | n.d. | n.d. | n.d. |

[a-e] different letters in each column indicate statistically different means ($p < 0.05$).

[n.d.] Not determinable

As expected, the firmness of the samples increased with increasing palm stearin concentration (Saghafi et al., 2019). However, samples crystallized under pressure showed significantly higher firmness values as compared to samples crystallized at ambient pressure (Table 11). In this instance, further trials were conducted to establish if maintaining samples under pressure for times longer than 1 h could provide additional improvement to their firmness. However, as reported in Table 12, only negligible changes in sample firmness were obtained by maintaining pressurization at 200 MPa even up to 24 h. In agreement with the literature, this indicates the incapability of hydrostatic pressure to further affect solid crystalline structures after their formation (Zulkurnain et al., 2016b). Based on these results, the attention was thus focused on samples maintained in the hyperbaric vessel for 1 h.

Table 12. Firmness of samples containing increasing concentrations of palm stearin (80, 90, 100%, w/w) in sunflower oil after

| | Palm stearin concentration (%, w/w) and pressure treatment | | | | | |
| | 80 | | 90 | | 100 | |
| Time (h) | 0.1 MPa | 200 MPa | 0.1 MPa | 200 MPa | 0.1 MPa | 200 MPa |
|---|---|---|---|---|---|---|
| 1 | $8.6 \pm 1.2^{cd}$ | $18.4 \pm 1.1^{b}$ | $13.9 \pm 1.5^{c}$ | $33.9 \pm 1.7^{a}$ | $30.7 \pm 3.4^{c}$ | $59.3 \pm 2.19^{b}$ |
| 2 | $7.4 \pm 1.3^{d}$ | $22.2 \pm 0.92^{a}$ | $18.6 \pm 2.2^{b}$ | $34.1 \pm 3.72^{a}$ | $29.9 \pm 2.9^{c}$ | $75.9 \pm 6.3^{a}$ |
| 4 | $7.2 \pm 0.6^{cd}$ | $19.9 \pm 1.5^{ab}$ | $14.4 \pm 1.5^{c}$ | $33.1 \pm 0.6^{a}$ | $30.8 \pm 8.4^{c}$ | $69.0 \pm 8.9^{ab}$ |
| 16 | $8.3 \pm 1.2^{cd}$ | $18.8 \pm 3.0^{b}$ | $13.7 \pm 0.5^{c}$ | $34.9 \pm 1.1^{a}$ | $36.9 \pm 2.7^{c}$ | $67.3 \pm 2.4^{ab}$ |
| 24 | $10.0 \pm 0.7^{c}$ | $18.2 \pm 1.7^{b}$ | $14.4 \pm 1.3^{c}$ | $36.0 \pm 2.0^{a}$ | $32.6 \pm 5.7^{c}$ | $65.6 \pm 8.0^{ab}$ |

[a,f]: different letters for the samples with equal palm stearin concentration indicate statistically different means ($p < 0.05$).

To better understand the effect of hydrostatic pressure on sample crystallization, rheological analyses were carried out under both non-linear (large strain) and linear (small strain) regimes (Figure 18). It must be highlighted that rheological analyses were not performed on the 100% (w/w) palm stearin samples since they presented the physical properties of a brittle solid.
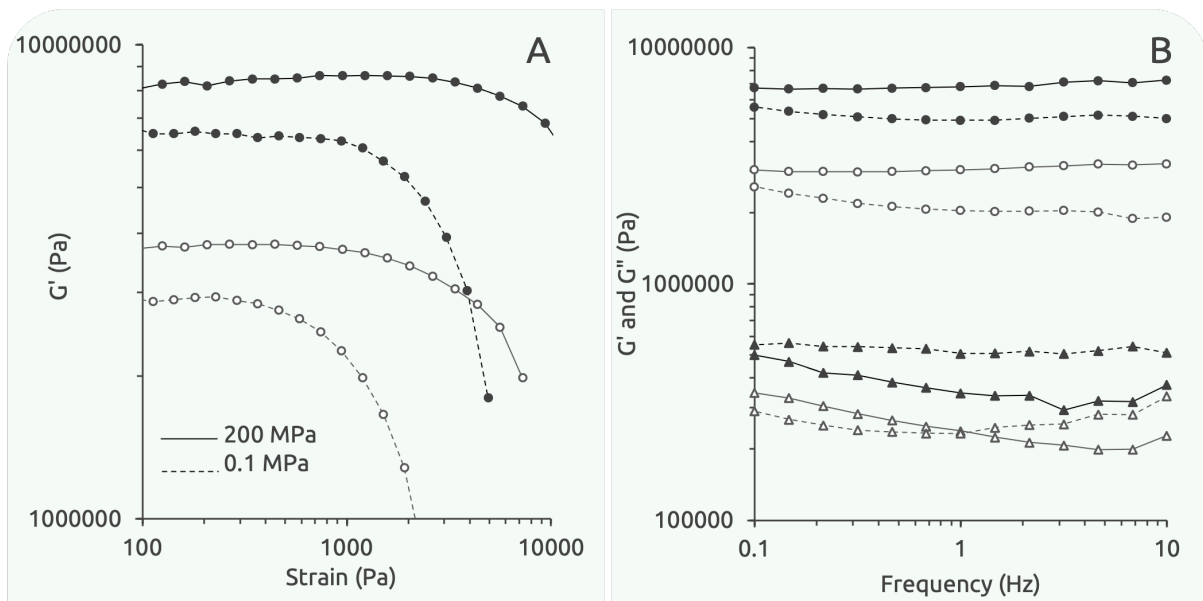


Figure 18. Changes in elastic (G', ○) and viscous (G'', △) moduli as a function of oscillatory strain (A) and frequency (B) of samples containing 80 (empty symbols) and 90 (full symbols) % palm stearin in sunflower oil and crystallized at 0.1 or 200 MPa.

Oscillatory stress sweep results at 1 Hz are reported in Figure 18A. In the linear region, both viscoelastic moduli were not stress-dependent (*plateau*) because the applied stresses produced a proportional strain response (reversible deformation). These data were used to

determine the critical stress ($\sigma^*$), corresponding to the shear stress above which structure breakage occurs (Table 11). Increasing the palm stearin concentration and applying pressure caused an increase in $\sigma^*$. This indicates that the networks formed with high palm stearin content and crystallized under pressure were more capable of withstanding mechanical strain without plastic deformation (Patel, Babaahmadi, et al., 2015).

Concerning frequency sweep curves (Figure 18B), G' was always higher than G'' in the tested frequency range, indicating that the elastic component was dominant for all the samples. Rheological parameters at a frequency of 1 Hz were used to compare the samples (Table 11). In agreement with firmness data, the increase of palm stearin content in the blend caused a significant increase in G'. Even in this case, pressurized samples showed G' significantly higher than the corresponding unpressurized blends. These results are in agreement with those obtained by (Zulkurnain et al., 2016a), who reported a G' increase in a blend of 30% fully hydrogenated soybean oil and soybean oil crystallized under pressure (600 MPa, 10 min, 25 °C). Samples loss tangent (tan δ) was also calculated using G' and G'' (*i.e.*, loss modulus) values. This parameter is commonly used to describe the structural order (in terms of molecular interactions) in viscoelastic food systems, with lower tan δ values referred to highly structured materials (Albano et al., 2014). As expected, all samples showed tan δ values lower than 1, indicating the predominance of the solid behavior of the systems over the liquid one (Chai et al., 2020). Both the increase in palm stearin content in the sample and crystallization pressure caused a significant decrease in tan δ.

### 3.3.3. Solid Fat Content and Thermal Profile

To understand the reasons behind the change in mechanical and rheological properties upon pressurization during crystallization, the solid fat content (SFC) at 20 °C of the considered fat blends crystallized at 0.1 and 200 MPa was assessed by LR-NMR (Figure 19).
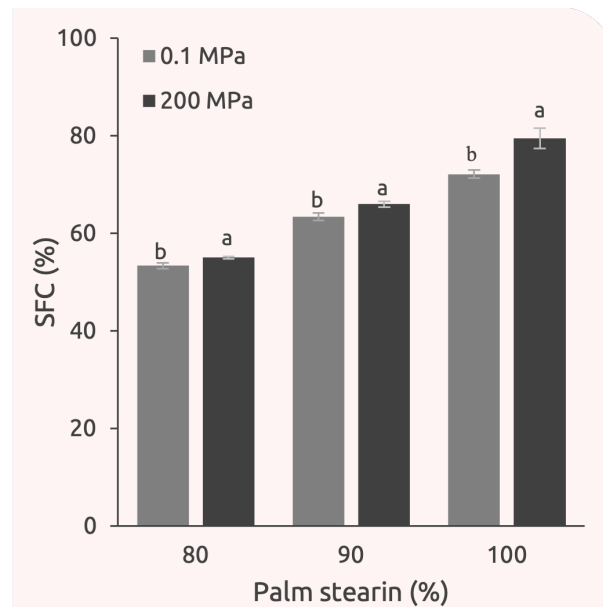


Figure 19. Solid fat content (%) at 20 °C of samples containing increasing concentrations of palm stearin (80, 90, and100%, w/w) in sunflower oil and crystallized at 0.1 or 200 MPa.
[a,b] different letters for the samples with equal palm stearin concentration indicate statistically different means (t-test; $p < 0.05$).

It can be noted that pressurization during crystallization caused a significant increase in SFC ($p < 0.05$). These results strongly indicate that the pressure-induced enhancement of sample mechanical/rheological properties can be associated with an increase in the crystallized palm stearin fraction in the blend. The higher fat content upon pressurization was also confirmed by the DSC thermal profile (Figure 20, Table 13).

Figure 20. DSC thermograms of samples containing increasing concentrations of palm stearin (80, 90, and 100%, w/w) in sunflower oil and crystallized at 0.1 or 200 MPa.

As expected, all samples showed a single endothermic peak, corresponding to the melting of the crystallized palm stearin fraction. In agreement with the literature, the increase of palm stearin concentration from 80 to 100% caused a visible peak shift towards higher temperature and an increase in melting enthalpy, due to the higher number of crystallizing components (Zhu et al., 2017). In agreement with (Zulkurnain et al., 2019), crystallizing samples under pressure caused a slight shift towards lower temperatures of the melting peak and a concomitant increase in melting enthalpy ($\Delta$H) (Table 13).

Table 13. Thermal parameters ($T_{onset}$ and $\Delta$H) of samples containing increasing concentrations of palm stearin (80, 90, and 100%, w/w) in sunflower oil and crystallized at 0.1 or 200 MPa.

| Palm Stearin (%, w/w) | Pressure (MPa) | $T_{onset}$ (°C) | $\Delta$H (J g$^{-1}$) |
|---|---|---|---|
| 80 | 0.1 | 32.2 ± 1.0[a] | 73.8 ± 0.1[f] |
| | 200 | 30.8 ± 0.1[c] | 74.9 ± 0.7[e] |
| 90 | 0.1 | 32.4 ± 1.4[a] | 78.1 ± 0.1[d] |
| | 200 | 31.2 ± 0.3[b] | 85.4 ± 2.0[c] |
| 100 | 0.1 | 32.8 ± 0.7[a] | 96.7 ± 3.6[b] |
| | 200 | 32.2 ± 0.5[a] | 102.3 ± 1.3[a] |
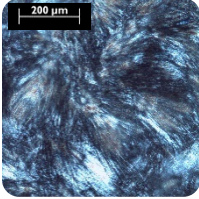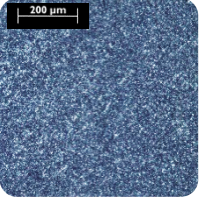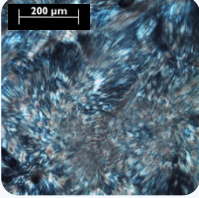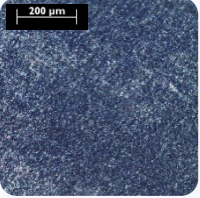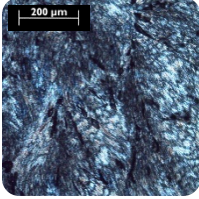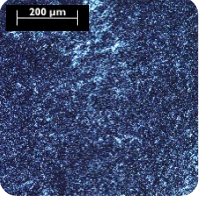
[a-f] different letters in each column indicate statistically different means ($p < 0.05$).

These results are in agreement with SFC data (Figure 19), clearly indicating the capability of hydrostatic pressure to promote crystallization phenomena.

Micro and Nanostructure Morphology

Table 14 shows the polarized light micrographs of samples containing 80, 90, and 100% (w/w) palm stearin upon crystallization at 0.1 or 200 MPa.
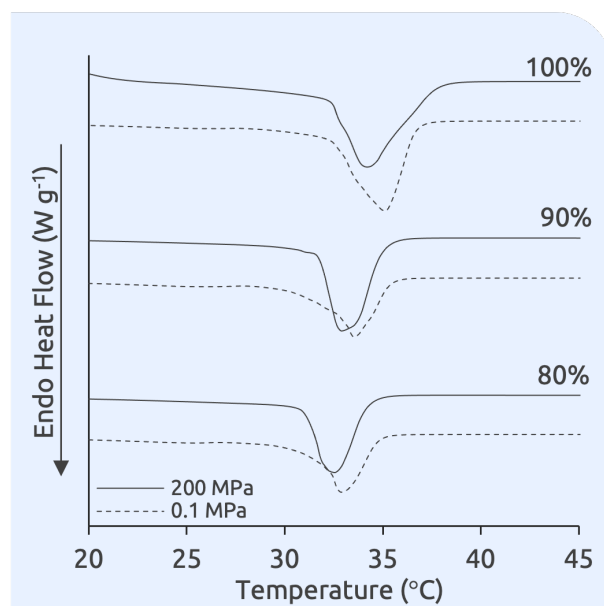
Table 14. Polarized light microscopy images of samples containing increasing concentrations of palm stearin (80, 90, 100%, w/w) in sunflower oil and crystallized at 0.1 or 200 MPa.

| Palm Stearin (%, w/w) | Pressure | |
|---|---|---|
| | 0.1 MPa | 200 MPa |
| 80 |  |  |
| 90 |  |  |
| 100 |  |  |

Samples crystallized at 0.1 MPa clearly showed a microstructure composed of large needle-shaped crystalline aggregates. The application of hyperbaric crystallization caused a clear modification of the fat crystal network microstructure with the formation of a higher number of evenly dispersed, small crystalline particles. These data, along with those reported in Table 11 and Table 13, indicate that pressure favored the formation of a larger amount of smaller, spherulitic crystal aggregates, which formed a more densely packed network as compared to samples crystallized at ambient pressure. This network feature, along with the higher SFC, ultimately led to fat materials with more pronounced solid-like behavior than the control samples. This agrees with previous studies highlighting that smaller crystals were associated with the formation of a stronger and more structured network (Campos et al., 2002; Pérez-Martínez et al., 2007).

Synchrotron-XRD analysis was performed to better determine the impact of pressurization on crystal morphology. Samples wide- and small-angle XRD diffractograms (WAXD and SAXD), which were produced by the crystal interplanar spacings related to inter-chain (shorter cell dimensions) and chain-length (longer cell dimension and higher reflection orders) distances, respectively, are reported in Figure 21.
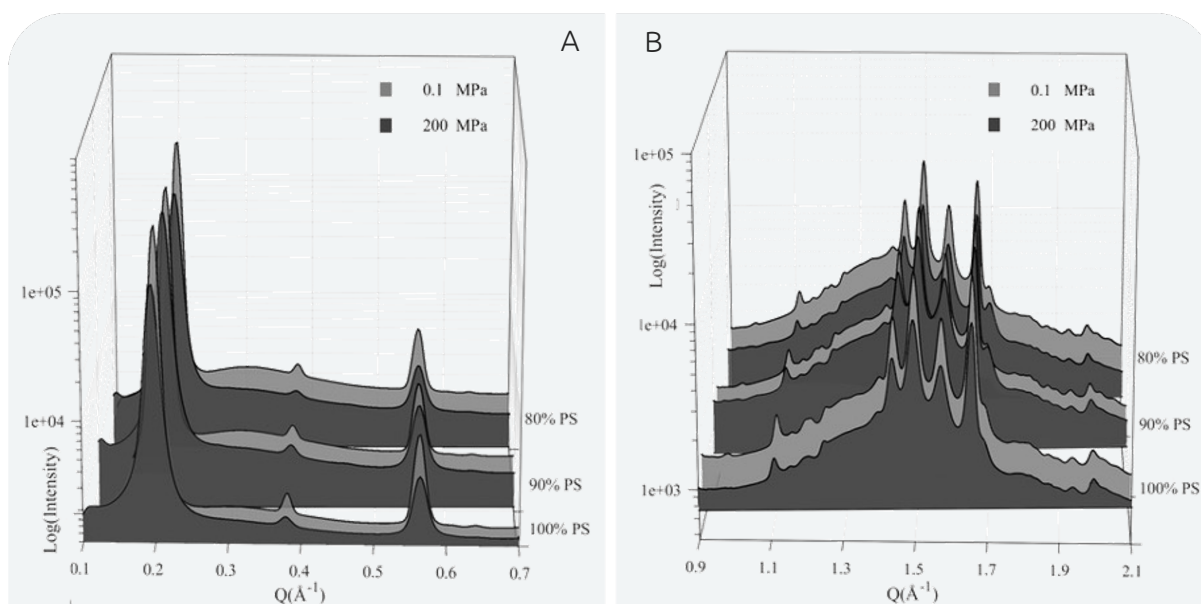
Figure 21. Normalized small-angle (A) and wide-angle (B) diffractograms of samples containing increasing concentrations of palm stearin (80, 90, and 100%, w/w) in sunflower oil and crystallized at 0.1 or 200 MPa.

WAXD revealed the typical palm oil XRD patterns, with 4 well-distinguishable peaks at 4.41, 4.20, 4.05 e 3.82 Å (Figure 21). In agreement with the literature, these peaks are attributable to the X-ray scattering of orthorhombic β' fat crystals (C. Liu et al., 2019). As clearly visible, no peak shifts or appearance of other polymorphs were observed in the WAXD region as a consequence of the application of pressure during crystallization. Similar results were obtained in the SAXD region, where the main peak at $d$ = 34.12 Å along with three higher order reflections were detected and associated with a double-chain lamellar length of crystallized triglycerides in palm oil (C. Liu et al., 2019; van Mechelen et al., 2006).

Despite the same position in the diffractograms, it can be noted that peaks associated with pressurized samples were broader in both WAXD and SAXD regions, as compared to unpressurized samples. This result is typically associated with an increase in the fat crystal network disorder (Ungár, 2004). To quantitatively evaluate the effect of pressure on the structural characteristic of palm stearin crystalline network, diffraction profiles were fitted and elaborated to determine the crystallite size ($D_s$), volume-adjusted crystallite size ($D_v$), microstrain and paracrystallinity index (Enzo et al., 1988; Hindeleh & Hosemann, 1991) (Table 15).

Table 15. Crystallite size ($D_s$), volume-adjusted crystallite size ($D_v$), microstrain and paracrystallinity of samples containing increasing concentrations (80, 90, and 100%, w/w) of palm stearin and crystallized at 0.1 or 200 MPa.

| Palm stearin (%, w/w) | Pressure (MPa) | $D_s$ [a] ($Å^3$) | $D_v$ (Å) [a] ($Å^3$) | Microstrain (-) | Paracrystallinity [b] (%) |
|---|---|---|---|---|---|
| 80 | 0.1 | 333.1 | 364.4 | 0.0104 | 3.8 |
|    | 200 | 320.2 | 346.1 | 0.0104 | 3.6 |
| 90 | 0.1 | 393.3 | 423.0 | 0.0095 | 3.8 |
|    | 200 | 340.9 | 368.2 | 0.0107 | 4.0 |
| 100 | 0.1 | 378.7 | 426.6 | 0.0086 | 3.4 |
|     | 200 | 306.1 | 328.6 | 0.0100 | 3.4 |

[a] estimated esd ~ 10 Å

[b] Lattice fluctuation vector relative to the two successive orders 020 and 040 of the same crystallographic direction.

As visible from the data reported in Table 15, the increase of palm stearin concentration from 80 to 100% caused an increase in the crystallite size and a decrease in the microstrain of crystals formed during cooling under atmospheric conditions. Although counterintuitive at first glance, this can be associated with crystal growth faster than nucleation phenomena, thus leading to larger crystals with lower interfacial tension (Greiner et al., 2012). When pressure was applied, a decrease of $D_s$ and $D_v$, with a concomitant microstrain increase, was observed, confirming that the application of pressure caused the formation of smaller crystallites. Interestingly, the effect of pressure resulted in much more effective in reducing crystal size as the palm stearin content increased. It can be inferred that pressurization further favored nucleation instead of crystal growth.

# 3.4. Conclusions

This study demonstrates the applicability of moderate hydrostatic pressure treatments to steer the crystallization of palm stearin in sunflower oil. Crystallization under pressure (200 MPa, 20 °C, 1 h) significantly enhanced the firmness, the elastic modulus, and the critical stress of all samples. This effect was attributed to the presence of a higher number of small, disordered, highly strained crystals.

The obtained results suggest the potential use of hydrostatic pressurization to tailor the techno-functional properties of fat-based ingredients. Notably, significant variations were observed between the samples and the controls when pressure was applied. Considering that the technology is already widely employed on a large scale within the food sector (*e.g.*, non-thermal pasteurization), its application to fat manufacturing will likely not pose significant technical hurdles. Future studies are needed to demonstrate the applicability of hydrostatic pressure treatments on oleogels made of crystalline networks, such as monoglycerides and waxes. Unfortunately, it was not possible due to time constraints to proceed on this aspect in this Thesis.

# PART 2

# STRUCTURING OIL THROUGH INDIRECT APPROACH

In Part 2 of this thesis, the focus moved to the use of a more innovative and, at the same time, challenging structuring approach, namely, the indirect approach. This approach opens the possibility of using hydrophilic molecules as oil structuring molecules, widening their possible use in food formulations and fostering the clean label consumer demand (Patel, 2018; Schatteman, 2013).

Among the different techniques presented in the literature, the dry template approach was selected and investigated on different biopolymers, mainly considering the effect of the hydrogel characteristics as well as the drying technologies applied (*i.e.*, supercritical-$CO_2$- and freeze-drying).

Cellulose, whey, and pea proteins were selected as target structuring biopolymers.

Cellulose is a particularly attractive biopolymer, already used in the food industry for its functional properties. It is naturally present in or added as an ingredient in various food products, serving as a thickener, stabilizer, filler, and bulking agent. Its ability to enhance textural attributes, such as viscosity, mouthfeel, and creaminess, makes it highly appreciated in dressings, sauces, and dairy alternatives (Mu et al., 2019). Consumers are familiar with cellulose as an ingredient, and its popularity is growing due to its plant origin and associated health benefits. As a non-digestible component, cellulose can be used as a filler to reduce caloric intake, but also to promote gastrointestinal health, acting as a prebiotic for gut microbes and acting as a gut-protection agent (Brownlee et al., 2006; David et al., 2014; Hervik & Svihus, 2019). From a sustainability perspective, cellulose is the Earth's most abundant polysaccharide, making it cost-effective. Moreover, it can be sourced from agro-industrial vegetable byproducts, utilizing a closed-loop approach that minimizes waste generation (Pires et al., 2022). To our knowledge, cellulose is an understudied polymer in the field of oleogelation. Among different cellulose types, microcrystalline cellulose (MCC) emerges as an excellent candidate for generating food-grade aerogels and cryogels porous materials, based on recent evidence (Budtova, 2019). Its widespread use in the food industry for diverse applications, such as a stabilizer, emulsifier, and anti-caking agent, makes it an ideal choice to be used also as a structuring agent (Merci et al., 2015), as will be described in Chapters 4 and 5.

Considering proteins, over the last two decades, proteins have experienced a surge in commercial popularity driven by their recognized health benefits and increasing ecological and environmental awareness (Nikbakht Nasrabadi et al., 2021).

Proteins are versatile and widely explored molecules that could offer promising potential in the form of porous materials for oleogelation. Whether of animal or plant origin, proteins can form gels through various mechanisms like denaturation, coagulation, or aggregation, opening possibilities to develop porous dry structures, and able to interact with liquid oil (Scholten, 2019). The interest in utilizing proteins as building blocks for oleogelation arises from their capacity to influence the texture, stability, and nutritional profile of food products while reducing the reliance on traditional solid fats.

Pea (PPI) and whey (WPI) protein isolates are the most notable among protein sources. PPI offers a plant-based alternative to allergenic soy protein in plant-based products. On the other hand, WPI is known for its versatility and is a significant byproduct of cheese production (Farooq et al., 2019; Lam et al., 2018).

The key studies presented in this part are the following:
- CELLULOSE
  - Chapter 4. Interactions of cellulose cryogels and aerogels with water and oil: structure-function relationships.
  - Chapter 5. Cellulose-based oleogels obtained through the cryogel template approach.
- PROTEINS
  - Chapter 6. Potentialities for oil structuring of pea protein cryogel monoliths prepared at different pH.
  - Chapter 7. Oil structuring capability of whey protein cryogel particles obtained through gelation at different pH.
  - Chapter 8. Interaction of whey protein cryogel-based oleogels with water.

# 4. INTERACTIONS OF CELLULOSE CRYOGELS AND AEROGELS WITH WATER AND OIL: STRUCTURE-FUNCTION RELATIONSHIPS

## 4.1. Introduction and Aim of the Study

In this Chapter, cellulose cryogels and aerogels were prepared and investigated for interaction with oil and water. The structure aerogel and cryogel samples were first characterized, including SEM microstructure analysis, BET-specific surface area measurement, and assessments of porosity, pore volume, and density. Then, their interactions with common food fluids, such as water and oil, were studied revealing various potential food applications for these porous cellulose-based templates.

Results here presented have been published in:

Ciuffarin, F., Négrier, M., Plazzotta, S., Libralato, M., Calligaris, S., Budtova, T., & Manzocco, L. (2023). Interactions of cellulose cryogels and aerogels with water and oil: Structure-function relationships. Food Hydrocolloids, 140, 108631. https://doi.org/10.1016/j.foodhyd.2023.108631

## 4.2.  Materials and Methods

### 4.2.1. Materials

Microcrystalline cellulose (Avicel®, pH-101, degree of polymerization 180 as declared by the manufacturer) was purchased from Sigma Aldrich. Sunflower oil was obtained from a local store. Deionized water was made with System advantage A10®, Millipore S.A.S, Molsheim, France); absolute ethanol (purity > 99%) and NaOH were purchased from Fisher Chemical.

### 4.2.2. Preparation of Cellulose Hydrogels, Cryogels, and Aerogels

Cellulose hydrogels were prepared as follows. Microcrystalline cellulose was first dried at 50 °C under vacuum for at least 2 h, pre-soaked in water for a few hours and then mixed with NaOH-water, pre-cooled at -16 °C, at 50 rpm using a mixer (Hei-Torque 100, Heidolph, Schwabach, Germany) for 2 h in a thermostatic cooling bath (Huber Compatible Control CC1, Offenburg, Germany) at -5 °C. Cellulose concentration was 3, 4, and 5 % (w/w) in 8% (w/w) NaOH-water. The obtained solutions were transparent and optically homogeneous. Around 6 mL of solution was poured into cylindrical polypropylene vials (2.7 cm in diameter) and heated at 50 °C for 2 h; in these conditions, cellulose-NaOH-water solutions are gelling (Budtova & Navard, 2016). The gels were then placed in successive water baths to dilute NaOH, as tested with pH-meter (BASIC pH meter, Denver Instrument, Bohemia, USA); the resulting material was a cellulose hydrogel at pH 7.0.

To obtain cryogels, cellulose hydrogels were frozen by immersion into liquid nitrogen (-196 °C) and freeze-dried for 72 h at -80 °C and 10 mTorr (Cryotec Cosmos, Saint-Gély-du-Fesc, France).

To obtain aerogels, water in hydrogels was first replaced by ethanol, a fluid miscible with $CO_2$ (Budtova, 2019): cellulose hydrogels were placed in successive water-ethanol baths with a gradual increase in ethanol concentration to completely remove water. The resulting alcogels were dried with supercritical $CO_2$ (homemade set-up of PERSEE Mines Paris, France); the details can be found elsewhere (Zou & Budtova, 2021). Briefly, alcogels were placed in a 1 L autoclave, pressurized at 80 bar and 37 °C and ethanol purged. Two dynamic washing steps were then performed for 1 and 2 h with a $CO_2$ output of 5 kg $h^{-1}$. In between those dynamic steps, a static mode of 2 h was used, with no $CO_2$ output. Finally, the system was slowly depressurized at 4 bar $h^{-1}$ and 37 °C and cooled down to room temperature.

The obtained dried monoliths were stored in a desiccator containing granular silica gel at room temperature until analysis.

### 4.2.3. Characterization

#### 4.2.3.1. Image Acquisition

Sample images were acquired using an image acquisition cabinet and a Google Pixel 6 camera (Alphabet, Mountain View, California, USA). The light was provided by a LED strip properly placed to minimize shadow and glare.

#### 4.2.3.2. Morphology by Scanning Electron Microscopy (SEM)

SEM micrographs were obtained using a MAIA-3 (Tescan, Brno, Czech Republic), equipped with detectors of secondary and back-scattered electrons. The internal cross-section of the samples was coated with a 14 nm layer of platinum with a Quorum Q150T metallizer (Quorum Technologies, East Sussex, UK) to prevent the accumulation of electrostatic charges and images' defaults. The observations were performed with an acceleration voltage of 3 kV.

#### 4.2.3.3. Volume Variation

Sample volume was calculated as the volume of the cylinder whose diameter and height were measured by a CD-15APXR digital caliber (Absolute AOS Digimatic, Mitutoyo Corporation, Kanagawa, Japan). Volume variation ($\Delta V$, %) during the conversion of hydrogels to cryogels or aerogels was expressed as follows (eq. 1).

$$\Delta V(\%) = \frac{V_H - V_D}{V_H} \cdot 100 \qquad (eq. 1)$$

where $V_H$ and $V_D$ are the volumes of the hydrogel and of the dried material (cryogel or aerogel), respectively.

#### 4.2.3.4. Envelope Density, Porosity, and Pore Volume

Envelope density ($\rho_{envelope}$) was measured using the Micromeritics GeoPyc 1360 Envelope Density Analyzer (Norcross, Georgia, USA) with the DryFlo® powder as a fluid medium. Each sample was measured in 5 cycles with an applied force of 27 N. Porosity (eq. 2) and pore volume (eq. 3) were calculated from the envelope ($\rho_{envelope}$) and cellulose skeletal density ($\rho_{skeletal}$ = 1.5 g cm$^{-3}$, Sun, 2005):

$$Porosity\ (\%) = \left(1 - \frac{\rho_{envelope}}{\rho_{skeletal}}\right) \cdot 100 \qquad (eq. 2)$$

$$Pore\ volume\ (cm^3 g^{-1}) = \frac{1}{\rho_{envelope}} - \frac{1}{\rho_{skeletal}} \qquad (eq. 3)$$

### 4.2.3.5. Specific Surface Area

The specific surface area ($S_{BET}$) was determined by measuring $N_2$-adsorption isotherm at 77 K with the Micromeritics ASAP 2020 (Norcross, Georgia, USA) and using Brunauer, Emmett and Teller (BET) approach (Brunauer et al., 1938). Prior to measurements, samples were degassed 5 h at 70 °C.

### 4.2.3.6. Firmness

Firmness was measured by a uniaxial compression test using an Instron 4301 (Instron LTD., High Wycombe, UK). Samples were tested at ambient conditions using a 6.2 mm diameter cylindrical probe mounted on a 1000 N compression head at a 25 mm min$^{-1}$ crosshead speed. Force-distance curves were obtained from the compression tests and firmness was taken as the maximum force (N) required to penetrate the sample for 2 mm.

### 4.2.3.7. Water Vapor Adsorption

The water vapor sorption isotherms were recorded with the ProUmid "Vsorp Basic" dynamic vapor sorption analyzer system (ProUmid, Ulm, Germany). The monoliths were cut using a microtome blade to obtain 0.4 g samples. The latter were placed in aluminium plates (86 mm in diameter) and kept in a climatic chamber at 25 ± 0.1 °C. The percentage of relative humidity (RH) in the sample headspace was automatically increased from 0 ± 0.1% RH to 90 ± 0.1% RH with 10% RH steps. The equilibrium of each step was considered to be reached when sample mass variation was lower than 0.01% for at least 300 min. The water vapor isotherms were expressed as moisture ($g_{H2O}/g_{dry\ matter}$) as a function of sample water activity ($a_w$), which corresponds to RH/100 in the headspace of the sample at equilibrium conditions.

### 4.2.3.8. Water and Oil Absorption Kinetics

Cryogels and aerogels were manually cut into cubes of 1 cm$^3$ volume and weighted ($W_0$). Cubes were immersed into Petri plates containing water or sunflower oil at room temperature (22 °C). At defined time intervals, samples were withdrawn, wiped with absorbent paper, and weighed ($W_t$). The experiment was carried out until a constant weight was reached (*plateau* or equilibrium value), as indicated by no weight variation in 3 consecutive measures. Absorbed water or oil at each time was expressed as the ratio between weight gain at time t (min) and the initial weight of the cryogel or aerogel sample (eq. 4).

$$Absorbed\ solvent\left(g_{fluid}/g_{dry\ matter}\right) = \frac{(W_t - W_0)}{W_0} \qquad \text{(eq. 4)}$$

The maximum solvent absorption capacity was taken at equilibrium.

### 4.2.3.9. Water and Oil Holding Capacity

When the absorption reached the equilibrium, around 100-200 mg of sample ($W_1$) was placed into 1.5 mL microtubes and centrifuged at 15,000$g$ for 30 min using a microcentrifuge (Mikro 120, Hettich Zentrifugen, Andreas Hettich GmbH and Co, Tuttlingen, Germany). After centrifugation, the released fluid was accurately wiped using absorbing paper and the sample was weighted again ($W_2$). Water (WHC) and oil holding capacity (OHC) were calculated as the percentage ratio between the weight of fluid retained in the sample after centrifugation and the total fluid weight initially present (eq. 5).

$$Fluid\ Holding\ Capacity\ (\%) = \frac{S \cdot W_1 - (W_1 - W_2)}{S \cdot W_1} \cdot 100 \qquad \text{(eq. 5)}$$

where $S$ represents the weight fraction (%) of the fluid initially present in the sample.

## 4.2.4. Data Analysis
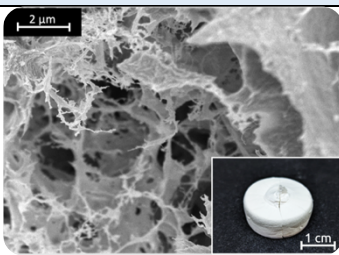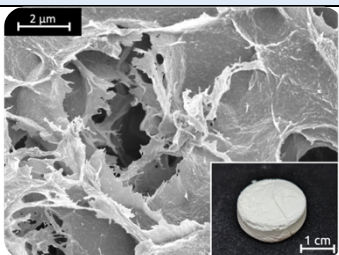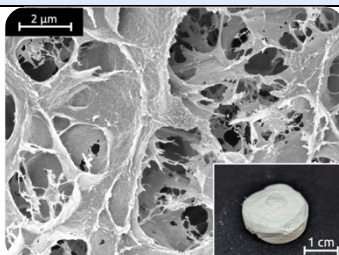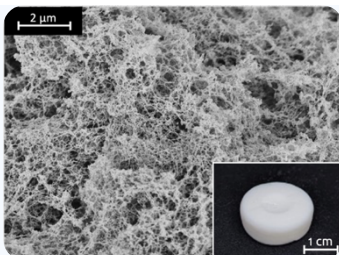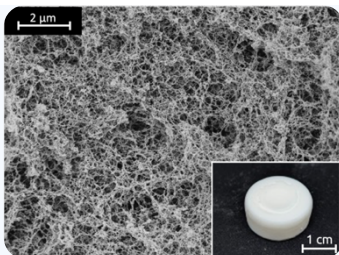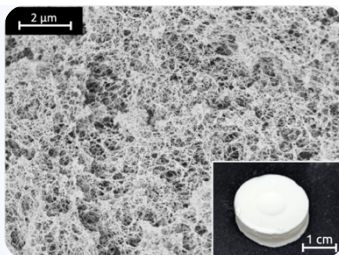
Data were expressed as the mean ± standard error of at least two measurements from two experimental replicates (n ≥ 4). Statistical analysis was performed by using R v. 4.0.3 (The R Foundation for Statistical Computing). ANOVA test was used to determine statistically significant differences between means ($p < 0.05$). Bartlett's test was used to check the homogeneity of variance ($p ≥ 0.05$) and the Tukey test was used as a *post-hoc* test ($p < 0.05$).

# 4.3. Results and Discussion

### 4.3.1. Characterization of Cryogels and Aerogels

Table 16 shows the visual appearance and microstructure of cryogels and aerogels prepared *via* freeze-drying (FD) and supercritical-CO$_2$ drying (SCD), respectively, of hydrogels obtained from cellulose solutions containing 3, 4, and 5% (w/w) cellulose.

Table 16. Visual appearance and SEM microstructure of cryogels and aerogels prepared from cellulose solutions containing 3, 4, and 5% (w/w) cellulose.

| Samples | Cellulose concentration in the initial solution (%, w/w) | | |
|---|---|---|---|
| | 3 | 4 | 5 |
| Cryogel |  |  |  |
| Aerogel |  |  |  |

Both cryogels and aerogels appeared visually opaque (Buchtová & Budtova, 2016; Gavillon & Budtova, 2008). Cryogels showed an uneven surface with evident cracking, whereas aerogels appeared more homogeneous without visible cracks (insets in Table 16). SEM revealed significant differences between aerogel and cryogel morphology (Table 16). In cryogels, larger pores (around and below 2-5 μm) with flat walls were observed, in agreement with previous literature (Buchtová & Budtova, 2016). Although ice crystal sublimation during FD avoids liquid-vapor interfaces and thus capillary surface tension (Fricke & Tillotson, 1997), ice crystal formation and growth during hydrogel freezing force cellulose chains to locally collapse and concentrate, resulting in large pores and non-porous pore walls (Assegehegn et al., 2019). By contrast, aerogels showed a more homogeneous microstructure (Table 16), characterized by a fibrillated network, with the majority of pores of diameter lower than 200 nm.

The conversion of hydrogels into cryogels led to a slight volume increase, as indicated by the positive volume variation (Table 16). This result can be attributed to the ice crystal growth during FD (Assegehegn et al., 2019). By contrast, aerogel preparation caused volume contraction (Table 16), which can be attributed to the increased difference in solubility parameters between cellulose (39 $MPa^{0.5}$), ethanol (26.5 $MPa^{0.5}$), and $CO_2$ (around 5 - 8 $MPa^{0.5}$ for the supercritical $CO_2$ in the conditions used in the present study) (Hansen, 2007; M. Zhang et al., 2017). Therefore, cryogels presented lower density than the aerogels made from cellulose solutions of the same concentration (Table 17). As expected, higher cellulose concentrations in the initial solution led to both cryogels and aerogels of higher density. The porosity of both materials was higher than 90% and it was slightly lower for aerogels as compared to cryogels. The pore volume of cryogels was higher than that of aerogels, and for both types of materials pore volume decreased with density increase (Table 17).

Table 17. Volume variation, envelope density, porosity, pore volume, BET-specific surface area, and firmness of cryogels and aerogels prepared from cellulose solutions containing 3, 4, and 5% (w/w) cellulose.

| Sample | Cellulose Solution Concentration (%, w/w) | ΔV (%) | Envelope density (g cm⁻³) | Porosity (%) | Pore Volume (cm³ g⁻¹) | $S_{BET}$ (m² g⁻¹) | Firmness (N) |
|---|---|---|---|---|---|---|---|
| Cryogel | 3 | 9.5 ± 4.7 [b] | 0.056 ± 0.002 [d] | 96.2 ± 0.1 [a] | 17.01 ± 0.60 [a] | 28 ± 0 [b] | 10.44 ± 1.1 [e] |
| | 4 | 7.7 ± 1.8 [b] | 0.071 ± 0.002 [c] | 95.3 ± 0.1 [b] | 13.40 ± 0.37 [b] | 31 ± 2 [b] | 19.9 ± 0.57 [d] |
| | 5 | 4.9 ± 0.8 [c] | 0.077 ± 0.004 [b] | 94.9 ± 0.3 [b] | 12.30 ± 0.64 [b] | 30 ± 1 [b] | 25.1 ± 0.48 [c] |
| Aerogel | 3 | - 25.9 ± 2.4 [a] | 0.077 ± 0.007 [b] | 93.8 ± 0.3 [c] | 10.08 ± 0.57 [c] | 384 ± 4 [a] | 21.0 ± 0.36 [d] |
| | 4 | - 23.3 ± 3.2 [a] | 0.098 ± 0.005 [ab] | 93.5 ± 0.4 [cd] | 9.54 ± 0.59 [c] | 380 ± 10 [a] | 35.8 ± 1.57 [b] |
| | 5 | - 20.8 ± 2.6 [a] | 0.112 ± 0.006 [a] | 92.9 ± 0.2 [d] | 8.69 ± 0.21 [c] | 371 ± 11 [a] | 44.1 ± 1.08 [a] |

[a-e] in the same column, mean values indicated by different letters are statistically different ($p < 0.05$).

Specific surface area ($S_{BET}$), which reflects the presence of mesopores and small macropores (< 200 nm), was more than 10-times higher for aerogels as compared to cryogels (Table 17), in line with SEM observations (Table 16) and results reported in the literature for bio-aerogels (Buchtová & Budtova, 2016; Zou & Budtova, 2021). It should be noted that large macropores are not detected by the BET approach, and thus a complete pore size distribution is not possible based on $S_{BET}$ results solely (Robitzer et al., 2011; Zou & Budtova, 2021).

All samples exhibited a solid nature, demonstrating a restricted elastic response to external mechanical forces before reaching the point of fracture. As a result of the lower density, cryogels presented lower firmness as compared to the aerogels prepared from cellulose solutions of the same concentration (Table 17). This is in line with the literature results. For instance, κ-carrageenan cryogels and aerogels showed firmness values of 1.2 and

47.1 N, respectively (Plazzotta et al., 2019); similarly, cryogels and aerogels prepared from whey protein hydrogels showed firmness of 18.5 and 29.5 N, respectively (Manzocco et al., 2021). As expected, since density increased with cellulose concentration, the firmness followed a similar trend, like the previously reported trend for Young's modulus of various porous cellulose materials (Buchtová et al., 2019; Schestakow et al., 2016).

### 4.3.2. Interaction with Water and Oil

In order to analyze the capacity of cellulose cryogels and aerogels to interact with water vapor, moisture adsorption isotherms were assessed. Figure 22 shows data relevant to cryogels and aerogels made from 3, 4, and 5% (w/w) cellulose solutions. The adsorption isotherm of microcrystalline cellulose is shown for comparison.
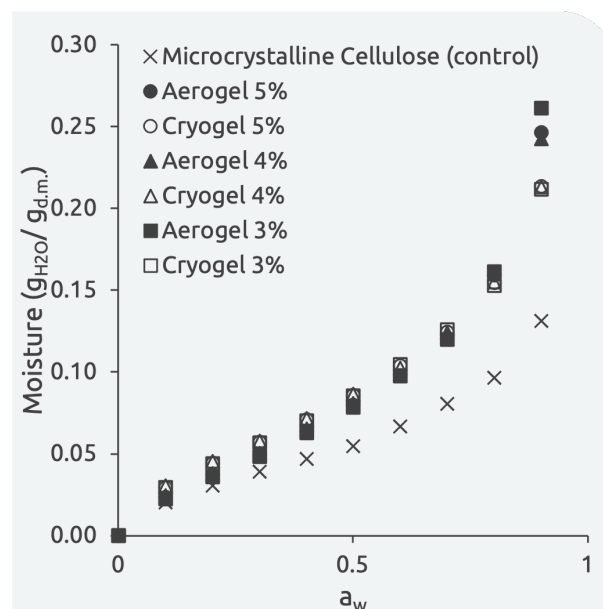


Figure 22. Water vapor adsorption isotherms of cryogels and aerogels prepared from 3, 4, and 5% (w/w) cellulose solution (see density and porosity values in Table 17) and microcrystalline cellulose. Error bars are not visible being smaller than the symbol size.

Microcrystalline cellulose isotherm was consistent with the literature data (Portugal et al., 2010). A steady increase in the moisture content was observed in the $a_w$ region up to 0.7, related to the saturation of hydrophilic cellulose sites. Upon further $a_w$ increase ($a_w > 0.7$), an inflection point in the adsorption isotherm was observed, followed by higher moisture adsorption (Figure 22). This is attributed to the cleavage of cellulose intermolecular hydrogen bonds by water, which interacts with cellulose and promotes fiber swelling (Portugal et al., 2010). The transformation of microcrystalline cellulose into cryogels and aerogels did not change the form of the isotherm but resulted in a shift towards higher moisture values over

the entire $a_w$ range (Figure 22), indicating an increased ability of cellulose to interact with water vapor; the same phenomenon was recorded for aerogels and cryogels made from cellulose solutions of 3% and 4%. It is known that microcrystalline cellulose actually contains a rather high crystalline fraction, limiting the interactions with water vapor (Bhandari, 2013). The conversion of microcrystalline cellulose into cellulose II-based cryogels and aerogels decreases the crystalline fraction, thus increasing cellulose accessibility to water vapor (Yue et al., 2012).

Figure 22 also shows that the isotherms were negligibly affected by the drying technique (freeze-drying *vs.* supercritical drying), and not influenced by material porosity or specific surface area either (Table 17).

The possibility of using cellulose cryogels and aerogels as innovative food ingredients requires the knowledge of their ability to absorb and retain the most common liquids used in foods, namely water and oil. The kinetics of water and oil absorption by aerogels and cryogels are shown in Figure 23.
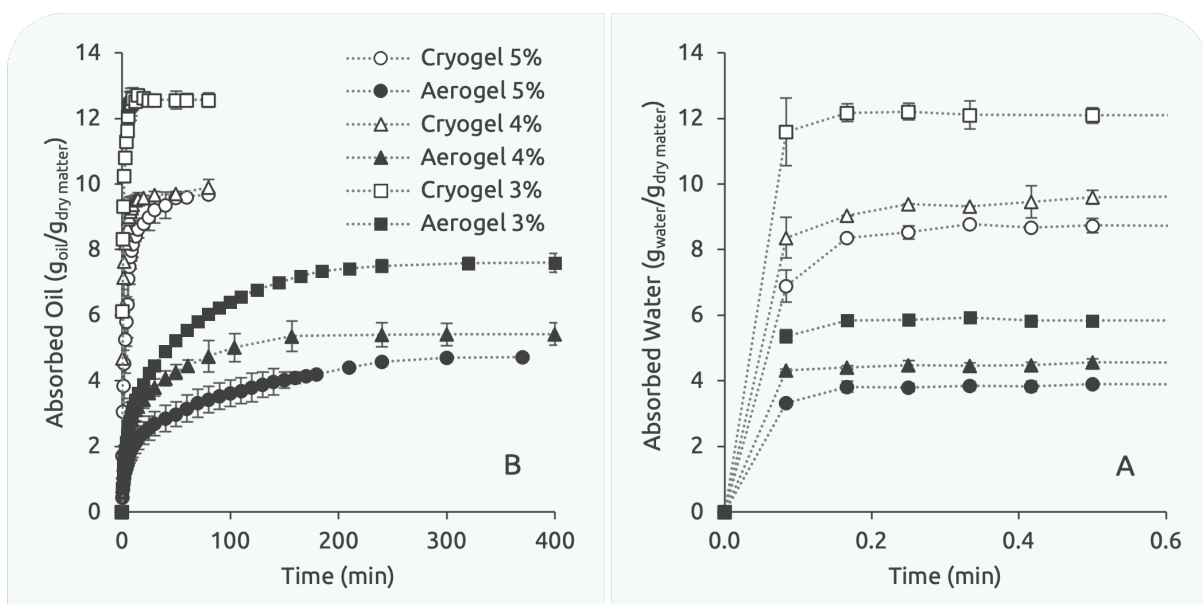


Figure 23. Water (A) and oil (B) absorbed by cryogels and aerogels prepared from cellulose solutions containing 3, 4, and 5% (w/w) cellulose. The symbols are the same for both figures. The dashed lines are given to guide the eyes.

Upon contact with water, an extremely fast absorption was observed for all the samples (Figure 23), so that the absorption equilibrium was reached after a few seconds. The absorption of oil was from one to three orders of magnitude slower than that of water (Figure 23). The faster absorption of water as compared to oil by both cryogels and aerogels can be attributed to the hydrophilic nature of cellulose as well as to the lower viscosity of water

(0.001 Pa s at 25 °C) as compared to that of sunflower oil (0.060 Pa s at 25 °C) (Lucas-Washburn equation).

Cryogels were found to absorb fluids faster than aerogels. For example, in the case of cryogels, oil absorption approached the equilibrium within 15-60 min, while aerogels showed a more gradual oil absorption, which leveled off only after 200-250 min. These differences in fluid absorption kinetics can be attributed to the different morphology of cryogels and aerogels. In particular, aerogels present much smaller pores as compared to cryogels, as seen in Table 16 and also deduced from the specific surface area of the materials (Table 17).

The maximum water and oil absorption values (or *plateau* values in Figure 23) of all the prepared materials were plotted as a function of material pore volume (Figure 24). These values varied from 4 to 8 $g_{fluid}/g_{dry\ matter}$ for aerogels and from 8 to 13 $g_{fluid}/g_{dry\ matter}$ for cryogels, due to different material pore volumes (see Table 17). Interestingly, all equilibrium values fell on the same linear trend ($R^2 = 0.92$; $p < 0.05$) as a function of material pore volume despite the hydrophilic nature of cellulose, and not depending on the type of liquid (oil *vs.* water) or pore dimensions. This highlights the pivotal role of material pore volume on fluid uptake values at equilibrium.
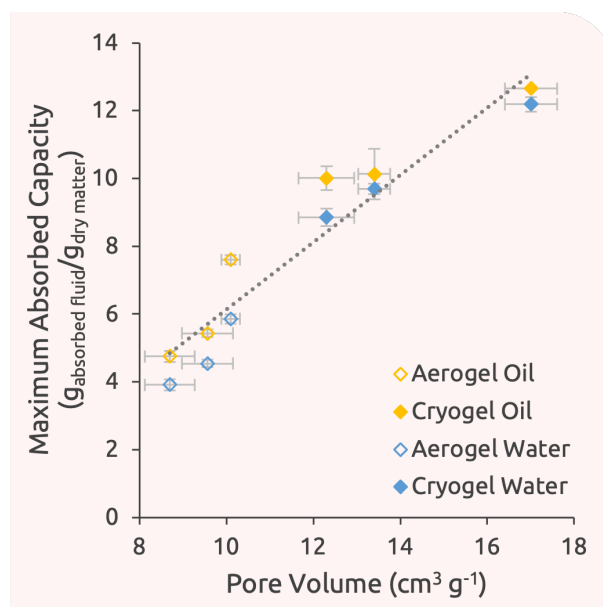


Figure 24. Maximum water and oil absorption capacity of cryogels and aerogels prepared from cellulose solutions containing 3, 4, and 5% (w/w) cellulose as a function of material porosity. The dashed line is the least square approximation with $R^2 = 0.96$.

The literature reports the use of porous cellulose for the absorption of various liquids. Most studies used functionalized freeze-dried cellulose II for oil absorption. After silylation (Lin et al., 2015), chemical vapor deposition (Liao et al., 2016), or plasma treatment (H. Zhang et al., 2016), absorption values were in the range from 20 to 60 $g_{oil}/g_{dry\ matter}$. Similar values

were also reported for functionalized freeze-dried nanocellulose. By contrast, very few examples are known about the absorption behavior of neat cellulose II aerogels. In the study of Chin et al. (2014) cellulose coated with $TiO_2$ showed a five times higher oil absorption capacity (up to 28 $g_{oil}/g_{dry\ matter}$), as compared to its non-coated counterpart (5 $g_{oil}/g_{dry\ matter}$). The results acquired in this study (Figure 23 and Figure 24) demonstrate that cellulose aerogels and cryogels absorb large quantities of water and oil without any chemical modification. This is particularly relevant for the food application of these porous materials: in fact, despite resulting in high fluid absorption, the chemical modifications cited above are not acceptable for food applications.

The effect of water and oil absorption on cryogel and aerogel firmness is reported in Figure 25, where firmness values of cryogels and aerogels prior to and after water and oil absorption are plotted against porosity.
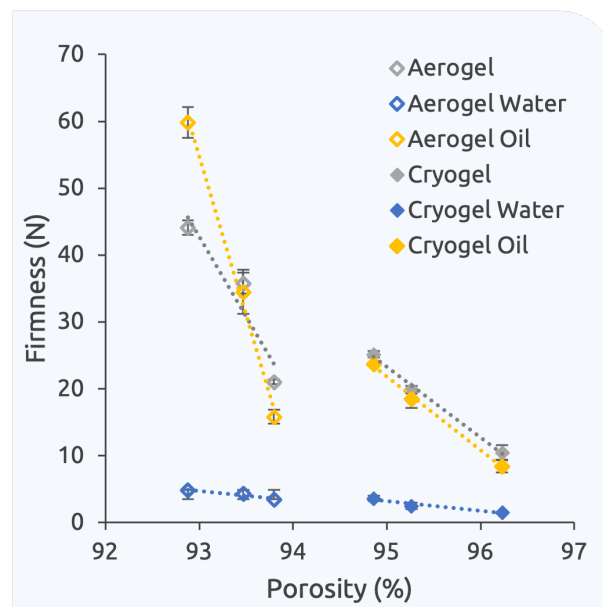


Figure 25. Firmness of cryogels and aerogels prepared from cellulose solutions containing 3, 4, and 5% (w/w) cellulose prior to and after water and oil absorption as a function of porosity. The dashed lines are added as a guide for the eyes.

Water absorption caused a significant decrease in sample firmness as compared to the dried materials (Figure 25). Differently from water-absorbed samples, oil absorption had a negligible effect on cryogel and aerogel firmness (Figure 25). The different effect of water and oil absorption on cryogels and aerogels firmness is probably attributable to the high hygroscopicity of cellulose, which causes the hydration of the cellulose network, weakening it, as also demonstrated for other porous materials based on vegetable fibers and proteins. By contrast, oil would simply fill the voids without significantly interacting with the polymer network (Manzocco et al., 2017, 2022).

Finally, the ability of cryogels and aerogels to retain the absorbed liquid was evaluated under centrifugal stress. All the samples showed similar ($p \geq 0.05$) high water and oil holding capacity, with values higher than 96%, independent from drying technique, material porosity, and specific surface area. These results were expected for aerogels, due to the ability of small pores (Table 16) to strongly entrap the fluid. Similar oil holding capacity (OHC) values (96.3 and 83.4%), were obtained for whey protein and κ-carrageenan aerogels, which presented pore sizes around 100 and 400 nm, respectively (Manzocco et al., 2017, 2022; Plazzotta et al., 2019). Remarkably, cellulose cryogels showed much higher water and oil-holding capacity values than those reported in the literature. For example, cryogels prepared from whey proteins or κ-carrageenan showed an OHC lower than 50% (Manzocco et al., 2022; Plazzotta et al., 2019). Those cryogels possess very large pores with diameters up to 900 µm. One of the reasons for the high water and oil holding capacity of the cellulose cryogels obtained in this work might be higher capillary forces due to the rather small pore size, around 2-5 µm (Table 16).

# 4.4. Conclusions

Cellulose aerogels and cryogels were made via supercritical- and freeze-drying, respectively, and tested for the absorption and holding capacity of water and vegetal oil. All materials possessed very high porosity, above 90%. By varying drying techniques, materials with different morphology were obtained: aerogels had a fine ramified network with pore size below 200 nm, while cryogels presented pores of few microns and lower, and continuous flat pore walls.

The kinetics of water and oil absorption were investigated: water was absorbed by aerogels and cryogels within one minute, while oil absorption was much slower due to oil higher viscosity and hydrophobicity. Oil absorption by cryogels was much faster than by aerogels, 15-60 min *vs* 200-250 min, respectively. This phenomenon was attributed to material morphology as described above.

The maximum absorption of oil and water was proportional to material pore volume, and all experimental values fell on the same linear plot. Pore volume turned out to be the main parameter governing fluid absorption at equilibrium, which did not depend on material morphology or fluid polarity.

Finally, the water and oil holding capacity, and firmness of aerogels and cryogels, both before and after water and oil loading, were analyzed. Firmness decreased with material porosity increase, as expected. Water loading caused firmness to decrease as compared to the unloaded aerogels and cryogels, while the firmness of materials filled with oil was comparable to the one with air in the pores.

These interesting results open new prospects in using cellulose aerogels and cryogels in food applications. Considering the attempt to produce oleogels by using cellulose, cryogels were particularly interesting for their high capability to absorb large quantities of oil. However, monoliths resulted in hard materials not applicable to mimic the functionalities of plastic fat. Thus, there is the need to go further by designing solutions allowing the conversion of cellulose cryogels into plastic materials.

# 5. CELLULOSE-BASED OLEOGELS OBTAINED THROUGH THE CRYOGEL TEMPLATE APPROACH

## 5.1. Introduction and Aim of the Study

As exposed in Chapter 4, the physical properties of the solid monolithic material entrapping oil were far from those of plastic required for a fat alternative, thus hardly fitting with its applicability as a food ingredient. A proposed solution presented in the literature is represented by the reduction in the size of the monoliths into dried porous particles, as already successfully applied to other biopolymers such as whey (De Vries, Gomez, et al., 2017; Plazzotta et al., 2020), potato (Jung et al., 2023), and egg white proteins (Alavi & Ciftci, 2023). To our knowledge, limited efforts are documented in the literature on the application of polysaccharides in oleogel production.

In this study, the potentiality of cellulose cryogel particles was investigated, by forming, grinding, and freeze-drying 5% (w/w) cellulose hydrogels. The obtained particles were sieved to separate the fraction with dimensions lower than 100 µm, compatible with a food application. The particles were then dispersed in sunflower oil at different cryogel-to-oil ratios and characterized for firmness, rheological properties, and physical stability (oil holding capacity). Moreover, the behavior of the oleogel upon gastrointestinal digestion was evaluated. Results open the possibility of exploiting cellulose as a novel oleogelator.

Results here presented are ready to be submitted to Polymers:

> Ciuffarin, F., Plazzotta, S., Calligaris, S., Gelas, L., Budtova, T., Manzocco, L. Structure and digestibility of cellulose oleogels though the cryogel template approach. Polymers.

# 5.2.  Materials and Methods

## 5.2.1. Materials

Microcrystalline cellulose (Avicel®, pH-101, degree of polymerization 180 as declared by the manufacturer) and NaOH were purchased from Sigma Aldrich. Sunflower oil was obtained from a local store. Deionized water was made with System Advantage A10® (Millipore S.A.S, Molsheim, France).

## 5.2.2. Cryogel Particles

Cellulose hydrogel monoliths (5%, w/w) were prepared according to Ciuffarin, Négrier, et al. (2023) from microcrystalline cellulose. Briefly, MCC was dissolved in sodium hydroxide solution (8%, w/w) at -5 for 2 h, gelled at 50 °C for 2 h, and coagulated with several washing steps of deionized water.

Hydrogel monoliths were added (2:1, w/w) with deionized water and ground using a high-speed homogenizer (DI 25 Basic, IKA Werke, Staufen im Breisgau, Germany) at 14,000 rpm for 3 min. The obtained dispersion was placed in aluminum trays (8 × 15 cm), frozen at -40 °C for 45 min in a blast chiller (FAB25 Electrolux, Italy), and finally freeze-dried. The freeze-dryer (EPSILON 2-4 LSCplus, Del Tek, Naples, Italy) was set at 0.2 mBar and the following steps were performed: 20 min at -30 °C, 24 h at -20 °C, 24 h at -10 °C, 8 h at 0 °C, 16 h at 10 °C, and finally at 20 °C for 8 h. The resulting cellulose cryogel powder was stored in a desiccator containing silica at room temperature until use.

The cryogel powder was finally sieved (FTS-0200, Filtra Vibracion, Barcelona, Spain) and the fraction size < 100 μm was used to prepare oleogels.

## 5.2.3. Cryogel-templated Oleogels

An amount of 1.0 g of cellulose cryogel particles was manually mixed with increasing amounts of sunflower oil (SO), leading to systems with an oil content ranging from 60 to 80% (w/w).

## 5.2.4. Cryogel Particles Characterization

### 5.2.4.1.  Image Acquisition

Sample images were acquired using an image acquisition cabinet and a Google Pixel 6 smartphone (Alphabet, Mountain View, California, USA). The light was provided by a LED strip properly placed to minimize shadow and glare.

### 5.2.4.2. Bulk Density

The cellulose cryogel powder was carefully filled into a graded cylinder (1.5 cm in diameter) and its weighed. The bulk density was then calculated from the particle mass (m) and the sample bulk volume ($V_b$) (Eq. 1):

$$\rho_b = \frac{m}{V_b}$$ 

(Eq. 1)

### 5.2.4.3. Porosity

Cryogel powder porosity (%) was estimated based on the following equation (Eq. 2) (Druel et al., 2018):

$$Porosity\ (\%) = \left(1 - \frac{\rho_b}{\rho_t}\right) \cdot 100$$ 

(Eq. 2)

where $\rho_b$ (g cm$^{-3}$) is the bulk density of the powder and $\rho_t$ (g cm$^{-3}$) is its true density (*i.e.*, skeletal density). In particular, $\rho_t$ was considered as MCC true density ($\rho_t$ = 1.46 g cm$^{-3}$) (C. Sun, 2005b).

### 5.2.4.4. Morphology

SEM micrographs were obtained using a MAIA-3 (Tescan, Brno, Czech Republic), equipped with detectors of secondary and back-scattered electrons. The internal cross-section of the samples was coated with a 14 nm layer of platinum with a Quorum Q150T metallizer (Quorum Technologies, East Sussex, UK) to prevent the accumulation of electrostatic charges and images' defaults. The observations were performed with an acceleration voltage of 3 kV.

### 5.2.4.5. Specific Surface Area

The specific surface area ($S_{BET}$) was determined by measuring $N_2$-adsorption isotherm at 77 K with the Micromeritics ASAP 2020 (Norcross, Georgia, USA) and using the BET approach (Brunauer et al., 1938). Before measurements, samples were degassed for 5 h at 70 °C.

## 5.2.5. Characterization of Cryogel-based Oleogels

### 5.2.5.1. Firmness

Firmness was measured by a uniaxial compression test using an Instron 4301 (Instron LTD., High Wycombe, UK) according to Jung et al. (2023). In brief, an accurate volume of oleogel (2 mL) was transferred in a 5 mL glass beaker, leveled, and analyzed using an 8.1 mm diameter cylindrical probe mounted on a 500 N compression head at a 25 mm min$^{-1}$ crosshead speed.

Force-distance curves were obtained from the compression tests and firmness was taken as the maximum force (N) required to penetrate the sample for 2 mm.

### 5.2.5.2. Oil Holding Capacity

About 1 g of oleogel was weighted into a microcentrifuge tube and centrifuged at 14,900 ×$g$ for 20 min at 20 °C (Mikro 120, Hettich Zentrifugen, Andreas Hettich GmbH and Co, Tuttlingen, Germany). The separated oil phase was accurately drained with absorbent paper and the sediment weighed. The oil holding capacity (OHC) was expressed as the percentage of oil retained by the oleogel as compared to the initial oil content.

### 5.2.5.3. Rheological Properties

The viscoelastic properties (moduli G', G" and tan δ) of the oleogels were tested using an RS6000 Rheometer (Thermo Scientific RheoStress, Haake, Germany), equipped with a Peltier system for temperature control. Measures were performed using a sand-blasted parallel plate geometry at 20 °C with a gap of 2.0 mm. Oscillatory sweep tests to identify the linear viscoelastic region (LVR) were performed increasing stress from 10 to $1 \times 10^4$ Pa at 1 Hz frequency. Critical stress (Pa) was identified as the stress value corresponding to a 10% drop in G' value. Frequency sweep tests were then performed increasing frequency from 0.1 to 10 Hz at stress values selected in the LVR previously recorded.

## 5.2.6. Data Analysis
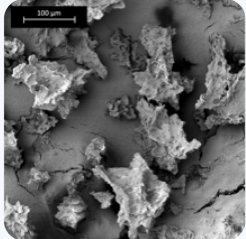
Data were expressed as the mean ± standard error of at least two measurements from two experimental replicates (n ≥ 3). Statistical analysis was performed by using R v. 4.0.3 (The R Foundation for Statistical Computing). ANOVA test was used to determine statistically significant differences between means ($p < 0.05$). Bartlett's test was used to check the homogeneity of variance ($p \geq 0.05$) and the Tukey test was used as a post hoc test ($p < 0.05$).

# 5.3. Results and Discussion

### 5.3.1. Characterization of Cellulose Cryogel Particles

Table 18 shows the macroscopic and microscopic features, density, porosity, and $S_{BET}$ of cellulose cryogel particles obtained from grinding 5% (w/w) cellulose hydrogels.

Table 18. Appearance, microstructure, bulk density, porosity, and specific surface area ($S_{BET}$) of cellulose cryogel powder.

| Macroscopic Appearance | SEM microstructure | Bulk density (g cm$^{-3}$) | Porosity (%) | $S_{BET}$ (m$^2$ g$^{-1}$) |
|---|---|---|---|---|
|  |  | 0.31 ± 0.01 | 78.4 ± 0.5 | 4.8 ± 0.9 |

The cryogel powder was made of particles having dimensions lower than 100 μm with irregular shapes and characterized by sharp edges and uneven surfaces. Similar particle morphology has been previously observed in particles obtained by freeze-drying and grinding of whey protein hydrogels as well as by combinations of maltodextrin with ι-carrageenan or soybean protein (Papoutsis et al., 2018; Plazzotta et al., 2020). These observations were compared to the SEM micrographs performed by Mahdi et al. (2018) on the original MCC. The latter was s formed by particles with spheroidal shape and smoother surfaces as compared to those observed for cryogel particles. The density and the porosity of the cryogel particles (Table 18) were respectively lower and higher than those of the native MCC (density 0.42 g cm$^{-3}$; porosity 71%). The internal surface area ($S_{BET}$), which is related to the presence of mesopores (*i.e.*, pores in the 2 – 50 nm range), was also higher than that of the MCC (0.59 – 0.64 m$^2$ g$^{-1}$, Vehovec et al., 2012).

Overall, the proposed cryogelation process caused the conversion of regular-shape particles of crystalline cellulose into cryogel particles characterized by rough surfaces, lower density, and higher porosity.

### 5.3.2. Cellulose Oleogels

To assess the capacity of cellulose cryogel particles to entrap oil, they were manually mixed with sunflower oil at different particle-to-oil ratios and the obtained systems were characterized.

The formation of a semi-solid material assimilable to an oleogel was visually evaluated by assessing the ability of the mixtures to form a cohesive and continuous material able to stick to the spatula when turned upside-down. The firmness of the samples was also evaluated. Figure 26 illustrates the visual appearance and the firmness of the particle-oil mixtures at varying oil content.
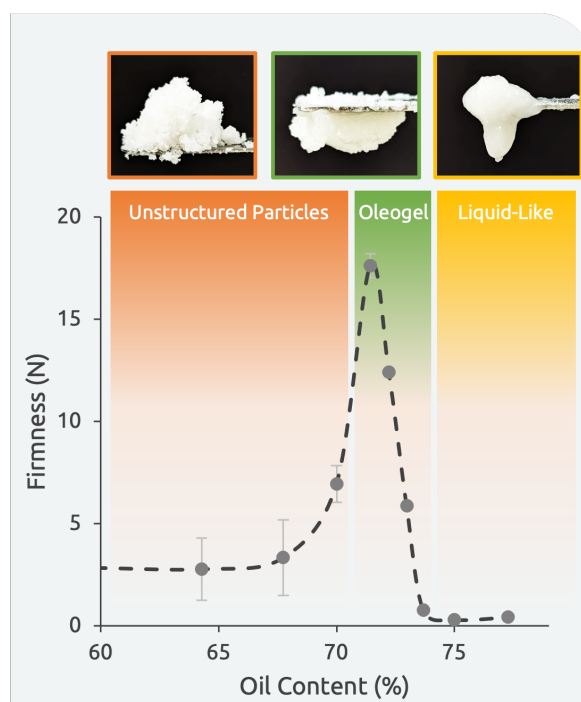


Figure 26. Visual appearance and firmness of mixtures of cellulose cryogel particles with sunflower oil at increasing oil content.

MCC exhibited no ability to structure oil, showing evident oil release independently from the particles/oil ratio (data not shown). A different behavior was noted for cellulose cryogel particles upon oil addition (Figure 26). At oil content lower than 71% (w/w), the cryogel-oil mixtures resulted in a grainy matrix with visible aggregates of particles not able to stick together (unstructured particles). According to these observations, the particle aggregates were easily displaced during compression, accounting for low firmness values (Figure 26). In these samples, the oil was probably mainly absorbed into the inner pores or adsorbed onto the cryogel particle surface, with no interaction among particles. By increasing the oil content up to 71-74% (w/w), spreadable materials with no evident oil release and creamy appearance were obtained. These mixtures showed significantly higher firmness than the other samples, which can be attributed to the formation of a gel network among cellulose particles. In particular, it can be hypothesized that, in this oil content range, the oil was not only absorbed into the cryogel pores or adsorbed onto particle surfaces but was also entrapped in a network made of cellulose particles interacting via surface hydrophilic interactions (De Vries, Lopez

Gomez, et al., 2017; Plazzotta et al., 2020; Jung et al., 2023). It should be noted that these samples showed no oil release during storage at ambient conditions for up to 4 months, as confirmed by the assessment of OHC, which resulted in all cases equal to 100%. Finally, upon further increasing the oil content (> 74%, w/w), samples showed a liquid-like behavior with reduced firmness. In these conditions, it can be hypothesized that the network formed by cellulose particles was weakened and eventually destructured, due to a dilution effect of increasing oil amount. Analogous firmness trends were previously reported by Jung et al. (2023), considering oleogels based on whey and potato protein porous powders with oil content in the 70-84%, (w/w) range.

To demonstrate the gel-like behavior of the samples containing oil in the range of 71-74%, their rheological properties were studied (Figure 27 and Table 19).
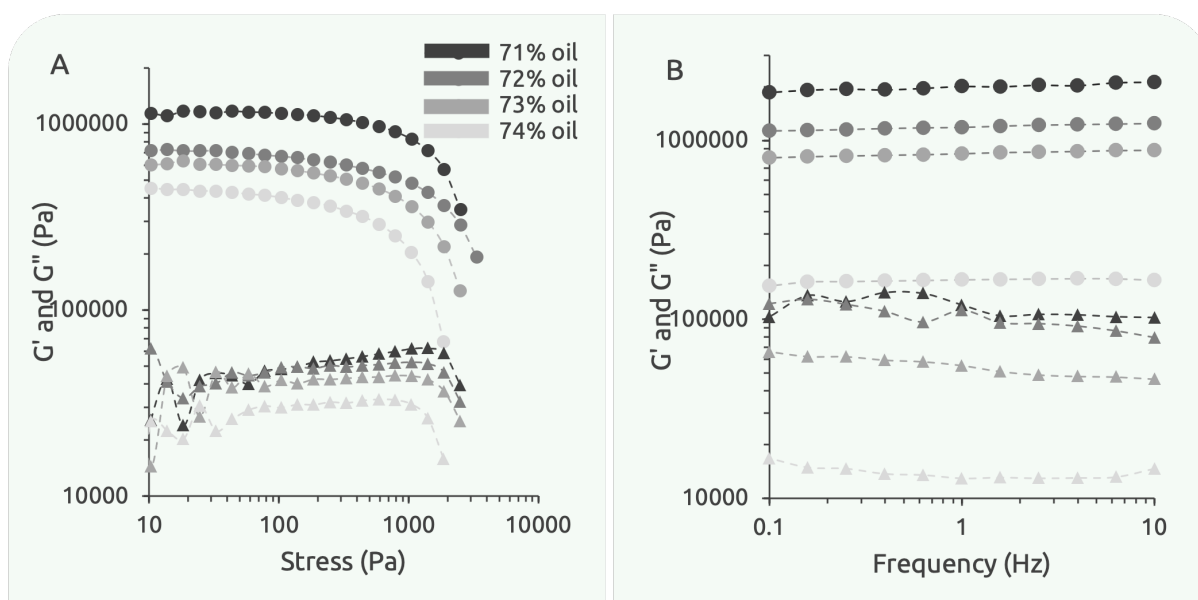


Figure 27. G' (○), and G'' (△) from amplitude (A) and frequency sweep (B) of cryogel particles at increasing oil content (71-74% range). Standard deviation bars were omitted to improve graph readability.

All the samples exhibited a gel-like behavior, being the elastic modulus (G') greater than the viscous one (G''). As the stress gradually increased, the critical value delimiting the linear viscoelastic region (LVR) was reached, resulting in a drastic drop in the response of the material (Figure 27A). As expected, with the increase in oil content, the critical stress and the G' value decreased (Figure 27A, Table 19), confirming firmness data (Figure 26). These results support the hypothesis of the formation of a particle-particle network, whose structure was weakened upon the increase of the oil fraction in the system. The viscoelastic behavior of the samples was further investigated through frequency sweep analysis (Figure 27B). The storage modulus (G') and the loss modulus (G'') exhibited parallel patterns, unaffected by the applied

frequency. Moreover, all systems showed the G''/G' ratio (*i.e.*, Tan δ, Table 19), close to 0 indicating their solid-like nature. However, the progressive addition of oil, increased the viscous response of the oleogels, as indicated by the increase in Tan δ value (Table 19). In the literature, G' and critical stress have been previously indicated as key parameters in the comparison of the rheological properties of oleogels with those of traditional fats (Blake & Marangoni, 2015). Notably, the values displayed by the cellulose oleogel were in the range of G' ($1 - 50 \times 10^5$ Pa) and critical stress ($150 - 1000$ Pa) values of most commercial fats (Calligaris et al., 2021; Patel et al., 2020).

Table 19. Rheological parameters (critical stress, G', G'' and Tan δ) of cryogel particles at increasing oil content.

| Oil Content (%) | Critical Stress (Pa) | G' × 10⁵ (Pa) | G'' × 10⁵ (Pa) | Tan δ |
|---|---|---|---|---|
| 71 | 403.0 ± 62.3 [a] | 21.3 ± 1.8 [a] | 1.2 ± 0.0 [a] | 0.055 ± 0.006 [b] |
| 72 | 154.4 ± 26.9 [b] | 10.6 ± 1.5 [b] | 0.7 ± 0.1 [b] | 0.072 ± 0.001 [a] |
| 73 | 142.8 ± 40.9 [b] | 8.1 ± 0.4 [c] | 0.5 ± 0.0 [c] | 0.070 ± 0.002 [a] |
| 74 | 127.3 ± 20.1 [b] | 1.4 ± 0.3 [d] | 0.1 ± 0.0 [d] | 0.068 ± 0.001 [a] |

[a-d]: In the same column, mean values indicated by different letters are statistically different ($p < 0.05$).

Based on the above-reported results, the conversion of cellulose into cryogel particles was demonstrated to give this biopolymer a peculiar capacity to entrap oil, forming viscoelastic oleogels in a restricted oil content range. Both the oil content and the rheological properties of the obtained cellulose oleogels resulted comparable to that reported for oleogels obtained through the dried template approach using both whey and potato proteins with 81-85% and 83-89% (w/w) oil content, respectively (I. Jung et al., 2023; Plazzotta et al., 2021).

# 5.4. Conclusions

This study demonstrates the feasibility of cellulose conversion into cryogel porous particles as a possible strategy to generate oleogels. Oleogels presenting rheological properties ascribable to those of fats were only obtained in a specific range of oil content (71 – 74%, w/w). The capability of cellulose particles to entrap oil was attributed not only to their ability to absorb or adsorb oil but also to the formation of a network among hydrophilic particles. These findings open interesting possibilities for potential further applications of cellulose oleogels in food products.

Moreover, these results also demonstrated the feasibility of the dried template approach to obtain oleogels, both in the form of monoliths and spreadable materials. In this context, the structure of the materials resulted in the pivotal factor in determining the further functionalities. So, it can be highly interesting to move ahead considering other biopolymers as possible oil structuring agents. Thus, in the next chapters, proteins were employed.

# 6. POTENTIALITIES FOR OIL STRUCTURING OF PEA PROTEIN CRYOGEL MONOLITHS PREPARED AT DIFFERENT pH

## 6.1. Introduction and Aim of the Study

Pea proteins exhibit distinctive nutritional characteristics, due to their low risk of allergenicity, and high antioxidant potential (Oliete et al., 2018). Additionally, they are the focus of many research efforts due to their interesting technological functionalities. Among others, the gelling capacity is the pivotal functionality in the attempt to use pea proteins as an oil structuring agent.

Pea proteins form gels by the heat-induced gelation is characterized. This process is reported to be a multi-stage mechanism (Zhu et al., 2022): the gelation of pea proteins requires the thermal unfolding of the native molecules, exposing interaction sites, followed by intermolecular interactions among the unfolded molecules. Ultimately, the formation of a network is achieved through the agglomeration of aggregates, contributing to the overall gelation process (Clark et al., 2001)

In this context, this Chapter focuses on the possibility of using a pea protein isolate as a building block for the formation of cryogel porous material intended for oil structuring. To this aim, this study focused on the characterization of pea protein-based hydrogel monoliths prepared at pH 7.0, at their isoelectric point (pI, 4.3), and using a pH-shifting approach (from pH 7 to 12 and again to 7). Furthermore, dried monoliths were tested for their ability to absorb oil. This study must be considered as a proof of concept for the development of porous materials for pea protein-oleogel production.

This study was carried out in collaboration with the Food Structure and Function group of Ghent University, Belgium, under the supervision of Filip van Bockstaele during the Erasmus period spent abroad in 2023.

# 6.2.   Materials and Methods

## 6.2.1. Materials

Pea protein isolate powder (PPI, Pisane 43071-C9; 80% protein, 7% moisture, 5% total fat, 5% total ash, and 3% carbohydrate) was bought from Bacare & Co Ltd. (United Kingdom). Nile Red and Fast Green dyes, HCl, and NaOH were purchased from Sigma Aldrich (Milan, Italy). Sunflower oil was purchased in a local store. Deionized water was also used.

## 6.2.2. Samples Preparation

### 6.2.2.1.   Hydrogel Preparation

Pea protein hydrogels were prepared using the method exposed by Betz et al. (2012) with some modifications. In particular, PPI was dispersed at 20% (w/w) concentration in deionized water at room temperature and mixed with a high-speed homogenizer (DI 25 Basic, IKA Werke, Staufen im Breisgau, Germany) at 14,000 rpm for 5 min to form a viscous matrix. The pH of the samples was adjusted to 7.0 or 4.3 (*i.e.*, the isoelectric point), obtaining samples called $PP_{7.0}$ and $PP_{4.3.}$ Additionally, one sample was prepared by applying a pH shift procedure as described by (Zhi et al., 2022): the dispersion pH was initially increased to pH 12, sonicated (Sonicator 250, Branson Ultrasonics Co., Danbury, U.S.) for 20 min, maintained at room temperature for 2 h, and finally, the pH was adjusted at 7. This sample was called $PP_{pHshift}$. In all cases, NaOH 2M or HCl 2 M were used to change the pH. The obtained samples were inserted into 50 mL and 2.5 cm in diameter plastic tubes and heated at 90 °C for 20 min in a temperature-controlled water bath to induce protein gelation.

Finally, samples were cooled in 4 °C water for 5 min, stored overnight at 4 °C, and cut into monoliths with a height of ~1.5 cm to obtain the hydrogel monolith.

### 6.2.2.2.   Cryogel Monolith

Hydrogel monoliths were frozen by immersing the sample into liquid nitrogen and dried using a freeze dryer (SP VirTis BenchTop SLC, SP scientific, NY, USA) for 2 days at a condenser temperature of -108 °C under a vacuum pressure of 0.015 kPa. Monoliths were stored in a desiccator at room temperature until use.

### 6.2.3. Dry templates Characterization

#### 6.2.3.1. Oil Structuring Capacity

Cryogels monoliths were immersed into a sunflower oil-containing baker at 20 °C. At defined time intervals, samples were withdrawn, wiped with absorbent paper, and weighed ($W_t$). The experiment continued until a stable weight, referred to as the *plateau* value, was achieved, as evidenced by three consecutive measurements showing no weight fluctuations. The absorption oil at each time point was quantified as the ratio between the weight gained at time t (in minutes) and the initial weight ($W_0$) of the cryogel or aerogel sample (equation 1).

$$Absorbed\ solvent\ \left(g_{solvent}/g_{dry\ matter}\right) = \frac{(W_t - W_0)}{W_0} \qquad \text{(Eq. 1)}$$

The maximum solvent absorption capacity was taken at *plateau* value.

#### 6.2.3.2. Image Acquisition

Sample images were acquired using a matte black background and a Google Pixel 6 smartphone (Alphabet, Mountain View, California, USA).

#### 6.2.3.3. Monolith Firmness

The firmness of the monolith was measured by a uniaxial compression test using a 5942 Instron TA 500 Texture Analyzer (Lloyd Instrument, Bognor Regis, West Sussex, UK). To this aim, a 2 cm-height monolith was cut and analyzed using a 6.2 mm diameter cylindrical probe mounted on a 1000 N compression head at a 25 mm min$^{-1}$ crosshead speed. Force-distance curves were obtained from the compression tests and firmness was taken as the maximum force (N) required to penetrate the sample for 2 mm.

#### 6.2.3.4. Envelope Density

Bulk and envelope density should not be confused. The envelope density ($\rho_e$) is determined for porous material when the pore void spaces are included in the measure, thus in the case of monoliths. In this regard, monolith cryogel envelope density was calculated as the ratio between the monolith volume and its weight.

The envelope density was calculated from the particle mass (m) and the sample volume ($V_b$) (Eq. 2):

$$\rho_b = \frac{m}{V_b} \qquad \text{(Eq. 2)}$$

### 6.2.3.5. Porosity

Cryogel porosity (%) was estimated based on the following equation (Eq. 3) (Druel et al., 2018):

$$Porosity\ (\%) = \left(1 - \frac{\rho_b}{\rho_t}\right) \cdot 100 \qquad \text{(Eq. 3)}$$

where $\rho_b$ (g cm$^{-3}$) is the bulk or envelope density of the powder and $\rho_t$ (g cm$^{-3}$) is its true density (*i.e.*, skeletal density). In particular, $\rho_t$ was considered as PP true density ($\rho_t = 1.35$ g cm$^{-3}$) (Fischer et al., 2009).

### 6.2.3.6. Cryo-scanning Electron Microscopy

The shape of the starch granules was visualized using a JSM-7100F TTLS LV TFEG-SEM (Jeol Europe BV, Zaventem, Belgium) under high vacuum and at an accelerated voltage of 5 keV. Prior to electron beam targeting, the samples were vitrified in liquid nitrogen and transferred to a PP3000T cryo-transfer system (Quorum Technologies Ltd., East Sussex, U.K.) at -140 °C. The samples were subjected to a short sublimation step of 10 min at -90 °C. Prior to the transfer from the cryo-preparation room to the scanning electron microscope (SEM) chamber, a thin layer of a conductive metal (Pt) was deposited on the samples.
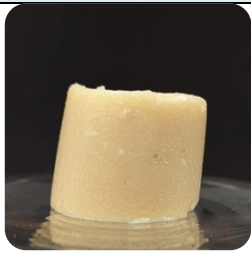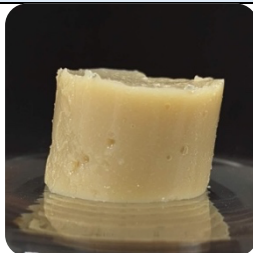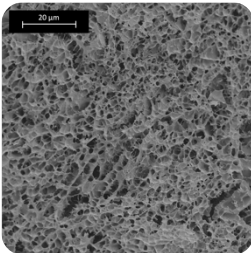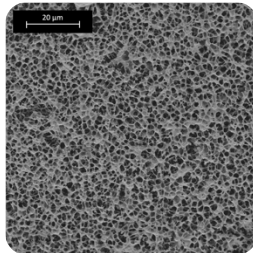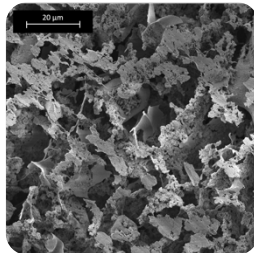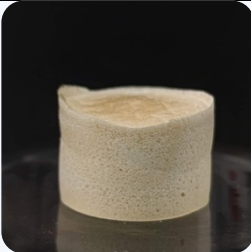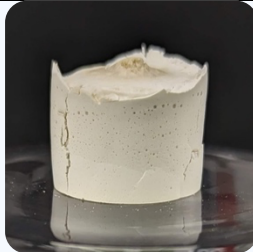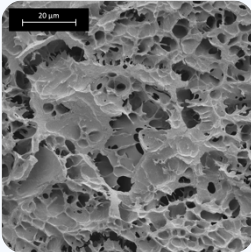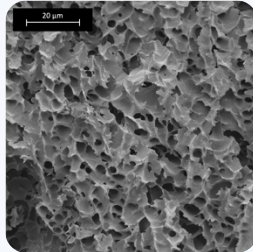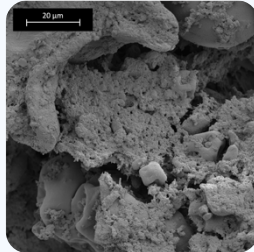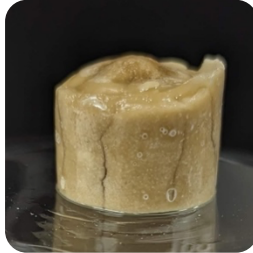
## 6.2.4. Data Analysis

Data were expressed as the mean ± standard error of at least two measurements from two experimental replicates (n ≥ 4). Statistical analysis was performed by using R v. 4.0.3 (The R Foundation for Statistical Computing). ANOVA test was used to determine statistically significant differences between means ($p < 0.05$). Bartlett's test was used to check the homogeneity of variance ($p \geq 0.05$) and the Tukey test was used as a post hoc test ($p < 0.05$).

# 6.3. Results and Discussion

Table 20 shows the macroscopic and microscopic morphology of PP-based hydrogel monoliths, the resulting systems after freeze-drying (cryogels) and finally the systems upon oil absorption (oleogel).

Table 20. Macroscopic and microscopic morphology of PP-based hydrogel, cryogel and oleogels.

| Samples | PP$_{7.0}$ | PP$_{pH-shift}$ | PP$_{4.3}$ |
|---|---|---|---|
| Hydrogel |  |  |  |
| Cryogel |  |  |  |
| Oleogel |  |  |  |

As shown in Table 20, PP$_{7.0}$ and PP$_{pH-shift}$ samples were self-standing materials able to maintain their shape, whereas the PP$_{4.3}$ mixture resulted in fragile and not self-standing. These differences can be attributed to the peculiar microstructure of the samples induced by the pH. Cryo-SEM micrographs revealed that the gelation at a neutral pH (*i.e.,* PP$_{7.0}$ and PP$_{pH-shift}$) resulted in the formation of a protein network in which water is entrapped. It is noteworthy that the pH-shift procedure led to the formation of smaller and uniform pores than the sample obtained by just adjusting the pH at 7.0. In contrast, the structure of the PP$_{4.3}$ monolith was predominantly composed of protein clusters not able to interact with the formation of a network able to retain water. The observed structures can be associated with the protein-protein interactions upon gelation. At the isoelectric point (pI), protein solubility is very low leading to the formation of protein aggregates impairing weak ionic protein-protein interactions during gelation (Felix et al., 2017). On the other side, for samples gelled at neutral pH, protein interactions were favored due to the increase of protein solubility as well as the development of disulfide bonds leading to the formation of a more developed network characterized by enhanced elasticity and firmness (Sun & Arntfield, 2011; Zhu et al., 2022). This was confirmed by the firmness value reported in Table 2, showing the highest firmness for those samples gelled at a neutral pH, and the lowest for that at the isoelectric point (PP$_{4.3}$).

As the freeze-drying process was performed, no increase in volume was recorded for monoliths (< 1%). As expected, the PP$_{4.3}$ monolith showed a general collapse of the structure with macropores associated with the inhomogeneous structure formed in the corresponding hydrogel. This is evident also by observing microstructure imaged by SEM. The other cryogels demonstrated a good capacity to maintain their structure also upon freeze-drying, with a very high porosity that resulted in 84.5 and 85.5% for PP$_{7.0}$ and PP$_{pH-shift}$, respectively (Table 21). The envelope density value in Table 21 confirmed this observation, with the sample PP$_{4.3 \, being}$ the lowest density value. By observing the microstructure, it is possible to note the gel network is still present with a general increase of void areas. This behavior is attributable to the ice crystal formation inside the structure leading to pore expansion. The different firmness recorded among PP$_{pH-shift}$ and PP$_{7.0}$ can be explained by the different strengths in molecule interactions experienced by the proteins during the shift towards pH 12. This hypothesis is in accordance with the study of Tanger et al. (2022) that measured the interaction strength of PP gels at different pH.

Table 21. Firmness, envelope density and porosity of PP-based hydrogel, cryogels and oleogels obtained by gelling PPI at different pH conditions.

| Sample | Firmness (N) | | | Envelope Density (g cm$^{-3}$) | Porosity (%) |
|---|---|---|---|---|---|
| | Hydrogel | Cryogel | "Oleogel" | | |
| PP$_{7.0}$ | 0.29 ± 0.02 [a] | 55.9 ± 7.4 [a] | 81.2 ± 22.1 [a] | 0.209 ± 0.007 [a] | 84.5 ± 0.5 [b] |
| PP$_{4.3}$ | 0.18 ± 0.02 [c] | 0.42 ± 0.10 [c] | - | - | - |
| PP$_{pH-shift}$ | 0.26 ± 0.03 [b] | 37.0 ± 5.0 [b] | 80.1 ± 28.8. [a] | 0.195 ± 0.006 [a] | 85.5 ± 0.5 [b] |

These outcomes underscore the feasibility of creating porous materials from PP using various gelation methods, thereby opening avenues for successful interactions with food solvents, such as oil. The kinetics of oil absorption in PP cryogel is shown in Figure 28.
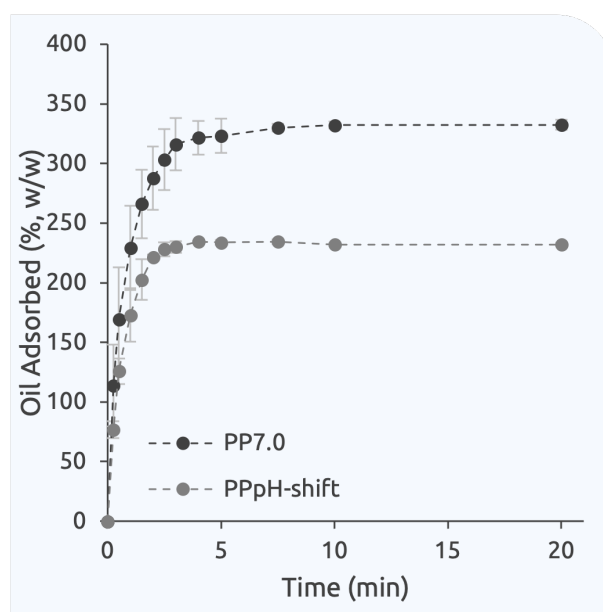


Figure 28. Oil absorbed by cryogel monoliths prepared by gelling PPI at pH 7.0 and with a 7-12-7 pH-shift.

Upon contact with oil, an extremely fast absorption was observed for both PP$_{STD}$ and PP$_{pH-shift}$ samples (Figure 28), reaching the absorption *plateau* in under 5 min. By comparing the maximum absorbing capability, PP$_{7.0}$ has proven to be able to absorb a higher amount of liquid oil, thus increasing its initial weight by 332% (w/w) compared to PP$_{pH-shift}$ (232%, w/w). This can be attributed to the micromorphology of the sample, characterized by pores of larger dimensions (Table 20). The absorbing capacity was compared with other similar studies retrievable in the literature and in this thesis (Table 22).

Table 22. Absorbing capacity of different monolith porous systems found in the literature.

| Gelator | Dry Template | Porosity (%) | Maximum absorption ($g_{oil}/g_{dry\ material}$) | References |
|---|---|---|---|---|
| Pea Proteins | Cryogel | ~ 85 | 2.4 – 3.5 | - |
| Cellulose | Cryogel | ~ 95 | 10 - 13 | Chapter 4 |
| | Aerogel | ~ 93 | 4 - 8 | |
| Whey Proteins | Cryogel | 84* | ~ 3 | Manzocco et al., 2022 |
| | Aerogel | 79* | ~ 4 | |
| κ-carrageenan | Aerogel | 94 | 4.7 | Plazzotta et al., 2019 |
| | Cryogel | 96 | 31 | |
| κ-carrageenan + Lettuce fillers | Aerogel | 90 | 16.6 | |
| | Cryogel | 88 | 18.9 | |
| Cellulose + TiO$_2$ coating (non-food-grade) | Aerogel | - | 28 | Chin et al., 2014 |
| Kapok/cellulose (non-food-grade) | Aerogel | 99 | 141 | Zhang et al., 2021 |

* Values estimated from density using Eq. 2.

As detailed in Table 22, pea protein (PP) cryogel samples exhibited lower oil absorption capacity (2.4 - 3.5 $g_{oil}/g_{cryogel}$) compared to that of cellulose. However, the oil absorption capacity resulted comparable to that of other protein-based systems, such as whey protein aerogel and cryogel (Manzocco et al., 2022). These results can be attributed to the distinct structure of the materials, influenced by the drying technique, the gelator type and concentration.

Despite the quite interesting results, both cryogel monoliths did not show any plastic behavior, thus limiting their application in the food sector. These promising results open the possibility of the formation of cryogel particles for structuring oil into plastic materials.

## 6.4. Conclusions

This Chapter demonstrated the feasibility of converting pea protein hydrogels into porous cryogels able to absorb liquid oil. The microstructure of the hydrogel and then of the resulting cryogel was shown to be the critical factor influencing the functionality of the material. Notably, the gelation at the isoelectric point was found to be ineffective in achieving the formation of a stable hydrogel and thus a cryogel able to maintain its shape. This behavior was attributed to the reduced interactions between proteins in these conditions. On the other hand, the gelation at neutral pH was identified as the optimal condition for achieving these objectives.

Starting from these findings it would be interesting to investigate how to improve the oil absorption capacity of pea proteins with the final aim of obtaining a fat-like material. The analysis in this way just started during the period spent in the Food Structure & Function laboratories under the supervision of Filip van Bockstaele, however the results, although promising, were in the early stages.

The research was thus further directed toward whey proteins as structuring agents, due to their well-known gelling capacity.

# 7. OIL STRUCTURING CAPABILITY OF WHEY PROTEIN CRYOGEL PARTICLES OBTAINED THROUGH GELATION AT DIFFERENT pH

## 7.1. Introduction and Aim of the Study

Whey protein, a byproduct of cheese production, has garnered significant attention for its versatile applications in the food industry (Królczyk et al., 2016). From a functional standpoint, whey protein displays remarkable properties as an emulsifier, stabilizer, and gelling agent, making it an attractive option for enhancing the texture and nutritional profile of various food products (Baldissera et al., 2011). Beyond its nutritional value, whey protein has emerged as a valuable resource in terms of sustainability. The use of whey protein helps reduce waste by transforming what would otherwise be considered byproducts into valuable ingredients. Incorporating whey protein into food side-stream processes not only aligns with sustainable practices but also contributes to the creation of innovative, value-added food formulations. In this context whey protein-based porous materials could enlarge the use of this material (Draijer et al., 2023).

From a processing perspective, forming a hydrogel from a whey protein isolate (WPI) is a straightforward procedure, typically involving the denaturation of a protein solution through heating (Andlinger et al., 2021; Kleemann et al., 2018; Selmer et al., 2015). This process results in a gel stabilized by disulfide bonds, hydrogen bonding, and hydrophilic interactions (Clark et al., 2001b; Shimada & Cheftel, 1988). pH considerations are crucial, as pH significantly influences the characteristics of the hydrogel and the resulting dry material, whether it becomes an aerogel or a cryogel (Betz et al., 2012; Clark et al., 2001b; Errington & Foegeding, 1998). In the case of WPI, heat treatment near the isoelectric point (pI) induces the formation of spherical particles, approximately 100 nm in diameter, known as microgels, a hydrated protein network (Donato et al., 2011; Nicolai, 2016; Nicolai & Durand, 2013). Adjusting the concentration of the WPI solution enables the aggregation of these microgels into structures that can be molded into self-supporting hydrogels with desired shapes and dimensions (Nicolai & Durand, 2013). These hydrogels can undergo different drying techniques to

produce aerogels, cryogels, or xerogels (Betz et al., 2012). The primary focus of the subsequent pivotal study was on forming and characterizing WP-based hydrogels from WPI solutions at various pH levels. The latter part of the investigation centered on reducing the size of these hydrogels into cryogel particles and assessing their performance as agents for structuring oil. In the last part, the best performing oleogel sample was used in a food formulation, a cocoa cream, in which traditionally, WPI and palm oil are used.

Part of this study was carried out in collaboration with the Food Structure and Function group of Ghent University, Belgium, under the supervision of Filip van Bockstaele during the Erasmus period spent in 2023.

# 7.2. Materials and Methods

### 7.2.1. Materials

In the study were used whey protein isolate (WPI, 94.7% protein content; 74.6% β-lactoglobulin, 23.8% α-lactalbumin, 1.6% bovine serum albumin, Davisco Food International Inc., Le Sueur, MN, USA), Nile Red and Fast Green dyes, and HCl purchased from Sigma Aldrich (Milan, Italy).

### 7.2.2. Hydrogel Preparation

Whey protein hydrogels were made according to the method of Betz et al. (2012). In particular, 20% (w/w) of whey protein isolate (WPI) was dissolved in double-distilled water, under continuous stirring at room temperature for 24 h. The pH of the WPI suspension was then adjusted to 4.8, 5.7, and 7.0 (HI5221, HANNA Instruments, Padua, Italy) using a 6 M HCl solution. Aliquots of 40 mL were then introduced in 50 mL and 2.5 cm in diameter plastic tubes and heated at 90 °C for 20 min in a temperature-controlled water bath to induce protein denaturation. Samples were finally cooled in ice water for 15 min, stored overnight at 4 °C, and cut into monoliths with a 1.5 cm height and 2.5 cm diameter.

### 7.2.3. Cryogel Particles Preparation

Monoliths were manually broken and added in a ratio of 2:1 v/v to water to be easily homogenized using a high-speed homogenizer (DI 25 Basic, IKA Werke, Staufen im Breisgau, Germany) at 14,000 rpm for 3 min. The obtained samples were placed in aluminum containers, frozen at -40 °C for 45 min in a blast chiller (FAB25 Electrolux, Italy), and freeze-dried (EPSILON 2-4 LSCplus, Del Tek, Naples, Italy). The freeze-dryer was set at 0.2 mBar at different time/temperature settings: 20 min at -30 °C, 24 h at -20 °C, 24 h at -10 °C, 8 h at 0 °C, 16 h at 10 °C, and finally at 20 °C for 8 h. The resulting freeze-dried particles were sieved by using a vibrating sieve (Digital Electromagnetic Sieve Shaker, Filtra Virbacion, Barcelona, Spain), and the <100 μm was collected. Particles were stored in a desiccator at room temperature until use.

### 7.2.4. Oleogel Preparation

An amount of 1.0 g of WP aerogels ore native WPI was weighed, and sunflower oil (SO) was gradually added, under continuous manual mixing. In this way, oleogels containing increasing oil amounts from 30 to 70% (w/w) were obtained.

### 7.2.5. Monolith Characterization

#### 7.2.5.1. Image Acquisition

Monolith images were acquired by using an image acquisition cabinet (Immagini and Computer, Bareggio, Italy) equipped with a digital camera (EOS 550D, Canon, Ota City, Tokyo, Japan) and 60 mm lens with 2.8 focal aperture (Canon, Ota City, Tokyo, Japan). The digital camera was placed on an adjustable stand positioned 40 cm in front of a black cardboard base where the sample was placed. The light was provided by four 23 W frosted photographic floodlights, in a position allowing minimum shadow and glare. Other camera settings were: shutter time 1/25 s, f/10, and ISO 100. Images were saved in jpg format.

#### 7.2.5.2. Monolith Firmness

The firmness of the monolith was measured by a uniaxial compression test using an Instron 4301 (Instron LTD., High Wycombe, UK). To this aim, a 2 cm-height monolith was cut and analyzed using a 6.2 mm diameter cylindrical probe mounted on a 1000 N compression head at a 25 mm min$^{-1}$ crosshead speed. Force-distance curves were obtained from the compression tests and firmness was taken as the maximum force (N) required to penetrate the sample for 2 mm.

### 7.2.6. Cryogel Particle Characterization

#### 7.2.6.1. Colour

Sample colour was obtained using a tristimulus colorimeter (Chromameter-2 Reflectance, Minolta, Osaka, Japan) equipped with a CR-300 measuring head and calibrated using a standard white tile. The samples were placed on a petri dish, which was positioned on top of the calibration tile. The color was then measured and expressed in L* (lightness), a* (green-red), b* (blue-yellow) of the Hunter Scale.

#### 7.2.6.2. Bulk Density

The WP cryogel powder was carefully filled into a graded cylinder and its weighed. The bulk density was then calculated from the particle mass (m) and the sample bulk volume ($V_b$) (Eq. 1):

$$\rho_b = \frac{m}{V_b} \qquad \text{(Eq. 1)}$$

### 7.2.6.3.  Porosity

Cryogel powder porosity (%) was estimated based on the following equation (Eq. 2) (Druel et al., 2018):

$$Porosity\ (\%) = \left(1 - \frac{\rho_b}{\rho_t}\right) \cdot 100 \qquad \text{(Eq. 2)}$$

where $\rho_b$ (g cm$^{-3}$) is the bulk density of the powder and $\rho_t$ (g cm$^{-3}$) is its true density (*i.e.*, skeletal density). In particular, $\rho_t$ was considered as WP true density ($\rho_t$ = 1.35 g cm$^{-3}$) (Fischer et al., 2004).

### 7.2.6.4.  Scanning Electron Microscopy

The WP particles were placed on double-side conductive adhesive tape. After that, they were gold-sprayed on their surface using an ion sputter Coater (108 Auto, Cressington, UK). The microstructures of the WP could be visualized using an FEI Quanta 250 SEM at 1.0 kV voltage with a magnification of × 30000.

## 7.2.7. Oleogel Characterization

### 7.2.7.1.  Image Acquisition

Oleogel sample images were acquired using an image acquisition cabinet and a Google Pixel 6 smartphone (Alphabet, Mountain View, California, USA). The light was provided by a LED strip properly placed to minimize shadow and glare.

### 7.2.7.2.  Confocal Microscopy

A 0.2 % aqueous solution of Fast Green and Nile Red (Sigma Aldrich, Milan, Italy) was used to stain the proteins and the oil, respectively, by gently hand-mixing the oleogel samples. The stained samples were then placed on the microscope slide, covered with a cover slide, and observed using a confocal laser scanning microscope at 100 times magnification (Leica TCS SP8 X confocal system, Leica Microsystems, Wetzlar, Germany). Images were imported in jpeg format using the software LasX 3.5.5 (Leica Microsystems, Wetzlar, Germany).

### 7.2.7.3.  Oleogel Firmness

The firmness of the oleogels was measured by a uniaxial compression test using a 5942 Instron TA 500 Texture Analyzer (Lloyd Instrument, Bognor Regis, West Sussex, UK). To this aim, an accurate volume of oleogel (2 mL) was transferred in a 2 mm-diameter cylindrical sample container and compressed for 30 s with a 10 g-cylinder. The oleogels were then analyzed using an 8.1 mm-diameter cylindrical probe mounted on a 500 N compression head at a 25 mm min$^{-1}$ crosshead speed. Force-distance curves were obtained from the

compression tests and firmness was taken as the maximum force (N) required to penetrate the sample for 2 mm.

### 7.2.7.4. Oil Holding Capacity

The oil holding capacity (OHC) was determined by weighing about 1 g of sample into a microcentrifuge tube. Samples were centrifuged at 10,000 rpm for 15 min at 20 ◦ C (Mikro 120, Hettich Zentrifugen, Andreas Hettich GmbH and Co, Tuttlingen, Germany) and decanted the excess oil. The samples were weighed and OHC was expressed as the percentage of oil retained by the sample.

### 7.2.7.5. Rheological Properties

The viscoelastic properties (moduli G' and G") were tested using an MCR Anton Paar 302 (Anton Paar, Graz, Austria) with a Peltier system for temperature control. Measures were performed using a 25 mm sandblasted parallel plate geometry (PP25S) at 20 °C with a gap of 2.0 mm. Oscillatory sweep tests to identify the linear viscoelastic region (LVR) were performed increasing stress from 1.0 to $1.0 \times 10^4$ Pa at 1 Hz frequency. Critical stress (Pa) was identified as the stress value corresponding to a 10% drop in G' value. Frequency sweep tests were then performed increasing frequency from 0.1 to 10 Hz at stress values selected in the LVR.

### 7.2.7.6. Spreadability

The spreadability test was performed using an Instron (34TM-5, Norwood, Massachusetts, United States) with a spreadability back extrusion food cell (Instron, P369927). The cup was filled with 30g of sample. The measuring parameters consisted of a 25 mm/s penetration speed and a 5 mm penetration upon auto-detected force of 0.05 N.

## 7.2.8. Data Analysis
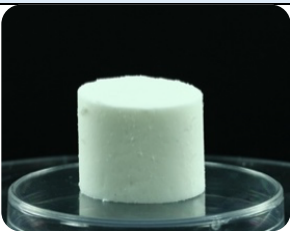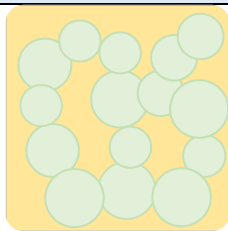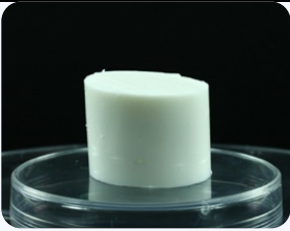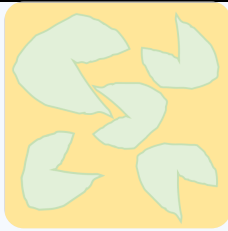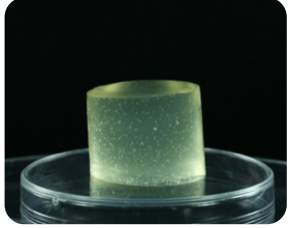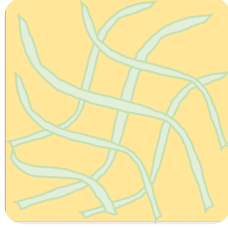
Data were expressed as the mean ± standard error of at least two measurements from two experimental replicates (n ≥ 4). Statistical analysis was performed using R v. 4.0.3 (The R Foundation for Statistical Computing). ANOVA test was used to determine statistically significant differences between means ($p < 0.05$). Bartlett's test was used to check the homogeneity of variance ($p \geq 0.05$) and the Tukey test was used as a post hoc test ($p < 0.05$).

# 7.3. Results and Discussion

## 7.3.1. Hydrogel Characterization

The appearance, color parameters and firmness values of hydrogels resulting from the gelling WPI solutions adjusted at pH 4.8 (corresponding to the isoelectric point, pI), 5.7, and 7.0 are reported in Table 23.

Table 23. Appearance, firmness, colour parameters and network schematic representation of hydrogels resulting from gelling whey protein solutions at pH 4.8, 5.7, and 7.0.

| pH | Appearance | Firmness (N) | Color | | | Network Representation |
|----|-----------|------|-------|-----|-----|----------|
| | | | L* | a* | b* | |
| 4.8 (pI) |  | 3.41 ± 0.12 [b] | 92.2 ± 0.0 [a] | -1.07 ± 0.05 [c] | 5.99 ± 0.03 [b] |  |
| 5.7 |  | 5.69 ± 0.14 [a] | 92.1 ± 0.2 [a] | -1.36 ± 0.05 [b] | 3.56 ± 0.02 [c] |  |
| 7.0 |  | 2.43 ± 0.06 [c] | 38.9 ± 1.1 [b] | 1.51 ± 0.10 [a] | 8.54 ± 0.21 [a] |  |

[a-c] means indicated by different letters are significantly different $(p < 0.05)$.

As expected, based on the literature, the pH of the WP dispersion strongly affected hydrogel properties. By gelling WP solutions at pH 7.0, a transparent light-yellow hydrogel was obtained, while the hydrogels deriving from WP solutions at pI (*i.e.*, 4.8) and pH 5.7 appeared white and opaque. These observations were confirmed by color parameters (Table 23). The hydrogels resulted also in different firmness: the highest firmness was recorded for the sample gelled at pH 5.7, followed by samples obtained at pH 4.8 and finally, that obtained at pH 7.0. The observed differences can be attributed to the peculiar gel structure induced by the pH.

According to the literature, pH 7.0 favors the unfolding of proteins that assume a fibrillar form mainly stabilized by covalent disulfide bridges, leading to the formation of a fine-stranded slightly yellow gel network (Fan et al., 2019; P. Zhu et al., 2022). By progressively reducing the pH, the charges distributed on the protein quaternary structure are increasingly neutralized, leading to protein self-folding phenomena. Under thermal gelation, folded proteins form globular strongly aggregated structures, also called microgels. The latter exhibit dimensions larger than that of natural light wavelength, favoring light scattering and resulting in an opaque hydrogel (Betz et al., 2012; Foegeding et al., 1995). These results agree with those reported by Fan et al. (2019), who characterized whey protein hydrogels in the 2-11 pH range.
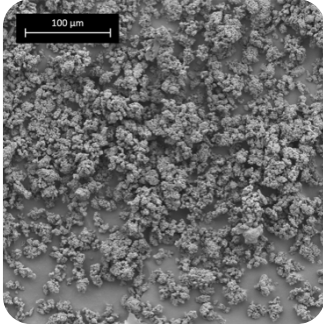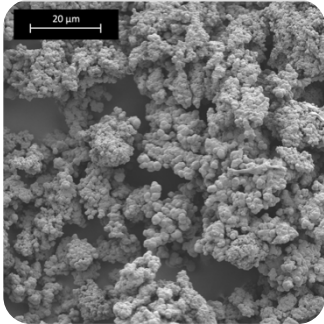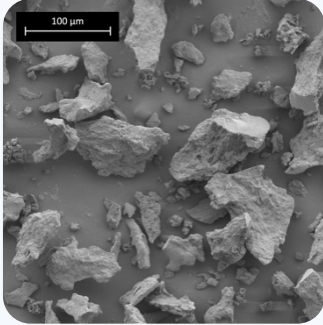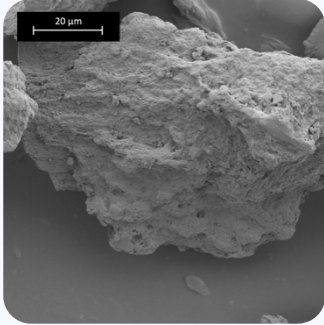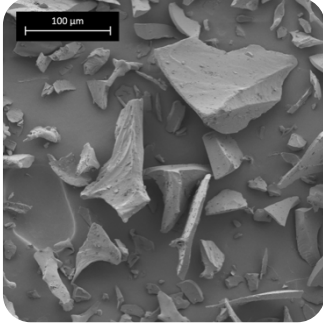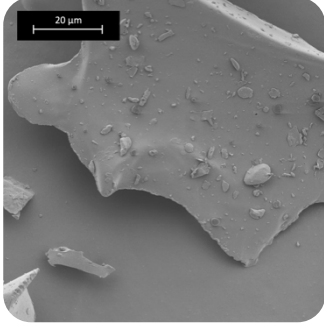
The different protein network organizations also accounted for different firmness values. The hydrogel obtained at 5.7 showed the highest firmness, followed by samples obtained at pH 4.8 and 7.0. This behavior can be explained by the different levels of entanglements of the protein microstructure. Being WPI gelled at pH 7 in the form of linear fibrils, a lower amount of entanglements is present, making them more susceptible to shear forces, ultimately resulting in reduced firmness (Vardhanabhuti et al., 2010). Conversely, as the pH approaches the pI, protein self-folding occurs, removing the interactions between different proteins, which restricts the material firmness. In the case of WPI gelled at pH 5.7, can be hypothesized that the higher firmness in comparison to the sample gelled at pH 4.8 can be attributed to the level of interactions among protein chains and the self-folding behavior occurring because of system pH. These results are in accordance with Lorenzen et al. (2006) which found pH 6 to give higher stiffness to the WPI gel, compared to that of pH 7 and 4.8.

These interesting features of protein hydrogels were further investigated to obtain cryogels intended for oil structuring.

### 7.3.2. Particle Characterization

The hydrogels having different pH were ground and freeze-dried obtaining WP particles. These particles were sieved to separate those with dimensions lower than 100 μm. Particle microstructure observed by SEM, porosity, and bulk density are reported in Table 24.

Table 24. SEM microscopic images at different magnifications, bulk density, and porosity of cryogel particles resulting from gelling whey protein solutions at pH 4.8, 5.7, and 7.0.

| pH | Density (g cm$^{-3}$) | Porosity (%) | SEM Microstructure | |
|---|---|---|---|---|
| 4.8 (pI) | 0.19 ± 0.01 [c] | 85.3 ± 0.6 [a] |  |  |
| 5.7 | 0.22 ± 0.00 [b] | 82.8 ± 0.6 [b] |  |  |
| 7.0 | 0.29 ± 0.02 [a] | 78.6 ± 0.5 [c] |  |  |

[a-d] means indicates significant differences among samples ($p < 0.05$).

First, it should be noted that the cryogel powders exhibited different density and porosity values depending on the pH, but in any case, lower than those of native WPI (0.39 ± 0.03 g cm$^{-3}$; 71.1 ± 0.3%, respectively). These results confirm the ability of hydro-gelation followed by freeze-drying to preserve the porous structure of the sample leading to particles with higher porosity than native ones, in agreement with the literature (Plazzotta et al., 2020). It is also clear observing Table 24 that the pH of the hydrogel and the protein-associated structure

greatly affected the structure of cryogels. Specifically, the cryogel obtained from hydrogels at pH 7.0 displayed the highest bulk density and the lower porosity, followed by the one at pH 5.7, and finally 4.8, suggesting an effect of the gelation pH on the morphological features of cryogel particles. To confirm this hypothesis, SEM was performed (Table 24).

The sample obtained from WPI solutions at pH 7.0 displayed particles ranging from several tenths of micrometers to 100 μm, characterized by irregular shapes with flat surfaces and sharp edges. A similar microstructure was imaged for the sample obtained at pH 5.7, but in this case, a pronounced surface roughness can be noted, confirming the literature results (Plazzotta et al., 2020). Freeze-drying of hydrogels obtained at the pI produced considerably smaller cryogel particles, not exceeding 20-30 μm, and preserving the initial microgel structure, characterized by spheroidal particles organized into aggregates, thus forming interstices, and enhancing porosity.

### 7.3.1. Oil Structuring Ability

The ability of the developed WP cryogel particles to structure liquid oil into oleogels was assessed by adding an increasing amount of oil to the powders. Figure 29 shows the visual appearance and firmness of the cryogel-oil mixtures having increasing oil content.
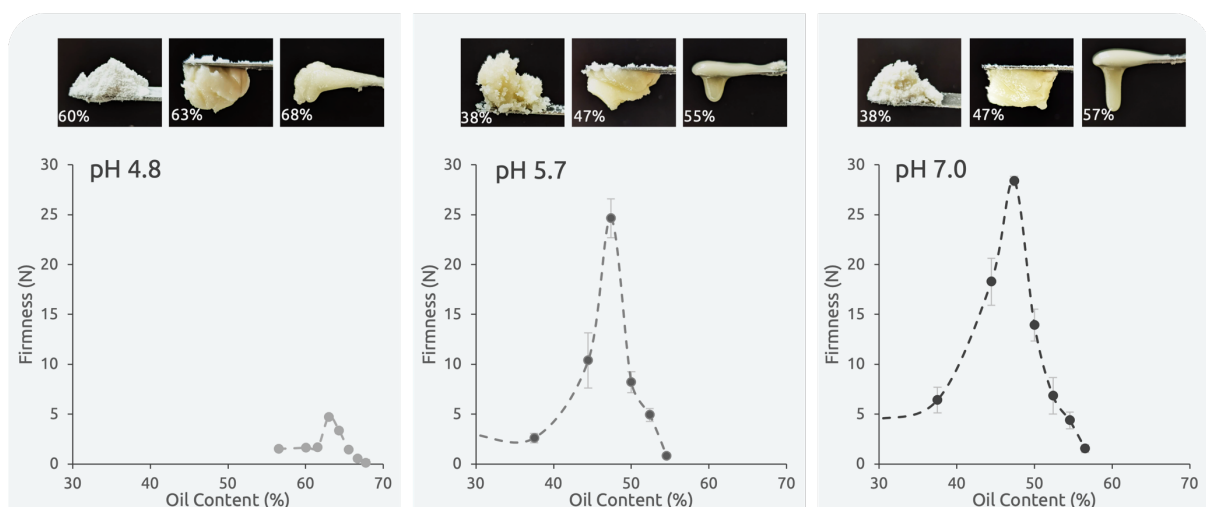


Figure 29. Appearance and firmness of sunflower oil and cryogel particle mixtures resulting from gelling whey protein solutions adjusted at the isoelectric point (pI, pH 4.8) and at pH of 5.7 and 7.0. Percentages in the macroscopic images refer to the oil content (%, w/w).

It should be noted that native WPI showed no oil structuring capability, independently from the oil content of the mixture, a particle suspension in oil was obtained with no oil retention capacity (data not shown). By contrast, all the cryogel samples displayed an oil structuring capability. Grainy mixtures were obtained below a certain oil content, which value

was specific for each cryogel sample. In these systems, the oil was probably mainly absorbed into the particle pores, resulting in non-connected particulate systems with low firmness (Figure 29). As the oil content increased, a homogeneous and self-standing material was obtained in correspondence with the firmness peak. In this situation, part of the oil occupied the spaces among the particles forming liquid oil bridges connecting the particles (Selmer et al., 2019). The latter was also demonstrated to interact *via* hydrogen bonding among the hydrophilic surface sites (DeVries et al., 2017; Plazzotta et al., 2020; Jung et al., 2023). As a result, a network efficaciously embedding the oil was formed. As the oil content further increased, the particles were progressively detached upon dilution in oil, leading to the formation of a suspension of particles in the oil. In this condition, interactions among particles were eventually lost, resulting in a drop in the firmness values, associated with a liquid-like behavior of the cryogel-oil mixtures (Figure 29).

Despite the firmness of all the samples exhibiting similar bell-shaped behavior, the pH of the initial hydrogel strongly affected the range of oil content in which the peak firmness was obtained. Indeed, for cryogel particles formed at pH 5.7 and 7.0, the firmness peak was detected at 47% (w/w) oil content. In comparison, particles formed at the pI presented the maximum firmness at a remarkably higher oil content (63%, w/w) (Figure 29). These differences can be associated with the particle microstructure (Table 24): being the particles obtained at the pI, smaller and more porous than those obtained at higher pH, they probably offered higher internal porosity for oil absorption and also a higher number of surface sites available for both oil adsorption, particle hydrophilic networking and oil bridging.

To better explore the effect of pH on the oil structuring capability of WP cryogel particles, the samples corresponding to the firmness peak were further characterized. All the samples showed no oil separation during storage at ambient temperature for up to 5 months. The high physical stability against phase separation was also confirmed by OHC values (100%). Figure 30 and Table 25 report the results of small-oscillation amplitude sweep tests of the three samples.
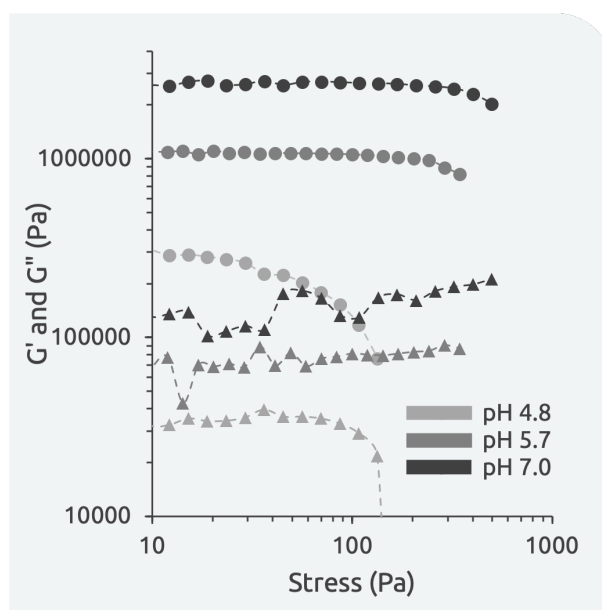
Figure 30. G' (○), and G'' (△) from amplitude sweep of mixtures of sunflower oil and cryogel particles resulting from gelling whey protein solutions at pH 4.8, 5.7, and 7.0. Samples had 63%, 47%, and 47% (w/w) oil content, respectively.

Table 25. Rheological parameters (critical stress, G', and G'') of mixtures of sunflower oil and cryogel particles resulting from gelling whey protein solutions at pH 4.8, 5.7, and 7.0. Samples had 63%, 47%, and 47% (w/w) oil content, respectively.

| pH | Oil Content (%, w/w) | Critical Stress (Pa) | G' × 10⁵ (Pa) | G'' × 10⁵ (Pa) |
|---|---|---|---|---|
| 7.0 | 47 | $355.5 \pm 61.9$ [a] | $21.6 \pm 3.2$ [a] | $0.9 \pm 0.1$ [a] |
| 5.7 | 47 | $263.7 \pm 23.8$ [b] | $12.2 \pm 1.3$ [b] | $0.5 \pm 0.1$ [b] |
| 4.8 | 63 | $50.7 \pm 13.6$ [c] | $4.0 \pm 0.8$ [c] | $0.3 \pm 0.0$ [c] |

[a-c] in the same column, different letters indicate significant differences ($p < 0.05$).

The obtained rheological results allow us to classify the cryogel-oil mixtures as gels since the samples were characterized by an elastic modulus (G') higher than the viscous one (G'') (Table 25, and Figure 30). As expected, the higher oil content structured by the cryogel particles obtained at the pI accounted for G' values lower than those detected for the oil-cryogel mixtures obtained with particles from hydrogels at higher pH confirming firmness data (Figure 29). A similar trend was also observed for critical stress, which indicates the stress value delimiting the linear viscoelastic region (LVR), where the material response is linear and reversible. It should be noted that the obtained values of G' and critical stress are within the range commonly associated with traditional fats, such as margarine and palm oil (*e.g.*, G' = 1 – 50 × 10⁵ Pa, and critical stress = 150 – 1000 Pa) (Calligaris et al., 2021; Patel et al., 2020). Based on this comparison, the obtained WP cryogel-oil mixtures present a gel behavior comparable to those of common food fats.

Since small-amplitude rheological parameters alone are insufficient for evaluating a material suitability as a fat replacer, it is crucial to consider conditions involving large deformations. The latter could mimic the deformations that the material will undergo during application as a food ingredient. For this reason, the WP cryogel-oil mixtures were subjected to spreadability analysis, which reflects the work required to spread a material under a given compressive deformation (Guichard et al., 2018). The results are reported in Figure 31.
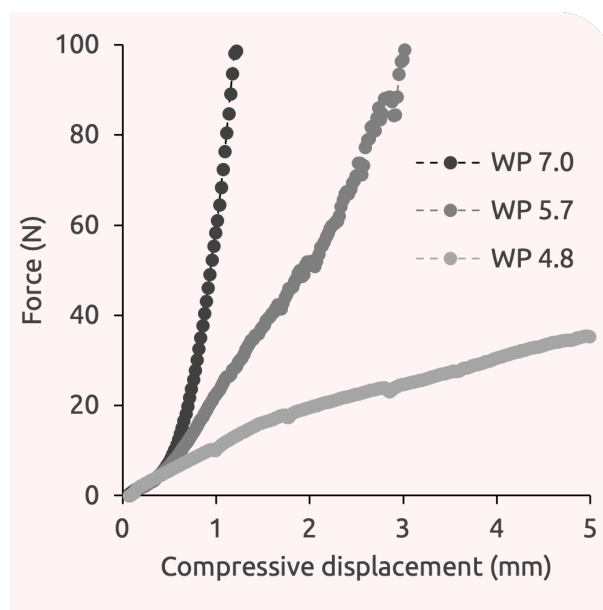


Figure 31. Force-displacement curves of mixtures of sunflower oil and cryogel particles obtained from hydrogels at pH 4.8, 5.7, and 7.0, and containing 63, 47, and 47% (w/w) oil content, respectively.

The typical profile of a plastic spreadable fat shows an initial increase of force with compressive displacement, followed by a progressive reduction of force dependence on the displacement, which indicates that a plastic, irreversible deformation is occurring (Guichard et al., 2018). Both mixtures of oil with cryogels obtained at pH 5.7 and 7.0 did not show such behavior, evidencing instead a progressive force increase with the displacement. This indicates that these samples were not deformable but tended to compact under the spreading tool, accounting for a progressively increasing force opposing compression. By contrast, the sample containing cryogel particles formed at the pI showed the typical force-displacement profile associated with spreadable food fats (Figure 31). This interesting behavior could be explained by considering the microstructure of the cryogel-oil mixtures, as evidenced by confocal microscopy (Figure 32).
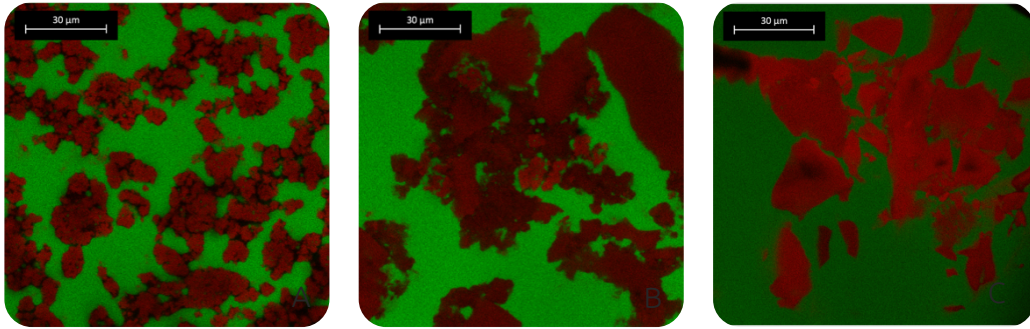
Figure 32. Confocal microscopy of mixtures of mixtures of sunflower oil and cryogel particles resulting from gelling whey protein solutions at pH 4.8, 5.7 and 7.0. Samples had 63%, 47%, and 47% (w/w) oil content, respectively.

The images show the presence of large particle agglomerates for samples containing cryogels formed at a pH higher than the pI. By contrast, the spheroidal cryogel particles formed at the pI appeared uniformly distributed in oil, and interacting on the surface, supporting the hypothesis that a deformable particle-particle network embedding free oil was formed. Based on these microscopic images, it can be hypothesized that, differently from particles prepared far from the pI, those formed at this pH value were able to efficaciously interact on the surface, leading to the formation of an articulated three-dimensional network. The latter would be able to structure a large oil amount while providing the obtained oleogel with peculiar spreadability (Figure 31). Thus, only the sample obtained by gelling WP at pH 4.8 behaved as an oleogel intended for fat substitution.

### 7.3.1. Proof of Concept: Cocoa Cream

Based on these results, cryogel particles obtained at the pI were used as ingredients in the formulation of a cocoa spread containing liquid oil solely as a lipid phase. In these products, the typical spreadable structure is provided by a high amount of fat rich in saturated fatty acids, such as palm and cocoa oils (Marra et al., 2023). Table 26 reports the physical properties of the samples prepared by using native WP or cryogel particles.

Table 26. Visual aspect, oil holding capacity, and rheological parameters (critical stress and G' module) of cocoa spreads prepared using native whey protein isolate (WPI), cryogel particles gelled at pH 4.8 (cryogel), and sunflower oil.

| Sample | Visual Aspect | OHC (%) | Viscoelastic Properties | |
| --- | --- | --- | --- | --- |
| | | | Critical Stress (Pa) | G' × 10$^5$ (Pa) |
| WPI |  | 96.3 ± 0.5$^c$ | 0.31 ± 0.05 $^b$ | 0.078 ± 0.006 $^b$ |
| Cryogel |  | 98.9 ± 0.2$^b$ | 918.8 ± 114.7 $^a$ | 41.1 ± 7.7 $^a$ |

[a-b] means indicates significant differences among values of the same column ($p < 0.05$).

n.d.: not detectable

The spread formulated with native WP (control) appeared as a fluid system well retaining the oil (OHC). When native WP was substituted with the porous cryogel particles prepared at the pI, a visibly more structured spread, with higher OHC was obtained (Table 26). This can be inferred by the ability of the cryogel particles to interact with each other via liquid oil bridges, thus connecting the particles and resulting in a self-standing material. The rheological analysis confirmed these observations, with the cryogel-containing spread showing a significantly higher critical stress and G' value than the WP one (Table 26). Spread samples were also assessed for spreadability, as shown in Figure 33.
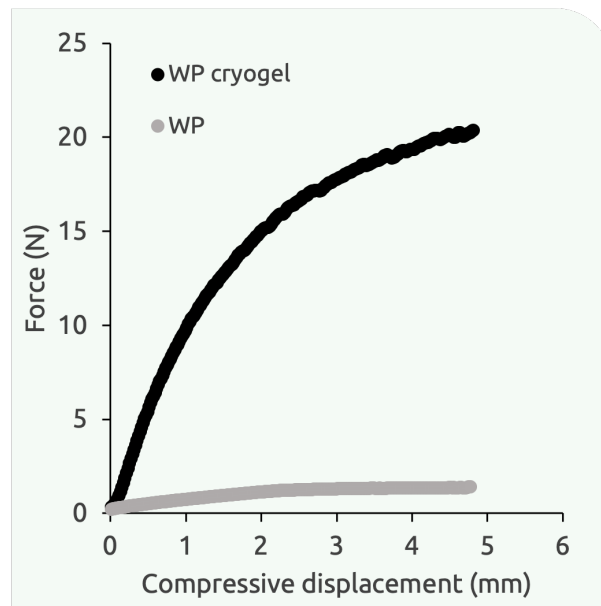
Figure 33. Force-displacement curves of cocoa spreads containing sunflower oil and native whey protein (WP), or WP cryogel particles obtained from hydrogel at pH 4.8.

As expected, the sample containing unstructured WP opposed minimum resistance to spreadability head movement, resulting in low force values, typical of fluid samples. By contrast, a displacement-sensitive force curve characterized by higher values was obtained from the cryogel-containing spread, showing the typical profile of spreadable matrices.

# 7.4. Conclusions

This study demonstrated the oil structuring potential of whey proteins in the form of cryogel. The critical role of the gelling pH in modifying the microstructure of the starting hydrogel and the deriving cryogel particles was demonstrated. At pH near the pI, highly porous small globular cryogel particles are obtained, which show the ability to retain large quantities of oil resulting in spreadable oleogels. Conversely, cryogel particles prepared from hydrogels obtained at pH values far from the pI, demonstrated a lower oil structuring ability due to the higher particle size and reduced porosity. Upon mixing with oil, these cryogel particles lead to elastic non-spreadable materials, which cannot be regarded as oleogels intended for fat substitution.

These results substantially enhanced the understanding of the impact of whey protein particle morphology on oil structuring, offering intriguing prospects for their potential applications in the food industry. This is particularly relevant considering that the developed porous cryogels can be considered novel structured materials produced with conventional and widely used technologies in food industries, such as freeze-drying and grinding.

Given the encouraging outcomes, further investigations were done to explore the behavior of oleogels made of whey protein cryogel particles in multi-phase systems containing water.

# 8. INTERACTION OF WHEY PROTEIN CRYOGEL-BASED OLEOGELS WITH WATER

## 8.1. Introduction and Aim of the Study

Based on the findings from Chapter 7, this part of the thesis focused on the interactions between whey protein oleogels and water. Despite the substantial research efforts in the literature regarding the formation of oleogels using hydrophilic biopolymers, there is limited information on their potential interaction with a water phase typically present in food formulations. To address this knowledge gap, the whey protein-based oleogel was mixed with increasing amounts of water, and the resulting systems were characterized by their morphological, mechanical, rheological, and microstructural attributes.

# 8.2. Materials and Methods

### 8.2.1. Materials

In the study the following materials were used: whey protein isolate (WPI, 94.7% protein content; 74.6% β-lactoglobulin, 23.8% α-lactalbumin, 1.6% bovine serum albumin, Davisco Food International Inc., Le Sueur, MN, USA); sunflower oil was purchased in a local grocery store; Nile Red and Fast Green dyes purchased from Sigma Aldrich (Milan, Italy). Deionized water was also used.

### 8.2.2. Oleogel Preparation

WP cryogel-based oleogel was prepared following the procedure described in paragraph 7.2.4. For the study, the WPI solution was gelled at a pH of 4.8, and the obtained cryogel particles were mixed with sunflower oil to obtain an oleogel with 63% oil content.

### 8.2.3. Oleogel-Water System Preparation

Oleogel was added with increasing quantities of water at 9500 rpm for 3 minutes (Polytron PT-MR3000, Kinematica AG, Littau, Switzerland). Table 27 shows the composition of the different considered emulsions.

Table 27. Composition of emulsions prepared by mixing the oleogel with water.

| Water (%, w/w) | Total (%) | Oil (%) | WPI (%) |
| --- | --- | --- | --- |
| 20 | 80 | 50.4 | 29.6 |
| 25 | 75 | 47.2 | 27.8 |
| 30 | 70 | 44.1 | 25.9 |
| 35 | 65 | 40.9 | 24.1 |
| 40 | 60 | 37.8 | 22.2 |
| 45 | 55 | 34.6 | 20.4 |
| 50 | 50 | 31.5 | 18.5 |
| 70 | 30 | 18.9 | 11.1 |
| 80 | 20 | 12.6 | 7.4 |
| 90 | 10 | 6.3 | 3.7 |

### 8.2.4. Analytical Determinations

#### 8.2.4.1. Visual Aspect

Samples were positioned on a petri dish with a resting time of 1 min, and placed inside a lightbox (Immagini & Computer, Bareggio, Italy). Pictures were taken using a digital camera equipped with a 60 mm fixed lens (EOS 550D, Canon Macro Lens EF-S, Milano, Italy) at 50 cm of distance. Acquisition parameters were as follows: ISO sensibility of 100, exposition time of 1/25, and diaphragm opening of f/10.

#### 8.2.4.2. Confocal Microscopy

Images were acquired with a confocal microscope system (Leica TCS SP8 X confocal system, Leica Microsystems, Wetzlar, Germany). The sample was prepared as follows: a 0.2% of an aqueous solution of Fast Green and Nile Red (Sigma Aldrich, Milan, Italy) was added in order to stain the protein and the oil contained in the oleogel samples, respectively. The samples were manually mixed until homogeneous, and an appropriate aliquot of each sample was placed on a sample-holding slide. A cover slide was then placed on top of the sample aliquot and fixed with transparent nail polish. Images were then acquired at 100× magnification and elaborated using the software LasX 3.5.5 (Leica Microsystems, Wetzlar, Germany).

#### 8.2.4.3. Firmness

Samples firmness was measured by a compression test using an Instron 4301 (Instron LTD., High Wycombe, UK) dynamometer equipped with a 1 kN load cell and a 6.2 mm (diameter) cylindrical probe. A 2 mm penetration at 25 mm/min cross-speed was performed for each measurement, and firmness was expressed as the maximum force opposed to such penetration by the sample.

#### 8.2.4.4. Rheological Properties

Sample rheological properties (Critical Stress and G') were analyzed using a RS6000 (Thermo Scientific RheoStress, Haake, Germany) rheometer equipped with a Peltier temperature control system. All measurements were performed at 20 °C using a parallel plates geometry, with a diameter of 35 mm, and a distance between the plates of 2.0 mm. Before each test, a waiting time of 5 minutes was applied to allow the relaxation of the sample. An amplitude sweep test was first performed at an oscillatory frequency of 1 Hz to identify the linear viscoelastic stress domain within a range of stress from 1 to 1000 Pa. From the resulting G' curve, the critical stress was calculated as a 10% drop of the G'. A frequency stress test was then carried out by decreasing the oscillatory frequency from 10 to 0.1 Hz at

a stress value selected in the viscoelastic region. Sample gel strength was expressed as the value of the elastic module (G') at 1 Hz.

### 8.2.4.5. Fluid Holding Capacity (FHC)

The FHC was determined by centrifuging (Mikro 20, Hettich Zentrifugen, Tuttlingen, Germania) 0.5 g of sample in 2 mL Eppendorf tubes at 14900 ×g per 20 min at 20 °C. The exceeded oil was then removed from the tubes using a cotton swab and the tubes were weighed again. FHC of samples was calculated as the percentual ratio between the fluid held inside the tube after the centrifugation and the initial fluid present in the oleogel.

### 8.2.5. Data Analysis

Data were expressed as the mean ± standard error of at least two measurements from two experimental replicates (n ≥ 4). Statistical analysis was performed by using R v. 4.0.3 (The R Foundation for Statistical Computing). ANOVA test was used to determine statistically significant differences between means ($p < 0.05$). Bartlett's test was used to check the homogeneity of variance ($p \geq 0.05$) and the Tukey test was used as a post hoc test ($p < 0.05$).

# 8.3. Results and Discussion

Figure 34 shows the oleogel-water mixtures obtained by increasing the amount of water (in the 20-90% range, w/w). After mixing, different samples obtained were evaluated based on their self-standing behavior (Figure 34).
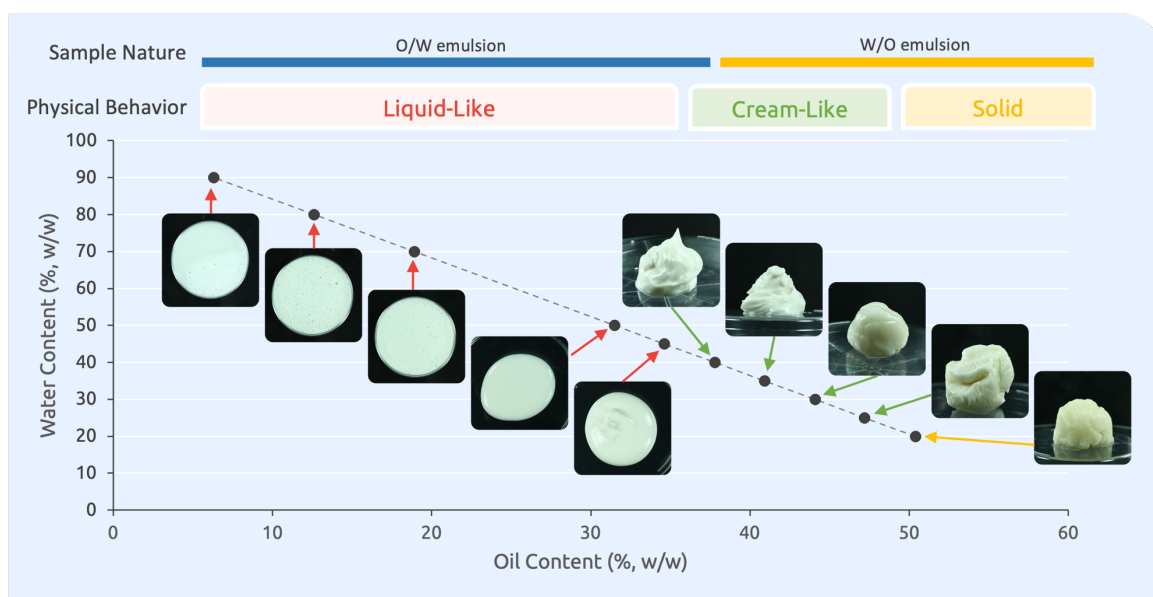


Figure 34. Visual aspect of the oleogel-water mixture at increasing amounts of water.

As visible in Figure 34, differently structured materials were obtained by the addition of increasing quantities of water to the oleogel. In all cases, no liquid phase separation was observed, regardless of the amount of water in the system. This interesting result can be attributed to the amphiphilic nature of the WP cryogel particles (Hong et al., 2022). Based on the formulation, different sample structures were observed. Specifically, at the lowest water content (<20%, w/w), a highly granular, brittle material characterized by an uneven and matte surface, was obtained. This macroscopic appearance deviates from that of the anhydrous oleogel (Figure 29) due to the increase in the presence of particles on the material surface. It can be speculated that proteins underwent a progressive swelling causing their appearance on the surface. This swelling phenomenon was well reported by Manzocco et al. (2022) in a study involving WP cryogel monoliths.

By further increasing water content in the 20 – 40% (w/w) range, self-standing materials with a cream-like appearance were obtained. Afterward, liquid systems were formed. Interestingly, all the samples resulted in stable emulsions with no phase separation upon centrifugation (data not shown). Considering the importance of designing novel lipid substitutes, further analyses were focused on the self-standing samples. Table 28 shows the

firmness and rheological parameters of the samples having from 20 to 40% (w/w) water content.

Table 28. Fluid holding capacity, firmness, critical stress, and G' rheological modulus of oleogel-water mixtures prepared by increasing amount of water.

| Water Content (%, w/w) | Fluid Holding Capacity (%) | Firmness (N) | Critical Stress (Pa) | $G' \times 10^4$ |
|---|---|---|---|---|
| 20 | $99.9 \pm 0.1^a$ | $0.59 \pm 0.10^c$ | $704.75 \pm 70.07^b$ | $17.42 \pm 0.03^b$ |
| 25 | $99.9 \pm 0.1^a$ | $2.53 \pm 0.73^a$ | $901.4 \pm 65.73^a$ | $42.84 \pm 3.59^a$ |
| 30 | $99.9 \pm 0.0^a$ | $0.82 \pm 0.05^b$ | $574.56 \pm 11.54^c$ | $10.36 \pm 1.27^c$ |
| 35 | $99.9 \pm 0.1^a$ | $0.35 \pm 0.01^d$ | $155.7 \pm 0.001^d$ | $3.79 \pm 0.37^d$ |
| 40 | $99.9 \pm 0.0^a$ | $0.10 \pm 0.01^e$ | $84.1 \pm 5.21^e$ | $0.02 \pm 0.0^e$ |

Samples in the 20 – 40% (w/w) water content range showed a fluid holding capacity of ~100%, confirming what is shown in Figure 29. Sample firmness, critical stress, and G' showed their peak value in correspondence of 25% (w/w) water content followed by a progressive decrease (Table 28). This behavior can be explained by the ability of whey protein to place themselves on the interface between the water and oil, building interactions. This result appears quite interesting due to the possibility of using whey protein not only as an emulsifier but also as a structuring agent when in the form of cryogel particles. Moreover, the possibility to steer the oleogel/water ratio in the attempt to modify the material mechanical characteristics appears promising to the attempt to use cryogel particles as food ingredients specific food formulation. To gain a better understanding of this mechanism, confocal microscopy analysis was performed in selected samples (Table 29).

Table 29. Confocal microscopy images of oleogels added with increasing water contents.



| Water Content (%, w/w) | | | |
|---|---|---|---|
| 30 | 40 | 45 | 80 |
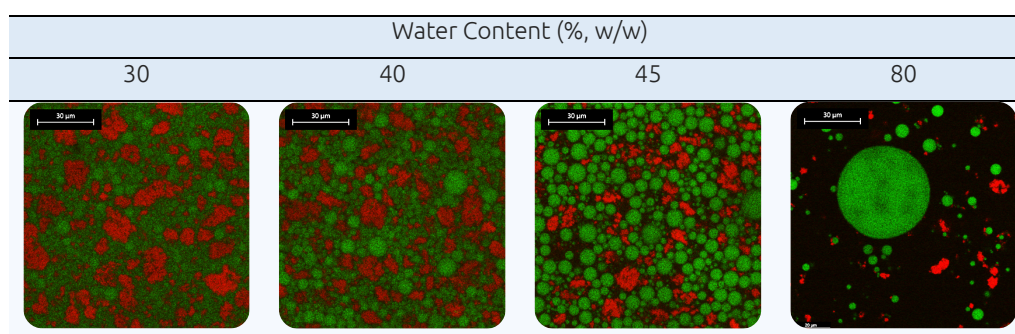
The confocal micrographs clearly show the systems microstructure organization. In particular, in the sample with the lower amount of water (*i.e.*, 30%, w/w), a microstructure similar to that of the anhydrous oleogel (Figure 32A) was observed, with oil (*i.e.*, green areas), almost evenly distributed among the protein network (*i.e.*, red areas, Table 29), describing the material as a W/O emulsion. As the water content increased (*i.e.*, 40-45%, w/w), the oil started

to be confined into spherical droplets surrounded by water, shifting the material nature into a O/W emulsion (Figure 33). In these systems, the network provided by proteins is maintained. However, it is expected also a swelling of protein particles posing at the water-oil interface stabilizes the emulsion. Just for comparison, a system with 80% water was also analyzed. It can be noted the presence of oil droplets dispersed in the water with portion particles still present in the medium (Table 29).

# 8.4. Conclusions

Considering the findings of this study, it can be asserted that WP cryogel-based oleogels are suitable materials to be used in multi-phase systems. In particular, the ability of proteins to interact with the oil and water phase concomitantly allows to generation of a number of structured emulsions with different potential applications.

# PART 3

# HEALTH FUNCTIONALITIES OF OLEOGELS

As already extensively presented in the introduction, oleogels have been traditionally studied and developed as a feasible alternative to saturated fats due to their good capability to mimic their technological functionalities (Patel & Dewettinck, 2016; Sivakanthan et al., 2022). However, more recently their potential health functionalities have been claimed, by affecting lipid digestibility (Ashkar et al., 2019; Calligaris et al., 2020; Marangoni et al., 2007; Marangoni & Garti, 2011b; O'Sullivan et al., 2017; Plazzotta et al., 2022) as well as the bioaccessibility of lipophilic compounds contained in the oil (Calligaris et al., 2020; Dent et al., 2022; N. Luo et al., 2021; Salvia-Trujillo et al., 2017; Zhao et al., 2022). While lipophilic gelators have been proven to reduce lipolysis hindering the access of lipolytic enzymes to their substrate (Calligaris et al., 2020; O'Sullivan et al., 2017; Ashkar et al., 2019), and modifying the bioaccessibility of liposoluble compounds, little is known regarding the ability of hydrophilic-based oleogels.

To study the impact of oleogel structure on their behavior upon digestion, the oleogels previously developed and described in Chapters 2 and 5 were *in vitro* digested also studying their destructuring behavior during the gastric and intestinal phase, the lipolysis degree and the bioaccessibility of key components, namely polyphenols. In particular, in Chapter 9 the effect of oleogelation of extra virgin olive oil by different gelators on lipid digestion and polyphenol bioaccessibility was studied. Furthermore, in Chapter 10 the digestion behavior of cellulose-based oleogels was studied.

# 9. OLEOGELATION OF EXTRA VIRGIN OLIVE OIL BY DIFFERENT GELATORS AFFECTS LIPID DIGESTION AND POLYPHENOL BIOACCESSIBILITY

## 9.1. Introduction and Aim of the Study

The objective of the present study aimed to address the knowledge gap regarding the digestion fate of EVOO-based oleogel systems, by investigating their destructuring behavior, lipid digestion, and the bioaccessibility of key polyphenols, namely tyrosol and hydroxytyrosol.

To this purpose, oleogels were prepared by using either the direct method (applied for saturated monoglycerides, phytosterol-phytosterol ester mixture, sunflower, and rice bran waxes) or the indirect method (in the case of whey protein aerogel particles). Oleogels were subjected to digestion simulation by using the INFOGEST standardized *in vitro* protocol (Brodkorb et al., 2019). The lipolysis degree and polyphenol bioaccessibility of the oleogels were compared to those of the unstructured EVOO. Results confirmed the possibility of steering the digestion fate of EVOO components by oleogelation.

Results here presented have been published in:

Ciuffarin, F., Alongi, M., Plazzotta, S., Lucci, P., Schena, F. P., Manzocco, L., & Calligaris, S. (2023). Oleogelation of extra virgin olive oil by different gelators affects lipid digestion and polyphenol bioaccessibility. Food Research International, 173, 113239. https://doi.org/10.1016/j.foodres.2023.113239

# 9.2. Materials and Methods

## 9.2.1. Materials

Commercial EVOO was used (fatty acid composition: 7.7% C18:0, 2.3% C18:0, 80.1% C18:1, 8.0% C18:2, 1.9% other; K232: 2.24; K270: 0.06; PV: 7.6 $mEqO_2$ $kg^{-1}$; viscosity: 77 mPa s). Saturated monoglycerides (Myverol$^{TM}$, fatty acid composition: 0.24% C12:0, 0.9% C14:0, 60.1% C16:0, 38.4% C18:0, 0.3% C20:0, 0.1% other; melting point 68.1 ± 0.5 °C) were purchased from Kerry Bioscience (Bristol, UK); rice bran wax (Karl Wax GmbH & Co. KG, Reinbek, Germany) was kindly provided by Spica Srl (Sulmona, Italy); sunflower wax was purchased from Kahlwax GmbH & Co. KG (Reinbek, Germany); β-sitosterol (75.5% β-sitosterol, 12.0% β-sitostanol, 8.4% campesterol, 3.0% other) and γ-oryzanol (99% purity) were purchased from Nutraceutica Srl (Monterenzio, Italy). Whey protein isolate (WP, 94.7% protein content; 74.6% β-lactoglobulin, 23.8% α-lactalbumin, 1.6% bovine serum albumin) was purchased from Davisco Food International Inc. (Le Sueur, MN, USA). Agar technical (Agar No. 3) was purchased from Oxoid Limited (Basingstoke, UK). Nile Red dye, porcine pepsin, porcine lipase, porcine pancreatin (8 × USP), porcine bile extract, HCl, NaOH, $CaCl_2$, $Na_2CO_3$, NaCl, KCl, $KH_2PO_4$, $MgCl_2(H_2O)_6$, $(NH_4)_2CO_3$, $MgSO_4$, hydroxytyrosol, tyrosol analytical standards, were purchased from Sigma Aldrich (Milan, Italy).

## 9.2.2. Sample Preparation

### 9.2.2.1. Preparation of Oleogels Containing Lipophilic Molecules (Direct Method)

Oleogels were prepared by using 90% (w/w) EVOO and 10% (w/w) of the following gelators: saturated monoglycerides (MG), rice waxes (RW), sunflower waxes (SW), or a mixture of β-sitosterol and γ-oryzanol (PS) (2:3 w/w). As previously described by Ciuffarin et al. (2023), the mixtures were stirred in dark conditions at 80 °C (MG, RW, and SW) or 90 °C (PS) until the gelator completely melted. Following, MG, RW, and SW mixtures were cooled down to 20 °C, while the PS mixture was kept at 4 °C for 12 h. All samples were then stored in dark conditions at 20 °C and analyzed 48 h after preparation to allow network setting.

### 9.2.2.2. Preparation of Oleogels Containing Hydrophilic Molecules (Indirect Method)

Oleogels were prepared as described by (Plazzotta et al., 2020). In brief, WP aerogel particles were dispersed into EVOO (0.1 g $mL^{-1}$), homogenized by a high-speed mixer (13,000

rpm, 3 min, Polytron PT-MR3000, Kinematica AG, Littau, Switzerland), and collected by centrifugation (14,000 ×$g$, 10 min, Beckman, Avanti J-25 centrifuge, Palo Alto, USA). This procedure was repeated twice, obtaining oleogels presenting 80% (w/w) oil content. The samples were stored in dark conditions at 20 °C and analyzed 48 h after preparation.

### 9.2.3. Analytical Determinations

#### 9.2.3.1. Firmness

Oleogel firmness was determined using a texture analyzer (TA.XT Plus, Stable Micro Systems Ltd, Godalming, UK) equipped with a 5 kg load cell. Forty grams of 25-mm-thick sample were compressed with a 35-mm-diameter compression platen at a crosshead speed of 1.5 mm/s (Giacintucci et al., 2018) and firmness was expressed as the maximum force (g) applied to the samples.

#### 9.2.3.2. *In vitro* Digestion

*In vitro* digestion was carried out according to the INFOGEST static protocol (Brodkorb et al. 2019). The simulated salivary (SSF), gastric (SGF), and intestinal (SIF) fluids were preheated at 37 °C just before *in vitro* digestion. Due to the lack of carbohydrates in the digested matrices, amylolytic enzymes were not considered. Four mL SSF, 25 µL 0.3 M $CaCl_2$, and 975 µL water were added to the sample to start the oral phase and the sample was continuously stirred at 37 °C for 2 min. Then, 8 mL SGF, 5 µL 0.3 M $CaCl_2$, and 667 µL of an aqueous pepsin solution providing 2,000 U/mL activity in the final chyme were added for the WP sample, while MG, RW, SW, PS, and control EVOO the enzyme solution was substituted with 667 µL of water. The gastric phase was started by adjusting the pH to 3.0 with 1 M HCl and making up the volume to 20 mL with water. The mix was continuously stirred at 37 °C for 2 h. Following, 8 mL SIF, 4 µL 0.3 M $CaCl_2$, 5 mL of a lipase-pancreatin solution, prepared in SIF and providing 2000 and 100 U/mL activity respectively in the final mixture, and 3 mL of 160 mM bile extract prepared in SIF were added to WP sample. For MG, RW, SW, PS, and control EVOO the lipase-pancreatin solution was substituted with 5 mL of lipase solution at 2000 U/mL activity. The intestinal phase was started by adjusting the pH to 8.00 ± 0.10 with 1 M NaOH and making up the volume to 40 mL with water. The mix was continuously stirred at 37 °C for up to 2 h. A 30 mL aliquot of the mixed micellar phase (*i.e.*, stabilized structures in which lipophilic bioactive components are encapsulated) was recovered after *in vitro* digestion by centrifugation at 30,000 ×$g$ for 70 min (Beckman, Avanti J-25 centrifuge, Palo Alto, USA).

### 9.2.3.3.  Confocal Light Scanning Microscopy (CLSM)

The fluorescent dye Nile Red (0.2% aqueous solution) was used to stain lipophilic molecules. The hanging-drop method was used (Gallier et al., 2012) to analyze samples collected after the gastric and intestinal digestion phases (*i.e.*, digestate). The stained samples were added with an agarose solution (1% w/w) preheated at 50 °C, in a sample:agarose solution ratio of 1:2 (v/v). Two µL of the fluid mix was placed on a microscope coverslip and left to set at room temperature for 1 min. The coverslip with the gelled droplet was then fixed on a concave microscope slide and observed at 100× by confocal laser scanning microscope (Leica TCS SP8 X confocal system, Leica Microsystems, Wetzlar, Germany). Images of confocal micrographs were imported in jpeg format (LasX 3.5.5, Leica Microsystems, Wetzlar, Germany). Image analysis was carried out to assess the oil droplet dimension (Image-Pro Plus 6.3, Media Cybernetics Inc., USA). Images were converted to an 8-bit grey scale and software calibration was applied. Droplet diameter data were provided by the software and further elaborated to obtain the $D_{32}$ using Excel (Microsoft, Redmond, Washington, USA).

### 9.2.3.4.  Particle Size and Zeta Potential of Digested Samples

The particle size distribution of the mixed micellar phase of digested oil and oleogels (recovered as described in paragraph 9.2.3.2) was measured by DLS (Zetasizer NanoZS, Malvern Instruments, Worcestershire, UK). Samples were diluted 1:100 (v/v) with deionized water and placed in a cell where the laser light, set at 173° angle, was scattered by the particles. Particle size was reported as the cumulative sum of volume-weighed mean diameter expressed in nm. The polydispersity index of distributions (PDI) was used to measure the homogeneity of particle size distribution. The ζ-potential was also measured by placing the diluted sample in a capillary cell equipped with two electrodes to assess particle electrophoretic mobility.

### 9.2.3.5.  Lipid Digestibility

The pH-stat approach was used to determine the extent of lipid digestibility (Mat et al., 2016). $NaHCO_3$ was replaced with NaCl in SSF, SGF, and SIF. According to oleogel composition (80% oil content for WP-based oleogels, 90% for MG, RW, SW, PS-based oleogel), an oleogel amount of 1.25 g for WP oleogel and 1.11 g for MG, RW, SW, PS-based oleogel, corresponding to 1 g oil, was used. The pH of the digestion mixture was monitored immediately after lipase addition (paragraph 2.2.4) and 0.25 M NaOH aliquots were added to maintain a value of 8.0 ± 0.1 (*i.e.*, the optimum of used lipase based on its technical specifications) and the volume of NaOH (mL) added to titrate the oleogels was recorded ($V_{oleogel}$). An aliquot of lipid-free WP gelator (0.25 g) corresponding to that contained in the oleogels was digested and the

required NaOH volume registered ($V_{aerogel}$) to account for the proteolysis contribution to pH lowering. Finally, the NaOH volume required to titrate unstructured EVOO (1 g) was also recorded ($V_{oil}$).

The percentage of free fatty acids (FFA) released during lipolysis was calculated (Eq 1):

$$\text{FFA (\%)} = \frac{V_e}{V_t} \times 100 \qquad \text{Eq. 1}$$

where $V_e$ is the experimental volume, represented by: (i) $V_{oil}$ in the case of EVOO and MG, RW, SW, and PS-based oleogels; (ii) the difference between $V_{oloegel}$ and $V_{aerogel}$ in the case of WP-based oleogel. $V_t$ represents the theoretical volume required to titrate the fatty acids released by complete hydrolysis of triglycerides in the reaction vessel, assuming 2 FFA are produced for each triacylglycerol molecule (Y. Li et al., 2011), and was calculated according to Eq. 2:

$$V_t = 2 \times \left[ \frac{m_{oil}}{MW_{oil}} \frac{1000}{c_{NaOH}} \right] \qquad \text{Eq. 2}$$

where $m_{oil}$ is the mass of oil in the reaction vessel (g), $MW_{oil}$ is the average molecular weight of EVOO (879.67 g mol$^{-1}$) and $C_{NaOH}$ is the concentration of the sodium hydroxide (mol L$^{-1}$).

### 9.2.3.6. Hydroxytyrosol and Tyrosol Quantification

Hydroxytyrosol (HTy) and tyrosol (Ty) were extracted and quantified from 2 g of oil as reported by Ciuffarin et al. (2023) and according to the official COI/T.20/Doc No 29 method in agreement with Reg. UE 432/2012. Acid hydrolysis was applied following the ISO 23942:2022 procedure. UHPLC analysis was performed as previously reported (Lucci et al., 2020).

Total polyphenol content was calculated as the sum of hydroxytyrosol and tyrosol values.

### 9.2.3.7. Polyphenol Bioaccessibility Computation

Phenolic compounds were extracted from the mixed micellar phase following the methodological approach reported by Calligaris et al. (2020). The method was modified to optimize the extraction of the compounds of interest, by modifying solvent mixture and by adding a d-SPE clean-up step. Briefly, aliquots of 10 mL of micellar phase were placed in a 50 mL falcon tube with 2.5 mL of acetonitrile. The sample was vigorously hand-shaken for 1 min. A 6 g salt mixture (MgSO$_4$/NaCl 2:1, w/w) was then added and shaking was repeated under the same conditions. The resulting mixture was centrifuged at 5000 ×$g$ for 10 min and 1.5 mL of supernatant was carefully taken and placed in a tube with 150 mg MgSO$_4$ and 50 mg PSA for d-SPE clean-up, vortexed, and centrifuged at 10,000 ×$g$ for 5 min (Mikro 120, Hettich Italia Srl, Milan, Italy). 1 mL of supernatant was then placed in a vial and dried by a gentle N$_2$ flow. Acid hydrolysis was applied before UHPLC analysis as described in section 9.2.3.6.

The extraction procedure for polyphenols analysis in digested samples was validated. Accuracy was determined by means of recovery experiments during which digested samples

of refined sunflower oil were fortified with three different amounts of polyphenols (25, 100, and 250 μg for tyrosol and hydroxytyrosol, each) and their content was assessed. Precision was determined in terms of relative standard deviation from recovery experiments at each fortification level. In all cases, the average recovery ranged from 75 to 100% with repeatability relative standard deviation lower than 2%, revealing the suitability of the procedure for the quantitative extraction of polyphenols from digested samples.

The BAC of HTy and Ty was calculated as the percentage ratio between the concentration of compound incorporated in the micellar phase recovered from *in vitro* digestion and its concentration in the undigested sample and was expressed as mg of Ty or HTy per $kg_{oil}$.

### 9.2.4. Statistical Analysis

Results are reported as means ± standard deviation and are averages of three measurements carried out on two replicated experiments. Bartlett's test was used to check the homogeneity of variance, the Tukey test, and the analysis of variance (ANOVA) were used to test for differences between means ($p < 0.05$), using R (v. 4.0.3, The R Foundation for Statistical Computing, Vienna, Austria). The correlation was measured by the Pearson coefficient.

# 9.3. Results and Discussion

### 9.3.1. Oleogel Physical Properties
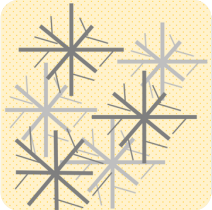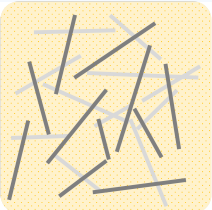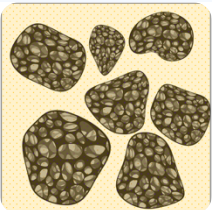
The firmness of the oleogels considered in this study is reported in Table 30. All samples have been previously characterized for their structural features elsewhere (Alongi et al., 2022; Ciuffarin, Alongi, Peressini, et al., 2023; Plazzotta et al., 2022). The 10% (w/w) concentration of liposoluble gelators was chosen since allowing to obtain self-standing oleogels (Table 30), while the WP-based oleogel contained 80% oil, which is the maximum quantity of the oil that can be included in the WP network (Plazzotta et al., 2020).

The oleogels presented firmness values decreasing in the order PS > SW > RW > WP > MG. This behavior can be explained by the different nature of the oleogel network and agrees with the literature (Alongi et al., 2022; Plazzotta et al., 2022; Valoppi et al., 2017). As represented in Table 30, MG, SW, and RW samples were characterized by a three-dimensional network of oleogelator crystals with different morphology. In particular, MG presents crystals with a spherulite conformation characterized by a dendritic shape, while RW and SW present needle-like crystals with different dimensions, smaller for the former and longer for the latter (Chapter 2, Doan et al., 2017; Valoppi et al., 2017). PS network was formed by hollow double-walled tubules smaller enough to be crossed by the light and accounting for a high firmness but a brittle structure (Scharfe et al., 2019). Finally, in the case of the WP-based oleogel, the oil was retained by multiple mechanisms, including:

- oil absorption into the protein particle pores, driven by capillary forces;
- oil adsorption onto particle surface;
- interactions between oil and hydrophobic protein residues;
- oil retainment in the interstices among particles, which creates a network based on weak hydrophilic interactions (De Vries, Gomez, et al., 2017).

As a result, a semi-solid material with rheological properties analogous to those of laminating fats is obtained, as demonstrated by Plazzotta et al. (2020, 2022).

Table 30. Structuring elements, network representation, macroscopic appearance, and firmness of EVOO-based oleogels obtained by using 10% (w/w) monoglycerides (MG), rice wax (RW), sunflower oil (SW), or phytosterols (PS), and 20% (w/w) whey protein aerogel (WP).

| Oleogelator | Structuring elements | Network representation | Macroscopic appearance | Firmness (g) |
|---|---|---|---|---|
| MG | Crystals |  |  | 33.6 ± 2.5 [e] |
| RW | Crystals |  |  | 115.0 ± 3.0 [c] |
| SW | Crystals |  |  | 532.7 ± 23.8 [b] |
| PS | Hollow tubules |  |  | 2534.0 ± 71.6 [a] |
| WP | Porous material |  |  | 96.7 ± 6.8 [d] |

[a–e]: indicate significant differences among oleogels ($p < 0.05$).

### 9.3.2. Destructuring Behavior under Gastrointestinal Conditions

The different oleogel structure (Table 30, Alongi et al., 2022; Ciuffarin et al., 2023) has been previously reported to affect the structural arrangement of samples also during digestion (Plazzotta et al., 2022). The digestive behavior of samples was thus analyzed and compared to that of unstructured EVOO, considered as a reference.

The microstructure generated upon gastric and intestinal phases was observed by CLSM to study the destructuring of oleogels under gastrointestinal conditions. Table 31 reports the confocal micrographs.

Table 31. CLSM of the digestate samples obtained upon gastric and intestinal digestion of unstructured EVOO (control) and EVOO-based oleogels obtained by using 10% (w/w) of monoglycerides (MG), rice wax (RW), sunflower oil (SW), or phytosterols (PS), and 20% whey protein aerogel (WP).



Upon gastric digestion, unstructured EVOO presented droplets with a $D_{32}$ around 4.5 μm. Analogous small droplets were also observed in the gastric digestate of MG, RW, SW, and PS oleogels (Table 31), which showed droplets with a $D_{32}$ of about 3.4, 2.7, 5.5, and 3.4 μm, respectively. It must be mentioned that after gastric digestion intact oleogel agglomerates, not homogeneously dispersed, were still found in the digestate. This is consistent with the lower number of droplets visually detectable in MG, RW, SW, and PS sample micrographs, as compared to that of the unstructured oil. Residual oleogel structures physically entrapped the oil, thus preventing its release in the form of droplets in the digestive medium. In the case of the WP oleogel, a $D_{32}$ of 4.4 μm was measured after the gastric phase. However, in the CLSM micrograph of this sample, a larger number of droplets was observed. This suggests that a higher amount of oil was released as compared to the other oleogels, resulting in a gastric digestate similar to that of unstructured oil. This behavior can be explained by the susceptibility of the WP-based aerogel template to gastric digestion. In this regard, the structure of WP-based oleogel, including protein location, has already been thoroughly

characterized in our previous work by Plazzotta et al. (2022), demonstrating that more than 70% of aerogel proteins were digested during this phase.

The differences among samples became even more evident after the intestinal phase (Table 31). Looking at the CLSM micrograph of EVOO, it can be observed that both the number and the $D_{32}$ (4.2 µm) of particles remained almost unchanged as compared to the gastric phase. Oil was dispersed into the digestive mixture since the beginning of digestion, due to the absence of an oleogel network able to entrap it. Conversely, the number of droplets observed in the CLSM micrograph of MG, RW, SW, and PS samples increased after the intestinal phase of digestion, indicating that oil was physically released from the oleogel network in the digestive mixture. It must be pointed out that, at the end of the intestinal phase, intact oleogel particles could be barely visually detected in the samples. Moreover, it was observed that the $D_{32}$ of MG and RW droplets almost doubled from the gastric to the intestinal phase, accounting for 6.7 and 5.9 µm, respectively, while the $D_{32}$ of SW and PS samples remained almost unchanged (6.3 and 4.3 µm, respectively). These differences could be attributed to the different firmness of the oleogels (Table 30). MG and RW actually presented a lower firmness compared to SW and PS. This may have increased their susceptibility to mechanical disruption during digestion, possibly accelerating oil release in the digestive mixture, and resulting in a more pronounced droplet coalescence (N. Luo et al., 2021). Moreover, gelator crystals are expected to place themselves at the oil/water interface, contributing to the increase in droplet size (Dong et al., 2020). Nevertheless, in all cases the presence of bile salts, combined with peristalsis simulation, favored oil emulsification, preventing the formation of large droplets. Oil droplets completely disappeared in the WP sample after the intestinal phase, in agreement with previous findings (Plazzotta et al., 2022). Besides allowing the physical release of oil already during the gastric phase, the WP released upon the digestion of the aerogel template would be able to act as surfactants, favoring the emulsification of oil and increasing the exposed surface area (Mat et al., 2020). This, in turn, is expected to increase the susceptibility of oil to lipolysis.

It must be pointed out that CLSM micrographs provide an overview of the appearance of digested samples on the micro-scale. However, when dealing with the digestibility of lipid matrices, it is crucial to characterize the mixed micellar fraction. Mixed micelles are self-assembled nanoscale-size structures, encapsulating free fatty acids and other lipophilic compounds released during lipid digestion. The micelles below 200 nm can be absorbed through the intestinal epithelium and therefore their role is to carry the encapsulated compounds through the epithelial cells of the small intestine for uptake (Salvia-Trujillo et al., 2017). Since the efficiency of this process is affected by mixed micelle size (Marze et al., 2015), the particle size distribution of the mixed micellar fractions obtained after the intestinal

digestion of oleogels and EVOO (control) were analyzed by DLS, and the cumulative distributions are shown in Figure 35.
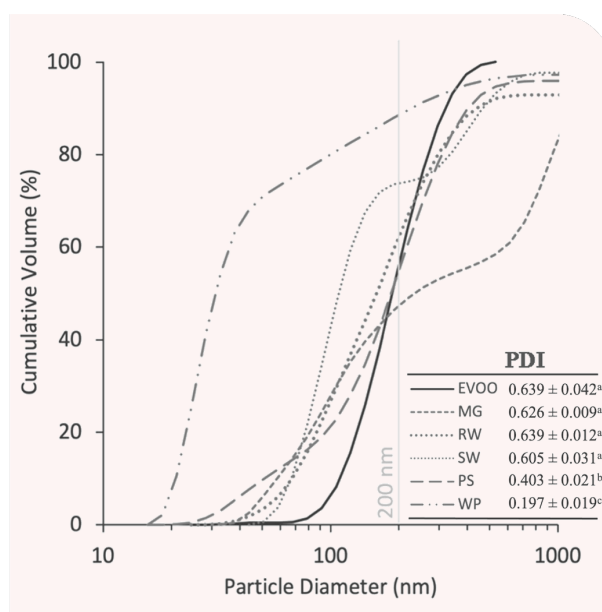


Figure 35. Cumulative particle size distribution and PDI of unstructured EVOO (control) and EVOO-based oleogels obtained by using 10% (w/w) of monoglycerides (MG), rice wax (RW), sunflower oil (SW), or phytosterols (PS), and 20% whey protein aerogel (WP).

The 51% of particles in the mixed micellar fraction of unstructured EVOO was smaller than 200 nm, *i.e.*, the threshold for intestinal uptake. A similar profile was observed also in the case of MG, RW, SW, and PS oleogels, in which the ratio of particles below 200 nm was around 50% (Figure 35). These findings agree with those reported in the literature for sunflower oil gelled by using the same liposoluble gelators here applied (Calligaris et al., 2020; Dong et al., 2020). Conversely, almost 90% of the micelles generated upon WP digestion presented a size below 200 nm, in agreement with the results reported by Plazzotta et al. (2022) on sunflower and flaxseed oil WP-based oleogels, possibly resulting in an increased lipid digestibility. The micellar fraction of the samples also showed different PDI values (Figure 35The PDI of EVOO micellar fraction was the lowest one (around 0.2), indicating that the micelles produced upon its digestion showed a rather homogeneous size. The PDI increased (~0.4) when WP-based oleogel was digested, but the highest values (>0.6) were observed in the micellar fraction deriving from the digestion of liposoluble gelator-based oleogels. This occurred regardless of the gelling agent used, indicating that the gelator nature affected the heterogeneity of the micellar phase size. These results can be possibly attributed to the de-structuring behavior of oleogels. It can be hypothesized that the presence of a network made of liposoluble gelators impaired the homogeneous breakage of the oleogel structure and the consequent release of oil. By contrast, in the case of WP oleogels, the oil present in the interparticle spaces was

readily released and digested, leading to micelles analogous to those found in the bioaccessible fraction of unstructured EVOO.

Besides particle dimension, also the surface electrical charge of particles at the oil-water interface is well known to play a role in intestinal uptake (McClements, 2004). The ζ-potential of the mixed micellar fractions was thus measured. A negative charge was found in all cases, due to the presence of anionic surfactants absorbed at the oil-water interface, such as bile salts and free fatty acids (Salvia-Trujillo et al., 2013). However, MG, RW, SW, PS, and EVOO presented similar values, ranging from -53 to -56 mV, while the WP ζ-potential was significantly higher (-41 mV). Such a difference can be attributed to the presence of positively charged free aminoacids and peptides derived from protein digestion (Qian et al., 2012).

Based on these results, the destructuring behavior of oleogels seems to be governed in a complex way by both the gel network strength and the oleogelator type. These differences could lead to changes in lipid digestibility and polyphenol bioaccessibility.

### 9.3.3. Lipolysis upon *in vitro* digestion

The lipid digestibility of oleogels and unstructured oil was monitored by measuring the free fatty acid (FFA) released during the intestinal phase of *in vitro* digestion (Figure 36).
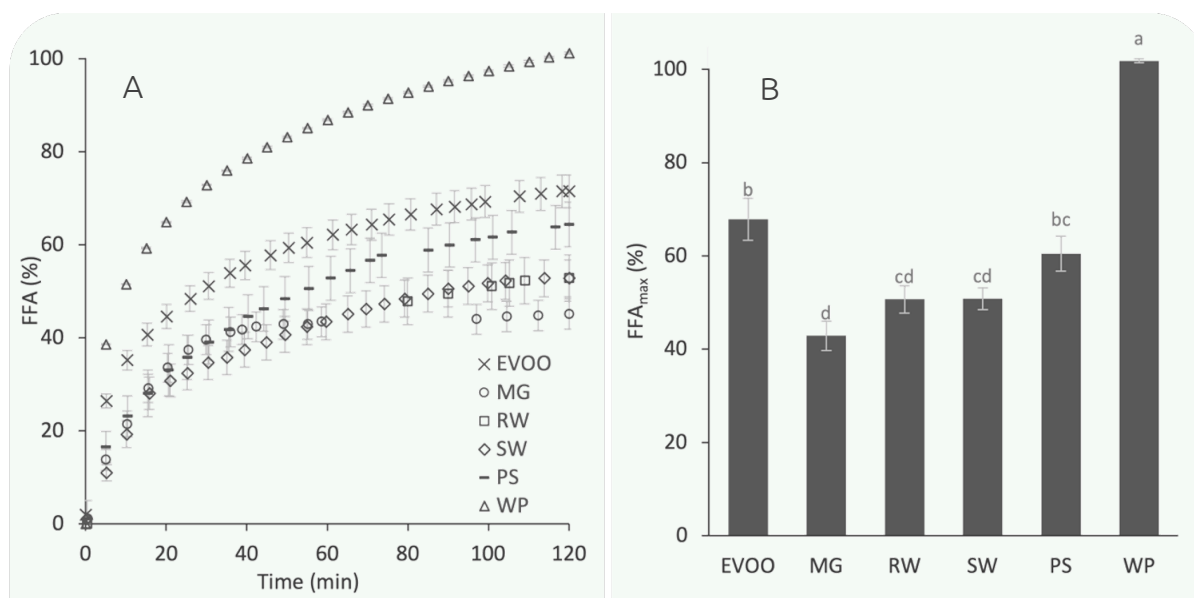


Figure 36. Free fatty acids (FFA) release kinetics (A) and total free fatty acids ($FFA_{max}$) released during in vitro intestinal digestion (B) of unstructured EVOO (control) and EVOO-based oleogels obtained by using 10% (w/w) of monoglycerides (MG), rice wax (RW), sunflower oil (SW), or phytosterols (PS), and 20% whey protein aerogel (WP).

[a–d]: indicate significant differences in polyphenol concentration in the same column ($p < 0.05$).

n.d.: not detectable.

The FFA release during intestinal digestion of all samples followed the typical profile reported in the literature (Li et al., 2011; O'Sullivan et al., 2017), with a steeper increase in the first minutes followed by a flattening until a *plateau* was approached (Figure 36A) (Mat et al., 2020; Salvia-Trujillo et al., 2017). However, the rate and extent of lipid digestion were affected by oil structuring. After 2 h intestinal digestion, $FFA_{max}$ accounted for nearly 70% (Figure 36B) of the unstructured EVOO, in agreement with the literature (Pascoviche et al., 2019). It must be pointed out that the theoretical value of FFA release under gastrointestinal conditions is 66%, due to the selective hydrolysis carried out by lipases preferably in positions 1- and 3- of the triglyceride, thus producing 2 free fatty acids and one monoglyceride (Hofmann & Borgstrem, 1964). However, different lipolysis extents were reported in the literature for oils with different compositions, ranging from 44% for unstructured canola oil (O'Sullivan et al., 2017), to 72% for palm oil (Ye et al., 2019). The remaining undigested oil was clearly visible as distinct droplets in the CLSM micrographs of the intestinal digestate (Table 31).

Oleogel structuring with liposoluble gelators led to an overall decrease in $FFA_{max}$ (PS ≥ SW ≈ RW ≥ MG). This behavior can be attributed to the presence of different network structures modulating the lipase accessibility to its active sites. In particular, the use of oleogelators forming crystalline networks reduced lipase activity more than the oleogelator forming fibrillar network (PS).

An opposite effect on lipolysis extent was observed when oil was structured through WP aerogel. The presence of proteins considerably improved the efficiency of lipid digestibility, leading to complete hydrolysis ($FFA_{max} ≈ 100\%$) after the 2-h intestinal digestion, in agreement with previous results on other vegetable oils (Plazzotta et al., 2022). This result was attributed to the ability of WP aerogel to act as an emulsifier in the digestive mix. The finely dispersed oil droplets were stabilized by partially undigested aerogel particles, which placed themselves at the droplet surface, supporting the easy attack by intestinal lipases and complete lipolysis. This evidence agrees with CLSM micrographs showing the complete absence of visible oil droplets in the intestinal digestate (Table 31). WP would actually increase oil susceptibility to gastric enzymes favoring the formation of small oil droplets already in the gastric phase and leading to their prompt lipolysis during the first stages of the intestinal phase (Plazzotta et al., 2022).

Overall, these results confirm the possibility of steering lipid digestion by oleogelation, thus suggesting the applicability of oleogels not only for their technological advantages but also to accomplish specific nutritional requirements (Qian et al., 2012; Salvia-Trujillo et al., 2017). In this regard, the possibility of tuning lipolysis

by selecting the proper oleogelator could be exploited to develop different products intended for specific consumer categories. For instance, the use of a lipophilic-based oleogel might be adopted to reduce caloric intake thanks to its ability to restrain lipid digestion, whereas protein-based oleogels can contribute to the efficient delivery of essential fatty acids.

### 9.3.4. Polyphenol Bioaccessibility

The bioaccessibility of the major phenolic compounds contained in EVOO (*i.e.*, hydroxytyrosol and tyrosol) was further investigated. Unstructured EVOO contained 248.1 ± 4.6 and 93.9 ± 3.3 mg kg$^{-1}$ hydroxytyrosol and tyrosol, respectively. Since the oleogel preparation process did not affect phenolic concentration (data not shown), these values were used to compute the bioaccessibility in MG, RW, SW, PS, and WP oleogels (Table 32

Table 32. Hydroxytyrosol and tyrosol content and bioaccessibility (BAC) in EVOO (control) and oleogels obtained by using 10% (w/w) of monoglycerides (MG), rice bran waxes (RW), sunflower waxes (SW), or phytosterols (PS), and 20% (w/w) of whey protein aerogels particle (WP) after *in vitro* digestion.

| Sample | Hydroxytyrosol | | Tyrosol | |
|---|---|---|---|---|
| | Concentration (mg kg$_{oil}^{-1}$) | BAC (%) | Concentration (mg kg$_{oil}^{-1}$) | BAC (%) |
| EVOO | n.d. | n.d. | 46.3 ± 3.2 [a] | 48.1 ± 3.38 [a] |
| MG | 17.2 ± 4.3 [b] | 7.0 ± 0.75 [b] | 25.1 ± 0.9 [bc] | 26.1 ± 0.97 [bc] |
| RW | 13.5 ± 1.2 [c] | 5.4 ± 0.49 [c] | 21.9 ± 1.7 [c] | 22.8 ± 1.77 [c] |
| SW | 13.2 ± 1.6 [c] | 5.3 ± 0.66 [c] | 30.4 ± 3.1 [b] | 31.6 ± 3.25 [b] |
| PS | 2.9 ± 0.2 [d] | 1.2 ± 0.08 [d] | 24.6 ± 1.7 [c] | 25.6 ± 1.81 [c] |
| WP | 42.1 ± 11.1 [a] | 17.0 ± 4.50 [a] | 50.3 ± 1.8 [a] | 52.3 ± 1.96 [a] |

[a–d]: indicate significant differences in polyphenol concentration in the same column ($p < 0.05$). n.d.: not detectable.

Overall, hydroxytyrosol (HTy) and tyrosol (Ty) decreased considerably upon digestion in all cases, but significant differences were detected among the samples.

When unstructured EVOO underwent *in vitro* digestion, hydroxytyrosol suffered a dramatic decrease, completely disappearing from digested unstructured EVOO, while tyrosol was halved. These results can be attributed to the different resistance toward the oxidizing conditions in the biological fluids of these two phenolic compounds (Cheng et al., 2002; Pripp et al., 2005). Tyrosol is actually reported to be more stable than hydroxytyrosol, maintaining its antioxidant activity also under critical conditions (Marković et al., 2019).

Our results differ from those reported by Reboredo-Rodríguez, et al. (2021), who observed the presence of HTy after intestinal digestion in the micellar phase. These contradictory

outputs could be associated with the diversity of both the starting material and the methods applied in the studies. In consideration of the limited literature on this topic, there is a need to reinforce the studies on this topic.

When EVOO was structured by liposoluble gelators, the BAC of hydroxytyrosol and tyrosol changed. The BAC of tyrosol significantly decreased, while that of hydroxytyrosol increased, being detected even after digestion. The increase in hydroxytyrosol concentration in the mixed micellar fraction and thus in its BAC can be associated with a retarded oil digestion (Figure 36A), leading to partial protection of the bioactive molecule through the shielding carried out by the gelled structure against the gastric environment, followed by a further release in the intestinal fluids. In the case of tyrosol, which is less water soluble than hydroxytyrosol, its BAC decreased due to the entrapment of the molecule into the undigested oleogel (Table 32). Additionally, a possible role of the interactions among phenolic compounds and gelators cannot be excluded as recently demonstrated in Chapter 2. Given these protection and binding mechanisms, the total phenolic BAC ultimately remained in the same range as observed for unstructured EVOO, accounting for 12.3, 10.0, 12.1, and 7.0% in MG, RW, SW, and PS-based oleogels, respectively. These values corresponded to an overall concentration of bioaccessible phenolic compounds of around 42.4, 34.5, 41.7, and 24.1 mg $kg^{-1}$ in MG, RW, SW, and PS, respectively.

On the contrary, WP allowed a higher retention of hydroxytyrosol and tyrosol than lipophilic gelators, resulting in an improvement of total phenolic BAC (27%, 26.9 mg $kg^{-1}$). This result can be linked to the presence of emulsifying WP, able to protect hydroxytyrosol from degradative events occurring under gastric conditions. It cannot be excluded also a protective role of whey proteins, especially β-lactoglobulin, as antioxidants during digestion (H. C. Liu et al., 2007).

# 9.4. Conclusions

The knowledge of the effect of oleogel structure on human digestion behavior appears promising to formulate oleogels with tailored health functionalities, widening their potential application beyond their use as fat-mimetic. This study highlighted how, based on the gelator choice, not only the caloric intake can be modified, but also the BAC of phenols naturally present in EVOO can be steered. In particular, WP-based oleogels presented the highest FFA release (*circa* 100%) and phenolic compound BAC, as a consequence of their peculiar destructuring behavior during digestion. Contrarily, EVOO gelled with lipophilic gelators showed reduced oil lipolysis and BAC, associated with possible entrapment in the undigested oleogel. The recorded BAC reduction may open the possibility for EVOO phenolic compounds to be carried to the colon, where they can further exert their bioactivity. Indeed, future research should be addressed to understand more in detail the actual fate of the non-bioaccessible fraction of EVOO phenolic compounds.

# 10. DIGESTION BEHAVIOR OF CELLULOSE-BASED OLEOGELS

## 10.1. Introduction and Aim of the Study

Cellulose is a widely used polymer in the food industry as an ingredient not only for its functional properties but also as a filler in various food products. The latter is exerted being cellulose a non-digestible component that helps to reduce caloric intake, promote gastrointestinal health, act as a prebiotic for gut microbes, and act as a gut-protection agent (Brownlee et al., 2006; David et al., 2014; Hervik & Svihus, 2019).

In this Chapter, cellulose oleogel digestion behavior was investigated by determining the lipid hydrolysis rate as well as the overall oil digestibility.

# 10.2. Material and Methods

## 10.2.1.  Oleogel Preparation

Oleogels were prepared by manually mixing oil and cryogel particles in order to obtain a self-standing material with 71% (w/w) oil content.

## 10.2.2.  *In vitro* Lipid Digestibility

### 10.2.2.1. *In vitro* Digestion

The *in vitro* digestion process followed the INFOGEST static protocol (Brodkorb et al., 2019), and the pH-stat approach was used to determine the extent of lipid digestibility (Mat et al., 2016), by replacing NaCl with $NaHCO_3$ in simulated salivary (SSF), gastric (SGF), and intestinal (SIF) fluids. According to oleogel composition (71% oil content), 1.4 g of cellulose-based oleogel, corresponding to 1 $g_{oil}$, was used.

SSF, SGF, and SIF were preheated to 37 °C. As the matrices being digested lacked carbohydrates and proteins, amylolytic and proteolytic enzymes were not used.

For the oral phase, 4 mL of SSF, 25 μL of 0.3 M $CaCl_2$, and 975 μL of water were added to the samples, which were continuously stirred at 37 °C for 2 min.

In the gastric phase, 8 mL of SGF, 5 μL of 0.3 M $CaCl_2$, and 667 μL of water were added to the oleogel sample. The gastric phase was initiated by adjusting the pH to 3.0 with 1 M HCl and making up the volume to 20 mL with water. The mixture was continuously stirred at 37 °C for 2 hours.

In the intestinal phase, 8 mL of SIF, 4 μL of 0.3 M $CaCl_2$, 5 mL of a lipase solution (prepared in SIF and providing 2,000 U/mL activity), and 3 mL of 160 mM bile extract (prepared in SIF) were added. The intestinal phase was initiated by adjusting the pH to 8.00 ± 0.10 with 1 M NaOH and making up the volume to 40 mL with water. The pH of the digestion mixture was monitored immediately after lipase addition and 0.25 M NaOH aliquots were automatically added by a TitroLine® 7000 titrator (SI Analytics GmbH, Mainz, Germany) to maintain a value of 8.0 ± 0.025 (*i.e.*, the optimum of used lipase based on its technical specifications). The volume of NaOH (mL) added to titrate the oleogels at a specific time, was recorded ($V_{oleogel}$).

The percentage of free fatty acids (FFA) released during lipolysis was calculated (Eq 1):

$$\text{FFA (\%)} = \frac{V_e}{V_t} \times 100 \qquad \text{(Eq. 1)}$$

where $V_e$ is the experimental volume of the oil, and $V_t$ represents the theoretical volume required to titrate the fatty acids released by complete hydrolysis of triglycerides in the

reaction vessel, assuming that 2 FFA are produced for each triacylglycerol molecule (Li et al., 2011), and was calculated according to Eq. 2:

$$V_t = 2 \times \left[ \frac{m_{oil}}{MW_{oil}} \frac{1000}{C_{NaOH}} \right]$$  (Eq. 2)

where $m_{oil}$ is the mass of oil in the reaction vessel (g), $MW_{oil}$ is the average molecular weight of sunflower oil (876.6p0 g mol$^{-1}$) and $C_{NaOH}$ is the concentration of the sodium hydroxide (mol L$^{-1}$).

After in vitro digestion, the digestion was stopped by placing the sample into an ice bath for 15 min, centrifugated at 30,000 ×g for 70 minutes using an Avanti J-25 centrifuge (Beckman, Palo Alto, USA), and a 30 mL aliquot of the mixed micellar phase (*i.e.,* stabilized structures encapsulating lipophilic bioactive components) was recovered.

### 10.2.2.2. Confocal Microscopy of Digested Samples

The hanging-drop method was used to analyze samples collected after the gastric and intestinal digestion phases (*i.e.,* digestate) (Gallier et al., 2012). Samples were stained by gently hand-mixed with 0.05 mL of a 0.2% (w/v) aqueous solution of Nile Red and 0.01% (w/v) of Fluorescent Brightener 28 (Sigma Aldrich, Milan, Italy), to selectively mark the oil and the cellulose fraction, respectively. Secondly, an agarose solution (1%, w/w) preheated at 50 °C, was added to the samples in a sample:agarose solution ratio of 1:2 (v/v). Two µL of the fluid mix was placed on a microscope coverslip and left to set at room temperature for 1 min. The stained samples were then placed on a microscope slide, covered with a cover slide, and observed using a confocal laser scanning microscope at 100× magnification (Leica TCS SP8 X confocal system, Leica Microsystems, Wetzlar, Germany). Images were imported in jpg format using the software LasX 3.5.5 (Leica Microsystems, Wetzlar, Germany).

Image analysis was carried out to assess the oil droplet dimension (Image-Pro Plus 6.3, Media Cybernetics Inc., USA). Images were converted to an 8-bit grey scale and software calibration was applied. Droplet diameter data were provided by the software and further elaborated to obtain the $D_{32}$ using Excel (Microsoft, Redmond, Washington, USA).

### 10.2.2.3. Particle Size and Zeta Potential of Digested Samples

The particle size distribution of the mixed micellar phase from digested oil and oleogels (recovered as described in section 2.3.4) was determined using Dynamic Light Scattering (DLS) with a Zetasizer NanoZS (Malvern Instruments, Worcestershire, UK). Samples were diluted 1:100 (v/v) with deionized water and introduced into a cell where the particles scattered laser light at a 173° angle. Particle size was expressed as the cumulative volume-weighted mean diameter in nanometers. Additionally, the ζ-potential was measured by placing the diluted sample in a capillary cell equipped with two electrodes to assess particle electrophoretic mobility.

# 10.3. Results and Discussion

### 10.3.1.　　Destructuring Behavior of Cellulose-based Oleogels under Gastrointestinal Conditions

Due to the possible effect on the digestion behavior of the oleogel structure (Alongi et al., 2022; Ciuffarin, Alongi, et al., 2023; Plazzotta et al., 2022), cellulose oleogel containing 71% (w/w) oil was submitted to *in vitro* simulated digestion. and compared to a control sample, containing MCC and SO at the same concentration. The destructuring behavior of the oleogel and the control upon the gastric and intestinal phase was first observed by CLSM (Figure 37).
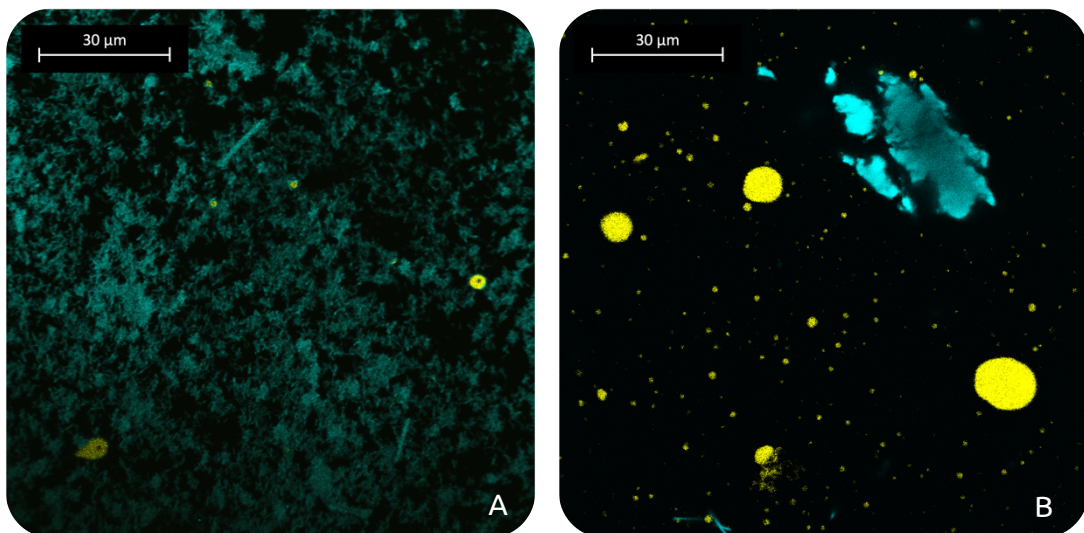


Figure 37. Confocal light scanning microscopy micrograph of the gastric (A) and intestinal (B) digestate samples of a cellulose oleogel containing 71% (w/w) oil. Cellulose is represented in turquoise, and oil in yellow.

As visible from Figure 37A, at the end of the gastric phase, a limited number of round oil droplets (yellow) were observed among swelled cellulose particles (turquoise). Conversely, their number increased drastically at the intestinal level. It can be hypothesized that cellulose, upon contact with the aqueous medium of the gastric fluid, interacted with water due to its hydrophilic characteristic. Consequently, the cellulose matrix largely released oil, which was visually noticed to separate at the surface of the digestate, and thus not analyzed in the CLSM analysis. The introduction of bile salts and lipase in the intestinal phase gradually favored both the separation of cellulose into dense hydrated aggregates and the dispersion of the oil phase into micelles (Figure 37B), with results similar to those of unstructured oil reported previously (Chapter 9) and in the literature (Plazzotta et al., 2022). Oil droplets with similar dimensions and distribution were obtained upon digestion of the unstructured control sample containing

MCC and SO (data not shown), suggesting that cellulose cryogel particles did not interfere with oil digestion, probably due to their strong hydrophilic nature and digestion resistance. The digestate CLSM observations differed from those obtained digesting whey protein-based oleogels in Chapter 9. In that case, protein particles favored oil digestion at the intestinal phase, making oil droplets no more detectable. This hypothesis was further confirmed by the analysis of FFA release during intestinal digestion (Figure 38).
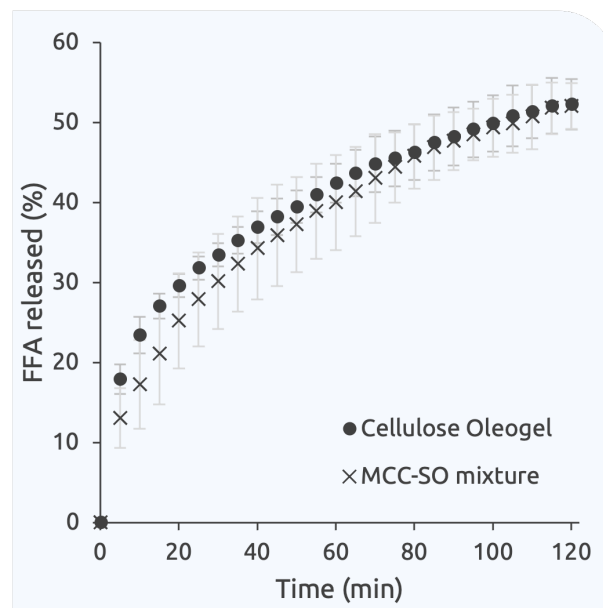


Figure 38. Free fatty acid (FFA) released kinetic during in vitro intestinal digestion of cellulose oleogel and unstructured MCC-oil mixture with 71% (w/w) oil content.

The release of free fatty acids (FFA) during intestinal digestion exhibited a pattern consistent with those of Chapter 9 and prior studies (Li et al., 2011; O'Sullivan et al., 2017), which shows a rapid increase in the initial phase, followed by a gradual slowing of FFA release until reaching a *plateau*. After 2 h of intestinal digestion, the $FFA_{max}$ was comparable (around 52%) between the cellulose oleogel and the unstructured MCC-oil mixture (Figure 38). This value is in line with the hydrolysis level of the unstructured sunflower oil (Calligaris et al., 2020). Moreover, no differences between the digested cellulose oleogel and the unstructured MCC-oil mixture were found in terms of oil particle size distribution and zeta-potential (around -67 mV in both cases) .

These findings clearly highlighted that the structuring of oil into a cellulose oleogel did not affect the digestion behavior of oil. This is probably due to the tendency of cellulose to release oil in the early stage of gastrointestinal digestion, thus being unable to protect it from the action of lipolytic enzymes. This behavior is certainly interesting since it demonstrates that the use of cellulose oleogels in foods as fat replacers would not affect the nutritional functionalities of the structured oil.

# 10.4. Conclusions

These findings clearly highlighted that the structuring of oil into a cellulose-based oleogel did not affect its digestion behavior. This is probably due to the tendency of cellulose to release oil in the early stage of gastrointestinal digestion, thus being unable to protect it from the action of lipolytic enzymes. This behavior is certainly interesting since it demonstrates that the use of cellulose oleogels in foods as fat replacers would not affect the nutritional functionalities of the structured oil.

# 11. GENERAL CONCLUSIONS

Today, the development of a new era of sustainable and healthy food products goes through a clear understanding of formulation-process-structure-function relationships. In this context, food structure, defined as the hierarchical organization of food elements, is strategic to deliver the desired food functionalities. On one side, food structure affects food acceptability and sensory perception being associated with the macroscopic feature of foods; on the other side, food structure deeply influences nutritional and health performances of macro and micronutrients, and bioactive components during digestion. It is not enough for the qualitative study of food products considering the different quality attributes, but it is imperative to design quantitative hypothesis-driven research to find out the links between food functionalities and food structure. These considerations are particularly important in the attempt to design healthier and sustainable foods for future generations.

I hope that this thesis - focused on oleogels- could contribute to addressing some of the nutritional and environmental issues today associated with fat consumption.

## 11.1. Main Findings

In Part 1 the direct oleogelation was studied considering the self-assembly properties of a considerable number of lipophilic oleogelators. As a general consideration, we can say that direct oleogelation is ready to be scaled up, despite some Regulatory constraints impairing the application of oleogels by the food industry. Based on our research findings, it is important not to underestimate the different variables potentially affecting oleogel structure. In particular, the presence of minor components in oil, such as polyphenols in extra virgin olive oil, was demonstrated to modify the oleogel structure, being able to create novel junction zones in the crystalline network made of saturated monoglycerides and waxes. On direct oleogelation, this thesis it was also explored the feasibility of changing the conventional paradigm in oleogel production by using controlled heating and cooling phases and shifting to innovative technologies, such as hydrostatic high-pressure treatments. It was highlighted that this technology is feasible to steer fat structuring being able to modulate fat crystal size and morphology.

In the second part of the research, the attention was moved to the indirect oleogelation approach. This approach is particularly interesting in the attempt to obtain clean-label oleogels. However, the use of hydrophilic polymers for oil structuring is challenging and requires more complex preparation methodologies as compared to direct oleogelation. The possibility of obtaining porous materials able to entrap large quantities of oil strictly depends on the ability of the molecule to form a gel in water. The further hydrogel drying must be controlled to reduce as much as possible the collapse of the matrix leaving a highly porous network in which oil can be absorbed. In this context, the thesis outcomes clearly show the importance of studying the structural changes occurring during the conversion from a hydrogel to a cryogel up to an oleogel. It was clearly demonstrated that the oleogel properties are related to the hydrogel characteristics that finally are associated with the gelling conditions adopted. Interestingly, cellulose, whey proteins, and pea proteins were all able to form networks with oil structuring ability. However, each biopolymer generated oleogels with different features as well as with different ability to interact with other food components, such as water.

Finally, in the third part of the thesis oleogel health functionalities were studied. Depending on the structuring molecules considered, different gastrointestinal behaviors were noted. Lipophilic molecules structured oleogels showed reduced oil lipolysis in comparison to the control oil. This was explained by the ability of the gelator network to hinder the action of lipase during intestinal digestion. On the contrary, when whey protein oleogels were considered, an enhancement of the lipolysis rate and degree was recorded, probably associated due to the emulsifying capacity of proteins. Finally, cellulose oleogels were not able to modify the oil digestion behavior. Similarly, polyphenol bioaccessibility wasaffected by oleogel structure and the considered structuring molecule. Whey protein-based oleogel enhanced polyphenol intestinal bioaccessibility, while lipophilic gelator reduced it. This outcome is interesting in the attempt to deliver molecules to the colon, where they can further exert their bioactivity.

These findings appear interesting to design oleogels with tailored functionalities, widening their potential beyond their use as fat substitutes.

## 11.2. Innovative Aspects

In this PhD Thesis, a deep investigation of oleogels and oleogelation methodologies oleogel was presented. Results could be useful to strategically design the new generation of oleogels taking into account technological, sustainable, and nutritional aspects. As emerged from this Thesis, depending on the final intended use the structure of oleogels can be tailored by modulating both processing conditions and formulation. Novel technologies and novel structured materials have been developed and proposed to obtain oleogels with specific characteristics in terms of technological performances, health properties as well as sustainability features. I hope that some of them could enlarge the exploitability of oleogels for the development of novel healthy, sustainable, and memorable from a sensory point of view. Finally, I guess to have contributed to my work for more sustainable and healthy diets.

## 11.3. Personal Considerations

I believe that each branch of the conceptual tree (Figure 11) delineated in this doctoral thesis adds something to our comprehension of food for designing more sustainable human diets in this way the objectives designed for my doctoral journey. This "Ph.D. expedition", originally structured to encompass various aspects of the oleogel world, occasionally veered along unforeseen trajectories due to serendipitous discoveries in the laboratory. This aspect was both challenging and motivational, furnishing me with the fortitude and impetus to progress in the research.

Additionally, my hope is that the publications associated to this thesis could generate interest on the fascinating world of oleogels, inspiring the curiosity of other young researchers.

# REFERENCES

Abdallah, D. J., & Weiss, R. G. (2000). Organogels and low molecular mass organic gelators. *Advanced Materials*, *12*(17). https://doi.org/10.1002/1521-4095(200009)12:17<1237::AID-ADMA1237>3.0.CO;2-B

Abdollahi, M., Goli, S. A. H., & Soltanizadeh, N. (2020). Physicochemical Properties of Foam-Templated Oleogel Based on Gelatin and Xanthan Gum. *European Journal of Lipid Science and Technology*, *122*(2), 1900196. https://doi.org/10.1002/ejlt.201900196

Abdolmaleki, K., Alizadeh, L., Nayebzadeh, K., Hosseini, S. M., & Shahin, R. (2020). Oleogel production based on binary and ternary mixtures of sodium caseinate, xanthan gum, and guar gum: Optimization of hydrocolloids concentration and drying method. *Journal of Texture Studies*, *51*(2), 290–299. https://doi.org/10.1111/jtxs.12469

Acevedo, N. C., & Marangoni, A. G. (2015). Nanostructured fat crystal systems. *Annual Review of Food Science and Technology*, *6*, 71–96. https://doi.org/10.1146/annurev-food-030713-092400

AIACHE, J. -M, GAUTHIER, P., & AIACHE, S. (1992). New gelification method for vegetable oils I: cosmetic application. *International Journal of Cosmetic Science*, *14*(5), 228–234. https://doi.org/10.1111/j.1467-2494.1992.tb00056.x

Alavi, F., & Ciftci, O. N. (2023). Superlight macroporous aerogels produced from cold-set egg white protein hydrogels show superior oil structuring capacity. *Food Hydrocolloids*, *136*, 108180. https://doi.org/10.1016/j.foodhyd.2022.108180

Albano, K. M., Franco, C. M. L., & Telis, V. R. N. (2014). Rheological behavior of Peruvian carrot starch gels as affected by temperature and concentration. *Food Hydrocolloids*, *40*, 30–43. https://doi.org/10.1016/j.foodhyd.2014.02.003

Alongi, M., Lucci, P., Clodoveo, M. L., Schena, F. P., & Calligaris, S. (2022). Oleogelation of extra virgin olive oil by different oleogelators affects the physical properties and the stability of bioactive compounds. *Food Chemistry*, *368*. https://doi.org/10.1016/j.foodchem.2021.130779

Alvarez-Ramirez, J., Vernon-Carter, E. J., Carrera-Tarela, Y., Garcia, A., & Roldan-Cruz, C. (2020). Effects of candelilla wax/canola oil oleogel on the rheology, texture, thermal properties and in vitro starch digestibility of wheat sponge cake bread. *Lwt*, *130*, 109701. https://doi.org/10.1016/j.lwt.2020.109701

Andlinger, D. J., Bornkeßel, A. C., Jung, I., Schröter, B., Smirnova, I., & Kulozik, U. (2021). Microstructures of potato protein hydrogels and aerogels produced by thermal

crosslinking and supercritical drying. *Food Hydrocolloids*, *112*, 106305. https://doi.org/10.1016/j.foodhyd.2020.106305

Apovian, C. M. (2016). Obesity: definition, comorbidities, causes, and burden. In *The American journal of managed care* (Vol. 22, Issue 7).

Ardia, A., Knorr, D., & Heinz, V. (2004). Adiabatic heat modelling for pressure build-up during high-pressure treatment in liquid-food processing. *Food and Bioproducts Processing*, *82*(1), 89–95. https://doi.org/10.1205/096030804322985362

Aschemann-Witzel, J., Asioli, D., Banovic, M., Perito, M. A., Peschel, A. O., & Stancu, V. (2023). Defining upcycled food: The dual role of upcycling in reducing food loss and waste. *Trends in Food Science and Technology*, *132*, 132–137. https://doi.org/10.1016/j.tifs.2023.01.001

Ashkar, A., Laufer, S., Rosen-Kligvasser, J., Lesmes, U., & Davidovich-Pinhas, M. (2019). Impact of different oil gelators and oleogelation mechanisms on digestive lipolysis of canola oil oleogels. *Food Hydrocolloids*, *97*. https://doi.org/10.1016/j.foodhyd.2019.105218

Assegehegn, G., Brito-de la Fuente, E., Franco, J. M., & Gallegos, C. (2019). The Importance of Understanding the Freezing Step and Its Impact on Freeze-Drying Process Performance. In *Journal of Pharmaceutical Sciences* (Vol. 108, Issue 4, pp. 1378–1395). https://doi.org/10.1016/j.xphs.2018.11.039

Baldissera, A. C., Betta, F. Della, Penna, A. L. B., & De Dea Lindner, J. (2011). Alimentos funcionais: uma nova fronteira para o desenvolvimento de bebidas protéicas a base de soro de leite. *Semina:Ciencias Agrarias*, *32*(4), 1497–1512. https://doi.org/10.5433/1679-0359.2011v32n4p1497

Bampidis, V., Azimonti, G., Bastos, M. de L., Christensen, H., Dusemund, B., Kos Durjava, M., Kouba, M., López-Alonso, M., López Puente, S., Marcon, F., Mayo, B., Pechová, A., Petkova, M., Ramos, F., Sanz, Y., Villa, R. E., Woutersen, R., Bories, G., Gropp, J., … Aquilina, G. (2020). Safety and efficacy of ethyl cellulose for all animal species. *EFSA Journal*, *18*(7). https://doi.org/10.2903/j.efsa.2020.6210

Bascuas, S., Hernando, I., Moraga, G., & Quiles, A. (2020). Structure and stability of edible oleogels prepared with different unsaturated oils and hydrocolloids. *International Journal of Food Science and Technology*, *55*(4), 1458–1467. https://doi.org/10.1111/ijfs.14469

Bemer, H. L., Limbaugh, M., Cramer, E. D., Harper, W. J., & Maleky, F. (2016). Vegetable organogels incorporation in cream cheese products. *Food Research International*, *85*, 67–75. https://doi.org/10.1016/j.foodres.2016.04.016

Bermejo-Prada, A., Colmant, A., Otero, L., & Guignon, B. (2017). Industrial viability of the hyperbaric method to store perishable foods at room temperature. *Journal of Food Engineering*, *193*, 76–85. https://doi.org/10.1016/j.jfoodeng.2016.08.014

Betz, M., García-González, C. A., Subrahmanyam, R. P., Smirnova, I., & Kulozik, U. (2012). Preparation of novel whey protein-based aerogels as drug carriers for life science applications. *Journal of Supercritical Fluids*, *72*, 111–119. https://doi.org/10.1016/j.supflu.2012.08.019

Bhandari, B. (2013). Introduction to food powders. *Handbook of Food Powders: Processes and Properties*, 1–25. https://doi.org/10.1533/9780857098672.1

Blake, A. I., Co, E. D., & Marangoni, A. G. (2014). Structure and physical properties of plant wax crystal networks and their relationship to oil binding capacity. *JAOCS, Journal of the American Oil Chemists' Society*, *91*(6), 885–903. https://doi.org/10.1007/s11746-014-2435-0

Blake, A. I., & Marangoni, A. G. (2015). The Effect of Shear on the Microstructure and Oil Binding Capacity of Wax Crystal Networks. *Food Biophysics*, *10*(4), 403–415. https://doi.org/10.1007/s11483-015-9398-z

Bot, A., Den Adel, R., & Roijers, E. C. (2008). Fibrils of γ-oryzanol + β-sitosterol in edible oil organogels. *JAOCS, Journal of the American Oil Chemists' Society*, *85*(12), 1127–1134. https://doi.org/10.1007/s11746-008-1298-7

Brodkorb, A., Egger, L., Alminger, M., Alvito, P., Assunção, R., Ballance, S., Bohn, T., Bourlieu-Lacanal, C., Boutrou, R., Carrière, F., Clemente, A., Corredig, M., Dupont, D., Dufour, C., Edwards, C., Golding, M., Karakaya, S., Kirkhus, B., Le Feunteun, S., … Recio, I. (2019). INFOGEST static in vitro simulation of gastrointestinal food digestion. *Nature Protocols*, *14*(4), 991–1014. https://doi.org/10.1038/s41596-018-0119-1

Brownlee, I., Dettmar, P., Strugala, V., & Pearson, J. (2006). The Interaction of Dietary Fibres with the Colon. *Current Nutrition & Food Science*, *2*(3), 243–264. https://doi.org/10.2174/157340106778017896

Brunauer, S., Emmett, P. H., & Teller, E. (1938). Adsorption of Gases in Multimolecular Layers. *Journal of the American Chemical Society*, *60*(2), 309–319. https://doi.org/10.1021/ja01269a023

Buchtová, N., & Budtova, T. (2016). Cellulose aero-, cryo- and xerogels: towards understanding of morphology control. *Cellulose*, *23*(4), 2585–2595. https://doi.org/10.1007/s10570-016-0960-8

Buchtová, N., Pradille, C., Bouvard, J. L., & Budtova, T. (2019). Mechanical properties of cellulose aerogels and cryogels. *Soft Matter*, *15*(39), 7901–7908. https://doi.org/10.1039/c9sm01028a

Buckland, G., & Gonzalez, C. A. (2015). The role of olive oil in disease prevention: a focus on the recent epidemiological evidence from cohort studies and dietary intervention trials. *British Journal of Nutrition*, *113*(S2), S94–S101. https://doi.org/10.1017/S0007114514003936

Budtova, T. (2019). Cellulose II aerogels: a review. In *Cellulose* (Vol. 26, Issue 1, pp. 81–121). https://doi.org/10.1007/s10570-018-2189-1

Budtova, T., & Navard, P. (2016). Cellulose in NaOH–water based solvents: a review. In *Cellulose* (Vol. 23, Issue 1, pp. 5–55). https://doi.org/10.1007/s10570-015-0779-8

Cacace, F., Bottani, E., Rizzi, A., & Vignali, G. (2020). Evaluation of the economic and environmental sustainability of high pressure processing of foods. *Innovative Food Science and Emerging Technologies*, *60*. https://doi.org/10.1016/j.ifset.2019.102281

Calligaris, S., Alongi, M., Lucci, P., & Anese, M. (2020). Effect of different oleogelators on lipolysis and curcuminoid bioaccessibility upon in vitro digestion of sunflower oil oleogels. *Food Chemistry*, *314*, 126–146. https://doi.org/10.1016/j.foodchem.2019.126146

Calligaris, S., Mirolo, G., Da Pieve, S., Arrighetti, G., & Nicoli, M. C. (2014). Effect of Oil Type on Formation, Structure and Thermal Properties of γ-oryzanol and β-sitosterol-Based Organogels. *Food Biophysics*, *9*(1), 69–75. https://doi.org/10.1007/s11483-013-9318-z

Calligaris, S., Plazzotta, S., Barba, L., & Manzocco, L. (2021). Design of Roll-In Margarine Analogous by Partial Drying of Monoglyceride-Structured Emulsions. *European Journal of Lipid Science and Technology*, *123*(3). https://doi.org/10.1002/ejlt.202000206

Campos, R., & Marangoni, A. G. (2014). Crystallization Dynamics of Shear Worked Cocoa Butter. *Crystal Growth & Design*, *14*(3), 1199–1210. https://doi.org/10.1021/cg4017273

Campos, R., Narine, S. S., & Marangoni, A. G. (2002). Effect of cooling rate on the structure and mechanical properties of milk fat and lard. *Food Research International*, *35*(10), 971–981. https://doi.org/10.1016/S0963-9969(02)00159-X

Cerqueira, M. Â. P. R., & Castro, L. M. P. (2023). Why does the food industry need fat mimetics? In *Fat Mimetics for Food Applications* (pp. 3–6). Wiley. https://doi.org/10.1002/9781119780045.ch1

Chai, X., Meng, Z., & Liu, Y. (2020). Relationship between lipid composition and rheological properties of colloidal fat crystal networks: A comparative study using chemometrics. *Lwt*, *118*, 108814. https://doi.org/10.1016/j.lwt.2019.108814

Chen, B., Mcclements, D. J., & Decker, E. A. (2011). Minor components in food oils: A critical review of their roles on lipid oxidation chemistry in bulk oils and emulsions. *Critical Reviews in Food Science and Nutrition*, *51*(10), 901–916. https://doi.org/10.1080/10408398.2011.606379

Chen, C. H., & Terentjev, E. M. (2009). Aging and Metastability of Monoglycerides in Hydrophobic Solutions. *Langmuir*, *25*(12), 6717–6724. https://doi.org/10.1021/la9002065

Chen, K., & Zhang, H. (2020). Fabrication of Oleogels via a Facile Method by Oil Absorption in the Aerogel Templates of Protein-Polysaccharide Conjugates. *ACS Applied Materials and Interfaces*, *12*(6), 7795–7804. https://doi.org/10.1021/acsami.9b21435

Cheng, Z., Ren, J., Li, Y., Chang, W., & Chen, Z. (2002). Study on the multiple mechanisms underlying the reaction between hydroxyl radical and phenolic compounds by qualitative structure and activity relationship. *Bioorganic and Medicinal Chemistry*, *10*(12), 4067–4073. https://doi.org/10.1016/S0968-0896(02)00267-5

Chin, S. F., Binti Romainor, A. N., & Pang, S. C. (2014). Fabrication of hydrophobic and magnetic cellulose aerogel with high oil absorption capacity. *Materials Letters*, *115*, 241–243. https://doi.org/10.1016/j.matlet.2013.10.061

Cicerale, S., Lucas, L. J., & Keast, R. S. J. (2012). Antimicrobial, antioxidant and anti-inflammatory phenolic activities in extra virgin olive oil. *Current Opinion in Biotechnology*, *23*(2), 129–135. https://doi.org/10.1016/j.copbio.2011.09.006

Ciuffarin, F., Alongi, M., Peressini, D., Barba, L., Lucci, P., & Calligaris, S. (2023). Role of the polyphenol content on the structuring behavior of liposoluble gelators in extra virgin olive oil. *Food Chemistry*, *412*, 135572. https://doi.org/10.1016/j.foodchem.2023.135572

Ciuffarin, F., Alongi, M., Plazzotta, S., Lucci, P., Schena, F. P., Manzocco, L., & Calligaris, S. (2023). Oleogelation of extra virgin olive oil by different gelators affects lipid digestion and polyphenol bioaccessibility. *Food Research International*, *173*, 113239. https://doi.org/10.1016/j.foodres.2023.113239

Ciuffarin, F., Négrier, M., Plazzotta, S., Libralato, M., Calligaris, S., Budtova, T., & Manzocco, L. (2023). Interactions of cellulose cryogels and aerogels with water and oil: Structure-function relationships. *Food Hydrocolloids*, *140*, 108631. https://doi.org/10.1016/j.foodhyd.2023.108631

Clark, A. H., Kavanagh, G. M., & Ross-Murphy, S. B. (2001). Globular protein gelation- Theory and experiment. *Food Hydrocolloids*, *15*(4–6), 383–400. https://doi.org/10.1016/S0268-005X(01)00042-X

Clark, M., Macdiarmid, J., Jones, A. D., Ranganathan, J., Herrero, M., & Fanzo, J. (2020). The Role of Healthy Diets in Environmentally Sustainable Food Systems. *Food and Nutrition Bulletin*, *41*(2_suppl), 31S-58S. https://doi.org/10.1177/0379572120953734

Clark, M., & Tilman, D. (2017). Comparative analysis of environmental impacts of agricultural production systems, agricultural input efficiency, and food choice. *Environmental Research Letters*, *12*(6). https://doi.org/10.1088/1748-9326/aa6cd5

Co, E. D., & Marangoni, A. G. (2012a). Organogels: An alternative edible oil-structuring method. In *JAOCS, Journal of the American Oil Chemists' Society* (Vol. 89, Issue 5). https://doi.org/10.1007/s11746-012-2049-3

Co, E. D., & Marangoni, A. G. (2012b). Organogels: An alternative edible oil-structuring method. In *JAOCS, Journal of the American Oil Chemists' Society* (Vol. 89, Issue 5, pp. 749–780). https://doi.org/10.1007/s11746-012-2049-3

Crippa, M., Solazzo, E., Guizzardi, D., Monforti-Ferrario, F., Tubiello, F. N., & Leip, A. (2021). Food systems are responsible for a third of global anthropogenic GHG emissions. *Nature Food*, *2*(3), 198–209. https://doi.org/10.1038/s43016-021-00225-9

da Pieve, S., Calligaris, S., Co, E., Nicoli, M. C., & Marangoni, A. G. (2010). Shear Nanostructuring of monoglyceride organogels. *Food Biophysics*, *5*(3), 211–217. https://doi.org/10.1007/s11483-010-9162-3

da Silva, T. L. T., Chaves, K. F., Fernandes, G. D., Rodrigues, J. B., Bolini, H. M. A., & Arellano, D. B. (2018). Sensory and Technological Evaluation of Margarines With Reduced Saturated Fatty Acid Contents Using Oleogel Technology. *JAOCS, Journal of the American Oil Chemists' Society*, *95*(6), 673–685. https://doi.org/10.1002/aocs.12074

da Silva, T. L. T., Fernandes, G. D., & Arellano, D. B. (2021). Development of reduced saturated fat cookie fillings using multicomponent oleogels. *JAOCS, Journal of the American Oil Chemists' Society*, *98*(11), 1069–1082. https://doi.org/10.1002/aocs.12527

Daniel, J., & Rajasekharan, R. (2003). Organogelation of plant oils and hydrocarbons by long-chain saturated FA, fatty alcohols, wax esters, and dicarboxylic acids. *JAOCS, Journal of the American Oil Chemists' Society*, *80*(5). https://doi.org/10.1007/s11746-003-0714-0

David, L. A., Maurice, C. F., Carmody, R. N., Gootenberg, D. B., Button, J. E., Wolfe, B. E., Ling, A. V., Devlin, A. S., Varma, Y., Fischbach, M. A., Biddinger, S. B., Dutton, R. J., & Turnbaugh, P. J. (2014). Diet rapidly and reproducibly alters the human gut microbiome. *Nature*, *505*(7484), 559–563. https://doi.org/10.1038/nature12820

Davidovich-Pinhas, M. (2019). Oil structuring using polysaccharides. In *Current Opinion in Food Science* (Vol. 27, pp. 29–35). https://doi.org/10.1016/j.cofs.2019.04.006

Davidovich-Pinhas, M., Barbut, S., & Marangoni, A. G. (2015). The gelation of oil using ethyl cellulose. *Carbohydrate Polymers*, *117*, 869–878. https://doi.org/10.1016/j.carbpol.2014.10.035

De Vries, A., Gomez, Y. L., Van der Linden, E., & Scholten, E. (2017). The effect of oil type on network formation by protein aggregates into oleogels. *RSC Advances*, *7*(19), 11803–11812. https://doi.org/10.1039/c7ra00396j

De Vries, A., Hendriks, J., Van Der Linden, E., & Scholten, E. (2015). Protein Oleogels from Protein Hydrogels via a Stepwise Solvent Exchange Route. *Langmuir*, *31*(51), 13850–13859. https://doi.org/10.1021/acs.langmuir.5b03993

De Vries, A., Lopez Gomez, Y., Jansen, B., Van der Linden, E., & Scholten, E. (2017). Controlling Agglomeration of Protein Aggregates for Structure Formation in Liquid Oil: A Sticky

Business. *ACS Applied Materials and Interfaces*, *9*(11), 10136–10147. https://doi.org/10.1021/acsami.7b00443

Deniz Gunez, Z., Schafer, O., Chisholm, H., Deyber, H., Pelloux, C., & Binks, B. P. (2020). *Lipid Based Foam US10765125B2* (Patent US10765125B2).

Dent, T., Hallinan, R., Chitchumroonchokchai, C., & Maleky, F. (2022). Rice bran wax structured oleogels and in vitro bioaccessibility of curcumin. *JAOCS, Journal of the American Oil Chemists' Society*, *99*(4), 299–311. https://doi.org/10.1002/aocs.12576

Di Mattia, C., Paradiso, V. M., Andrich, L., Giarnetti, M., Caponio, F., & Pittia, P. (2014). Effect of Olive Oil Phenolic Compounds and Maltodextrins on the Physical Properties and Oxidative Stability of Olive Oil O/W Emulsions. *Food Biophysics*, *9*(4), 396–405. https://doi.org/10.1007/s11483-014-9373-0

Dikhtyar, A., Andrieieva, S., Fedak, N., Grinchenko, O., & Pyvovarov, Y. (2021). Determining Patterns in the Formation of Functionaltechnological Properties of a Fatbased Semi-Finished Product in the Technology of Sponge Cake Products. *Eastern-European Journal of Enterprise Technologies*, *6*(11(114)), 15–31. https://doi.org/10.15587/1729-4061.2021.246006

Doan, C. D., Patel, A. R., Tavernier, I., De Clercq, N., Van Raemdonck, K., Van de Walle, D., Delbaere, C., & Dewettinck, K. (2016). The feasibility of wax-based oleogel as a potential co-structurant with palm oil in low-saturated fat confectionery fillings. *European Journal of Lipid Science and Technology*, *118*(12), 1903–1914. https://doi.org/10.1002/ejlt.201500172

Doan, C. D., Tavernier, I., Okuro, P. K., & Dewettinck, K. (2018). Internal and external factors affecting the crystallization, gelation and applicability of wax-based oleogels in food industry. In *Innovative Food Science and Emerging Technologies* (Vol. 45, pp. 42–52). https://doi.org/10.1016/j.ifset.2017.09.023

Doan, C. D., To, C. M., De Vrieze, M., Lynen, F., Danthine, S., Brown, A., Dewettinck, K., & Patel, A. R. (2017). Chemical profiling of the major components in natural waxes to elucidate their role in liquid oil structuring. *Food Chemistry*, *214*, 717–725. https://doi.org/10.1016/j.foodchem.2016.07.123

Doan, C. D., Van De Walle, D., Dewettinck, K., & Patel, A. R. (2015). Evaluating the oil-gelling properties of natural waxes in rice bran oil: Rheological, thermal, and microstructural study. *JAOCS, Journal of the American Oil Chemists' Society*, *92*(6), 801–811. https://doi.org/10.1007/s11746-015-2645-0

Donato, L., Kolodziejcyk, E., & Rouvet, M. (2011). Mixtures of whey protein microgels and soluble aggregates as building blocks to control rheology and structure of acid induced cold-set gels. *Food Hydrocolloids*, *25*(4), 734–742. https://doi.org/10.1016/j.foodhyd.2010.08.020

Dong, L., Lv, M., Gao, X., Zhang, L., Rogers, M., Cao, Y., & Lan, Y. (2020). In vitro gastrointestinal digestibility of phytosterol oleogels: Influence of self-assembled microstructures on emulsification efficiency and lipase activity. *Food and Function*, *11*(11), 9503–9513. https://doi.org/10.1039/d0fo01642j

Draijer, N., Rivera del Rio, A., Lie-Piang, A., Janssen, A. E. M., & Boom, R. M. (2023). Nutritional value in sustainability assessment of protein-rich ingredients and foods: A 'farm-to-faeces' approach. *Journal of Cleaner Production*, *417*, 137864. https://doi.org/10.1016/j.jclepro.2023.137864

Druel, L., Niemeyer, P., Milow, B., & Budtova, T. (2018). Rheology of cellulose-[DBNH][CO2Et] solutions and shaping into aerogel beads. *Green Chemistry*, *20*(17), 3993–4002. https://doi.org/10.1039/c8gc01189c

Edenbrandt, A. K., & Lagerkvist, C. J. (2023). Motives, propensities and consistencies among Swedish consumers in relation to the food choice concept of clean eating. *British Food Journal*, *125*(13), 125–145. https://doi.org/10.1108/BFJ-03-2022-0217

The menu for change - A manifesto for the food system, (2021). https://www.eitfood.eu/media/news-pdf/FutureFoodMakers_-_Menu_for_Change.pdf

Enzo, S., Fagherazzi, G., Benedetti, A., & Polizzi, S. (1988). A profile-fitting procedure for analysis of broadened X-ray diffraction peaks. I. Methodology. *Journal of Applied Crystallography*, *21*(5), 536–542. https://doi.org/10.1107/S0021889888006612

Errington, A. D., & Foegeding, E. A. (1998). Factors Determining Fracture Stress and Strain of Fine-Stranded Whey Protein Gels. *Journal of Agricultural and Food Chemistry*, *46*(8), 2963–2967. https://doi.org/10.1021/jf980112y

Espert, M., Hernández, M. J., Sanz, T., & Salvador, A. (2021). Reduction of saturated fat in chocolate by using sunflower oil-hydroxypropyl methylcellulose based oleogels. *Food Hydrocolloids*, *120*. https://doi.org/10.1016/j.foodhyd.2021.106917

Espert, M., Salvador, A., & Sanz, T. (2020). Cellulose ether oleogels obtained by emulsion-templated approach without additional thickeners. *Food Hydrocolloids*, *109*, 106085. https://doi.org/10.1016/j.foodhyd.2020.106085

European Commission. (2020). Farm to Fork Strategy. In *DG SANTE/Unit 'Food information and composition, food waste'* (Issue DG SANTE/Unit 'Food information and composition, food waste'). https://ec.europa.eu/food/sites/food/files/safety/docs/f2f_action-plan_2020_strategy-info_en.pdf

Fabiani, R. (2016). Anti-cancer properties of olive oil secoiridoid phenols: A systematic review of: In vivo studies. *Food and Function*, *7*(10), 4145–4159. https://doi.org/10.1039/c6fo00958a

Fan, L., Ge, A., Chen, X. D., & Mercadé-Prieto, R. (2019). The role of non-covalent interactions in the alkaline dissolution of heat-set whey protein hydrogels made at gelation pH 2–11. *Food Hydrocolloids*, *89*, 100–110. https://doi.org/10.1016/j.foodhyd.2018.10.035

FAO. (2017). The future of food and agriculture: Trends and challenges. https://www.fao.org/3/i6583e/i6583e.pdf. In *Food and Agriculture Organization of the United Nations*. https://www.fao.org/3/i6583e/i6583e.pdf

Farooq, M. A., Aquib, M., Ghayas, S., Bushra, R., Haleem Khan, D., Parveen, A., & Wang, B. (2019). Whey protein: A functional and promising material for drug delivery systems recent developments and future prospects. *Polymers for Advanced Technologies*, *30*(9), 2183–2191. https://doi.org/10.1002/pat.4676

Fayaz, G., Calligaris, S., & Nicoli, M. C. (2020). Comparative Study on the Ability of Different Oleogelators to Structure Sunflower Oil. *Food Biophysics*, *15*(1), 42–49. https://doi.org/10.1007/s11483-019-09597-9

Fayaz, G., Goli, S. A. H., Kadivar, M., Valoppi, F., Barba, L., Calligaris, S., & Nicoli, M. C. (2017). Potential application of pomegranate seed oil oleogels based on monoglycerides, beeswax and propolis wax as partial substitutes of palm oil in functional chocolate spread. *Lwt*, *86*, 523–529. https://doi.org/10.1016/j.lwt.2017.08.036

Fayaz, G., Polenghi, O., Giardina, A., Cerne, V., & Calligaris, S. (2021). Structural and rheological properties of medium-chain triacylglyceride oleogels. *International Journal of Food Science and Technology*, *56*(2), 1040–1047. https://doi.org/10.1111/ijfs.14757

Feichtinger, A., Nibbelink, D. G., Poppe, S., Bozzo, L., Landman, J., & Scholten, E. (2022). Protein oleogels prepared by solvent transfer method with varying protein sources. *Food Hydrocolloids*, *132*, 107821. https://doi.org/10.1016/j.foodhyd.2022.107821

Felix, M., Perez-Puyana, V., Romero, A., & Guerrero, A. (2017). Development of thermally processed bioactive pea protein gels: Evaluation of mechanical and antioxidant properties. *Food and Bioproducts Processing*, *101*, 74–83. https://doi.org/10.1016/j.fbp.2016.10.013

Fischer, H., Polikarpov, I., & Craievich, A. F. (2009). Average protein density is a molecular-weight-dependent function. *Protein Science*, *13*(10), 2825–2828. https://doi.org/10.1110/ps.04688204

Foegeding, E. A., Bowland, E. L., & Hardin, C. C. (1995). Factors that determine the fracture properties and microstructure of globular protein gels. *Topics in Catalysis*, *9*(4), 237–249. https://doi.org/10.1016/S0268-005X(09)80254-3

Fowles, J., Boatman, R., Bootman, J., Lewis, C., Morgott, D., Rushton, E., Van Rooij, J., & Banton, M. (2013). A review of the toxicological and environmental hazards and risks of tetrahydrofuran. *Critical Reviews in Toxicology*, *43*(10), 811–828. https://doi.org/10.3109/10408444.2013.836155

Fricke, J. U., & Tillotson, T. (1997). Aerogels: production, characterization, and applications. *Thin Solid Films*, *297*(1–2), 212–223. https://doi.org/10.1016/S0040-6090(96)09441-2

Fu, H., Lo, Y. M., Yan, M., Li, P., & Cao, Y. (2020). Characterization of thermo-oxidative behavior of ethylcellulose oleogels. *Food Chemistry*, *305*. https://doi.org/10.1016/j.foodchem.2019.125470

Gallier, S., Gordon, K. C., & Singh, H. (2012). Chemical and structural characterisation of almond oil bodies and bovine milk fat globules. *Food Chemistry*, *132*(4), 1996–2006. https://doi.org/10.1016/j.foodchem.2011.12.038

Gao, Y., & Wu, S. (2019). Thermal and oxidation stability of functional oleogels formed by edible wax/starch and Schisandra chinensis oil. *Food and Function*, *10*(12), 8056–8068. https://doi.org/10.1039/c9fo01727e

Gavillon, R., & Budtova, T. (2008). Aerocellulose: New highly porous cellulose prepared from cellulose-NaOH aqueous solutions. *Biomacromolecules*, *9*(1), 269–277. https://doi.org/10.1021/bm700972k

Giacintucci, V., Di Mattia, C. D., Sacchetti, G., Flamminii, F., Gravelle, A. J., Baylis, B., Dutcher, J. R., Marangoni, A. G., & Pittia, P. (2018). Ethylcellulose oleogels with extra virgin olive oil: the role of oil minor components on microstructure and mechanical strength. *Food Hydrocolloids*, *84*, 508–514. https://doi.org/10.1016/j.foodhyd.2018.05.030

Giacomozzi, A. S., Carrín, M. E., & Palla, C. A. (2018). Muffins Elaborated with Optimized Monoglycerides Oleogels: From Solid Fat Replacer Obtention to Product Quality Evaluation. *Journal of Food Science*, *83*(6), 1505–1515. https://doi.org/10.1111/1750-3841.14174

Giacomozzi, A. S., Carrín, M. E., & Palla, C. A. (2021). Storage Stability of Oleogels Made from Monoglycerides and High Oleic Sunflower Oil. *Food Biophysics*, *16*(3), 306–316. https://doi.org/10.1007/s11483-020-09661-9

Gómez-Estaca, J., Pintado, T., Jiménez-Colmenero, F., & Cofrades, S. (2019). Assessment of a healthy oil combination structured in ethyl cellulose and beeswax oleogels as animal fat replacers in low-fat, PUFA-enriched pork burgers. *Food and Bioprocess Technology*, *12*(6), 1068–1081. https://doi.org/10.1007/s11947-019-02281-3

Gómez-Pinilla, F. (2008). Brain foods: The effects of nutrients on brain function. *Nature Reviews Neuroscience*, *9*(7), 568–578. https://doi.org/10.1038/nrn2421

Gravelle, A. J. (2023). Polysaccharide-based oleogels. *Fat Mimetics for Food Applications*, 155–191. https://doi.org/10.1002/9781119780045.ch9

Gravelle, A. J., Marangoni, A. G., & Davidovich-Pinhas, M. (2018). Ethylcellulose Oleogels. In *Edible Oleogels* (pp. 331–362). Elsevier. https://doi.org/10.1016/b978-0-12-814270-7.00014-9

Greiner, M., Reilly, A. M., & Briesen, H. (2012). Temperature- and Pressure-Dependent Densities, Self-Diffusion Coefficients, and Phase Behavior of Monoacid Saturated Triacylglycerides: Toward Molecular-Level Insights into Processing. *Journal of Agricultural and Food Chemistry*, *60*(20), 5243–5249. https://doi.org/10.1021/jf3004898

Guichard, E., Galindo-Cuspinera, V., & Feron, G. (2018). Physiological mechanisms explaining human differences in fat perception and liking in food spreads-a review. *Trends in Food Science & Technology*, *74*, 46–55. https://doi.org/10.1016/j.tifs.2018.01.010

Hagemann, J. W., & Rothfus, J. A. (1983). Polymorphism and transformation energetics of saturated monoacid triglycerides from differential scanning calorimetry and theoretical modelling. *Journal of the American Oil Chemists' Society*, *60*, 1123–1131.

Hansen, C. M. (2007). Methods of characterization - surfaces. In *Hansen Solubility Parameters: A Users Handbook, Second Edition*. CRC Press. https://doi.org/10.1201/9781420006834

Heller, M., & Keoleian, G. (2018). *Beyond Meat's Beyond Burger Life Cycle Assessment: A detailed comparison between*. https://css.umich.edu/sites/default/files/publication/CSS18-10.pdf

Hindeleh, A. M., & Hosemann, R. (1991). Microparacrystals: The intermediate stage between crystalline and amorphous. *Journal of Materials Science*, *26*(19), 5127–5133. https://doi.org/10.1007/BF01143202

Hiramatsu, N., Inoue, T., Suzuki, M., & Sato, K. (1989). Pressure study on thermal transitions of oleic acid polymorphs by high-pressure differential thermal analysis. *Chemistry and Physics of Lipids*, *51*, 47–53.

Hofmann, A. F., & Borgstrem, B. (1964). the Intraluminal Phase of Fat Digestion in Man: the Lipid Content of the Micellar and Oil Phases of Intestinal Content Obtained During Fat Digestion and Absorption. *The Journal of Clinical Investigation*, *43*(2), 247–257. https://doi.org/10.1172/JCI104909

Hong, Z., Xiao, N., Li, L., Li, Y., & Xie, X. (2022). Glycation of whey protein isolate and emulsions prepared by conjugates. *Journal of Food Engineering*, *316*, 110852. https://doi.org/10.1016/j.jfoodeng.2021.110852

Hooper, L., Martin, N., Jimoh, O. F., Kirk, C., Foster, E., & Abdelhamid, A. S. (2020). Reduction in saturated fat intake for cardiovascular disease. In *Cochrane Database of Systematic Reviews* (Vol. 2020, Issue 8). https://doi.org/10.1002/14651858.CD011737.pub3

Huang, H., Hallinan, R., & Maleky, F. (2018). Comparison of different oleogels in processed cheese products formulation. *International Journal of Food Science and Technology*, *53*(11), 2525–2534. https://doi.org/10.1111/ijfs.13846

Hyun, K., Kim, S. H., Ahn, K. H., & Lee, S. J. (2002). Large amplitude oscillatory shear as a way to classify the complex fluids. *Journal of Non-Newtonian Fluid Mechanics*, *107*(1–3), 51–65. https://doi.org/10.1016/S0377-0257(02)00141-6

I Brown, O. L. (2023). The Clausius-Clapeyron equation. *Journal of Chemical Education*, *28*, 428–429. https://pubs.acs.org/sharingguidelines

IPCC. (2019). *The Ocean and Cryosphere in a Changing Climate [EN/AR/RU/ZH] - World | ReliefWeb. September*. https://doi.org/https://www.ipcc.ch/report/srocc/

Jaberi, R., Pedram Nia, A., Naji-Tabasi, S., Elhamirad, A. H., & Shafafi Zenoozian, M. (2020). Rheological and structural properties of oleogel base on soluble complex of egg white protein and xanthan gum. *Journal of Texture Studies*, *51*(6), 925–936. https://doi.org/10.1111/jtxs.12552

Jahed, F. S., Hamidi, S., Zamani-Kalajahi, M., & Siahi-Shadbad, M. (2023). Biomedical applications of silica-based aerogels: a comprehensive review. *Macromolecular Research*, *31*(6), 519–538. https://doi.org/10.1007/s13233-023-00142-9

Jeong, S., Lee, S., & Oh, I. (2021). Development of antioxidant-fortified oleogel and its application as a solid fat replacer to muffin. *Foods*, *10*(12), 3059. https://doi.org/10.3390/foods10123059

Jiang, Z., & Bai, X. (2022). Effects of Polysaccharide Concentrations on the Formation and Physical Properties of Emulsion-Templated Oleogels. *Molecules*, *27*(17), 5391. https://doi.org/10.3390/molecules27175391

Jung, D., Oh, I., Lee, J. H., & Lee, S. (2020). Utilization of butter and oleogel blends in sweet pan bread for saturated fat reduction: Dough rheology and baking performance. *Lwt*, *125*, 109194. https://doi.org/10.1016/j.lwt.2020.109194

Jung, I., Schroeter, B., Plazzotta, S., De Berardinis, L., Smirnova, I., Gurikov, P., & Manzocco, L. (2023). Oleogels from mesoporous whey and potato protein based aerogel microparticles: Influence of microstructural properties on oleogelation ability. *Food Hydrocolloids*, *142*, 108758. https://doi.org/10.1016/j.foodhyd.2023.108758

Kleemann, C., Selmer, I., Smirnova, I., & Kulozik, U. (2018). Tailor made protein based aerogel particles from egg white protein, whey protein isolate and sodium caseinate: Influence of the preceding hydrogel characteristics. *Food Hydrocolloids*, *83*, 365–374. https://doi.org/10.1016/j.foodhyd.2018.05.021

Kościesza, R., Kulisiewicz, L., & Delgado, A. (2010). Observations of a high-pressure phase creation in oleic acid. *High Pressure Research*, *30*(1), 118–123. https://doi.org/10.1080/08957951003625555

Królczyk, J. B., Dawidziuk, T., Janiszewska-Turak, E., & Sołowiej, B. (2016). Use of Whey and Whey Preparations in the Food Industry - A Review. *Polish Journal of Food and Nutrition Sciences*, *66*(3), 157–165. https://doi.org/10.1515/pjfns-2015-0052

Lam, A. C. Y., Can Karaca, A., Tyler, R. T., & Nickerson, M. T. (2018). Pea protein isolates: Structure, extraction, and functionality. *Food Reviews International*, *34*(2), 126–147. https://doi.org/10.1080/87559129.2016.1242135

Li, J., Zhang, C., Li, Y., & Zhang, H. (2022). Fabrication of aerogel-templated oleogels from alginate-gelatin conjugates for in vitro digestion. *Carbohydrate Polymers*, *291*, 119603. https://doi.org/10.1016/j.carbpol.2022.119603

Li, L., Taha, A., Geng, M., Zhang, Z., Su, H., Xu, X., Pan, S., & Hu, H. (2021). Ultrasound-assisted gelation of β-carotene enriched oleogels based on candelilla wax-nut oils: Physical properties and in-vitro digestion analysis. *Ultrasonics Sonochemistry*, *79*, 105762. https://doi.org/10.1016/j.ultsonch.2021.105762

Li, L., Wan, W., Cheng, W., Liu, G., & Han, L. (2019). Oxidatively stable curcumin-loaded oleogels structured by β-sitosterol and lecithin: physical characteristics and release behaviour in vitro. *International Journal of Food Science and Technology*, *54*(7), 2502–2510. https://doi.org/10.1111/ijfs.14208

Li, Y., Hu, M., Du, Y., Xiao, H., & McClements, D. J. (2011). Control of lipase digestibility of emulsified lipids by encapsulation within calcium alginate beads. *Food Hydrocolloids*, *25*(1), 122–130. https://doi.org/10.1016/j.foodhyd.2010.06.003

Liao, Q., Su, X., Zhu, W., Hua, W., Qian, Z., Liu, L., & Yao, J. (2016). Flexible and durable cellulose aerogels for highly effective oil/water separation. *RSC Advances*, *6*(68), 63773–63781. https://doi.org/10.1039/c6ra12356b

Limpimwong, W., Kumrungsee, T., Kato, N., Yanaka, N., & Thongngam, M. (2017). Rice bran wax oleogel: A potential margarine replacement and its digestibility effect in rats fed a high-fat diet. *Journal of Functional Foods*, *39*, 250–256. https://doi.org/10.1016/j.jff.2017.10.035

Lin, R., Li, A., Zheng, T., Lu, L., & Cao, Y. (2015). Hydrophobic and flexible cellulose aerogel as an efficient, green and reusable oil sorbent. *RSC Advances*, *5*(100), 82027–82033. https://doi.org/10.1039/c5ra15194e

Liu, C., Meng, Z., Chai, X., Liang, X., Piatko, M., Campbell, S., & Liu, Y. (2019). Comparative analysis of graded blends of palm kernel oil, palm kernel stearin and palm stearin. *Food Chemistry*, *286*, 636–643. https://doi.org/10.1016/j.foodchem.2019.02.067

Liu, H. C., Chen, W. L., & Mao, S. J. T. (2007). Antioxidant nature of bovine milk β-lactoglobulin. *Journal of Dairy Science*, *90*(2), 547–555. https://doi.org/10.3168/jds.S0022-0302(07)71538-2

Lizhi, H., Toyoda, K., & Ihara, I. (2008). Dielectric properties of edible oils and fatty acids as a function of frequency, temperature, moisture and composition. *Journal of Food Engineering*, *88*(2), 151–158. https://doi.org/10.1016/j.jfoodeng.2007.12.035

Lorenzen, P. C., Schrader, K., Lorenzen, P. C., & Schrader, K. (2006). A comparative study of the gelation properties of whey protein concentrate and whey protein isolate. *Le Lait*, *86*(4), 259–271. https://doi.org/10.1051/lait:2006008

Lucci, P., Bertoz, V., Pacetti, D., Moret, S., & Conte, L. (2020). Effect of the refining process on total hydroxytyrosol, tyrosol, and tocopherol contents of olive oil. *Foods*, *9*(3). https://doi.org/10.3390/foods9030292

Luo, C., Liu, Z., Mi, S., & Li, L. (2022). Quantitative investigation on the effects of ice crystal size on freeze-drying: The primary drying step. *Drying Technology*, *40*(2), 446–458. https://doi.org/10.1080/07373937.2020.1806865

Luo, N., Ye, A., Wolber, F. M., & Singh, H. (2021). Effect of gel structure on the in vitro gastrointestinal digestion behaviour of whey protein emulsion gels and the bioaccessibility of capsaicinoids. *Molecules*, *26*(5). https://doi.org/10.3390/molecules26051379

Mahdi, F., Hassanpour, A., & Muller, F. (2018). An investigation on the evolution of granule formation by in-process sampling of a high shear granulator. *Chemical Engineering Research and Design*, *129*, 403–411. https://doi.org/10.1016/j.cherd.2017.10.038

Maleky, F., Smith, A. K., & Marangoni, A. (2011). Laminar Shear Effects on Crystalline Alignments and Nanostructure of a Triacylglycerol Crystal Network. *Crystal Growth & Design*, *11*(6), 2335–2345. https://doi.org/10.1021/cg200014w

Manzocco, L., Mikkonen, K. S., & García-González, C. A. (2021). Aerogels as porous structures for food applications: Smart ingredients and novel packaging materials. In *Food Structure* (Vol. 28). https://doi.org/10.1016/j.foostr.2021.100188

Manzocco, L., Plazzotta, S., Powell, J., de Vries, A., Rousseau, D., & Calligaris, S. (2022). Structural characterisation and sorption capability of whey protein aerogels obtained by freeze-drying or supercritical drying. *Food Hydrocolloids*, *122*. https://doi.org/10.1016/j.foodhyd.2021.107117

Manzocco, L., Valoppi, F., Calligaris, S., Andreatta, F., Spilimbergo, S., & Nicoli, M. C. (2017). Exploitation of κ-carrageenan aerogels as template for edible oleogel preparation. *Food Hydrocolloids*, *71*, 68–75. https://doi.org/10.1016/j.foodhyd.2017.04.021

Manzoor, S., Masoodi, F. A., Naqash, F., & Rashid, R. (2022). Oleogels: Promising alternatives to solid fats for food applications. *Food Hydrocolloids for Health*, *2*, 100058. https://doi.org/10.1016/j.fhfh.2022.100058

Marangoni, A. G., Acevedo, N., Maleky, F., Co, E., Peyronel, F., Mazzanti, G., Quinn, B., & Pink, D. (2012). Structure and functionality of edible fats. *Soft Matter*, *8*(5), 1275–1300. https://doi.org/10.1039/c1sm06234d

Marangoni, A. G., & Garti, N. (2011a). An Overview of the Past, Present, and Future of Organogels. In *Edible Oleogels: Structure and Health Implications* (pp. 1–17). https://doi.org/10.1016/B978-0-9830791-1-8.50004-8

Marangoni, A. G., & Garti, N. (2011b). Edible Oleogels: Structure and Health Implications. In *Edible Oleogels: Structure and Health Implications*. Elsevier Inc. https://doi.org/10.1016/C2015-0-02413-3

Marangoni, A. G., & Garti, N. (2018). Edible Oleogels. In *Edible Oleogels*. Elsevier. https://doi.org/10.1016/c2017-0-00541-4

Marangoni, A. G., Idziak, S. H. J., Vega, C., Batte, H., Ollivon, M., Jantzi, P. S., & Rush, J. W. E. (2007). Encapsulation-stucturing of edible oil attenuates acute elevation of blood lipids and insulin in humans. *Soft Matter*, *3*(2), 183–187. https://doi.org/10.1039/b611985a

Marković, A. K., Torić, J., Barbarić, M., & Brala, C. J. (2019). Hydroxytyrosol, tyrosol and derivatives and their potential effects on human health. In *Molecules* (Vol. 24, Issue 10). https://doi.org/10.3390/molecules24102001

Martinez, R. M., Rosado, C., Velasco, M. V. R., Lannes, S. C. S., & Baby, A. R. (2019). Main features and applications of organogels in cosmetics. In *International Journal of Cosmetic Science* (Vol. 41, Issue 2). https://doi.org/10.1111/ics.12519

Martini, S. (2013). *Sonocrystallization of Fats*. Springer New York. https://doi.org/10.1007/978-1-4614-7693-1

Martins, A. J. (2023). Phytosterols and other sterols. In *Fat Mimetics for Food Applications* (pp. 38–56). Wiley. https://doi.org/10.1002/9781119780045.ch4

Martins, A. J., Cerqueira, F., Vicente, A. A., Cunha, R. L., Pastrana, L. M., & Cerqueira, M. A. (2022). Gelation Behavior and Stability of Multicomponent Sterol-Based Oleogels. *Gels*, *8*(1). https://doi.org/10.3390/gels8010037

Martins, A. J., Lorenzo, J. M., Franco, D., Vicente, A. A., Cunha, R. L., Pastrana, L. M., Quiñones, J., & Cerqueira, M. A. (2019). Omega-3 and Polyunsaturated Fatty Acids-Enriched Hamburgers Using Sterol-Based Oleogels. *European Journal of Lipid Science and Technology*, *121*(11). https://doi.org/10.1002/ejlt.201900111

Martins, A. J., Vicente, A. A., Cunha, R. L., & Cerqueira, M. A. (2018). Edible oleogels: An opportunity for fat replacement in foods. In *Food and Function* (Vol. 9, Issue 2, pp. 758–773). https://doi.org/10.1039/c7fo01641g

Marze, S., Gaillard, C., & Roblin, P. (2015). In vitro digestion of emulsions: high spatiotemporal resolution using synchrotron SAXS. *Soft Matter*, *11*(26), 5365–5373. https://doi.org/10.1039/c5sm01205h

Mat, D. J. L., Le Feunteun, S., Michon, C., & Souchon, I. (2016). In vitro digestion of foods using pH-stat and the INFOGEST protocol: Impact of matrix structure on digestion kinetics of macronutrients, proteins and lipids. *Food Research International*, *88*, 226–233. https://doi.org/10.1016/j.foodres.2015.12.002

Mat, D. J. L., Souchon, I., Michon, C., & Le Feunteun, S. (2020). Gastro-intestinal in vitro digestions of protein emulsions monitored by pH-stat: Influence of structural properties

and interplay between proteolysis and lipolysis. *Food Chemistry*, *311*. https://doi.org/10.1016/j.foodchem.2019.125946

McClements, D. J. (2004). Food emulsions: Principles, practices, and techniques: Second edition. In *Food Emulsions: Principles, Practices, and Techniques, Second Edition*.

Menendez, J. A., Joven, J., Aragonès, G., Barrajón-Catalán, E., Beltrán-Debón, R., Borrás-Linares, I., Camps, J., Corominas-Faja, B., Cufí, S., Fernández-Arroyo, S., Garcia-Heredia, A., Hernández-Aguilera, A., Herranz-López, M., Jiménez-Sánchez, C., López-Bonet, E., Lozano-Sánchez, J., Luciano-Mateo, F., Martin-Castillo, B., Martin-Paredero, V., … Segura-Carretero, A. (2013). Xenohormetic and anti-aging activity of secoiridoid polyphenols present in extra virgin olive oil: A new family of gerosuppressant agents. *Cell Cycle*, *12*(4), 555–578. https://doi.org/10.4161/cc.23756

Merci, A., Urbano, A., Grossmann, M. V. E., Tischer, C. A., & Mali, S. (2015). Properties of microcrystalline cellulose extracted from soybean hulls by reactive extrusion. *Food Research International*, *73*, 38–43. https://doi.org/10.1016/j.foodres.2015.03.020

Miyashita, K. (2017). Polyunsaturated lipid oxidation in aqueous systems. In C. C. Akoh (Ed.), *Food Lipids: Chemistry, Nutrition, and Biotechnology, Fourth Edition*. CRC Press. https://doi.org/10.1201/9781315151854

Moghtadaei, M., Soltanizadeh, N., & Goli, S. A. H. (2018). Production of sesame oil oleogels based on beeswax and application as partial substitutes of animal fat in beef burger. *Food Research International*, *108*, 368–377. https://doi.org/10.1016/j.foodres.2018.03.051

Morales, M. E., Gallardo, V., Clarés, B., García, M. B., & Ruiz, M. A. (2009). Study and description of hydrogels and organogels as vehicles for cosmetic active ingredients. *Journal of Cosmetic Science*, *60*(6). https://doi.org/10.1111/j.1468-2494.2010.00580_4.x

Mu, R., Hong, X., Ni, Y., Li, Y., Pang, J., Wang, Q., Xiao, J., & Zheng, Y. (2019). Recent trends and applications of cellulose nanocrystals in food industry. *Trends in Food Science and Technology*, *93*, 136–144. https://doi.org/10.1016/j.tifs.2019.09.013

Müller, R. (2014). Production of Lubricants (Patent US2397956A). In *Encyclopedia of Lubricants and Lubrication* (US2397956A). https://doi.org/10.1007/978-3-642-22647-2_326

Nguyen, V., Rimaux, T., Truong, V., Dewettinck, K., & Van Bockstaele, F. (2020). Fat crystallization of blends of palm oil and anhydrous milk fat: A comparison between static and dynamic-crystallization. *Food Research International*, *137*, 109412. https://doi.org/10.1016/j.foodres.2020.109412

Nicolai, T. (2016). Formation and functionality of self-assembled whey protein microgels. *Colloids and Surfaces B: Biointerfaces*, *137*, 32–38. https://doi.org/10.1016/j.colsurfb.2015.05.055

Nicolai, T., & Durand, D. (2013). Controlled food protein aggregation for new functionality. *Current Opinion in Colloid and Interface Science*, *18*(4), 249–256. https://doi.org/10.1016/j.cocis.2013.03.001

Nikbakht Nasrabadi, M., Sedaghat Doost, A., & Mezzenga, R. (2021). Modification approaches of plant-based proteins to improve their techno-functionality and use in food products. *Food Hydrocolloids*, *118*, 106789. https://doi.org/10.1016/j.foodhyd.2021.106789

Nowak, D., & Jakubczyk, E. (2020). The freeze-drying of foods⇔the characteristic of the process course and the effect of its parameters on the physical properties of food materials. *Foods*, *9*(10), 1488. https://doi.org/10.3390/foods9101488

O'Brien, R. D. (2004). Fats and oils: formulating and processing for applications. In *New York*.

Öğütcü, M., & Yilmaz, E. (2014). Oleogels of virgin olive oil with carnauba wax and monoglyceride as spreadable products. *Grasas y Aceites*, *65*(3). https://doi.org/10.3989/gya.0349141

Oh, I. K., Amoah, C., Lim, J., Jeong, S., & Lee, S. (2017). Assessing the effectiveness of wax-based sunflower oil oleogels in cakes as a shortening replacer. *Lwt*, *86*, 430–437. https://doi.org/10.1016/j.lwt.2017.08.021

Oh, J. H., & Swanson, B. G. (2006). Polymorphic transitions of cocoa butter affected by high hydrostatic pressure and sucrose polyesters. *JAOCS, Journal of the American Oil Chemists' Society*, *83*(12), 1007–1014. https://doi.org/10.1007/s11746-006-5155-2

Ojijo, N. K. O., Kesselman, E., Shuster, V., Eichler, S., Eger, S., Neeman, I., & Shimoni, E. (2004). Changes in microstructural, thermal, and rheological properties of olive oil/monoglyceride networks during storage. *Food Research International*, *37*(4), 385–393. https://doi.org/10.1016/j.foodres.2004.02.003

Okuro, P. K., Martins, A. J., Vicente, A. A., & Cunha, R. L. (2020). Perspective on oleogelator mixtures, structure design and behaviour towards digestibility of oleogels. In *Current Opinion in Food Science* (Vol. 35, pp. 27–35). https://doi.org/10.1016/j.cofs.2020.01.001

Oliete, B., Potin, F., Cases, E., & Saurel, R. (2018). Modulation of the emulsifying properties of pea globulin soluble aggregates by dynamic high-pressure fluidization. *Innovative Food Science and Emerging Technologies*, *47*, 292–300. https://doi.org/10.1016/j.ifset.2018.03.015

O'Sullivan, C. M., Davidovich-Pinhas, M., Wright, A. J., Barbut, S., & Marangoni, A. G. (2017). Ethylcellulose oleogels for lipophilic bioactive delivery-effect of oleogelation on: In vitro bioaccessibility and stability of beta-carotene. *Food and Function*, *8*(4), 1438–1451. https://doi.org/10.1039/c6fo01805j

Palla, C. A., Wasinger, M. F., & Carrín, M. E. (2021). Monoglyceride oleogels as fat replacers in filling creams for sandwich cookies. *Journal of the Science of Food and Agriculture*, *101*(6), 2398–2405. https://doi.org/10.1002/jsfa.10863

Pandolsook, S., & Kupongsak, S. (2017). Influence of bleached rice bran wax on the physicochemical properties of organogels and water-in-oil emulsions. *Journal of Food Engineering*, *214*, 182–192. https://doi.org/10.1016/j.jfoodeng.2017.06.030

Papoutsis, K., Golding, J. B., Vuong, Q., Pristijono, P., Stathopoulos, C. E., Scarlett, C. J., & Bowyer, M. (2018). Encapsulation of citrus by-product extracts by spray-drying and freeze-drying using combinations of maltodextrin with soybean protein and ι-carrageenan. *Foods*, *7*(7), 115. https://doi.org/10.3390/foods7070115

Park, C., Bemer, H. L., & Maleky, F. (2018). Oxidative Stability of Rice Bran Wax Oleogels and an Oleogel Cream Cheese Product. *JAOCS, Journal of the American Oil Chemists' Society*, *95*(10), 1267–1275. https://doi.org/10.1002/aocs.12095

Parkinson, L., & Cicerale, S. (2016). The health benefiting mechanisms of virgin olive oil phenolic compounds. *Molecules*, *21*(12), 1734. https://doi.org/10.3390/molecules21121734

Pascoviche, D. M., Goldstein, N., Fishman, A., & Lesmes, U. (2019). Impact of fatty acids unsaturation on stability and intestinal lipolysis of bioactive lipid droplets. *Colloids and Surfaces A: Physicochemical and Engineering Aspects*, *561*, 70–78. https://doi.org/10.1016/j.colsurfa.2018.09.081

Patel, A. R. (2018). Structuring Edible Oils with Hydrocolloids: Where Do we Stand? In *Food Biophysics* (Vol. 13, Issue 2, pp. 113–115). Springer New York LLC. https://doi.org/10.1007/s11483-018-9527-6

Patel, A. R. (2020). Biopolymer-based oleocolloids. In K. Pal, I. Banerjee, P. Sarkar, D. Kim, W.-P. Deng, N. K. Dubey, & K. B. T.-B.-B. F. Majumder (Eds.), *Biopolymer-Based Formulations: Biomedical and Food Applications* (pp. 587–604). Elsevier. https://doi.org/10.1016/B978-0-12-816897-4.00024-2

Patel, A. R., Babaahmadi, M., Lesaffer, A., & Dewettinck, K. (2015). Rheological Profiling of Organogels Prepared at Critical Gelling Concentrations of Natural Waxes in a Triacylglycerol Solvent. *Journal of Agricultural and Food Chemistry*, *63*(19), 4862–4869. https://doi.org/10.1021/acs.jafc.5b01548

Patel, A. R., Cludts, N., Bin Sintang, M. D., Lewille, B., Lesaffer, A., & Dewettinck, K. (2014). Polysaccharide-based oleogels prepared with an emulsion-templated approach. *ChemPhysChem*, *15*(16), 3435–3439. https://doi.org/10.1002/cphc.201402473

Patel, A. R., Cludts, N., Sintang, M. D. Bin, Lesaffer, A., & Dewettinck, K. (2014). Edible oleogels based on water soluble food polymers: Preparation, characterization and potential application. *Food and Function*, *5*(11), 2833–2841. https://doi.org/10.1039/c4fo00624k

Patel, A. R., & Dewettinck, K. (2015). Comparative evaluation of structured oil systems: Shellac oleogel, HPMC oleogel, and HIPE gel. *European Journal of Lipid Science and Technology*, *117*(11), 1772–1781. https://doi.org/10.1002/ejlt.201400553

Patel, A. R., & Dewettinck, K. (2016). Edible oil structuring: An overview and recent updates. *Food and Function*, *7*(1), 20–29. https://doi.org/10.1039/c5fo01006c

Patel, A. R., Nicholson, R. A., & Marangoni, A. G. (2020). Applications of fat mimetics for the replacement of saturated and hydrogenated fat in food products. *Current Opinion in Food Science*, *33*, 61–68. https://doi.org/10.1016/j.cofs.2019.12.008

Patel, A. R., Rajarethinem, P. S., Cludts, N., Lewille, B., De Vos, W. H., Lesaffer, A., & Dewettinck, K. (2015). Biopolymer-based structuring of liquid oil into soft solids and oleogels using water-continuous emulsions as templates. *Langmuir*, *31*(7), 2065–2073. https://doi.org/10.1021/la502829u

Pehlivanoglu, H., Ozulku, G., Yildirim, R. M., Demirci, M., Toker, O. S., & Sagdic, O. (2018). Investigating the usage of unsaturated fatty acid-rich and low-calorie oleogels as a shortening mimetics in cake. *Journal of Food Processing and Preservation*, *42*(6). https://doi.org/10.1111/jfpp.13621

Pérez-Martínez, D., Alvarez-Salas, C., Charó-Alonso, M., Dibildox-Alvarado, E., & Toro-Vazquez, J. F. (2007). The cooling rate effect on the microstructure and rheological properties of blends of cocoa butter with vegetable oils. *Food Research International*, *40*(1), 47–62. https://doi.org/10.1016/j.foodres.2006.07.016

Perța-Crișan, S., Ursachi, C. Ștefan, Chereji, B. D., & Munteanu, F. D. (2023). Oleogels—Innovative Technological Solution for the Nutritional Improvement of Meat Products. *Foods*, *12*(1), 131. https://doi.org/10.3390/foods12010131

Perța-Crișan, S., Ursachi, C. Ștefan, Chereji, B. D., Tolan, I., & Munteanu, F. D. (2023). Food-Grade Oleogels: Trends in Analysis, Characterization, and Applicability. *Gels*, *9*(5), 386. https://doi.org/10.3390/gels9050386

Pires, J. R. A., Souza, V. G. L., Gomes, L. A., Coelhoso, I. M., Godinho, M. H., & Fernando, A. L. (2022). Micro and nanocellulose extracted from energy crops as reinforcement agents in chitosan films. *Industrial Crops and Products*, *186*, 115247. https://doi.org/10.1016/j.indcrop.2022.115247

Piroddi, M., Albini, A., Fabiani, R., Giovannelli, L., Luceri, C., Natella, F., Rosignoli, P., Rossi, T., Taticchi, A., Servili, M., & Galli, F. (2017). Nutrigenomics of extra-virgin olive oil: A review. *BioFactors*, *43*(1), 17–41. https://doi.org/10.1002/biof.1318

Plazzotta, S., Alongi, M., De Berardinis, L., Melchior, S., Calligaris, S., & Manzocco, L. (2022). Steering protein and lipid digestibility by oleogelation with protein aerogels. *Food and Function*. https://doi.org/10.1039/d2fo01257j

Plazzotta, S., Calligaris, S., & Manzocco, L. (2019). Structure of oleogels from κ-carrageenan templates as affected by supercritical-CO 2 -drying, freeze-drying and lettuce-filler addition. *Food Hydrocolloids*, *96*, 1–10. https://doi.org/10.1016/j.foodhyd.2019.05.008

Plazzotta, S., Calligaris, S., & Manzocco, L. (2020). Structural characterization of oleogels from whey protein aerogel particles. *Food Research International*, *132*, 109099. https://doi.org/10.1016/j.foodres.2020.109099

Plazzotta, S., Calligaris, S., & Manzocco, L. (2023). Feasibility of protein aerogel particles as food ingredient: The case of cocoa spreads. *Journal of Food Engineering*, *351*, 111522. https://doi.org/10.1016/j.jfoodeng.2023.111522

Plazzotta, S., Jung, I., Schroeter, B., Subrahmanyam, R. P., Smirnova, I., Calligaris, S., Gurikov, P., & Manzocco, L. (2021). Conversion of whey protein aerogel particles into oleogels: Effect of oil type on structural features. *Polymers*, *13*(23). https://doi.org/10.3390/polym13234063

Portugal, I., Dias, V. M., Duarte, R. F., & Evtuguin, D. V. (2010). Hydration of cellulosesilica hybrids assessed by sorption isotherms. *Journal of Physical Chemistry B*, *114*(11), 4047–4055. https://doi.org/10.1021/jp911270y

Principato, L., Carullo, D., Bassani, A., Spigno, G., Gruppi, A., Duserm Garrido, G., & Dordoni, R. (2021). Effect of dietary fiber and thermal conditions on rice bran wax-based structured edible oils. *Foods*, *10*(12), 3072. https://doi.org/10.3390/foods10123072

Pripp, A. H., Vreeker, R., & Van Duynhoven, J. (2005). Binding of olive oil phenolics to food proteins. *Journal of the Science of Food and Agriculture*, *85*(3), 354–362. https://doi.org/10.1002/jsfa.1992

Puscas, A., Muresan, V., Socaciu, C., & Muste, S. (2020). Oleogels in food: A review of current and potential applications. In *Foods* (Vol. 9, Issue 1). https://doi.org/10.3390/foods9010070

Qian, C., Decker, E. A., Xiao, H., & McClements, D. J. (2012). Nanoemulsion delivery systems: Influence of carrier oil on β-carotene bioaccessibility. *Food Chemistry*, *135*(3), 1440–1447. https://doi.org/10.1016/j.foodchem.2012.06.047

Ramel, P. R., Co, E. D., Acevedo, N. C., & Marangoni, A. G. (2016). Structure and functionality of nanostructured triacylglycerol crystal networks. *Progress in Lipid Research*, *64*, 231–242. https://doi.org/10.1016/j.plipres.2016.09.004

Reboredo-Rodríguez, P., González-Barreiro, C., Martínez-Carballo, E., Cambeiro-Pérez, N., Rial-Otero, R., Figueiredo-González, M., & Cancho-Grande, B. (2021). Applicability of an in-vitro digestion model to assess the bioaccessibility of phenolic compounds from olive-related products. *Molecules*, *26*(21), 6667. https://doi.org/10.3390/molecules26216667

Rémond, D., Shahar, D. R., Gille, D., Pinto, P., Kachal, J., Peyron, M. A., Dos Santos, C. N., Walther, B., Bordoni, A., Dupont, D., Tomás-Cobos, L., & Vergères, G. (2015). Understanding the gastrointestinal tract of the elderly to develop dietary solutions that prevent malnutrition. *Oncotarget*, *6*(16), 13858–13898. https://doi.org/10.18632/oncotarget.4030

Rigacci, S., & Stefani, M. (2016). Nutraceutical properties of olive oil polyphenols. An itinerary from cultured cells through animal models to humans. *International Journal of Molecular Sciences*, *17*(6), 843. https://doi.org/10.3390/ijms17060843

Robitzer, M., Renzo, F. Di, & Quignard, F. (2011). Natural materials with high surface area. Physisorption methods for the characterization of the texture and surface of polysaccharide aerogels. *Microporous and Mesoporous Materials*, *140*(1–3), 9–16. https://doi.org/10.1016/j.micromeso.2010.10.006

Rodríguez-Morató, J., Xicota, L., Fitó, M., Farré, M., Dierssen, M., & De La Torre, R. (2015). Potential role of olive oil phenolic compounds in the prevention of neurodegenerative diseases. *Molecules*, *20*(3), 4655–4680. https://doi.org/10.3390/molecules20034655

Roisnel, T., & Rodríguez-Carvajal, J. (2001). WinPLOTR: A windows tool for powder diffraction pattern analysis. *Materials Science Forum*, *378–381*(I), 118–123. https://doi.org/10.4028/www.scientific.net/msf.378-381.118

Roman, C., García-Morales, M., Eugenio, M. E., Ibarra, D., Martín-Sampedro, R., & Delgado, M. A. (2021). A sustainable methanol-based solvent exchange method to produce nanocellulose-based ecofriendly lubricants. *Journal of Cleaner Production*, *319*, 128673. https://doi.org/10.1016/j.jclepro.2021.128673

Rovellini, P. (2017). Oli, grassi animali e vegetali e loro sottoprodotti, semi e frutti oleaginosi". Progetto UNI1603053 Determinazione del Contenuto di Idrossitirosolo e Tirosolo Negli Oli di Olive—Metodo HPLC. *Uni/Ct 003/Gl 18*.

Saget, S., Porto Costa, M., Santos, C. S., Vasconcelos, M., Styles, D., & Williams, M. (2021). Comparative life cycle assessment of plant and beef-based patties, including carbon opportunity costs. *Sustainable Production and Consumption*, *28*, 936–952. https://doi.org/10.1016/j.spc.2021.07.017

Saghafi, Z., Naeli, M. H., Tabibiazar, M., & Zargaraan, A. (2019). Modeling the Rheological Behavior of Chemically Interesterified Blends of Palm Stearin/Canola Oil as a Function of Physicochemical Properties. *JAOCS, Journal of the American Oil Chemists' Society*, *96*(11), 1219–1234. https://doi.org/10.1002/aocs.12272

Sagiri, S. S., Behera, B., Rafanan, R. R., Bhattacharya, C., Pal, K., Banerjee, I., & Rousseau, D. (2014). Organogels as matrices for controlled drug delivery: A review on the current state. *Soft Materials*, *12*(1), 47–72. https://doi.org/10.1080/1539445X.2012.756016

Sagiri, S. S., Kasiviswanathan, U., Shaw, G. S., Singh, M., Anis, A., & Pal, K. (2016). Effect of sorbitan monostearate concentration on the thermal, mechanical and drug release properties of oleogels. *Korean Journal of Chemical Engineering*, *33*(5), 1720–1727. https://doi.org/10.1007/s11814-015-0295-4

Şahin, İ., Özbakır, Y., İnönü, Z., Ulker, Z., & Erkey, C. (2018). Kinetics of supercritical drying of gels. In *Gels* (Vol. 4, Issue 1). https://doi.org/10.3390/gels4010003

Salvia-Trujillo, L., Qian, C., Martín-Belloso, O., & McClements, D. J. (2013). Influence of particle size on lipid digestion and β-carotene bioaccessibility in emulsions and nanoemulsions. *Food Chemistry*, *141*(2), 1472–1480. https://doi.org/10.1016/j.foodchem.2013.03.050

Salvia-Trujillo, L., Verkempinck, S. H. E., Sun, L., Van Loey, A. M., Grauwet, T., & Hendrickx, M. E. (2017). Lipid digestion, micelle formation and carotenoid bioaccessibility kinetics: Influence of emulsion droplet size. *Food Chemistry*, *229*, 653–662. https://doi.org/10.1016/j.foodchem.2017.02.146

Sangwal, K., & Sato, K. (2018). Nucleation and Crystallization Kinetics of Fats. *Structure-Function Analysis of Edible Fats*, 21–72. https://doi.org/10.1016/B978-0-12-814041-3.00002-2

Sato, K., Ueno, S., & Yano, J. (1999). Molecular interactions and kinetic properties of fats. *Progress in Lipid Research*, *38*(1), 91–116. https://doi.org/10.1016/S0163-7827(98)00019-8

Scharfe, M., Ahmane, Y., Seilert, J., Keim, J., & Flöter, E. (2019). On the Effect of Minor Oil Components on β-Sitosterol/γ-oryzanol Oleogels. *European Journal of Lipid Science and Technology*, *121*(8). https://doi.org/10.1002/ejlt.201800487

Scharfe, M., & Flöter, E. (2020). Oleogelation: From Scientific Feasibility to Applicability in Food Products. In *European Journal of Lipid Science and Technology* (Vol. 122, Issue 12). https://doi.org/10.1002/ejlt.202000213

Schatteman, D. (2013). Alternative routes to oil structuring using oleogelators. *Springer*, *JUNE*.

Schestakow, M., Karadagli, I., & Ratke, L. (2016). Cellulose aerogels prepared from an aqueous zinc chloride salt hydrate melt. *Carbohydrate Polymers*, *137*, 642–649. https://doi.org/10.1016/j.carbpol.2015.10.097

Scholten, E. (2019). Edible oleogels: how suitable are proteins as a structurant? In *Current Opinion in Food Science* (Vol. 27, pp. 36–42). https://doi.org/10.1016/j.cofs.2019.05.001

Selmer, I., Kleemann, C., Kulozik, U., Heinrich, S., & Smirnova, I. (2015). Development of egg white protein aerogels as new matrix material for microencapsulation in food. *Journal of Supercritical Fluids*, *106*, 42–49. https://doi.org/10.1016/j.supflu.2015.05.023

Shang, J., Zhong, F., Zhu, S., Huang, D., & Li, Y. (2021). Formation, structural characteristics and physicochemical properties of beeswax oleogels prepared with tea polyphenol loaded gelators. *Food and Function*, *12*(4), 1662–1671. https://doi.org/10.1039/d0fo02772c

Shimada, K., & Claude Cheftel, J. (1988). Texture characteristics, protein solubility, and sulfhydryl group/disulfide bond contents of heat-induced gels of whey protein isolate. *Journal of Agricultural and Food Chemistry*, *36*(5), 1018–1025. https://doi.org/10.1021/jf00083a029

Singh, V. K., Pal, K., Pradhan, D. K., & Pramanik, K. (2013). Castor oil and sorbitan monopalmitate based organogel as a probable matrix for controlled drug delivery.

*Journal of Applied Polymer Science*, *130*(3), 1503–1515. https://doi.org/10.1002/app.39315

Sivakanthan, S., Fawzia, S., Madhujith, T., & Karim, A. (2022). Synergistic effects of oleogelators in tailoring the properties of oleogels: A review. *Comprehensive Reviews in Food Science and Food Safety*, *21*(4), 3507–3539. https://doi.org/10.1111/1541-4337.12966

Springmann, M., Clark, M., Mason-D'Croz, D., Wiebe, K., Bodirsky, B. L., Lassaletta, L., de Vries, W., Vermeulen, S. J., Herrero, M., Carlson, K. M., Jonell, M., Troell, M., DeClerck, F., Gordon, L. J., Zurayk, R., Scarborough, P., Rayner, M., Loken, B., Fanzo, J., … Willett, W. (2018). Options for keeping the food system within environmental limits. *Nature*, *562*(7728), 519–525. https://doi.org/10.1038/s41586-018-0594-0

Sun, C. (2005a). True density of microcrystalline cellulose. *Journal of Pharmaceutical Sciences*, *94*(10). https://doi.org/10.1002/jps.20459

Sun, C. (2005b). True density of microcrystalline cellulose. *Journal of Pharmaceutical Sciences*, *94*(10), 2132–2134. https://doi.org/10.1002/jps.20459

Sun, X. D., & Arntfield, S. D. (2011). Dynamic oscillatory rheological measurement and thermal properties of pea protein extracted by salt method: Effect of pH and NaCl. *Journal of Food Engineering*, *105*(3), 577–582. https://doi.org/10.1016/j.jfoodeng.2011.03.008

Tan, C. H., Lee, C. J., Tan, S. N., Poon, D. T. S., Chong, C. Y. E., & Pui, L. P. (2021). Red palm oil: A review on processing, health benefits and its application in food. *Journal of Oleo Science*, *70*(9), 1201–1210. https://doi.org/10.5650/jos.ess21108

Tan, S. Y., Peh, E., Lau, E., Marangoni, A. G., & Henry, C. J. (2017). Physical form of dietary fat alters postprandial substrate utilization and glycemic response in healthy Chinese men. *Journal of Nutrition*, *147*(6), 1138–1144. https://doi.org/10.3945/jn.116.246728

Tan, S. Y., Peh, E., Siow, P. C., Marangoni, A. G., & Henry, C. J. (2017). Effects of the physical-form and the degree-of-saturation of oil on postprandial plasma triglycerides, glycemia and appetite of healthy Chinese adults. *Food and Function*, *8*(12), 4433–4440. https://doi.org/10.1039/C7FO01194F

Tan, S. Y., Wan-Yi Peh, E., Marangoni, A. G., & Henry, C. J. (2017). Effects of liquid oil vs. oleogel co-ingested with a carbohydrate-rich meal on human blood triglycerides, glucose, insulin and appetite. *Food and Function*, *8*(1), 241–249. https://doi.org/10.1039/c6fo01274d

Tanger, C., Müller, M., Andlinger, D., & Kulozik, U. (2022). Influence of pH and ionic strength on the thermal gelation behaviour of pea protein. *Food Hydrocolloids*, *123*, 106903. https://doi.org/10.1016/j.foodhyd.2021.106903

Tanti, R., Barbut, S., & Marangoni, A. G. (2016). Hydroxypropyl methylcellulose and methylcellulose structured oil as a replacement for shortening in sandwich cookie creams. *Food Hydrocolloids*, *61*, 329–337. https://doi.org/10.1016/j.foodhyd.2016.05.032

Tarté, R., Paulus, J. S., Acevedo, N. C., Prusa, K. J., & Lee, S. L. (2020). High-oleic and conventional soybean oil oleogels structured with rice bran wax as alternatives to pork fat in mechanically separated chicken-based bologna sausage. *Lwt*, *131*, 109659. https://doi.org/10.1016/j.lwt.2020.109659

Tavernier, I. (2018). *Oil structuring through biopolymer and crystal networks*. Ghent University.

Tavernier, I., Doan, C. D., Van De Walle, D., Danthine, S., Rimaux, T., & Dewettinck, K. (2017). Sequential crystallization of high and low melting waxes to improve oil structuring in wax-based oleogels. *RSC Advances*, *7*(20), 12113–12125. https://doi.org/10.1039/c6ra27650d

Tavernier, I., Patel, A. R., Van der Meeren, P., & Dewettinck, K. (2017a). Emulsion-templated liquid oil structuring with soy protein and soy protein: κ-carrageenan complexes. *Food Hydrocolloids*, *65*. https://doi.org/10.1016/j.foodhyd.2016.11.008

Tavernier, I., Patel, A. R., Van der Meeren, P., & Dewettinck, K. (2017b). Emulsion-templated liquid oil structuring with soy protein and soy protein: κ-carrageenan complexes. *Food Hydrocolloids*, *65*, 107–120. https://doi.org/10.1016/j.foodhyd.2016.11.008

Tefelski, D. B., Siegoczyński, R. M., Rostocki, A. J., Kos, A., Kościesza, R., & Wieja, K. (2008). The investigation of the dynamics of the phase transformation in triolein and oleic acid under pressure. *Journal of Physics: Conference Series*, *121*(14), 142004. https://doi.org/10.1088/1742-6596/121/4/142004

Terech, P., & Weiss, R. G. (1997). Low molecular mass gelators of organic liquids and the properties of their gels. *Chemical Reviews*, *97*(8). https://doi.org/10.1021/cr9700282

Umeh, C., Gupta, R. C., Gupta, R., Kaur, H., Kazourra, S., Maguwudze, S., Torbela, A., & Saigal, S. (2021). Acetone Ingestion Resulting in Cardiac Arrest and Death. *Cureus*. https://doi.org/10.7759/cureus.18466

Ungár, T. (2004). Microstructural parameters from X-ray diffraction peak broadening. *Scripta Materialia*, *51*(8 SPEC. ISS.), 777–781. https://doi.org/10.1016/j.scriptamat.2004.05.007

Valoppi, F., Calligaris, S., Barba, L., Šegatin, N., Poklar Ulrih, N., & Nicoli, M. C. (2017). Influence of oil type on formation, structure, thermal, and physical properties of monoglyceride-based organogel. *European Journal of Lipid Science and Technology*, *119*(2). https://doi.org/10.1002/ejlt.201500549

van Mechelen, J. B., Peschar, R., & Schenk, H. (2006). Structures of mono-unsaturated triacylglycerols. I. The $\beta_1$ polymorph. *Acta Crystallographica Section B Structural Science*, *62*(6), 1121–1130. https://doi.org/10.1107/S0108768106037074

Vardhanabhuti, B., Khayankan, W., & Foegeding, E. A. (2010). Formation of elastic whey protein gels at low pH by acid equilibration. *Journal of Food Science*, *75*(5), E305–E313. https://doi.org/10.1111/j.1750-3841.2010.01647.x

Vehovec, T., Gartner, A., Planincek, O., & Obreza, A. (2012). Influence of different types of commercially available microcrystalline cellulose on degradation of perindopril erbumine and enalapril maleate in binary mixtures. *Acta Pharmaceutica*, *62*(4), 515–528. https://doi.org/10.2478/v10007-012-0039-5

Vernon-Carter, E. J., Alvarez-Ramirez, J., Meraz, M., Bello-Perez, L. A., & Garcia-Diaz, S. (2020). Canola oil/candelilla wax oleogel improves texture, retards staling and reduces in vitro starch digestibility of maize tortillas. *Journal of the Science of Food and Agriculture*, *100*(3), 1238–1245. https://doi.org/10.1002/jsfa.10135

Verstringe, S., Moens, K., De Clercq, N., & Dewettinck, K. (2015). Crystallization behavior of monoacylglycerols in a hydrophobic and a hydrophilic solvent. *Food Research International*, *67*, 25–34. https://doi.org/10.1016/j.foodres.2014.10.027

Vijay, V., Pimm, S. L., Jenkins, C. N., & Smith, S. J. (2016). The impacts of oil palm on recent deforestation and biodiversity loss. *PLoS ONE*, *11*(7). https://doi.org/10.1371/journal.pone.0159668

Wagh, A., Birkin, P., & Martini, S. (2016). High-Intensity Ultrasound to Improve Physical and Functional Properties of Lipids. *Annual Review of Food Science and Technology*, *7*(1), 23–41. https://doi.org/10.1146/annurev-food-041715-033112

Wei, F., Lu, M., Li, J., Xiao, J., Rogers, M. A., Cao, Y., & Lan, Y. (2022). Construction of foam-templated oleogels based on rice bran protein. *Food Hydrocolloids*, *124*, 107245. https://doi.org/10.1016/j.foodhyd.2021.107245

Weibel, G. L., & Ober, C. K. (2003). An overview of supercritical $CO_2$ applications in microelectronics processing. *Microelectronic Engineering*, *65*(1–2), 145–152. https://doi.org/10.1016/S0167-9317(02)00747-5

Werner-Cárcamo, E. R., Rubilar, M., Macias-Rodriguez, B. A., & Marangoni, A. G. (2023). Impact of cooling rate and shear flow on crystallization and mechanical properties of wax-crystal networks. *Physics of Fluids*, *35*(9). https://doi.org/10.1063/5.0162427

Wijarnprecha, K., Aryusuk, K., Santiwattana, P., Sonwai, S., & Rousseau, D. (2018). Structure and rheology of oleogels made from rice bran wax and rice bran oil. *Food Research International*, *112*, 199–208. https://doi.org/10.1016/j.foodres.2018.06.005

Wijaya, W., Van der Meeren, P., Wijaya, C. H., & Patel, A. R. (2017). High internal phase emulsions stabilized solely by whey protein isolate-low methoxyl pectin complexes: effect of pH and polymer concentration. *Food and Function*, *8*(2), 584–594. https://doi.org/10.1039/c6fo01027j

Wilson, C. (2023, August 22). *Plant-based meat market at a crossroads amid declining sales*. Food Business News.

Woern, C., Marangoni, A. G., Weiss, J., & Barbut, S. (2021). Effects of partially replacing animal fat by ethylcellulose based organogels in ground cooked salami. *Food Research International*, *147*. https://doi.org/10.1016/j.foodres.2021.110431

Wolfer, T. L., Acevedo, N. C., Prusa, K. J., Sebranek, J. G., & Tarté, R. (2018). Replacement of pork fat in frankfurter-type sausages by soybean oil oleogels structured with rice bran wax. *Meat Science*, *145*, 352–362. https://doi.org/10.1016/j.meatsci.2018.07.012

Wright, A., Pinto, C., Tulk, H., McCluskey, J., Goldstein, A., Huschka, B., Marangoni, A., & Seetharaman, K. (2014). Monoacylglycerol gel offers improved lipid profiles in high and low moisture baked products but does not influence postprandial lipid and glucose responses. *Food and Function*, *5*(5), 882–893. https://doi.org/10.1039/c3fo60596e

Xiong, Y. L. (2023). Meat and meat alternatives: where is the gap in scientific knowledge and technology? *Italian Journal of Animal Science*, *22*(1), 482–496. https://doi.org/10.1080/1828051X.2023.2211988

Ye, Z., Cao, C., Li, R., Cao, P., Li, Q., & Liu, Y. (2019). Lipid composition modulates the intestine digestion rate and serum lipid status of different edible oils: A combination of in vitro and in vivo studies. *Food and Function*, *10*(3), 1490–1503. https://doi.org/10.1039/c8fo01290c

Yue, Y., Zhou, C., French, A. D., Xia, G., Han, G., Wang, Q., & Wu, Q. (2012). Comparative properties of cellulose nano-crystals from native and mercerized cotton fibers. *Cellulose*, *19*(4), 1173–1187. https://doi.org/10.1007/s10570-012-9714-4

Zhang, H., Li, Y., Xu, Y., Lu, Z., Chen, L., Huang, L., & Fan, M. (2016). Versatile fabrication of a superhydrophobic and ultralight cellulose-based aerogel for oil spillage clean-up. *Physical Chemistry Chemical Physics*, *18*(40), 28297–28306. https://doi.org/10.1039/c6cp04932j

Zhang, H., Zhang, G., Zhu, H., Wang, F., Xu, G., Shen, H., & Wang, J. (2021). Multiscale kapok/cellulose aerogels for oil absorption: The study on structure and oil absorption properties. *Industrial Crops and Products*, *171*, 113902. https://doi.org/10.1016/j.indcrop.2021.113902

Zhang, M., Dou, M., Wang, M., & Yu, Y. (2017). Study on the solubility parameter of supercritical carbon dioxide system by molecular dynamics simulation. *Journal of Molecular Liquids*, *248*, 322–329. https://doi.org/10.1016/j.molliq.2017.10.056

Zhang, Y., Xu, J., Tang, C., & Li, Y. (2023). Crystallization Behavior and Physical Properties of Monoglycerides-Based Oleogels as Function of Oleogelator Concentration. *Foods*, *12*(2), 345. https://doi.org/10.3390/foods12020345

Zhao, W., Wei, Z., & Xue, C. (2022). Recent advances on food-grade oleogels: Fabrication, application and research trends. *Critical Reviews in Food Science and Nutrition*, *62*(27), 7659–7676. https://doi.org/10.1080/10408398.2021.1922354

Zhao, W., Wei, Z., Xue, C., & Meng, Y. (2023). Development of food-grade oleogel via the aerogel-templated method: Oxidation stability, astaxanthin delivery and emulsifying application. *Food Hydrocolloids*, *134*, 108058. https://doi.org/10.1016/j.foodhyd.2022.108058

Zhi, Z., Yan, L., Li, H., Dewettinck, K., Van der Meeren, P., Liu, R., & Van Bockstaele, F. (2022). A combined approach for modifying pea protein isolate to greatly improve its solubility and emulsifying stability. *Food Chemistry*, *380*, 131832. https://doi.org/10.1016/j.foodchem.2021.131832

Zhu, P., Huang, W., & Chen, L. (2022). Develop and characterize thermally reversible transparent gels from pea protein isolate and study the gel formation mechanisms. *Food Hydrocolloids*, *125*, 107373. https://doi.org/10.1016/j.foodhyd.2021.107373

Zhu, T., Zhao, Y., Zong, M., Li, B., Zhang, X., & Wu, H. (2017). Improvement of physical properties of palm stearin and soybean oil blends by enzymatic interesterification and their application in fast frozen food. *RSC Advances*, *7*(55), 34435–34441. https://doi.org/10.1039/C7RA02829F

Zou, F., & Budtova, T. (2021). Tailoring the morphology and properties of starch aerogels and cryogels via starch source and process parameter. *Carbohydrate Polymers*, *255*, 117344. https://doi.org/10.1016/j.carbpol.2020.117344

Zulim Botega, D. C., Marangoni, A. G., Smith, A. K., & Goff, H. D. (2013). The potential application of rice bran wax oleogel to replace solid fat and enhance unsaturated fat content in ice cream. *Journal of Food Science*, *78*(9). https://doi.org/10.1111/1750-3841.12175

Zulkurnain, M., Balasubramaniam, V. M., & Maleky, F. (2019). Effects of lipid solid mass fraction and non-lipid solids on crystallization behaviors of model fats under high pressure. *Molecules*, *24*(15). https://doi.org/10.3390/molecules24152853

Zulkurnain, M., Maleky, F., & Balasubramaniam, V. M. (2016a). High pressure crystallization of binary fat blend: A feasibility study. *Innovative Food Science and Emerging Technologies*, *38*, 302–311. https://doi.org/10.1016/j.ifset.2016.06.025

Zulkurnain, M., Maleky, F., & Balasubramaniam, V. M. (2016b). High Pressure Processing Effects on Lipids Thermophysical Properties and Crystallization Kinetics. *Food Engineering Reviews*, *8*(4), 393–413. https://doi.org/10.1007/s12393-016-9144-4

Zulkurnain, M., Maleky, F., & Balasubramaniam, V. M. (2016c). High Pressure Processing Effects on Lipids Thermophysical Properties and Crystallization Kinetics. *Food Engineering Reviews*, *8*(4), 393–413. https://doi.org/10.1007/s12393-016-9144-4

# ABOUT THE AUTHOR

Francesco Ciuffarin was born in Gorizia on the 21$^{st}$ of February 1996. After spending five years at the University of Udine enrolled in the Food Science and Technology course, he joined the FoodTech Group in 2020 as a Ph.D. student as part of the XXXIII Ph.D. cycle of the course in Food and Human Health. There, under the supervision of Prof. Sonia Calligaris, he studied the possibility of substituting saturated fats with healthier and more sustainable ingredients in food formulations.

During his doctoral studies, Ciuffarin contributed to the field through awards, publications, and oral presentations at international congresses. He was recognized for his speaking and artistic skills, and his work was acknowledged by winning the "What for… 2023" national award held in Naples in 2023.

Outside of academia, Ciuffarin enjoyed working as a coach to a roller-skating team and as a photographer for ceremonies, private events, and company catalogs, adding a unique dimension to his character. He aspires to continue contributing to the innovation of the food sector by focusing on sustainability.

This thesis stands as a testament to Ciuffarin dedication to advancing knowledge in the food sector, and he looks forward to contributing even more on that.

# PUBLICATIONS RELEVANT TO THE Ph.D. ACTIVITY

## Publications on International Peer-Reviewed Journals

- Ciuffarin, F., Alongi, M., Peressini, D., Barba, L., Lucci, P., & Calligaris, S. (2023). Role of the polyphenol content on the structuring behavior of liposoluble gelators in extra virgin olive oil. Food Chemistry, 412, 135572.
- Ciuffarin, F., Alongi, M., Plazzotta, S., Lucci, P., Schena, F. P., Manzocco, L., & Calligaris, S. (2023). Oleogelation of extra virgin olive oil by different gelators affects lipid digestion and polyphenol bioaccessibility. Food Research International, 173, 113239.
- Ciuffarin, F., Négrier, M., Plazzotta, S., Libralato, M., Calligaris, S., Budtova, T., & Manzocco, L. (2023). Interactions of cellulose cryogels and aerogels with water and oil: Structure-function relationships. Food Hydrocolloids, 140, 108631.
- Calligaris, S., Ciuffarin, F., Nicoli, M.C. (2022). *Oleogel: definition, possible applications and further developments.* La Rivista Italiana delle Sostaze Grasse.

## In Progress Manuscripts

- Effect of moderate hydrostatic pressure on crystallization of palm stearin-sunflower oil binary systems. Current Opinion in Food Science. 2024. *Submitted.*
- Structure and digestibility of cellulose oleogels obtained through the cryogel template approach. Polymers. 2024. *Ready to be submitted.*

## Contributions to National and International Congresses

Poster Contributions:

- Ciuffarin, F., Alongi, M., Calligaris, S. Application of DSC analysis to study oil gelation. XLII National Conference on Calorimetry, Thermal Analysis and Applied Thermodynamics, Udine/online January 27th-28th 2021.
- Ciuffarin, F., Calligaris, S. Oil structuring for improving healthy and sustainable diets. 25th Workshop on the Development of the Italian Ph.D. Research on food Science and Technology and Biotechnology, Palermo, Italy, 14th-15th September 2021.
- Ciuffarin, F., Alongi, M., Calligaris, S., Nicoli, M.C. Modulation of extra virgin olive oil digestibility through oleogelation. 7th International Conference on Food Digestion, Cork, Ireland, 3rd-5th May 2022.

- Ciuffarin, F., Negrier, M., Plazzotta, S., Calligaris, S., Budtova, T., Manzocco, L. Exploring the potentialities of cellulose aerogels and cryogels as food ingredients. 5th Food Structure and Functionality Symposium Structuring Foods for a Sustainable World, Cork, Ireland, 18th-21st September 2022.
- Ciuffarin, F., Calligaris, S. Oil structuring for improving healthy and sustainable diets: the case study of extra virgin olive oil oleogelation. 26th Workshop on the Development of the Italian Ph.D. Research on food Science and Technology and Biotechnology, Asti, Italy, 18th-21st September 2022.

Oral Contributions:
- Ciuffarin, F., Alongi, M., Lucci, P., Calligaris, S., Nicoli, M. C. (2021). The impact of polyphenol content and gelator type on the structure of extra virgin olive oil-based oleogels. SISSG Congress "Edible oils and fats: Innovation and sustainability in production and control", Perugia, Italy, $15^{th}$-$17^{th}$ June 2022.
- Ciuffarin, F., Négrier, M., Plazzotta, S., Calligaris, S., Budtova, T., Manzocco, L. Exploring the potentialities of cellulose aerogels and cryogels as food ingredients. $2^{nd}$ International Conference on Aerogels for Biomedical and Environmental Applications, Athens, Greece, $29^{th}$ June-$1^{st}$ July 2022.
- Ciuffarin, F., Plazzotta, S., Calligaris, S., Gelas, L., Budtova, T., Manzocco, L. Feasibility of cellulose porous materials as oleogel-templates for the development of fat-replacers. $3^{rd}$ International Conference on Aerogels for Biomedical and Environmental Applications, Maribor, Slovenia, $5^{th}$ - $7^{th}$ July 2023.

# Relevant Research Grants

- Ph.D. scholarship at the University of Udine.
- COST Aerogel "Short Term Scientific Mission" travel grant for a research stay, Jan-Feb 2022, Sophie Antipolis, France.
- COST Aerogel travel grant to participate in the $2^{nd}$ International Conference on Aerogels for Biomedical and Environmental Applications, July 2022, Athens, Greece.
- ERASMUS Traineeship+ for a research stay, April-July 2023, Ghent, Belgium
- COST Aerogel travel grant to participate in the $3^{rd}$ International Conference on Aerogels for Biomedical and Environmental Applications, July 2023, Maribor, Slovenia.

## Award

- First prize in the video contest "What for... 2023" award held by FederAlimentare ([link](link)). Naples, September 2023.